Geowissenschaftliche Sammlung FB5

University of Bremen

Ontogenetic and macroevolutionary patterns of Anisian (Middle Triassic) ammonoids from Nevada, USA

DISSERTATION

zur Erlangung des Doktorgrades

der Naturwissenschaften

~ Dr. rer. nat. ~

Fachbereich Geowissenschaften der Universität Bremen

Eva Alexandra Bischof

März 2021

Reviewer

Prof. Dr. Jens Lehmann (University of Bremen, Germany)

Prof Dr. Marco Balini (University of Milan)

Date Colloquium: July 14, 2021

Table of contents

Ontogenetische und makroevolutionäre Entwicklungsmuster von Ammonoideen aus dem Anisium (Mittlere Trias) aus Nevada, USA

Zusammenfassung

Die meisten Evolutions- und Entwicklungsstudien in der Paläontologie haben mit einer großen Herausforderung zu kämpfen: Die überwiegende Mehrheit aller Fossilien gehören Tier- und Pflanzenarten an, die schon, lange bevor es die ersten Menschen auf der Erde gab, ausgestorben sind. Aussagen über viele biologische Eigenschaften wie phylogenetische Verwandschaftsbeziehungen, Wachstumsraten oder Verhaltensmuster sind daher oft spekulativ. Das soll aber nicht die Bedeutung von paläontologischen Evolutions- und Entwicklungsstudien schmälern; ganz im Gegenteil. Es gibt viele, leicht unterschiedliche Zitate aus den verschiedensten Forschungsbereichen, die alle mehr oder weniger das Folgende aussagen: Man muss die Vergangenheit verstehen, um die Zukunft vorhersagen zu können. Eine Möglichkeit, die Tatsache zu überwinden, dass in der Paläontologie keine direkten Beobachtungen gemacht werden können, besteht darin, so viele verschiedene Parameter wie möglich einzubeziehen. Um ontogenetische und makroevolutionäre Muster von Ammonoideen aus dem Anisium (Mittlere Trias) zu erforschen, haben wir daher einen integrierten Ansatz verwendet, der eine Vielzahl verschiedener Methoden und Proxys einschließt.

Das Ziel dieser Dissertation ist es, unser Verständnis von Prozessen zu erweitern, die morphologische Veränderungen von Ammonoideen beeinflussen. Die ausgestorbenen, marinen Kopffüßer lebten in einem Gehäuse aus Aragonit und sind mit modernen Tintenfischen, Kraken und Sepien verwandt. Um morphologische Entwicklungsmuster zu entschlüsseln, wurden ontogenetische und makroevolutionäre Prozesse von Ammonoideen des anisischen Fossil Hill Member in NW Nevada, USA analysiert. Dazu wurden Gesteine und Fossilien von drei Hauptlokalitäten aus zwei verschiedenen Regionen untersucht: (1) der Fossil Hill in der Humboldt Range, (2) der Muller Canyon und (3) der Favret Canyon in den Augusta Mountains. Die untersuchten Sequenzen gehören zu den weltweit bekanntesten Lokalitäten für anisische Ammonoideen. Für die paläoökologische Rekonstruktion haben wir hochauflösende lithostratigraphische Profile (cm-Skala) aufgenommen und an allen Lokalitäten Gesteinsproben gesammelt, die nach der Präparation 186 Dünnschliffe ergaben. Insgesamt sammelten wir zudem mehr als 8000 Fossilien, von denen mehr als 7800 Ammonoideen sind. Um ein besseres Verständnis für die morphologischen Veränderungen der gefundenen Arten zu bekommen, haben wir die morphometrische Analyse der Ammonoideen mit paläoökologischen Beobachtungen gepaart. Das übergeordnete Forschungsziel kann daher in drei Hauptthemen unterteilt werden: (1) Rekonstruktion der

Paläoumwelt der Lokalitäten, (2) Ammonoideen-Vergesellschaftungen, und (3) die Morphologie der Ammonoideen. Diese drei Hauptthemen wurden in vier verschiedenen Publikationen abgehandelt.

Das erste Hauptthema dieser Arbeit ist die Paläoumweltrekonstruktion einschließlich einer Analyse der Mikrofazies und der Bio- und Lithostratigraphie der untersuchten Profile. Bereits schon während der Feldarbeit zeigte sich, dass die einzelnen untersuchten Sequenzen relativ einheitlich sind. Sie bestehen alle aus abwechselnden Schichten von kalkhaltigem Silt- und Tonsteinen, die immer wieder mit linsenförmigem Kalkstein versetzt sind. Die Uniformität der Fazies wurde bei den Laborarbeiten bestätigt. Weder die Analyse der Dünnschliffe noch die Geochemie ergaben größere Faziesveränderungen innerhalb der untersuchten Abfolgen. Die Laminierung der meisten Schichten deutet auf eine zumindest kurzzeitige Sauerstoffanreicherung der untersten Wassersäule und damit auf kleinere paläoökologische Veränderungen hin. Aufgrund seiner allgemein stabilen und eher ruhigen Umweltbedingungen hat sich das Fossil Hill Member von Nevada als optimales Intervall erwiesen, um intrinsische Faktoren zu untersuchen, die Diversitäts- und Disparitätsmuster von Ammonoideen beeinflussen.

Das zweite Hauptthema dieser Arbeit ist die Analyse der Ammonoideen-Vergesellschaftung. Dies beinhaltete die Untersuchung möglicher Verschiebungen in der Alphataxonomie der Fauna während des untersuchen Zeitintervalles. Insgesamt wurden mehr als 50 verschiedenen Ammonoideenarten bestimmt, die zu 32 Gattungen aus 15 Familien gehören. Der Fossilbestand des untersuchten Zeitintervalls (*Nevadisculites taylori* bis *Frechites occidentalis* Zone) wird eindeutig von der Familie Ceratitidae Mojsisovics, 1879 (insbesondere der Unterfamilie Beyrichitinae Spath, 1934) dominiert. Es gibt mehrere besonders häufige Beyrichitinae wie *Frechites occidentalis* (Smith, 1914) und *Gymnotoceras rotelliformis* (Meek, 1877). Innerhalb dieses Intervalls konnten keine abrupten Veränderungen in Bezug auf die Artenvielfalt festgestellt werden, was eine Periode besonderer paläoökologischer Instabilität widerspiegelt hätte.

Das letzte und sogleich bedeutendste Hauptthema dieser Studie sind morphologische Veränderungen der Ammonoideen während ihrer ontogenetischen Entwicklung. Die evolutionären Entwicklungsmuster der untersuchen Arten wurden mit Methoden aus den Bereichen der Traditional Morphometrics und Geometric Morphometrics analysiert. Dabei erwies sich der geometrisch-morphometrische Ansatz als besonders wertvoll. Mit der R-Software wurde eine neue Methode zur Analyse der morphologischen Entwicklung von Ammonoideen entwickelt. Dieser neu entwickelte Ansatz basiert hauptsächlich auf einer Reihe verschiedener Funktionen aus den R-Paketen *geomorph*, *RRPP* und *Morpho*. Die geometrisch-morphometrische Analyse erlaubte es, die Heterochronie der untersuchten Arten zu quantifizieren und ontogenetische Schwankungen der intra- und interspezifischen Variabilität zu verfolgen. Bei Ammonoideen der Unterfamilie Beyrichitinae sind die ontogenetische Allometrie und

die intra- und interspezifische Variabilität eng miteinander verbunden. Die morphologische Variation scheint das Ergebnis von Verschiebungen des allometrischen Wachstumsmusters (d.h. Heterochronie) zu sein. Dies unterstützt die allgemeine Meinung, dass in stabilen Habitaten generell die pädomorphe Entwicklung gegenüber der Peramorphose begünstigt ist. Es konnten keine dominante Evolutionsprozesse nachgewiesen werden. Dies wird als Folge der allgemein stabilen Paläoumwelt und des damit verbundenen geringen paläoökologischen Drucks interpretiert.

Eines der wichtigsten Ergebnisse dieser Dissertation ist es, dass die morphologischen Veränderungen der untersuchten Arten vor allem von intrinsischen Faktoren beeinflusst wird. Die dokumentierten evolutionären Trends der Ceratitiden wurden höchstwahrscheinlich nicht oder nur schwach durch paläoökologische Veränderungen getriggert. Die in dieser Arbeit vorgestellten Methoden stellen ein wertvolles Werkzeug für zukünftige biogeographische und phylogenetische Untersuchungen und Diversitätsanalysen dar.

Zukünftige Studien sollten daher versuchen, die hier vorgestellten Methoden auf ein breiteres Spektrum verschiedener Morphologien auszuweiten. In diesem Zusammenhang wäre ein globaler Vergleich der morphologischen Muster besonders interessant. Um ein umfängliches Bild des Morphospaces von Ammonoideen zu erhalten, muss der hier vorgestellte methodische Ansatz auf die morphologische Analyse verschiedener Gehäuseformen erweitert werden. Dies wird es uns ermöglichen, morphologische Veränderungen verschiedener Taxa während ihrer Ontogenese zu vergleichen und damit auch ihre komplexe Entwicklungsbiologie und Evolution zu verstehen.

Ontogenetic and macroevolutionary patterns of Anisian (Middle Triassic) ammonoids from Nevada, USA

Summary

Most evolutionary and developmental studies in palaeontology have to cope with one major challenge: the vast majority of fossil species went extinct long before the first humans arose on earth. Statements about many biological properties such as phylogenetic relationships, growth rate or behavioural patterns are therefore often somewhat speculative. Yet, this should not diminish the importance of studying evolutionary und developmental patterns of past life; on the contrary. There are many slightly different quotes from different fields of research that all say more or less the following: *You have to know the past to predict the future*. One way to overcome the fact that no direct observations can be made in palaeontology is to include as many different parameters as possible. To untangle ontogenetic and macroevolutionary patterns of Anisian (Middle Triassic) ammonoids we therefore used an integrated approach that includes a variety of different methods and proxies.

The aim of the present PhD thesis is to increase our understanding of processes influencing morphologic changes of ammonoids, which are marine, shelled organisms related to modern squids, octopuses, and cuttlefish. To untangle morphologic relationships, ontogenetic and macroevolutionary patterns of Anisian ammonoids of the Fossil Hill Member in NW Nevada, USA were investigated. Therefore, three main localities in two different regions were studied: (1) The Fossil Hill in the Humboldt Range, (2) the Muller Canyon and (3) the Favret Canyon in the Augusta Mountains. The studied sequences are amongst the world's most famous bearing Anisian ammonoids assemblages. For the palaeoenvironmental reconstruction we measured lithostratigraphic sections in high-resolution (cm-scale) and collected rock samples at all localities. The rock samples provided 186 thin sections. In total we collected more than 8000 fossils, of which more than 7800 are ammonoids. In order to get a better understanding of the morphologic changes of those species, morphometric analyses on ammonoids were paired with palaeoenvironmental observations. The major research aim can therefore be broken down to three objectives: (1) palaeoenvironmental reconstruction of localities, (2) ammonoid associations, (3) ammonoid morphology. These objectives were addressed in four different paper.

The first objective of this thesis is the palaeoenvironmental reconstruction including an analysis of the microfacies and the bio- and lithostratigraphy of the analysed stratigraphic sequences. During the fieldwork, it was apparent that the individual sequences studied are relatively uniform. They all consist of alternating layers of calcareous siltstone and mudstone, partly with lenticular limestone. The

uniformity of the facies was confirmed during the laboratory work. Neither the analysis of the thin sections nor the geochemistry revealed major facies changes within the studied successions. Nevertheless, the lamination of most beds indicates at least short-term oxygenation of the bottom waters and thus small-scale palaeoenvironmental perturbations. Due to its generally stable and calm environmental conditions, the Anisian Fossil Hill Member of Nevada has emerged to be an optimal interval to study intrinsic factors influencing diversity and disparity patterns of ammonoids.

The second objective was addressed by studying ammonoid associations. This involved an analysis of possible shifts in the alpha taxonomy of the fauna over time. The taxonomic determination involved the discrimination of more than 50 species belonging to 32 genera and 15 families. The fossil record of the investigated time interval (*Nevadisculites taylori* to *Frechites occidentalis* zones) is clearly dominated by the family Ceratitidae Mojsisovics, 1879 (particularly the subfamily Beyrichitinae Spath, 1934). There are several extremely common Beyrichitinae such as *Frechites occidentalis* (Smith, 1914) and *Gymnotoceras rotelliformis* (Meek, 1877). Within this interval no significant changes in terms of biodiversity, reflecting a period of particular palaeoenvironmental instability, could be detected.

Lastly, this study investigated morphologic changes of ammonoids through their ontogenetic development. These evolutionary trends of Anisian ammonoids are investigated by using Traditional and Geometric Morphometric Methods. Thereby, particularly the latter proved to be of great value. Using R software, a new method was developed to analyse morphologic development of ammonoids. This newly developed approach is mainly based on a set of different functions from the R packages *geomorph*, *RRPP* and *Morpho*. The Geometric Morphometric analysis in R allowed the quantification of heterochronic processes and to trace fluctuations of intra- and interspecific variability through ontogeny. In beyrichitine ammonoids, the observed ontogenetic allometry pattern and the intra- and interspecific variability are closely linked to one another. Morphologic variation seems to be the result of perturbations of the allometric growth pattern (i.e. heterochrony). This supports the common view that paedomorphic development is favoured over peramorphosis in more stable environments. Omnipresent directional evolutionary processes could not be detected. This is interpreted to be the result of the generally stable palaeoenvironment and therefore only a limited amount of palaeoenvironmental pressure.

In summary, one of the most significant result of this dissertation is the significant role of intrinsic factors influencing the morphologic changes of the investigated species. The documented evolutionary trends within ceratitid ammonoids were most likely not caused by small scale palaeoenvironmental changes and may therefore only partly reflect adaption. The methods introduced in this thesis represent a highly valuable tool for comprehensive biogeographical and phylogenetic investigations in future studies. In addition, they yield important potential for forthcoming broad-scale diversity analyses.

Future research should therefore attempt to extend the herein introduced methods to a broader scope. In this regard, the global comparison of morphologic patterns would be of particular interest. To obtain a compound picture of ammonoid morphospace, the methodological approach introduced herein needs to be extended to the morphologic analysis of various conch shapes. This will enable us to compare the morphologic changes of different taxa of ammonoids throughout their ontogeny and thus also to understand their complex developmental biology and evolution.

Ontogenetischi und makroevolutionäri Entwickligsmuster vo Ammonoideen usem Anisium (Mittleri Trias) vo Nevada, USA

(Bärndütsch, Bernese dialect)

Zämäfassig

Di meistä Evolutions- und Entwickligsstudiä ir Paläontologie hei mit eirä grossä Challenge ds kämpfä: Di überwiegendi Mehrheit vo aunä Fossiliä ghört zu Tier- und Pflanzäartä, wo scho lang bevors überhoupt di erstä Mönschä het gäh usgstorbä sy. Darum sy viu Ussagä über biologischi Eigäschaftä wi zum Bispiu phylogenetischi Verwandschaftsbeziigä, Wachstumsratä oder Verhautensmuster rächt spekulativ. Das söu aber uf ke Fau d Bedütig vo paläontologische Evolutions- und Entwickligsstudiä schmelerä; ganz im Gägäteil! Äs git viu, liächt ungerschidlächi Zitat wo meh oder minger ds folgende sägä: Mä muess d Vergangäheit verstah um Ussagä über d Zuekunft chönne ds machä. Ei Müglächkeit, wiemer dä Paläontologie-Gap cha übrwindä, besteit darin, dasmer so viu verschidnägi Parameter analüsiert, wiä numä müglächh. Für ontogenetischi und makroevolutionäre Muster vo Ammonoideen us em Anisium (Mittleri Trias) ds erforschä, hei mir darum ä integrierte Asatz brucht. Das heisst, dasi möglechscht viu verschidnägi Methodä und Proxies mitänäng ha kombiniert.

Ds Ziu vo dere Diss isches, äs bessers Verständnis vodä Prozässe, wo morphologischi Veränderigä vo Ammonoidee bewürke, ds becho. Di usgstorbnige, marine Chopffüässer hei immne Ghüüs us Aragonit ghuuset u si mit modernä Tintäfisch, Krakä und Sepiä verwandt. Für morphologischi Entwickligsmuster ds entschlüsslä, heimer ontogenetischi und makroevolutionäri Prozässä vo Ammonoidee vom anisische Fossil Hill Member vo NW Nevada, USA analüsiert. Daderzuä hani Gstei und Fossiliä vo drüü Houptlokalitätä us zwo verschidnigä Regione ungersuecht: (1) dr Fossil Hill ir Humboldt Range, (2) dr Muller Canyon und (3) dr Favret Canyon idä Augusta Mountains. Di ungersuechtä Sequänzä ghörä zudä wäutwyt bekannteste Lokalitäte womer anisischi Ammonoidee cha fingä. Für di paläoökologischi Rekonstruktion hei mir hochuflösendi lithostratigraphischi Profil (cm-Skala) ufgno. Währenddesse hei mer aui wichtigä Schichtä gsampled und Gsteisprobä gsammlet, us dene insgesammt 186 Dünnschliff präpariert si wordä. Insgesamt heimer zudem meh aus 8000 Fossiliä, vo drvo meh aus 7800 Ammonoidee si, gsammlet. Umnes bessers Verständnis vodä morphologische Veränderige vode gfungnigä Artä ds becho, heimer di morphometrisch Analyse vode Ammonoidee mit paläoökologischä Beobachtigä ergänzt. Ds übergeordnete Forschigsziu cha i drü Houptthemene ungerteilt wärdä: (1) Rekonstruktion vor Paläoumwäut vodä Lokalitätä, (2) Ammonoideen-

Vergseuschaftigä, und (3) Morphologie vo Ammonoideen. Diä drü Houptthemene sy i vier verschidnigä Paper abghandlet wordä.

Ds erstä Houptthema vo dere Arbeit ischd Paläoumweltrekonstruktion inklusive ere Analyse vor Mikrofazies und dr Bio- und Lithostratigraphie vode ungersuechtä Profiu. Bereits scho während der Fäudarbeit hetsech zeigt, dass di einzelnä ungersuechtä Sequenzä intern relativ iiheitläch si. Si bestöh aui usere Wächsulagerig vo chauchhautigä Silt- und Tonsteinä, wo immer widr mit linsäförmigä Chauchsteinä versetzt sy. D Uniformität vodä Fazies isch idä Laborarbeit bestätigt wordä. Weder d Analüsä vodä Dünnschliffe, no d Geochemie hei irgendwelchi grösserä Faziesveränderigä innerhaub vodä ungersuechtä Abfougä zeigt. D Laminierig vodä meistä Schichtä dütet auerdings of churzzytigi Suurstoffariicherigä vor ungerstä Wassersüülä und somit uf chlinneri paläoökologischi Veränderigä hy. Wägä dä augemein stabilä und ender ruigä Umwäutbedingigä hetsech ds Fossil Hill Member z Nevada aus es optimaus Intervau usägsteut um intrinischi Faktorä ds ungersuechä, wo Diversitäts- und Disparitätsmuster vo Ammonoidee beiflussä.

Ds zwöitä Houptthema vo dere Arbeit isch d Analüsä vodä Ammonoidee-Vergesellschaftigä. Das beeinhautet vorauem d Ungersuechig vo müglächä Verschiebigä ir Alphataxonomie vor Fauna während em ungersuechät Zytintervau. Insgesamt si meh aus 50 verschydnegi Ammonoideeartä bestimmt wordä, wo zu 32 Gattigä us 15 Familiä ghörä. Dr Fossiubestang vom ungersuechtä Zytintervau (*Nevadisculites taylori* bis *Frechites occidentalis* Zone) wird ganz klar vor Familiä Ceratitidae Mojsisovics, 1879 (insbesondere d Ungrfamiliä Beyrichitinae Spath, 1934) dominiert. Äs git mehreri extrem hüüfigi Beyrichitinae wi zum bispiu *Frechites occidentalis* (Smith, 1914) und *Gymnotoceras rotelliformis* (Meek, 1877). Innerhaub vo dämm Intervau hei keiner abruptä Änderigä in Bezug ufd Arteviufaut chönnä festgsteut wärdä, was ä Periodä vo bsungriger Paläoökologischer Instabilität bedütet hetti.

Ds letzte und glichzytig ou ds bedüütenstä Houptthema vo dere Arbeit si morphologischi Veränderigä vo Ammonoidee währen ihrer ontogenetisch Entwicklig. Di evolutionäre Entwickligsmuster vode ungersuechtä Artä si mit Methodene usem Beriich vo Traditional Morphometrics und Geometric Morphometrics analüsiert wordä. Daderbi hetsech der geometrisch-morphometrisch Asatz aus bsungers wärtvou erwisä. Mit der R-Software isch e neui Methode zur Analüsä vo morphologischä Entwickligä vo Ammonoidee entwicklet wordä. Dä neu Asatz basiert houptsächlech uf ennere Reihä vo verschidnigä Funktionä vodä R-Paket *geomorph*, *RRPP* und *Morpho*. Di geometrisch-morphometrisch Analüsä hets müglächh gmacht, dass d Heterochrony vodä ungersuechtä Artä ds quantifizerä und ontogenetischi Schwankigä vor intra- und interspezifischä Variabilität ds verfougä. Bi Ammonoidee vor Ungerfamiliä Beyrichitinae sy di ontogenetisch Allometrie

und d intra- und interspezifisch Variabilität äng mitenang vrbungä. Di morphologischi Variation schiint ds Ergäbnis vodä Verschiebigä vom allometrischä Wachstumsmuster (d.h. Heterochronie) ds sy. Das ungerstützt di augemein Meinig, dass i stabilä Habitat generell di pädomorphi Entwicklig gägänüber dr Peramorphosä begünstigt isch. Es hei kener dominantä Entwickligsprozässe chönnä nachägwisä wärdä. Das isch auä d Foug vor allgemein stabilä Paläoumwäut und vom dermit verbundnigä gringä paläoökologische Druck.

Eis vodä wichtigstä Ergäbnis vo dere Diss isch es, dass di morphologischä Veränderigä vodä ungersuechtä Artä vorauem vo intrinsischä Faktorä beeiflust wärdä. Di gfungnigä evolutionäre Trends vodä Ceratitidä si höchstwahrschinläch nid oder numä schwach dür paläoökologischi Veränderigä triggered wordä. Die i derä Arbeit vorgstöutä Methodene stöuä äs wärtvous Wärchzüg für zuekünftigi biogeographischi und phylogenetischi Ungersuechigä und Diversitätsanalüsä dar.

Zuekünftigi Studie söttä drum versuechä, diä hiä vorstöutä Methodene ufnes breiters Spektrum a verschidnigä Morphologiä usdswiitä. I dämm Zämähang wär ä globale Vergliich vo morphologischä Muster bsungers interessant. Um es umfänglechs Biud vodä Morphospaces vo Ammonoidee ds becho, muäss der hiä vorstöut Asatz ufne morphologischi Analüsä vo verschidnigä Ghüüsformä erwiiteret wärde. Das wirds üs ermüglächä, morphologischi Veränderigä vo verschidnigä Taxa während ihrer Ontogenese ds vergliichä und dadermit ou ihri komplexi Entwickligsbiologie und Evolution ds verstaa.

Abbreviations

$\delta^{13}C$	Delta-13-C, ratio of ^{13}C to ^{12}C isotopes in a sample
GMM	Geometric Morphometric methods
GSUB	Geowissenschaftliche Sammlung am Fachbereich Geowissenschaften der Universität Bremen; Geosciences Collection at the Faculty of Geosciences, University of Bremen
MfN	Museum für Naturkunde (MfN), Natural History Museum, Berlin, Germany
PCA	Principal Component Analysis
PIMUZ	Paläontologisches Institut und Museum (PIMUZ), Palaeontological Institute and Museum, University of Zurich, Switzerland
RW-PCA	Relative warp Principal Component Analysis
TM	Traditional Morphometric methods
TOC	Total organic content

Versicherung an Eides Statt / *Affirmation in lieu of an oath*

gem. § 5 Abs. 5 der Promotionsordnung vom 18.06.2018 /
according to § 5 (5) of the Doctoral Degree Rules and Regulations of 18 June, 2018

Ich / I, _____
(Vorname / First *Name*, Name / *Name*, Anschrift / *Address*, ggf. Matr.-Nr. / *student ID no., if applicable)*

versichere an Eides Statt durch meine Unterschrift, dass ich die vorliegende Dissertation selbständig und ohne fremde Hilfe angefertigt und alle Stellen, die ich wörtlich dem Sinne nach aus Veröffentlichungen entnommen habe, als solche kenntlich gemacht habe, mich auch keiner anderen als der angegebenen Literatur oder sonstiger Hilfsmittel bedient habe und die zu Prüfungszwecken beigelegte elektronische Version (PDF) der Dissertation mit der abgegebenen gedruckten Version identisch ist. / *With my signature I affirm in lieu of an oath that I prepared the submitted dissertation independently and without illicit assistance from third parties, that I appropriately referenced any text or content from other sources, that I used only literature and resources listed in the dissertation, and that the electronic (PDF) and printed versions of the dissertation are identical.*

Ich versichere an Eides Statt, dass ich die vorgenannten Angaben nach bestem Wissen und Gewissen gemacht habe und dass die Angaben der Wahrheit entsprechen und ich nichts verschwiegen habe*. / I affirm in lieu of an oath that the information provided herein to the best of my knowledge is true and complete.*

Die Strafbarkeit einer falschen eidesstattlichen Versicherung ist mir bekannt, namentlich die Strafandrohung gemäß § 156 StGB bis zu drei Jahren Freiheitsstrafe oder Geldstrafe bei vorsätzlicher Begehung der Tat bzw. gemäß § 161 Abs. 1 StGB bis zu einem Jahr Freiheitsstrafe oder Geldstrafe bei fahrlässiger Begehung. / *I am aware that a false affidavit is a criminal offence which is punishable by law in accordance with § 156 of the German Criminal Code (StGB) with up to three years imprisonment or a fine in case of intention, or in accordance with § 161 (1) of the German Criminal Code with up to one year imprisonment or a fine in case of negligence.*

_____ _____
Ort / *Place*, Datum / *Date* Unterschrift / *Signature*

1 Introduction

1.1 Palaeogeography

Nothing in the world is given, everything is in constant change. Even the ground we are standing on—the continents—are constantly transforming. Slowly, but continuously they drift on the surface of the earth. It is assumed that there have been at least three times in earth history when all of the continents were fused into one large supercontinent (Rogers & Santosh 2003): Columbia (~1800–1500 Ma); Rodinia (~1100–700 Ma); and Pangaea (~250 Ma).

Due to its shorter geological history of the youngest supercontinent, comparatively much is known about Pangaea. During the Triassic stage, the landmass was mainly surrounded by the Panthalassic Ocean (Fig. 1.1-1). To the west, Panthalassa was connected to the Tethys, which was a deep oceanic gulf, cutting into the supercontinent (Preto et al. 2010). Due to the tropical-subtropical location and the shielding by Pangea, the palaeoclimatic conditions in the Tethyan realm were different from the Panthalassic Ocean (Arias 2008). Tethys was a warm seaway (Totman Parrish 1999), that was significantly affected by the Pangaean mega-monsoon belt (e.g. Parrish 1993; Arias 2008). Even though Panthalassa and the Tethyan realm were connected, they represented separate habitats with characteristic fauna assemblages (Hyatt & Smith 1905; Ogg et al. 2020).

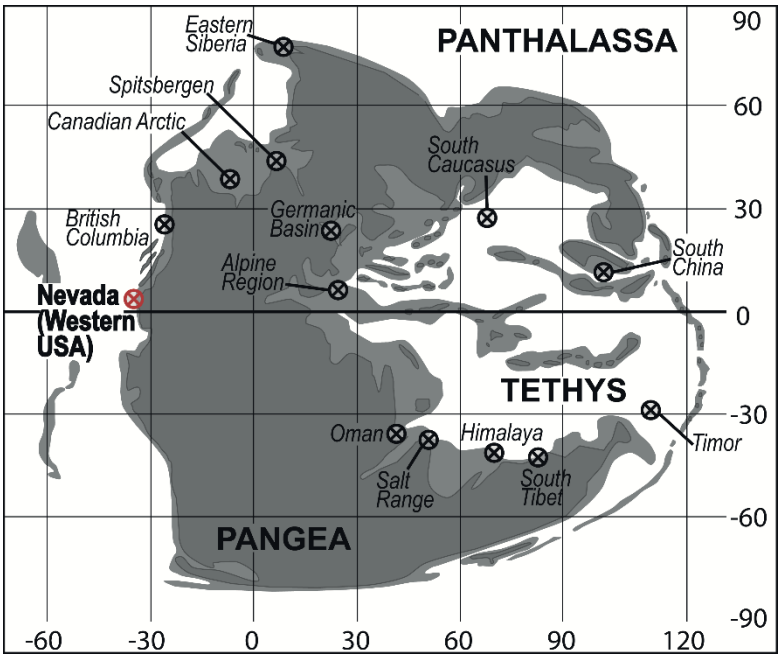

Fig. 1.1-1: Middle Triassic (~245 Ma) palaeogeographic setting. Nevada as well as other important localities where Triassic ammonoids assemblages can be found are marked. Palaeoposition after Brosse et al. (2013) and palaeogeographic map of the Middle Triassic modified after Péron et al. (2005), Skrzycki et al. (2018).

1.2 The rocks of Nevada

The study area of this thesis is located in the desert of NW Nevada, which is situated in the Great Basin of the Western USA (Fig. 1.2-1). The rocks of the Triassic of Nevada were deposited in an epicontinental part of the Panthalassic Ocean (Fig. 1.1-1). Whereas the depositional history of the investigated sequences is not characterised by major disturbances, the geological history, on the other hand, is very complex. In their book about the geology of Nevada Decourten & Biggar (2017) aptly describe the situation: "*Exploring the geology of Nevada's roadsides is rather like twisting a geological kaleidoscope: every bend in the road brings new rocks into view.*"

Fig. 1.2-1: Large scale map with geographic locations of the Humboldt Range and the Augusta Mountains in NW Nevada, USA.

1.2.1 Geologic and tectonic history

The main reason for the stratigraphic complexity of Nevada is the region's eventful geological past. The following paragraph represents a very brief summary of the several billion years long developmental history of rocks the rocks of Nevada.

The oldest rocks in Nevada can be found in the East Humboldt Range in the north-eastern part of the state and have an age of about 2500 Ma (Price 2002). The Proterozoic and Archean basement rocks of Nevada were part of the ancient supercontinent Rodinia (Decourten & Biggar 2017). About 700 Ma ago, Rodinia—and the area of today's Nevada—was affected by continental rifting, tearing the landmass apart (Rogers & Santosh 2003). Thereafter, an ocean basin with a passive continental margin with no earthquakes or intense volcanic activity was formed (Decourten & Biggar 2017).

In the Late Devonian to Early Mississippian time (~360 Ma) the extension reached its maximum and a subduction zone (Antler Orogeny) began to form on the future west coast of Pangaea (Price 2002). All throughout the late Palaeozoic until the end of the Mesozoic, many crustal blocks/terranes (i.e. volcanic islands, carbonate reefs, and microcontinents) were accreted on the continental margin (Ingersoll 2008).

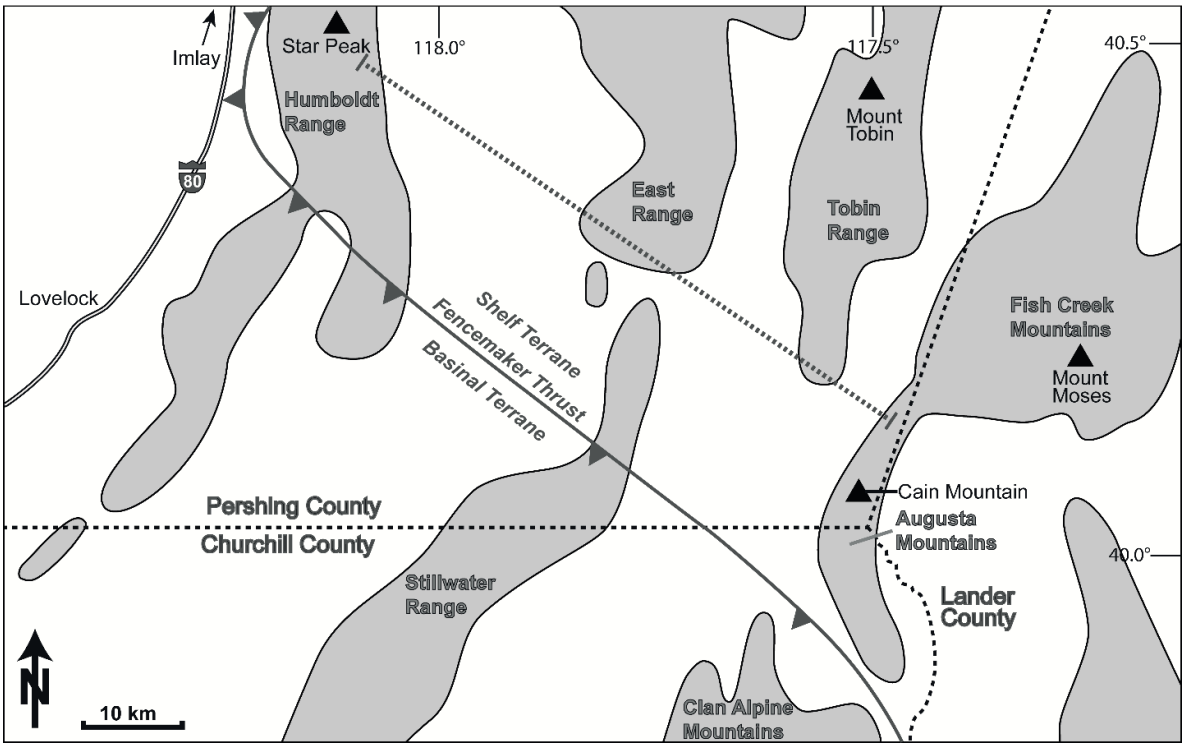

Fig. 1.2-2: Location of the study area in NW Nevada, USA. Location of Fencemaker Thrust after Wyld (2000). Grey dotted line: Approximate course of the cross-section in Fig. 1.2-3. Map modified from Bischof & Lehmann (2020).

A complex mosaic of rocks of accreted terranes, crumpled layers of deep-ocean sediment, and volcanic and intruded igneous rocks started to extend the coastline westward (Decourten & Biggar 2017). By the end of Mesozoic time, all of Nevada was exposed as dry land above sea level (Decourten & Biggar 2017).

The Triassic strata in NW Nevada can be divided into two main lithologic successions Wyld (2000): a shallow marine succession that was deposited carbonate platform system (shelf terrane) and a deep-marine basinal succession dominated by fine-grained siliciclastic rocks (basinal terrane). The rocks in focus of this study are part of the shelf terrane, which is separated from the adjacent fine-grained siliciclastic rocks of the basinal terrane by the Fencemaker Thrust (Wyld 2000) (Fig. 1.2-2).

The Basin and Range extension began about 30 to 40 million years ago (Price 2002). The collision of the oceanic Farallon Plate with the North American continental plate caused the development of a magmatic arc and an orogenetic belt along the subduction zone (Fiero 2009). The subduction also caused an extension of the North American plate and therefore the formation of the Great Basin (Decourten & Biggar 2017). The displacement through the Jurassic/Cretaceous strike-slip faults system adds an additional complication to the complex stratigraphy of Nevada (Wyld 2000). The thinning and the extension of the Great Basin area of up to 100 % lead to a general uplift of the region (Fiero 2009; Decourten & Biggar 2017). The complex interplay between tectonic processes, orogenesis and volcanic

activity continued until about 7 Ma ago (Ingersoll 2019). While the volcanic activity of the region has almost come to a standstill, the San Andreas Fault is still a continuing threat (Fiero 2009).

1.2.2 Stratigraphy

From a stratigraphic point of view, the Anisian (early Middle Triassic) sediments of Nevada are associated to the Fossil Hill Member of the Prida (NW) and the Favret Formation (SE) that belong to the Star Peak Group (Tab. 1.2-1; Fig. 1.2-3). The Group is a succession of mostly carbonate rocks of a carbonate platform complex that covers an area of more than 5000 km^2 (Nichols & Silberling 1977). The name "Star Peak" was first mentioned in literature by King (1878; p. 269) and was applied to a “body of 10000 feet of strata” that overlies the volcanic and sedimentary clastic rocks Koipato Group in the western Humboldt Region. The original definition of the Star Peak Group was later refined by Smith (1914); Cameron (1939), Ferguson et al. (1951) and Silberling & Wallace (1967). To my knowledge the most recent and comprehensive stratigraphic treatise on the group was done by Silberling & Wallace (1969) and Nichols & Silberling (1977). The latter estimates an average thickness of the group of about 1000 m (~3300 feet). In Nevada there is no other marine stratigraphic unit known of same or even older age (Nichols & Silberling 1977), which makes the observed successions even more valuable. A more general discussion on the geology and stratigraphy of the western USA can be found in Wyld (2000).

All stratigraphic successions of the Star Peak Group were deposited during the Triassic period (King 1878). During this time, Pangaea was on the verge of breaking apart, carbonate platform systems developed between the landmasses and the Sierra Nevada magmatic arc became established (Wyld 2000; Fiero 2009). Therefore, the sedimentary sequences of the Star Peak Group were deposited in the context of contemporaneous tectonics, volcanic activity and the associated regional uplift and subsidence of the carbonate platform complex (Tab. 1.2-1). Carbonate platform deposits are especially sensitive to relative changes in sea level. Therefore, especially the episodes of tectonism resulted in striking facies changes (Nichols & Silberling 1977). In the vicinity of the China Mountain (Stillwater range, central region) the Fossil Hill Member is unusually thin and locally absent because of erosion and secondary dolomitisation beneath the overlying Panther Canyon member (Nichols & Silberling 1977). Because all other stratigraphic successions of Anisian or Ladinian Ages are missing, the corresponding deposits are called Fossil Hill Formation instead of Fossil Hill Member.

In accordance with its name, the type locality of the Fossil Hill Member is on the southern flank of Fossil Hill in the south-eastern Humboldt Range (Silberling & Nichols 1982), where the member attains a thickness of about 60 m. However, due to local relative uplift and erosion during early Anisian time and the associate facies transition, the member is much thicker (~120 m) in the northern part of the

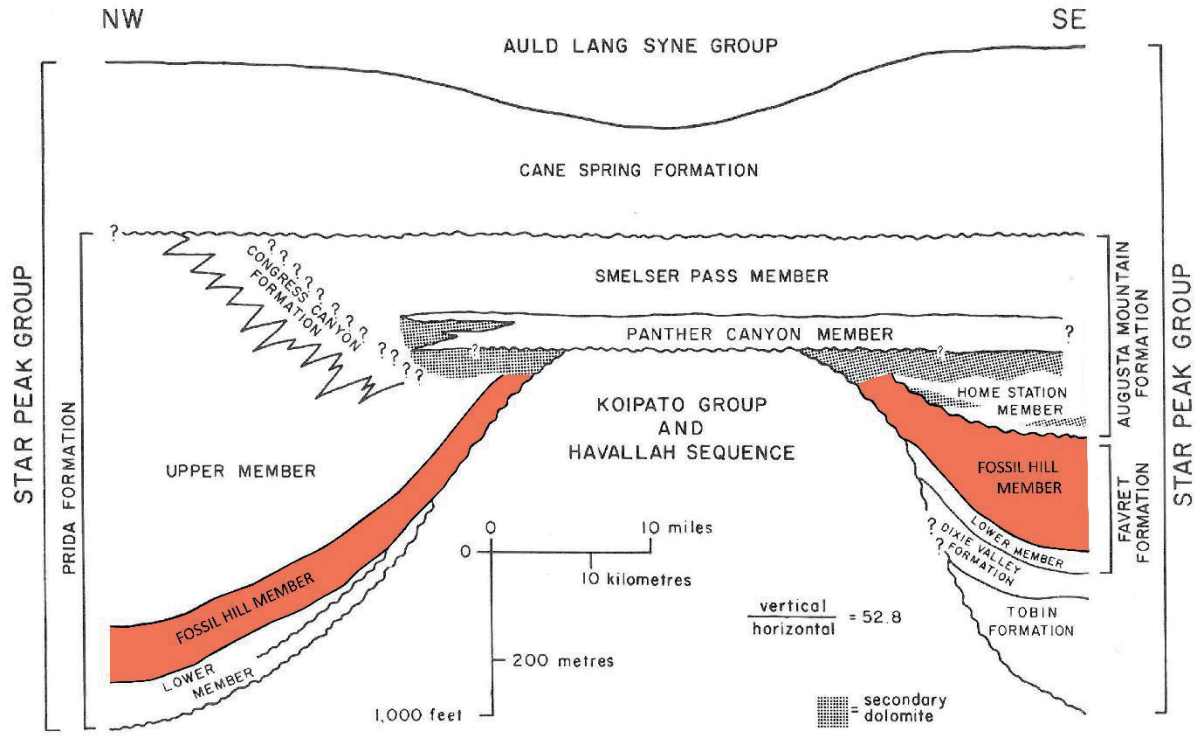

Fig. 1.2-3: Diagrammatic cross section of the Star Peak group trending from the northern Humboldt Range (NW) through the southern Tobin Range to the Augusta Mountains (SE). Figure slightly adapted from Nichols & Silberling (1977). Approximate course of the cross-section in Fig. 1.2-2 (grey dotted line). More information on the individual stratigraphic entities can be found in Tab. 1.2-1.

range (Silberling & Nichols 1982). In the Augusta Mountains the base of the member is not eroded and it therefore attains its greatest thickness of about 200 m (Nichols & Silberling 1977). In order to highlight lateral differences and to take the tectonic displacement into account, the NW and SE parts of the Fossil Hill Member (see Fig. 1.2-3) are attributed to different formations (Nichols & Silberling 1977). Overall, we could not observe any fundamental stratigraphic differences between the Fossil Hill Member in the Humboldt Range (NW) and the Augusta Mountain (SE). The microfacies of the observed successions herein are described in chapter 1.2.3 of this thesis.

While the topography in the Humboldt Mountains is characterised by gently sloping hills, the Augusta Mountains feature impressive rock formations with deeply incised canyons. Therefore, the predominant geomorphologic process in the Humboldt Range is *in situ* weathering, while in the Augusta Mountains mostly active erosion is taking place. As a result, much more coherent stratigraphic profiles can be measured in the vicinity of the Augusta Mountains. However, probably because the sections are much less accessible in this area, they are by far not as famous as the corresponding one in the Humboldt Range. The Anisian and lower Ladinian succession in the Humboldt Range is, in fact, one of the world's most famous sequences of Anisian ammonoid assemblages.

Tab. 1.2-1. Explanation on stratigraphic entities of Star Peak Group and the overlying Auld Lang Syne Group (Fig. 1.2-3). Summary of Silberling & Wallace (1969), Nichols & Silberling (1977), Brueckner & Snyder (1985) and own observations. Abbreviations: Fm: Formation; Mb.: Member.

Name		Approx. age	Depositional environment and rock type
Auld Lang Syne Group		Upper Triassic	Terrestrial: Calcareous and argillaceous (rich in clay) sandstone
Star Peak Group	**Cane Spring Fm.**	Carnian to Norian	Intertidal and lagoonal, inner-platform, occasionally subaerial: Carbonates (Mud- to pelleted wackestone, rare grainstone with ooids). Base: volcaniclastics and sandstone
	Smelser Pass Mb. (SE)	early Carnian	Open-platform intertidal to shallow subtidal: Cliff-forming, bioturbated limestone, overlain by mafic volcanic rocks
	Panther Canyon Mb. (SE)	late Ladinian	Sabkha to terrestrial: Fine-grained, laminated, stromatolitic and saccharoidal dolomite. Conglomeratic, coarse- and fine-grained redbeds
	Congress Canyon Fm. (NW)	Ladinian to early Carnian	Platform margin: Cliff-forming massive, mostly dark-grey, limestone, Packstone. Hydrothermally recrystallised, secondary dolomitisation
	Upper Mb. (NW)	early Carnian	Platform Margin: Massive, dark-grey, mostly recrystalised carbonates, Wackestone, quartz-silty, dark chert layers
	Home Station Mb. (SE)	late Anisian to upper Ladinian	Platform: Interstratified calcareous or dolomitic limestone, algal-laminate fine-grained dolomite, siliceous siltstone and sandstone. Massive, cliff-forming saccharoidal secondary dolomite containing chert blebs.
	Fossil Hill Mb.	middle to late Anisian	Deep marine, below storm wave base: Alternating layers of lenticular limestone and calcareous siltstone. Very fossiliferous
	Lower Mb. (SE)	late Spathian	Shallow-water: High-energy deposits. Thick-bedded to massive, light-grey limestone. Forms benchlike outcrops. Fossiliferous
	Lower Mb. (NW)	late Spathian	Terrestrial: Sandstone, secondary dolomite, limestone of various kinds, and mafic volcanic rocks
	Dixie Valley Fm. (SE)	late Spathian to middle Anisian	Alluvial to marine-influenced supratidal: Unfossiliferous alternating layers of yellow and brown conglomerate, sandstone, dolomites and maroon siltstone beds.
	Tobin Fm. (SE)	Spathian	Terrestrial: Mostly dark, unfossiliferous, laminated, irregularly fractured, silty mudstone. Probably deposited under euxinic conditions.
Koipato Group		Triassic	Terrestrial: Volcanic and clastic sedimentary rocks, partially eroded
Havallah Sequence (Golconda allochthon)		Latest Devonian to Permian	Deep marine: Various lithologies, but mostly radiolarian ribbon chert and argillite associated with siliciclastic, calcarenitic, and volcaniclastic turbidites and slump deposits. Partially hydrothermally altered.

1.2.3 Microfacies and palaeoenvironment

Considering how eventful the geological past of this area is, it is remarkable how tectonically undisturbed the Fossil Hill Member is. In total we measured seven stratigraphic sections (Fig. 1.2-4). No major syn- or post-sedimentary disturbances have been detected. Apart from some rare drainage

structures, hardly any synsedimentary disturbances were found. Detailed stratigraphic sections (cm resolution) can be found in in Appendix 1.

The herein studied successions all consist of alternating layers of lenticular limestone and calcareous siltstone. Following the classification of Folk (1962) and Dunham (1962) most lenticular limestone beds are classified as micritic to biomicritic mud- to wackestone and sometimes even packstone. There are some rare oil inclusions in ammonoid shells and other traps. The lenticular limestone beds are all thinly layered. Apart from some very rare burrows that can be observed under the microscope, there is no evidence of biological reworking of the sediment. Therefore, major benthic biological activity can be excluded. Towards the top of the member the individual carbonate beds are getting slightly thicker and more competent. The bottom water (or at least the sediment-water interface) was dysoxic to anoxic with oxygenated water above (Schatz 2000, 2005). The rather hostile environment allowed only little to no benthic fauna. Small-scale environmental changes most likely occurred in relation to short-term oxygenation of the bottom waters (chapter 4.5). The results of the microfacies analysis indicate a rather calm depositional environment below the storm wave base. Since the whole member consists of more or less regular sequences, relatively stable depositional conditions can be assumed.

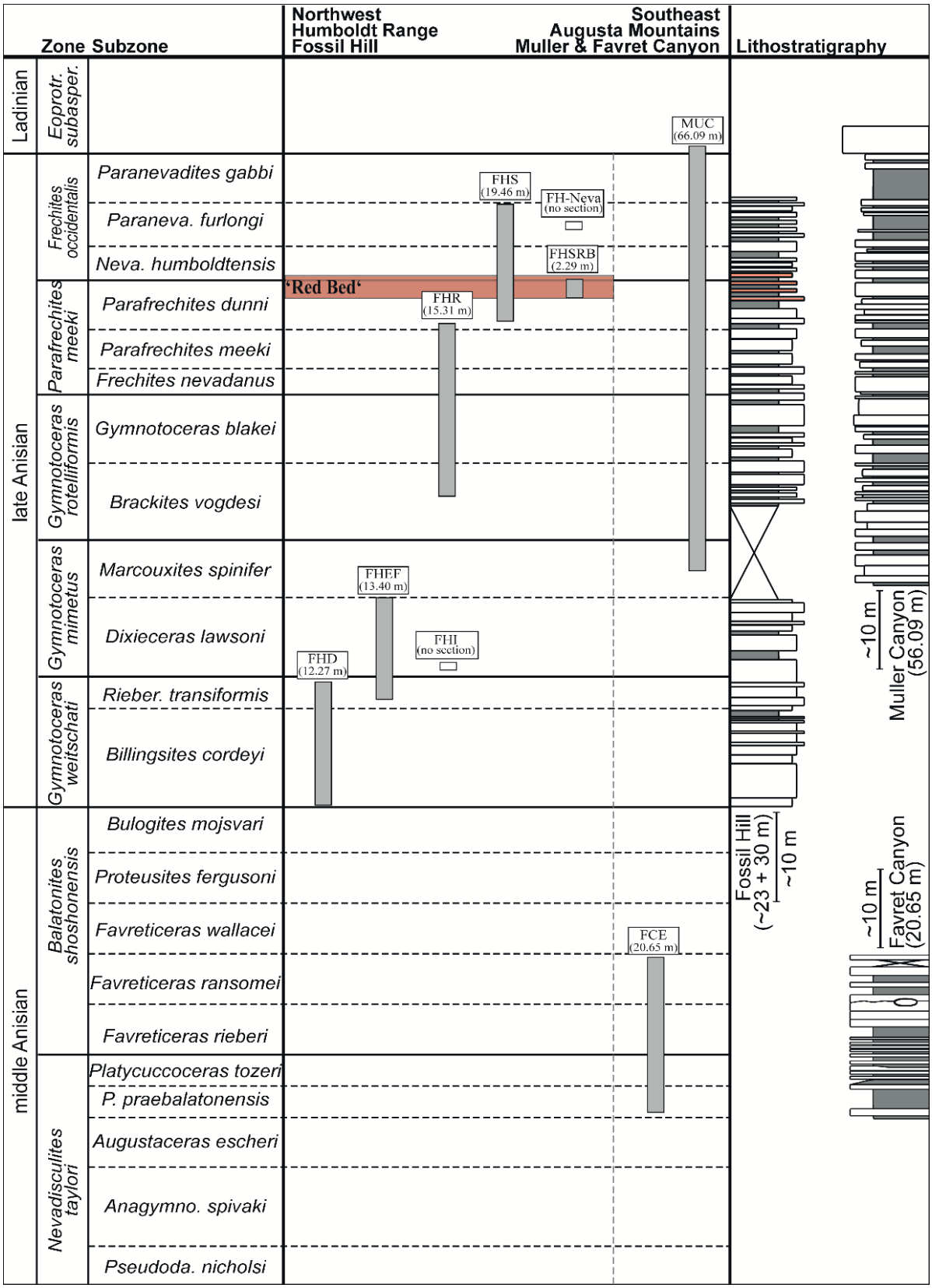

Fig. 1.2-4: Biostratigraphic correlation of measured sections in the Humboldt Range and in the Augusta Mountains in NV Nevada, USA. For sampling areas see Fig. 3.1-1. Biostratigraphic framework of Nevada after Jenks et al. (2015).

1.2.4 Triassic biostratigraphy

The foundation of Triassic biostratigraphy was laid by Mojsisovics et al. (1895). Although being limited to Europe and Asia, this study represented an important cornerstone for the worldwide correlation of Triassic marine strata. Depending on the time interval analysed, there are many different micro- and macrofossils that can be used as index fossils. For biostratigraphic purposes the fossil occurrences must meet certain requirements: (1) They must be abundant; (2) they must be well preserved; (3) they must occur continuously in the stratigraphic record; (4) they must be short lived as a species; (5) they must be geographically widespread. For the Triassic Conodonts and ammonoids are the main correlation tools for marine deposits (Monnet et al. 2015; Ogg et al. 2020). These two biostratigraphic frameworks should not be seen as competing theories but rather two different systems that complement each other (Balini et al. 2010).

The rich fauna of the succession of the Fossil Hill Member primarily consists of halobiid bivalves and ammonoids but also vertebrates, conodonts, gastropods, brachiopods, ostracods and foraminifera. In the case of the Fossil Hill Member, ammonoids and conodonts are most suitable for a biostratigraphic classification. Whereas ammonoids are the taxonomic group with the highest temporal resolution within Triassic marine environments, (Balini et al. 2010), conodonts provide a more widespread method of correlation (Ogg et al. 2020). The general advantage of micro- over macrofossils is the ubiquity in some strata (Lucas 2010). However, the down side of the small size is the invisibility of conodonts in the outcrop so they cannot be used to determine the age of strata during fieldwork (Lucas 2010). Furthermore, the analysis of large bulk samples is needed for conodont biostratigraphy. This represents a logistical problem at both locations investigated for this work. Whereas Triassic conodont biostratigraphy is a comparably young field (Balini et al. 2010), there are more than 120 years of ammonoid research in this discipline. In fact, most of the traditional stages (Anisian, Ladinian, Carnian, Norian, Rhaetian) were named from ammonoid-rich successions of the Northern Calcareous Alps of Austria (Ogg et al. 2020).

In the late 19th century Mojsisovics et al. (1895) published his work on a first attempt to establish a standardised biostratigraphic scheme of the Triassic Period in the Tethyan region. In 1897, Alpheus Hyatt spent three weeks in the museum of the Geological Survey of Austria in Vienna (*kaiserlich-königliche Geologische Reichsanstalt*), under the guidance of Dr. Edmund von Mojsisovics (Hyatt & Smith 1905; p. 11). His research stay enabled Hyatt & Smith (1905) to make “a careful comparison” of the American and European faunas in that were available at that time. The work on the Triassic cephalopod genera of America also represented the starting point for the era of more thorough ammonoid collecting in the Anisian rocks of NW Nevada. More than a century later, ammonoids have now become one of the most important biostratigraphic tools (Monnet et al. 2015; Ogg et al. 2020).

The Anisian and lower Ladinian ammonoid assemblages in NW Nevada are among the world's most famous of this age (Silberling & Nichols 1982; Monnet & Bucher 2005b). In their pioneering work of Silberling & Tozer (1968) on the biostratigraphy of Northern America, they correlated the biostratigraphy of Lower and Middle Triassic successions in Idaho, Nevada, California, Oregon, British Columbia, Alaska, and the Arctic Islands of Canada. Subsequently, improvements of the biostratigraphic framework were mainly achieved by revisions of the local stratigraphy (e.g. Silberling & Wallace 1969; Nichols & Silberling 1977) and the ammonoid alphataxonomy (e.g. Silberling & Nichols 1982; Bucher 1988, 1989, 1992a, b, 1994; Monnet & Bucher 2005b; Monnet et al. 2010). The state-of-the-art consensus on Anisian ammonoid biostratigraphic zones and subzones of Nevada after Jenks et al. (2015) and the observed biostratigraphic distribution of Anisian ammonoid species are illustrated in Fig. 3.4-1 and discussed in chapter 1.3.1 herein.

In the context of the very complicated depositional history of the Great Basin, it is extremely valuable to have such a reliable proxy as ammonoids. What holds true on a regional scale, applies to the large picture as well. Anisian ammonoid assemblages are also of great significance for biochronological correlation across the low palaeolatitude belt from the eastern Pacific to the western end of the Tethys (Monnet & Bucher 2005b). For a review of Middle Triassic ammonoid biostratigraphy including a worldwide correlation see Jenks et al. (2015; figs. 13.13 and 13.14).

1.3 Ammonoids

Ammonoids are a group of extinct cephalopods that were an important part of the marine biota from the Early Devonian until the Cretaceous period (Klug et al. 2015c). Even though their external shell strongly reminds of nautiloids and gastropods, they are in fact more closely related to coleoids (Engeser 1996; Kröger et al. 2011; Klug et al. 2015c). They major difference of ammonoids to nautiloids is the ventral position and the diameter of the siphuncle, the mode of mineralisation and the shape of the embryonic conch of the former (Engeser 1996; Klug et al. 2015c). Maybe the most important standard literature about ammonoids are the somewhat older "Red Books" of Lehmann, U. (1990) and Landman et al. (1996a) and the even more comprehensive two-volume work of Klug et al. (2015a, 2015b).

Particularly due to their rapid evolution and extinction (Yacobucci 2015) ammonoids are acknowledged as powerful index fossil (Landman et al. 1996a; Gradstein 2020) and are considered to be the most

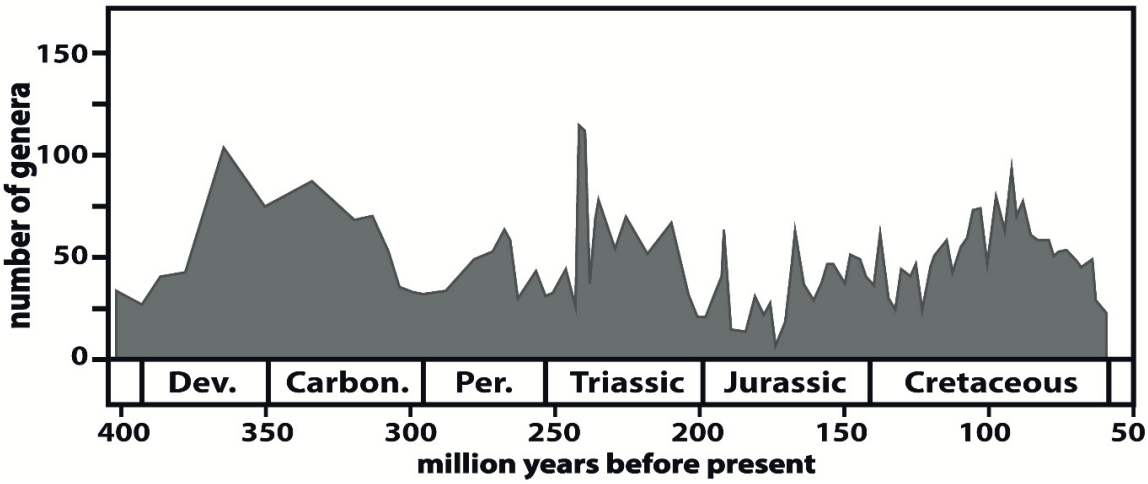

Fig. 1.3-1. Total generic richness of ammonoids through time. Composite image with data from following sources: Korn et al. (2015) from Devonian to Permian, Brayard & Bucher (2015) from the late Carboniferous until the end of the Triassic, and Yacobucci (2015) for the late Upper Triassic to the Upper Cretaceous. The three publications used slightly different approaches to measure diversity. Therefore, this illustration serves as a general guideline only.

important group for the dating and correlation of Triassic marine strata (Monnet & Bucher 2005b; Monnet et al. 2015). In fact, all Triassic substages are currently defined by ammonoid bioevents (Monnet et al. 2015). This mainly because they are abundant fossil occurrences that can be found in most Mesozoic marine rocks of the world. Their most important and complete records of Triassic ammonoid assemblages can be found in eastern Siberia, Spitsbergen (Svalbard), the Canadian Arctic (Sverdrup Basin), British Columbia, the western USA Basin (mainly Nevada, Utah, Idaho), South Caucasus (Iran), the Germanic Basin, Alpine Region (Austria, Italy, Hungary and Bosnia), Oman, Salt Range (Pakistan), Himalayas (Spiti), Southern Tibet, South China (Guangxi and Guizhou provinces) and Timor (Balini et al. 2010; see also Fig. 1.2-1 herein).

1.3.1 Ammonoid diversity through time

Ammonoid extinction rates are interpreted to be vulnerable to palaeoenvironmental changes (Yacobucci 2015). In Earth's history, life struggled with five major mass extinctions (Raup & Sepkoski 1986). During these events, more than three-quarters of all species went extinct in a geologically short time interval (Barnosky et al. 2011). The most severe biodiversity crisis of the Phanerozoic took place about 252 Ma ago at the Permian/Triassic boundary (e.g. Sepkoski 1984; Erwin 1994; Benton 1995), with 80–96 % of all marine species becoming extinct (Sahney & Benton 2008). The Permian/Triassic erathem boundary correlates with the disappearance of many organisms, which were typical for the Palaeozoic (e.g. trilobites, rugose- and tabular corals). This opened up ecological niches that were

subsequently filled by taxa typical for modern faunas (e.g. bivalves, gastropods, osteichthyan fishes, echinoids; Sepkoski 1984).

As most other groups, ammonoids were strongly decimated at the Permian/Triassic boundary as well (Brayard & Bucher 2015). Only a few species crossed the Permian/Triassic mass extinction leading to a quasi-monophyletic group during the Triassic (Monnet et al. 2015; Fig. 1.3-1). However, ammonoids were amongst the organisms with the fastest recovery rates in the aftermath of the mass extinction (Brayard et al. 2009a; Zakharov & Popov 2014; Close et al. 2020). The Triassic was characterised by the flourishing and dominance of the suborder Ceratitina (Monnet et al. 2015; Gradstein 2020). Ammonoid recovery during the Early Triassic is interpreted as the combined outcome of (1) the rapid refilling of a vacated ecological niches after the mass extinction, and (2) the successive extinction events and recurrent stressful environmental conditions that may have enhanced their high turnover rates (Brayard & Bucher 2015). Already in the Smithian (middle Lower Triassic) ammonoids reached diversity levels much higher than during the Permian (Brayard et al. 2009b; Zakharov & Mousavi Abnavi 2013; Brayard et al. 2015; Fig. 1.3-1). Therefore, the Triassic is a key interval in the evolutionary history of ammonoids (Monnet et al. 2015). However, despite this long history of biostratigraphic research and key evolutionary steps, the evolution of Triassic ammonoids still remains poorly studied (Monnet et al. 2015). Due to its stable environmental conditions, the Anisian Fossil Hill Member of Nevada (chapter 4.5) is a suitable interval to study intrinsic factor influencing diversity and disparity patterns (chapter 4.4).

1.3.2 Anisian ammonoids of Nevada

Modern mining in Nevada – and the Humboldt Range – began in the middle of the 19th century (Decourten & Biggar 2017). Fortunately, the most fossiliferous beds in the Humboldt Range are associated with a silver deposit that was found in 1860 (Silberling & Nichols 1982). Some of the fossils found by the mining men were acquired by the Geological Survey of California and subsequently described by William More Gabb (1864; Palæontology: Volume 1). These fossils were among the first American Triassic marine invertebrates that were scientifically described and examined (Silberling & Nichols 1982). More than a decade later, Fielding Bradford Meek (1877; Part 1: Palæontology) in collaboration with Alpheus Hyatt, described additional fossil material that was collected by members of Clarence King's U.S. Geological Exploration of the Fortieth Parallel.

The first extensive palaeontological field campaign in the Humboldt Range ("*Saurian Expedition*") was financed and coordinated by Annie Montague Alexander in 1905 and officially lead by Professor John Campbell Merriam (UCMP History (n.d.)). Even though the focus of this expedition was on vertebrate fossils, it enabled James Perrin Smith to collect some more fossil material for his comprehensive

monographic treatment of the Triassic invertebrate faunas of America (Smith 1914). Smith's publication of 1914 was preceded by the publication of Hyatt & Smith (1905) on Triassic cephalopod genera of America in which the Humboldt Range featured less prominently.

In keeping accordance to the scientific practice of his time, Smith (1914) described and listed a total of 110 ammonoid species from Fossil Hill in the Humboldt Range. The original alphataxonomy was then mainly refined using contemporaneous methods by Silberling & Nichols (1982) and Monnet & Bucher (2005b) that reduced number to 81 valid species (Brosse et al. 2013). However, there is also a number of studies that contributed significantly to the description of Anisian ammonoids assemblages from NV Nevada: i.e. Bucher (1988, 1989, 1991, 1992a, 1992b, 1994); Monnet & Bucher (2005a); Jenks et al. (2007); Monnet et al. (2010); Ji & Bucher (2018).

The area around the Fossil Hill-Saurian Hill (Humboldt Range) is considered to be the world's most complete sequence of low-palaeolatitude Anisian ammonoid assemblages (Monnet & Bucher 2005b) and has become a standard for the collection of Anisian ammonoids (Silberling & Nichols 1982). However, it must be noted, that the Humboldt Range is not the only area where the carbonates of the Anisian shelf terrane (i.e. Fossil Hill Member) are exposed in Nevada (Fig. 3.1-1). Due to the flat topography at many sites, it is often not possible to measure continuous stratigraphic sections and the fossil material has to be collected loosely. Even at Fossil Hill, excavations are required to obtain continuous sections. In the Augusta Mountains, however, the deeply incised canyons with a lot of active erosion offer perfect conditions for a thorough geological and stratigraphic documentation of the collected fossil material. However, the sites in the area of the Augusta Mountains are far less well documented. This is most likely because the mountainous topography of the wilderness study area is not as easily accessible as the vicinity of Fossil Hill. In conclusion, both localities investigated herein, have their advantages and disadvantages. In the end, however, they both offer a unique opportunity to analyse morphologic change and species associations of ammonoids through time and therefore provide new insights into the interrelation evolutionary processes and taxonomic concepts of the species.

1.3.3 Ontogeny of ammonoids

Ontogeny is the study of the sum of all developmental stages of an individual from the earliest to the most adult stages. The observation and especially the quantification of ontogenetic development can yield important information on the evolution of the observed individuals and groups. In morphometric studies, ontogenetic pathways are often visualised using ontogenetic trajectories. These vectors represent a series of measurement values of different ontogenetic stages of an individual or a group, called longitudinal data (Klingenberg 1998). Therefore, either several individuals of different ages, or

several “snapshots” in the course of an individual’s life are necessary for the analysis of the ontogeny of most living beings.

For the analysis of the ontogeny of ammonoids, however, a single (adult) individual is sufficient. This, because ammonoids retain a record of growth in their shells (Landman et al. 1996b). At the beginning of their life (embryonic stage, i.e. ammonitella), most ammonoid species look very similar (Lehmann 1990). They consist of an initial chamber (i.e. protoconch) and about one planispiral whorl. The average diameter of the protoconch of ceratitine ammonoids is 0.30–0.65 mm (Landman et al. 1996b). The majority of ammonoid species develop perfectly planispiral conches. The growth of the conches occurs through adding additional chambers to the existing conch (Korn 2012; Fig. 1.3-2 herein). The actual ammonoid body occupied only the last chamber which is therefore called living chamber (Lehmann, U. 1990). All preceding chambers and coils (phragmocone) are overgrown and conserved (Korn 2012). This allows the investigation of complete ontogenetic transformations of a set of traits, such as the conch geometry and septal characters (Korn 2012). Particularly the analysis of ontogenetic trajectories of ammonoids provides useful information about diversity and disparity at higher but also at the species level (Hoffmann et al. 2019). Therefore, ontogenetic analyses are an ideal tool to unravel phylogenetic and taxonomic relationships between ammonoid groups (Rieber 1962). This makes them ideal for the study of evolutionary change in ontogeny through time (Naglik et al. 2015). However, especially the field of Geometric Morphometric Methods and the associated statistical quantification of ontogenetic stages is far from being fully exploited.

Modified rate/timing of shape change in relation to any ancestor, descendent respectively, within an evolutionary framework is called heterochrony (Zelditch et al. 2012, p. 317). There are two main heterochronic developments: Peramorphosis and paedomorphosis (Fig. 1.3-3). Whereas peramorphic descendants develop morphologic features that are “beyond” those of their ancestors (i.e. overmaturation,

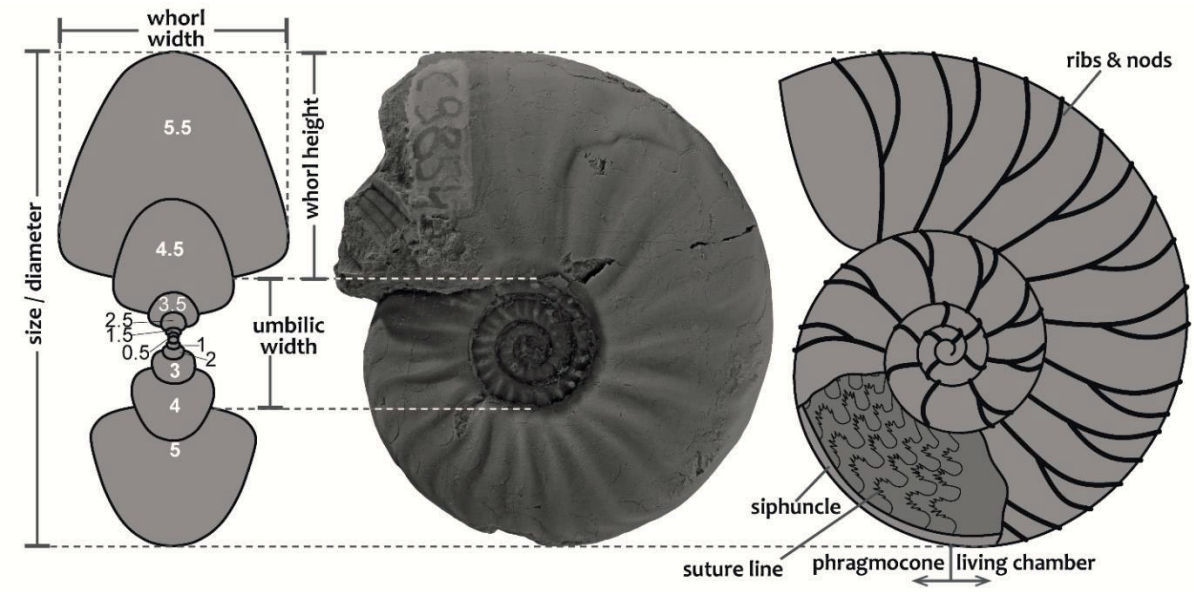

Fig. 1.3-2: Simplified sketches of shell bauplan and cross-sections of ammonoids. Photograph: Specimen number GSUB C9854.

paedomorphic descendants retain juvenile ancestral features (i.e. juvenilisation) (McNamara 2012). For more detailed and graphic explanations see Figure 1.3-3.

Even though the study of heterochrony in ammonoids extends back decades, it is still an active area of research (i.e. Alberch et al. 1979; Gould 1988; Klingenberg 1998; Gerber et al. 2007; Gerber 2011; McNamara 2012; Yacobucci 2015). The question–what drives evolutionary and ontogenetic change–is not yet and will probably never be fully resolved. However, there is evidence that certain heterochronic changes are adaptively favoured in particular environments (Yacobucci 2015). More stable environments can rather be associated with slowed down growth of the paedomorphic development (Gould 1977, chap. 8; McKinney & McNamara 1991, chap. 4). In the context of this thesis, the analysis of heterochronic processes yielded important insights into the speciation of Anisian ceratitid ammonoids of Nevada, USA (chapter 4.3 and 4.4 herein).

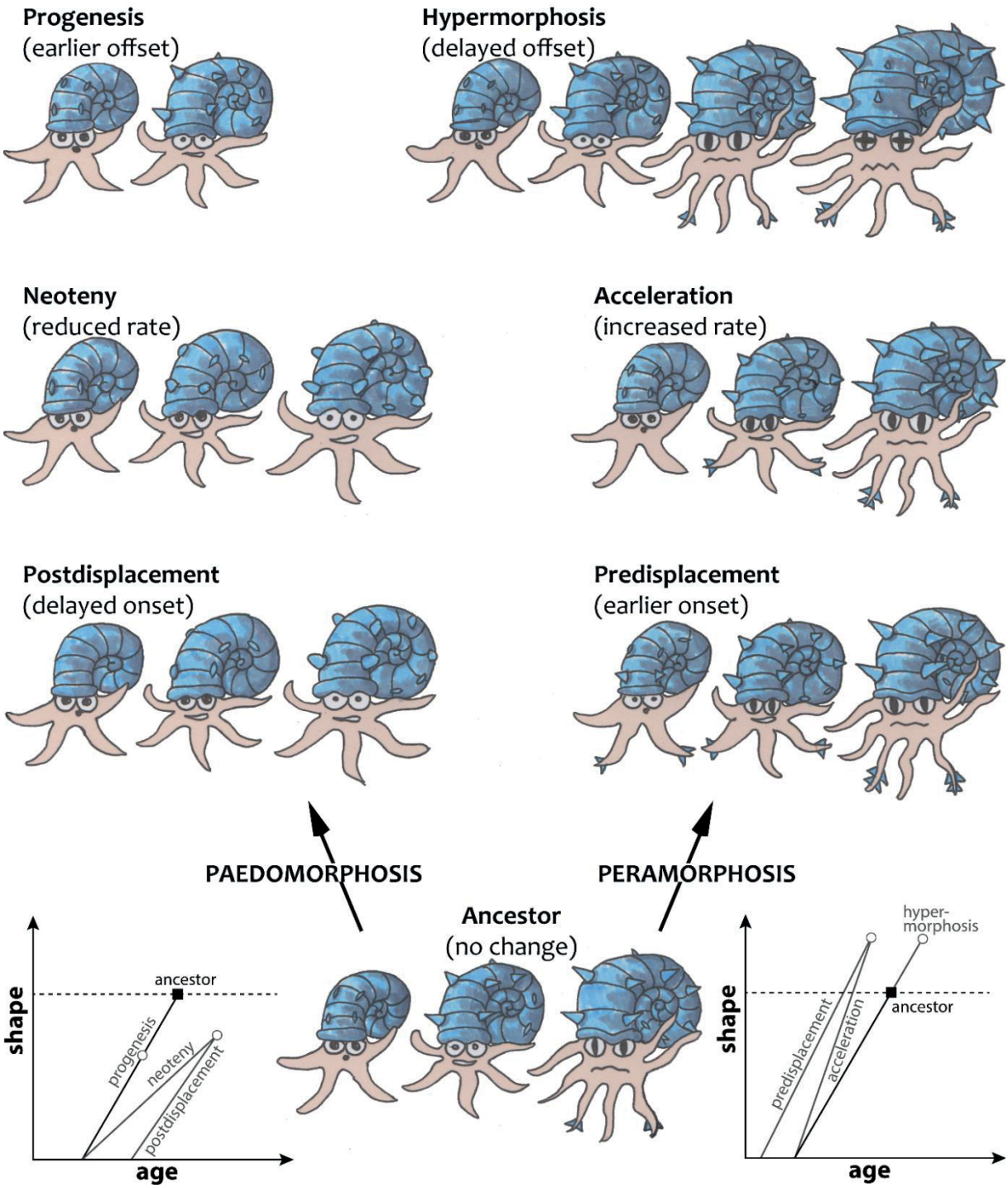

Fig. 1.3-3: Heterochronic pathways of hypothetical ammonoid-like animal that undergo a number of morphologic changes. Peramorphic descendants develop "beyond" the ancestor; paedomorphic descendants retain juvenile ancestral features. Illustration inspired by McNamara (2012) and diagrams adapted from Alberch et al (1979).

2 Objectives and relevance of this thesis

The main objective of the DFG project “AmMorphology” and this dissertation is to investigate drivers of morphologic changes in ammonoids. Thereby a key issue is the interrelation of morphologic change and total morphologic variation. To untangle evolutionary processes of ammonoids, a multi-approach including taxonomy, morphometry, lithostratigraphy, and microfacies analyses was needed (Fig. 2.1-1). All analyses were based on fossil and rock material from the Anisian of NW Nevada. As summarised in Figure 2.1-1, this thesis can be divided into three main research topics each with different goals:

2.1 Palaeoenvironmental reconstruction

How stable was the palaeoenvironment during the deposition of the Fossil Hill Member?

Palaeoenvironmental changes are generally considered as a key driving force for evolutionary and morphologic change (Yacobucci 2015). A particular emphasis was put on the question whether there are any recurring shifts or patterns in the palaeoenvironment.

- Measuring of detailed lithostratigraphic sections: The analysed stratigraphic sequences are characterised by very alternating layers of lenticular limestone and calcareous siltstone with an average thickness of 2–30 cm. In order to sufficiently investigate the sedimentary structures, lithostratigraphic sections had to be measured at centimetre resolution.
- Analysis of thin sections: Carbonate microfacies analysis enables carbonate classification via the analysis of individual components and sedimentary structures. It furthermore allows a detailed interpretation of fossil carbonate habitats and depositional environments including their evolution through time.
- Geochemistry: Analyses of total organic carbon (TOC) and δ13C can be used as a proxy to determine the source of organic carbon in the sediment. Of particular interest was the amount of biologic productivity in the depositional area.

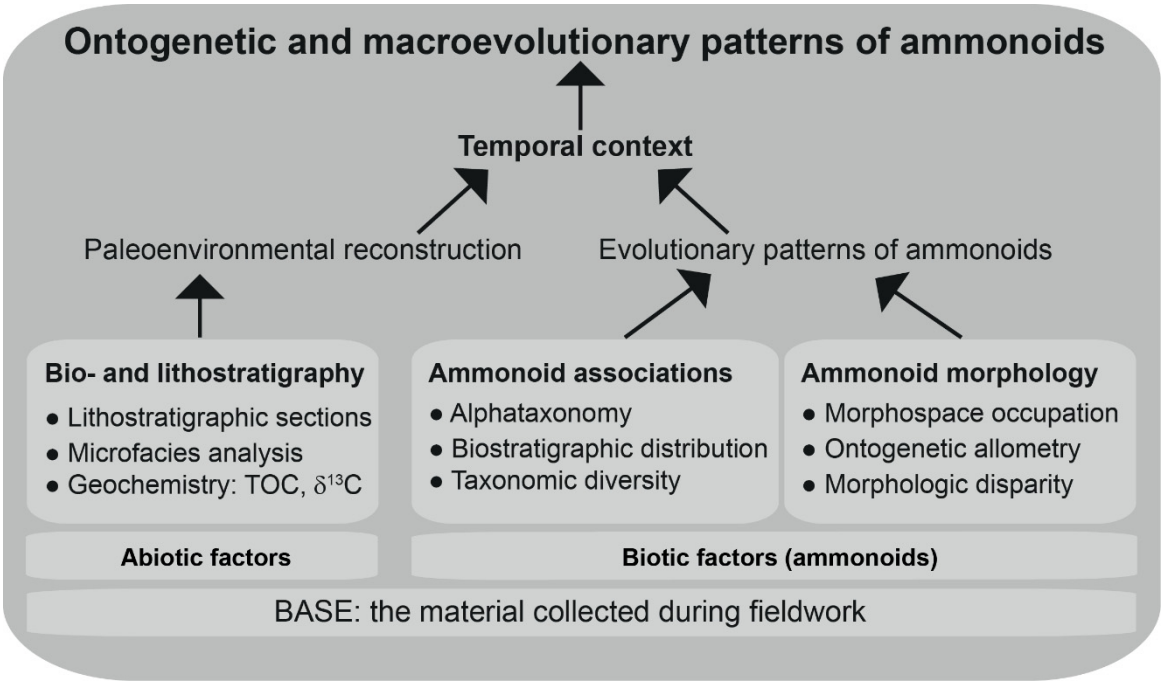

Fig. 2.1-1. Graphical representation of research topics and objectives of this thesis.

2.2 Ammonoid associations

Are there any taxonomic patterns or major shifts in biostratigraphic distribution of ammonoid associations?

In general, the mostly complete sections allow us to trace changes in the assemblage of ammonoids through time. Some Anisian ammonoid species of Nevada (especially representatives of the family Ceratitidae) are described based on a stratophenetic view. This means that species are distinguished by their stratigraphic occurrence, with anatomical features then identified as diagnostic for those groupings (Yacobucci 2015). In this context, arguments over biostratigraphy often reduce to arguments over taxonomy (Lucas 2010).

- Alphataxonomy. The first step for the evaluation of Anisian ammonoids associations was to evaluate and verify the alphataxonomy of the fossil material in a comprehensive literature search. This revealed the need for quantification and objectification of the taxonomic concept.
- Biostratigraphic distribution. Possible fluctuations in species distribution patterns provide insights to the stability of ecosystem. Furthermore, ammonoid biostratigraphy is an excellent tool to reliably correlate individual stratigraphic sequences in the complex geologic framework of Middle Triassic rocks in NW Nevada.
- Taxonomic diversity. The severity of mass extinction events is often measured as “percent/number of biologic groups that disappeared”. In this context, it is also directly related to

the prevailing diversity during balanced phases. Understanding diversity pattern in times of stable palaeoenvironmental conditions is therefore crucial for biodiversity studies.

2.3 Ammonoid morphology

What are the main factors influencing morphologic changes in Anisian ceratitid ammonoids of Nevada, USA?

As defined by Mayr (1949; Chapter VII, p. 119), the biological species definition is "If two animals produce fertile offspring, they usually belong to the same species". In palaeontology – dealing with mostly extinct organisms – this is, however, more intricate. Therefore, in most cases individual species are defined through their morphologies, following the philosophy of "what looks alike, must be the same". Intraspecific variation can therefore tremendously complicate species definition in palaeontology. The complex alphataxonomy of Anisian ammonoids in NW Nevada, clearly demonstrated the need for a more quantifiable and objective morphologic methodology. Which approach should be used, always depends on the specific research question.

- Morphospace occupation: For the evaluation and quantification of morphologic changes in ammonoids three different morphologic approaches were used:
    1. Linear measurements of ammonoid conches (Traditional Morphometrics). Measurements of the external shell are a basic and very comprehensible tool for species descriptions. However, especially in the case of the complex morphologic relationship of Anisian ammonoids revealing high amounts of intraspecific variability, this method lacks flexibility and quantifiability.
    2. Raupian parameters on ontogenetic cross-sections (Traditional Morphometrics). The Raupian parameters (Raup 1966) were introduced to describe the coiled conch morphospace and are calculated with the relationship of two or more linear measurements. Applied to ontogenetic cross-sections, Raupian parameters are an easy tool to track morphologic changes through ontogeny.
    3. Geometric Morphometric Methods (GMM) on ontogenetic cross-sections. The field of Geometric Morphometrics is based on very similar principles as Traditional Morphometrics. However, the use of methods such as Fourier analysis, and landmarks and semi-landmarks, allows a more flexible description of outlines. In addition, GMM are easier to quantify and are more suitable for statistical testing.
- Ontogenetic allometry. Evolutionary differences from ancestors to descendants are usually expressed by a positive or negative allometric coefficient. Therefore, the quantification of the

size-shape relationship during ontogeny can yield important information on the taxonomic context of individual species.

- Morphologic disparity. Animal as well as plant species are naturally influenced by a certain amount of morphologic variation. Thereby the question “how much variation is needed for the discrimination of a new species” might never be completely and universally clarified. However, the quantification of intra- and interspecific variability allows the description of the status quo and enables the comparison of different assemblages. Tracing morphologic disparity through time provides important insights to evolutionary processes affecting speciation.

The above stated research topics are addressed in this thesis and in four different publications that represent chapter 4.2–4.5 herein:

(1) Ontogenetic analysis of Anisian (Middle Triassic) ptychitid ammonoids from Nevada, USA
(2) Ontogeny of highly variable ceratitid ammonoids from the Anisian (Middle Triassic)
(3) Morphologic disparity and ontogenetic allometry of beyrichitine ammonoids
(4) Palaeoenvironment of the Fossil Hill Member (Middle Triassic) in Nevada, USA

The conclusions and a summary of the results are discussed in chapter 5. These investigations will lead to a better understanding of in- and extrinsic factors influencing morphologic changes in ammonoids. In addition, the methods introduced in this thesis will particularly promote the applicability of Geometric Morphometric methods using landmarks and sliding semi landmarks on ontogenetic cross-sections of ammonoids.

3 Material and Methods

3.1 Study sites

In summer 2017 and 2018, we – the members of the Geosciences Collection of the University of Bremen, Germany; GSUB – undertook each one field expedition in the desert of NW Nevada, USA. During a total of 11 weeks in the field, we collected the bulk of the fossil and rock material of this study. Due to the large geographical distance between the Humboldt Range and the Augusta Mountains, we set up two different base camps during both expeditions: (1) North side of Fossil Hill in the Humboldt Range, and (2) at the base of Favret Canyon in the Augusta Mountains (for geographic locations see Fig. 3.1-1).

As explained in chapter 1.2., the Fossil Hill Member is exposed at various locations (Fig. 3.1-1). However, stratigraphically coherent sections could only be measured at Fossil Hill (Fig. 3.1-2 A) and in the Augusta Mountains (Fig. 3.1-2 B and C). Which is why we put a clear focus on these localities in our fieldwork and subsequent analyses.

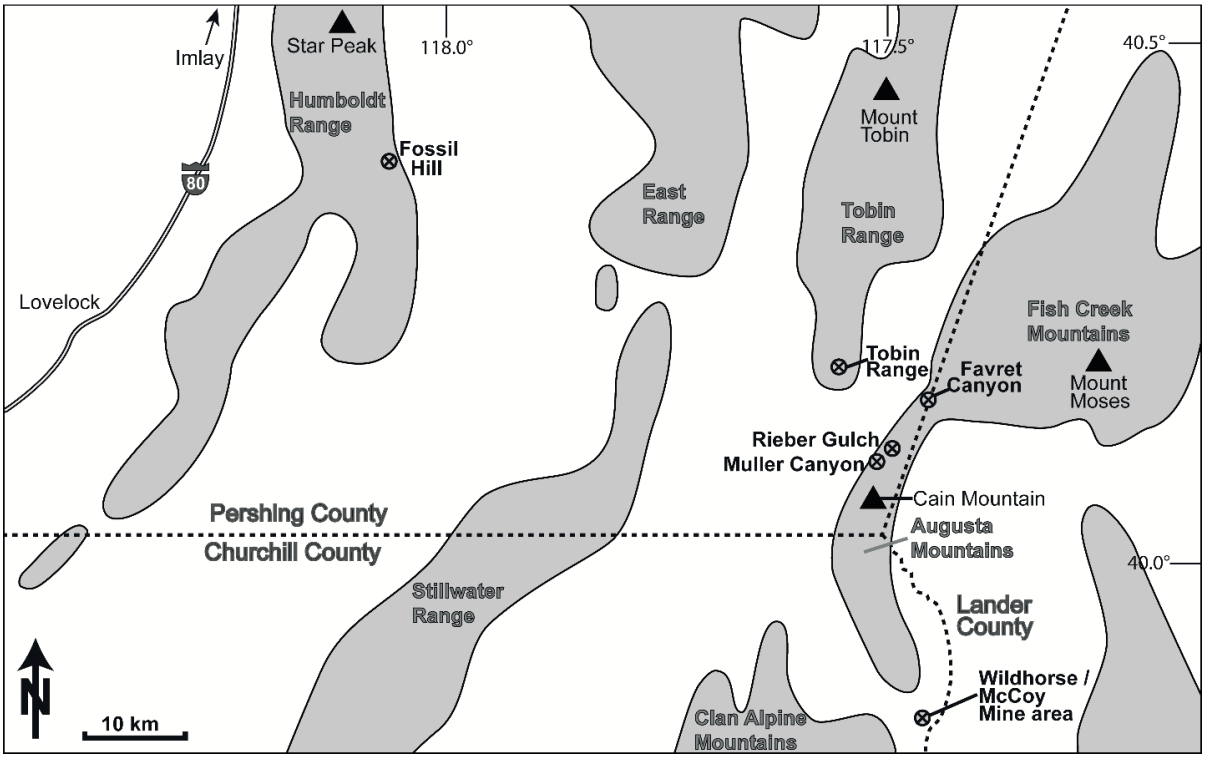

Fig. 3.1-1: Location of the study area in NW Nevada, USA. The most important localities of Fossil Hill Member outcrops are marked. Map modified from Bischof & Lehmann (2020).

Fig. 3.1-2. A) Southern Flank of Fossil Hill at the Humboldt Range. **B)** Base of measured section in the Muller Canyon. **C)** Aerial view of Muller Canyon. Dotted rectangle marks the measured section. **D)** Fossil and rock material (and a frying pan) were stored in steel drums for shipping. All pictures taken by members of the GSUB.

3.2 Rock and fossil material

In total, we collected material with a gross weight of over 4 tons (Fig. 3.1-2 D), which led to the preparation of over 8000 fossils and 186 thin sections. The fossil material collected by us is stored in the collection of the Geosciences collection of the University of Bremen (GSUB). In order to close smaller gaps, I have analysed additional fossil material from the following collections:

- Paläontologisches Institut und Museum (PIMUZ), University of Zurich, Switzerland
- Museum für Naturkunde (MfN), Berlin, Germany
- P. Embree: Resource Exploration and Drilling, LLC, Orangevale, CA, USA
- J. Jenks: private collector; West Jordan, UT, USA. The specimens used in this thesis are now housed in New Mexico Museum of Natural History & Science, Albuquerque, USA

3.3 Methods

This project can be subdivided in three major areas of research (Fig. 2.1-1, chapter 2): (1) Bio- and lithostratigraphy; (2) ammonoid associations; (3) ammonoid morphology. This threefold subdivision can also be detected in the methods used in the course of this study. Figure 3.3-1 provides an overview of the different methods that were used in the course of this thesis. More detailed descriptions are provided for each manuscript individually in the corresponding chapters (chapter 4.2–4.4).

The final Geometric Morphometric analysis was written in R language. The resulting R scripts are published in two publications of this thesis (chapter 4.3 and 4.4) and made available to third parties.

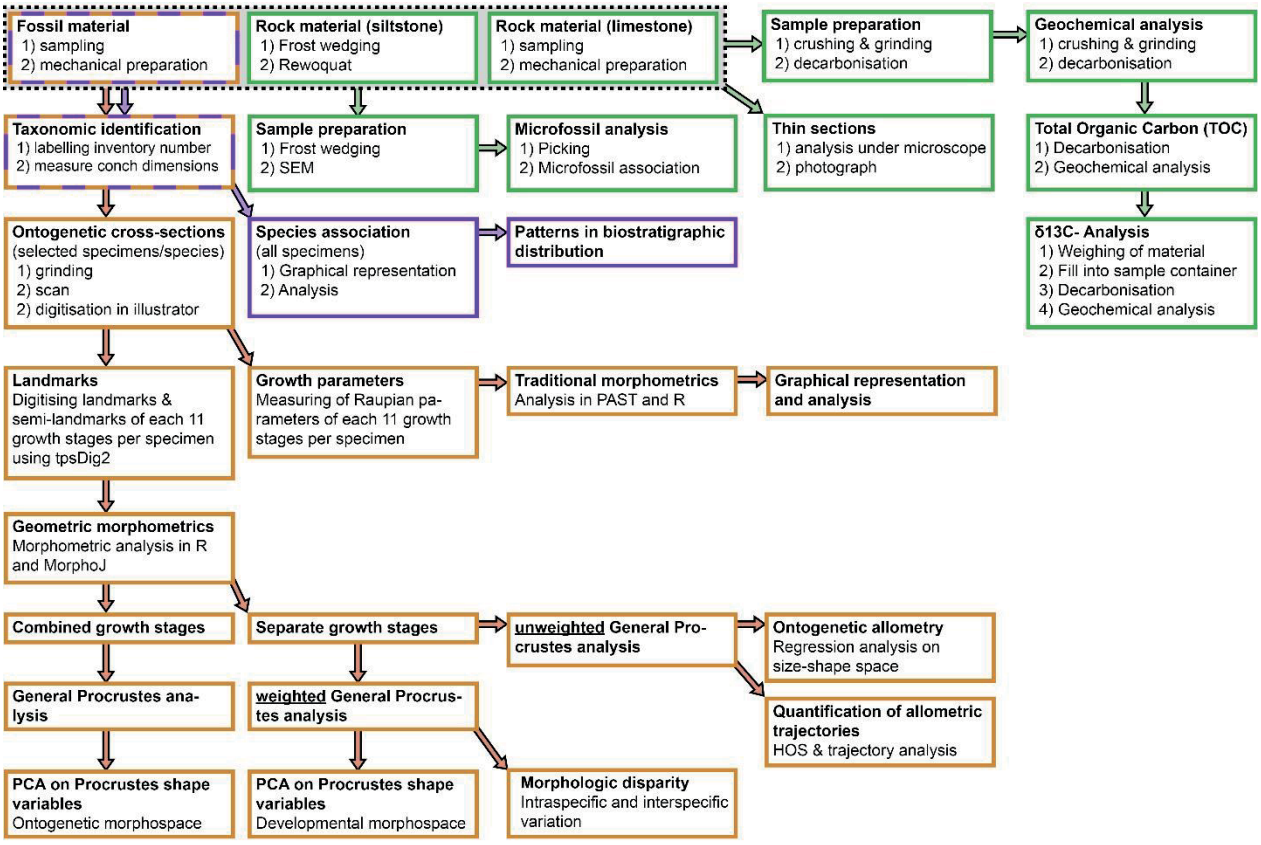

Fig. 3.3-1: Flow diagram of methods used. Divided according to the three subject areas with a colour code. Green: Bio- and Lithostratigraphy, purple: ammonoid associations, orange: ammonoid morphology. More detailed descriptions are provided for each manuscript individually in the corresponding chapters (chapter 4.2–4.4).

3.4 Biostratigraphic distribution

A total of 7809 ammonoids, 131 coleoids, 10 nautiloids, 15 gastropods and 4 brachiopods were collected and prepared. Associated with the many ammonoid samples are countless daonellid bivalves. Figure 4.3-1 shows the biostratigraphic distribution of the sampled material. Over all, the observed biostratigraphic pattern of the 53 Anisian ammonoid species is in agreement with the biostratigraphic distributions published by Silberling & Nichols (1982) and Monnet & Bucher (2005b). Patterns in biostratigraphic distribution are discussed in chapter 5.2 of this thesis.

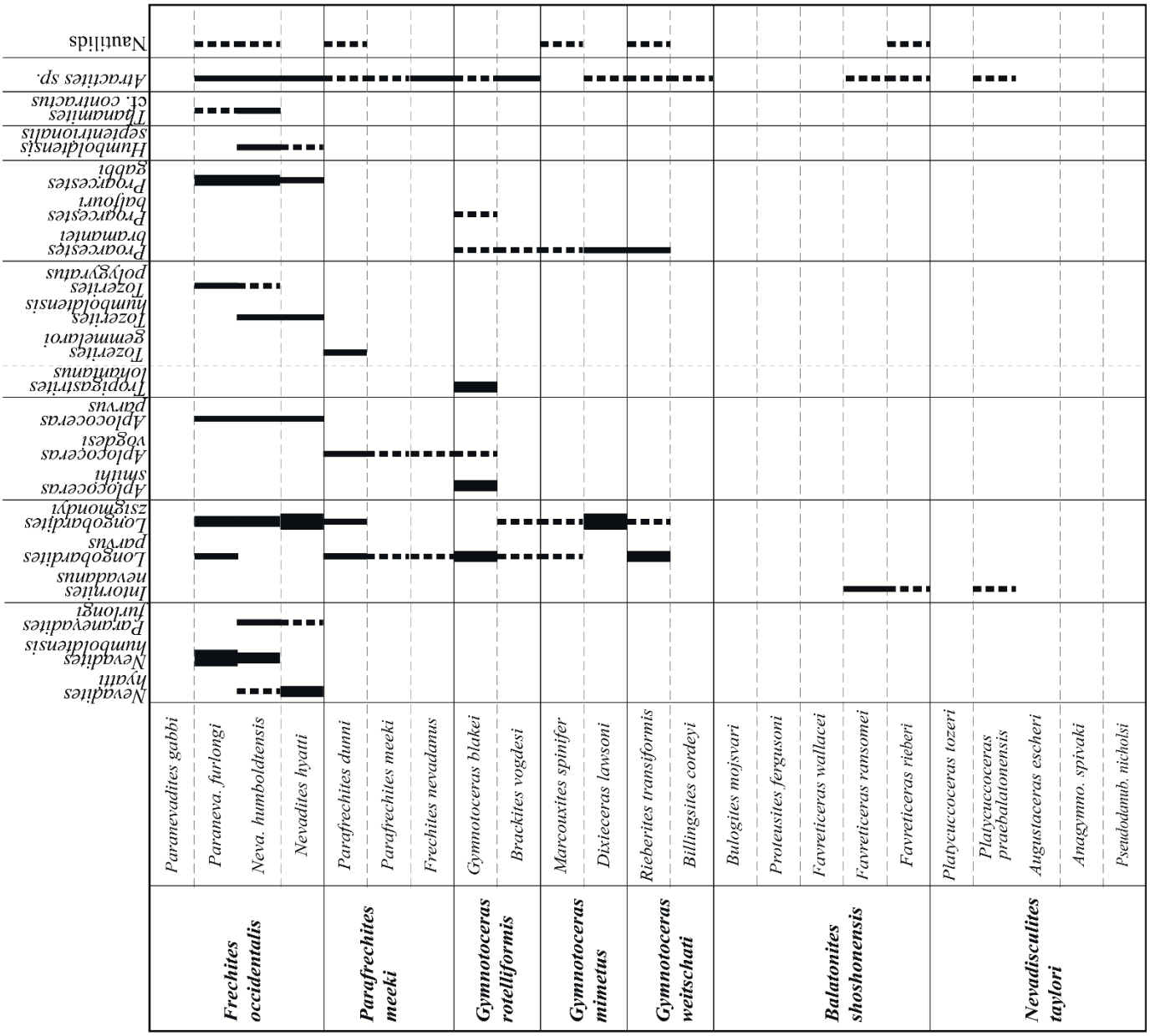

Fig. 3.4-1 part 1 and 2: Biostratigraphic distribution of Anisian Ammonoid species in Nevada, USA in two parts. Raw data can be found in Appendix 2.

Explanations
1–10 specimens
11–50 specimens
51–100 specimens
101–500 specimens
501–1000 specimens
>1000 specimens
Frechites occidentalis
Parafrechites meeki
Gymnotoceras rotelliformis
Gymnotoceras mimetus
Gymnotoceras weitschati
Balatonites shoshonensis
Nevadiscultites taylori
Paramevadites gabbi
Paraneva. furlongi
Neva. humboldtensis
Nevadites hyatti
Parafrechites dunni
Parafrechites meeki
Frechites nevadamus
Gymnotoceras blakei
Brackites vogdesi
Marcouxites spinifer
Dixieceras lawsoni
Rieberites transiformis
Billingsites cordeyi
Bulogites mojsvari
Proteusites fergusoni
Favreticeras wallacei
Favreticeras ransomei
Favreticeras rieberi
Platycuccoceras tozeri
Platycuccoceras praebalatonensis
Augustaceras escheri
Anagymno. spivaki
Pseudoamb. nicholsi
Acrochordiceras carolinae
Nevadiscultites depressus
Nevadiscultites smithi
Platycuccoceras cainense
Ptychites gradinarui
Ptychites guloensis
Ptychites embreei
Anagymnites sp.
Lissunites cf. arthaberi
Sageceras walteri
Favreticeras ransomei
?Eogymnotoc. tuberculatum
Brackites vogdesi
Billingsites cordeyi
Dixieceras lawsoni
Gymnotoceras praecursor
Gymnotoceras weitschati
Gymnotoceras mimetus
Gymnotoceras rotelliformis
Gymnotoceras rotelli.-blakei
Gymnotoceras blakei
Parafrechites meeki
Parafrechites dunni
Frechites nevadamus
Frechites occidentalis
Jenkinsites jexicostatus
Rieppelites boletzkyi
Riebertites transiformis
Silberlingia clarkei
Silberlingia praecursor
Ceccaceras sieckii
Eutomoceras dunni
Eutomoceras tauberi
Marcouxites spinifer
Metadinarites desertorus

4 Case studies

This thesis is written in a cumulative form and is based on three case studies on the morphology and ontogeny of Anisian (Middle Triassic) ammonoids and one case study about the palaeoenvironment of the Anisian of NW Nevada. All case studies are mainly using fossil and rock material retrieved from the Fossil Hill Member of Fossil Hill in the Humboldt Range and Muller Canyon of the Augusta Mountains (Pershing County), north-western Nevada, USA. The first case study, however, also contains some specimens that were collected by J. Jenks in the Rieber Gulch and Favret Canyon of the Augusta Mountains (Pershing County), and the Wildhorse-McCoy Mine area (Churchill County). The manuscripts are either published in or submitted to peer-reviewed scientific journals. Chapter 4.1 represents a short outline of my own and my co-authors' contributions to each of the four manuscripts.

4.1 Author's contribution

First case study: Ontogenetic analysis of Anisian (Middle Triassic) ptychitid ammonoids from Nevada, USA

Eva A. Bischof, Jens Lehmann, Journal of Palaeontology, 94 (2020) 829–851.

This study addresses scientific objective 3.3. Both authors collected the specimens and contributed in a discussion about the general idea of this paper. While I was in charge of the taxonomic and morphologic description, as well as the traditional morphometric analysis (grinding and polishing samples, sketching in illustrator, analysis in Excel), J. Lehmann analysed and interpreted the suture lines of the ammonoids, which I drew in Adobe illustrator. The results were interpreted and discussed by J. Lehmann and myself. The manuscript was written and reviewed by both authors.

	E. A. Bischof	J. Lehmann
Idea / Hypothesis	80 %	20 %
Data acquisition	70 %	30 %
Data evaluation	80 %	20 %
Interpretation	70 %	30 %
Writing of manuscript	80 %	20 %

Second case study: Ontogeny of highly variable ceratitid ammonoids from the Anisian (Middle Triassic)

Eva A. Bischof, Nils Schlüter, Dieter Korn, Jens Lehmann, PeerJ (2021)

This study addresses scientific objectives 3.2 and 3.3. I had the underlying idea for this paper that was subsequently improved by a discussion between N. Schlüter and me. J. Lehmann and I collected the specimens. D. Korn provided some additional specimens which, however, were not considered in the analysis. I did the taxonomic inventory and interpretation of the material. I did the cross-sectioning and polishing of the ammonoids specimens with some help from D. Korn. The subsequent placing of the landmarks on digitised sketches of the specimens was done by myself. The multivariate statistics methods were chosen by N. Schlüter and myself. I wrote the R script for the computation the geometric morphometric analysis. The interpretation of the results was done by N. Schlüter, J. Lehmann and I, but all authors discussed the interpretation. I wrote the manuscript, which was reviewed by all other authors.

	E. A. Bischof	N. Schlüter	D. Korn	J. Lehmann
Idea / Hypothesis	65 %	20 %	5 %	10 %
Data acquisition	90 %	/	10 %	/
Data evaluation	70 %	30 %	/	/
Interpretation	70 %	20 %	5 %	5 %
Writing of manuscript	80 %	10 %	5 %	5 %

Third case study: Morphologic disparity and ontogenetic allometry of beyrichitine ammonoids

Eva A. Bischof, Nils Schlüter, Jens Lehmann, to be submitted to PlosOne

This study addresses mainly scientific objective 3.3. The paper was based on ideas of N. Schlüter and me, but J. Lehmann added details as well. The specimens were collected by J. Lehmann and myself. I did the taxonomic inventory and interpretation of the material. I did the cross-sectioning, polishing and scanning of the ammonoids specimens. The underlying Procrustes shape data were obtained by me. The multivariate statistics methods were chosen by N. Schlüter and me. I wrote the R script for the computation the geometric morphometric analysis. N. Schlüter used the R script for his part of the analysis. N. Schlüter and I wrote the manuscript, which was reviewed by J. Lehmann.

	E. A. Bischof	N. Schlüter	J. Lehmann
Idea / Hypothesis	65 %	30 %	5 %
Data acquisition	100 %	/	/
Data evaluation	70 %	30 %	/
Interpretation	70 %	20 %	10 %
Writing of manuscript	70 %	20 %	10 %

Additional case study: Palaeoenvironment of the Fossil Hill Member (Middle Triassic) in Nevada, USA

Jens Lehmann, Eva Bischof, Thomas Lis, Martin Sander, Patrick G. Embree (manuscript in progress)

This study addresses scientific objective 3.1. The paper was based on ideas of J. Lehmann, T. Lis, M. Sander, P.G. Embree and me. The data used for the analysis was mainly part of the Master's thesis of T. Lis. The stratigraphic sections were measured by J. Lehmann and me. Patrick G. Embree is the owner of the Fossil Hill Locality and was of tremendously help during conducting the field work. Most of the rock material was processed by T. Lis, but a smaller part was also prepared by me. I drew the stratigraphic columns and synoptic sections in illustrator and provided the biostratigraphic framework. J. Lehmann, M. Sander and I wrote the manuscript, which was reviewed by T. Lis.

	J. Lehmann	E. A. Bischof	T. Lis	M. Sander	P. G. Embree
Idea / Hypothesis	50 %	20 %	20 %	5 %	5 %
Data acquisition	30 %	30 %	20 %	10 %	10 %
Data evaluation	40 %	20 %	30 %	10 %	/
Interpretation	40 %	20 %	20 %	10 %	10 %
Writing of manuscript	70 %	15 %	5 %	5 %	5 %

4.2 First case study

Ontogenetic analysis of Anisian (Middle Triassic) ptychitid ammonoids from Nevada, USA

Eva A. Bischof, Jens Lehmann

Published in Journal of Palaeontology, 94 (2020) 829–851.

Please cite the following publication as a journal article and not as a thesis chapter: Bischof EA, and Lehmann J. 2020. Ontogenetic analysis of Anisian (Middle Triassic) ptychitid ammonoids from Nevada, USA. Journal of Paleontology 94:829-851. 10.1017/jpa.2020.25.

https://doi.org/10.1017/jpa.2020.25

Journal of Paleontology, page 1 of 23

0022-3360/20/1937-2337
doi: 10.1017/jpa.2020.25

JOURNAL OF PALEONTOLOGY
A PUBLICATION OF THE Paleontological SOCIETY

Ontogenetic analysis of Anisian (Middle Triassic) ptychitid ammonoids from Nevada, USA

Eva A. Bischof[1]* and Jens Lehmann[1]

[1]Geowissenschaftliche Sammlung, Fachbereich Geowissenschaften, Universität Bremen, Leobener Strasse 8, 28357 Bremen, Germany <bischof@uni-bremen.de>, <jens.lehmann@uni-bremen.de>

Abstract.—*Ptychites* is among the most widely distributed ammonoid genera of the Triassic and is namesake of a family and superfamily. However, representatives of the genus mostly show low-level phenotypic disparity. Furthermore, a large number of taxa are based on only a few poorly preserved specimens, creating challenges to determine ptychitid taxonomy. Consequently, a novel approach is needed to improve ptychitid diversity studies. Here, we investigate *Ptychites* spp. from the middle and late Anisian of Nevada. The species recorded include *Ptychites embreei* n. sp., which is distinguished by an average conch diameter that is much smaller and shows a more evolute coiling than most of its relatives. The new species ranges from the *Gymnotoceras mimetus* to the *Gymnotoceras rotelliformis* zones, which makes it the longest-ranging species of the genus. For the first time, the ontogenetic development of *Ptychites* was obtained from cross sections where possible. Cross-sectioning highlights unique ontogenetic trajectories in ptychitids. This demonstrates that, despite showing little phenotypic disparity, *Ptychites* was highly ontogenetically differentiated, and thus the high taxonomic diversity at the species level is justified for the species investigated.

UUID: http://zoobank.org/5abe2487-8a00-4b48-adc7-ec7db7a097f7

Introduction

Ptychitid ammonoids appear at the lower-middle Anisian boundary with *Malletoptychites*, as well constrained only in the Tethys Himalaya (Krystyn et al., 2004), and are a typical component of the open-marine ammonoid assemblages during Anisian and partially Ladinian times (Balini, 1998). The family fills the gap after a minor ammonoid extinction event when almost all gram-bergiids disappeared (Konstantinov, 2008). The type genus itself, *Ptychites*, is one of the most characteristic ammonoids in the fossil record that was erected by Mojsisovics in Neumayr (1875), based on material from the Tethys Realm. Only a limited number of species was known in the early years after erecting the genus, but Mojsisovics' (1882) monograph boosted its importance. This work is regarded as a milestone in the history of Triassic ammonoids and chronostratigraphy (e.g., Tozer, 1971, 1984; Balini et al., 2010; Lucas, 2010; Jenks et al., 2015). Mojsisovics enlarged the number of species of *Ptychites*, and advanced the organization of this genus in several groups. After the group featured prominently in Mojsisovics (1882), it became one of the guide fossils for Triassic correlations. Its iconic status was also reflected by being a part of Ernst Haeckel's ammonoid selection in his influential book "Kunstformen der Natur"—a trendsetting issue, connecting science and art more than a century ago (Haeckel, 1899, 1900). In fact, *Ptychites* has been described from almost all over the world: (1) Nevada (Smith, 1914; Monnet and Bucher, 2005); (2) British Columbia (McLearn, 1948; Tozer, 1994); (3) Spitsbergen (Lindström, 1865; Mojsisovics, 1886; Köhler-Lopez and Lehmann, 1984); (4) the Himalayas (Diener, 1895a, 1907, 1913; Waterhouse, 1994, 1999, 2002a; Krystyn et al., 2004); (5) the Northern Alps (Hallstatt area, Schreyeralm Limestone, condensed Ammonitico-Rosso facies; Mojsisovics, 1882; Diener, 1900); (6) the Balaton Highlands (Vörös, 2018), and (7) the Dinarids and Hellenids (Han Bulog Limestone; von Hauer, 1892; Renz, 1910; Salopek, 1911; Pomoni and Tselepidis, 2013). In the Triassic of Spitsbergen and the Western Tethys, namely the wider Alpine and the Himalayan regions, the genus *Ptychites* is especially characteristic (e.g., Mojsisovics, 1886; Weitschat and Lehmann, 1983; Harland and Geddes, 1997; Balini, 1998). Therefore, scientists introduced the terms "Ptychitenkalke" (*Ptychites* limestone; Mojsisovics, 1882, 1886; Gugenberger, 1927; Rosenberg, 1952) and "*Ptychites* beds" (Spath, 1921; Harland and Geddes, 1997). *Ptychites* were well adapted to quite a large number of different paleoenvironments (Balini, 1998). Despite this fact, the genus shows a low morphological disparity. The new species described herein does not challenge this picture.

In this paper, we describe a new species of *Ptychites* and discuss the taxonomic diversity and morphologic disparity of this genus during the Middle Triassic of the west coast of North America. Our study area in north-western Nevada,

*Corresponding author

USA, belongs to the world's most complete low-paleolatitude sequences, revealing late Anisian ammonoid faunas (Monnet and Bucher, 2005). The continuous sequences, which include a very diverse and abundant ammonoid fauna, provide a good basis for ontogenetic studies on a high-resolution scale. Due to their distinctive ontogenetic trajectories (model curves), ptychitids will act as an important cornerstone in future quantification of ontogenetic analyses.

Because *Ptychites* is found all over the world, this study also contributes to the worldwide correlation of Middle Triassic sediments. Representatives of this group were described from many different localities all over the world. However, most of these records originate from condensed facies, with significant uncertainty regarding the number and age of the faunas, and the composition of the populations. This makes correlative work particularly challenging. The problems of correlation and condensation are discussed by Tozer (1971) and are, for example, reported from Epidauros (Greece) by Krystyn and Mariolakos (1975) and Krystyn (1983). Furthermore, Balini (1998, p. 144) emphasized that the alpha taxonomy of *Ptychites* is characterized by a lack of information on the stratigraphic relationships between the type specimens. The study of ptychitid ammonoids therefore holds great potential for both biostratigraphic and paleobiological work.

Geological setting and material

The bulk of the fossil material used here was collected by members of the Geosciences Collection of the University of Bremen (Germany). It derives from the Muller and Favret Canyon of the Augusta Mountains (Pershing County), north-western Nevada, USA (see Fig. 1). A complete section of the upper portion of the late Anisian Fossil Hill Member of the Favret Formation and the lowermost part of the early Ladinian Home Station Member of the Augusta Mountain Formation was meticulously documented and measured. Furthermore, J. Jenks collected additional material in Rieber Gulch and Favret Canyon of the Augusta Mountains, Pershing County, and the Wildhorse-McCoy Mine area, Churchill County (see also Fig. 1). Since the fossil material of J. Jenks was loosely collected, no measured sections are associated with this material. However, the sites where the fossil material was found are thoroughly documented and the biostratigraphic framework is well known (Jenks et al., 2015).

Biostratigraphically, *Ptychites* spp. from Nevada that are the focus of this study were collected in the *Balatonites shoshonensis* and the *Gymnotoceras mimetus–Gymnotoceras rotelliformis* zones of the Fossil Hill Member (middle and late Anisian; see Fig. 2). The Fossil Hill Member consists of alternating layers of calcareous siltstone and mudstone with lenticular limestone. The rich fauna of the succession primarily consists of halobiid bivalves and ammonoids. Ceratitids are quite abundant and diverse throughout the member. The Anisian faunas of the Humboldt Range were previously described in the 19th and early 20th century (Gabb, 1864; Hyatt and Smith, 1905; Smith, 1914). Recently, Silberling and Nichols (1982) and Monnet and Bucher (2005) refined the original alpha taxonomy and the biostratigraphy.

Methods and conventions

In order to underpin the description of *Ptychites embreei* new species, we performed an ontogenetic analysis of selected specimens of *Ptychites*. The methods introduced by Korn (2010) and Klug et al. (2015) were used. All samples used for ontogenetic analysis were first removed from the rock matrix by mechanical preparation and were then measured along the longest axis. The conch dimensions of the growth stages were obtained from digitized sketches of high-precision cross-sections intersecting the protoconch. In order to find a non-destructive method, a CT scan of selected specimens with a GE Phoenix v device, tome, x s 240 with a nanoray tube NF 180 kV was performed at the University of Erlangen, Germany. Unfortunately, the differences in density were marginal, and therefore the contrast of the internal structures on the scan images were not sufficient for further analysis.

The basic conch parameters (dm: diameter; ww: whorl width; wh: whorl height) for all available specimens were measured at every distinct growth stage (i.e., half whorl), starting at the protoconch. For the ontogenetic analysis, the growth parameters whorl expansion rate ($WER_n = [dm_n/dm_{n-0.5}]^2$), whorl width index ($WWI_n = ww_n/wh_n$), umbilical width index ($UWI_n = uw_n/dm_n$), and the conch width index ($CWI_n = ww_n/dm_n$) were calculated (for further explanations see Korn, 2010; Klug et al., 2015).

Ontogenetic morphospace.—The growth parameters WER, UWI, and CWI were also analyzed in a principal component analysis (PCA). The dataset comprises the values for all distinct growth stages of an individual. In contrast to most other ontogenetic studies using ternary plots or multivariate statistics (e.g., Korn and Klug, 2007; Klug et al., 2016; Walton and Korn, 2017, 2018), herein every individual is defined by the sum of all parameters of all ontogenetic stages. In order to omit missing values in the analysis, the PCA data set was limited to the last growth stage of the specimen with the fewest number of half whorls (here growth stage number 5.0; see Appendix). All parameters are numbered consecutively, starting with the first half whorl (i.e., $WER_{0.5}$, $CWI_{0.5}$, $UWI_{1.0}$) to the last one of the analysis (i.e., $WER_{5.0}$, $CWI_{5.0}$, $UWI_{5.0}$). Therefore, the space opened up by this analysis is not a classical morphospace showing the morphology of an individual at a specific growth stage, but in an artificial state of combined morphologies of different ontogenetic stages. It illustrates how the ontogeny of the groups differ. To prevent confusion, we introduce the term "ontogenetic morphospace." The PCA with correlation matrix was run using PAST (version 3.25; Hammer et al., 2001).

Suture lines.—The preservation of the ammonoids occasionally permits the drawing of suture lines. Among the fossil material herein, GSUB C13194 (*P. guloensis* Tozer, 1994) and C13196 (*P. gradinarui* Bucher, 1992) were the only specimens with a nicely preserved suture line. We used the suture terminology of Wedekind (1916), as applied by Kullmann and Wiedmann (1970) and modified by Korn et al. (2003)—E: external lobe; A: adventive lobe (that corresponds

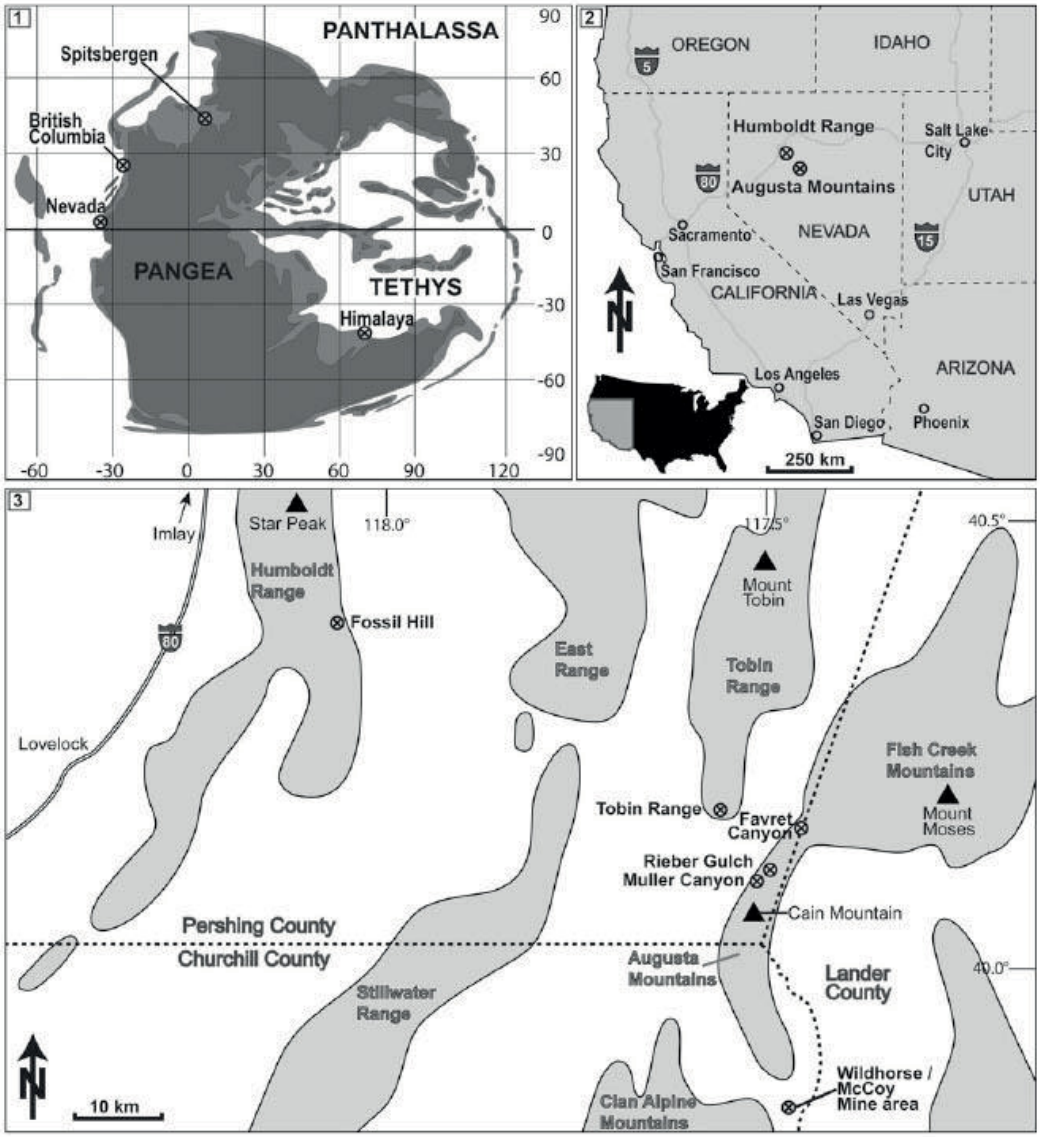

Figure 1. (1) Middle Triassic paleogeographical setting. Nevada as well as other important localities of Ptychites spp. are marked. Redrawn from Péron et al. (2005), Brayard et al. (2006), and Skrzycki et al. (2018). (2, 3) Location of the study area in NW Nevada, USA. The most important localities of Fossil Hill Member outcrops are marked.

to letter L of the traditional nomenclature); U: umbilical lobe; I: internal lobe; E/A (that is E/L of traditional nomenclature) is the saddle between E and A; A/U (that is L/U of traditional nomenclature) corresponds to the saddle between A and U.

Repositories and institutional abbreviations.—Geosciences Collection of the University of Bremen (GSUB), Germany; Paleontological Institute and Museum University of Zurich (PIMUZ), Switzerland; New Mexico Museum of Natural History & Science (NMMNH), Albuquerque, New Mexico,

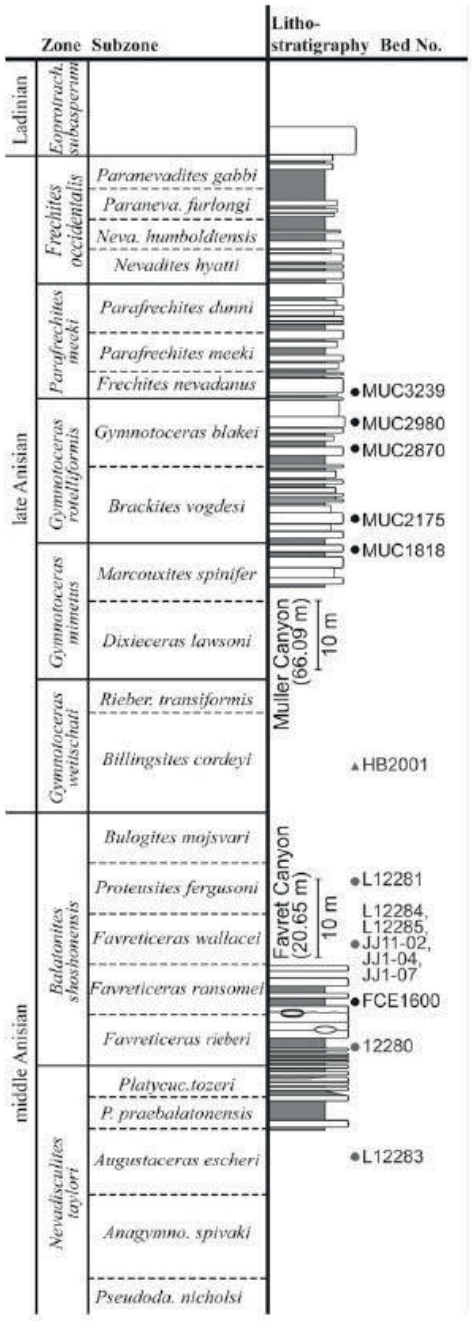

Figure 2. Measured lithostratigraphic sections in the Muller and Favret canyons of the Augusta Mountains, Pershing County, NW Nevada, USA from where our specimens were collected. Black dots: Beds within our measured sections; Gray dots: JJ-localities documented by J. Jenks, Salt Lake City, Utah, USA; Gray triangle: HB-locality, documented by H. Bucher, Zurich, Switzerland (Monnet and Bucher, 2005).

USA. The abbreviation JJ refers to localities of J. Jenks, Salt Lake City, Utah, USA, and HB refers to localities of H. Bucher, Zurich, Switzerland.

In the synonymy list we used '[n.s.]' for publications we have not seen, because we could not get hold of a copy of that paper.

Systematic paleontology

Order Ceratitida Hyatt, 1884
Superfamily Ptychitoidea Mojsisovics, 1882
Family Ptychitidae Mojsisovics, 1882
Genus *Ptychites* Mojsisovics in Neumayr, 1875

Type species.—*Ammonites rugifer* Oppel, 1863 (designated by Tozer, 1994, see discussion on p. 133). Tozer (1981, p. 94) was used as reference for the family-group taxonomy.

Ptychites guloensis Tozer, 1994
Figures 3.5–3.7, 4

1994 *Ptychites guloensis*; Tozer, p. 133, pl. 48, figs. 1, 2, text-figs. 35d, e.

Holotype.—Holotype is GSC 70993 from the Sulphur Mountain Formation, Minor Zone, near south end of Hook Lake, NTS Kinuseo Falls (GSC loc. 83873), Canada; several paratypes from other localities in the same area.

Diagnosis.—The diagnosis of *Ptychites guloensis* by Tozer (1994, p. 133) is as follows: "*Ptychites* attaining a diameter of at least 70 mm; H about 50 per cent, W 60–70 per cent, U about 15 per cent of diameter. Whorl section ovoid, the flanks and venter merging to form a perfect arch. Distinct ribbing absent, growth striae nearly or perfectly radial. Suture line with four lateral saddles, the outer two large and the inner two small. The inner two are depressed in relation to the large saddles. The outer large saddles are not bifid; the inner small saddles weakly bifid. Moderately sized to large *Ptychites* with a perfectly rounded venter. Rather narrow umbilicus with a steep umbilical wall. Almost smooth conch with only fine growth striae."

Occurrence.—Favret Canyon, Augusta Mountains, Pershing County: GSUB loc. FCE, *F. ransomei* Subzone, *B. shoshonensis* Zone, Fossil Hill Member of the Augusta Mountain Formation. According to Tozer (1994, p. 133), *P. guloensis* also occurs in the Middle Anisian, Middle Triassic, *H. minor* Zone, Toad Formation of north-eastern British Columbia.

Description.—Measurements of the selected specimen are provided in Table 1. Specimen GSUB C13194 (Fig. 3.5–3.7) is a complete conch with a maximum diameter of 26.71 mm. The pachyconic conch (ww/dm = 0.69) is subinvolute (uw/dm = 0.22) and has a perfectly rounded venter. The narrow umbilicus is deeply incised revealing a steep umbilical wall. The umbilical shoulders merge into the venter in a wide arch. The largest part of the shell is not preserved. The remnants of the shell and some

https://doi.org/10.1017/jpa.2020.25

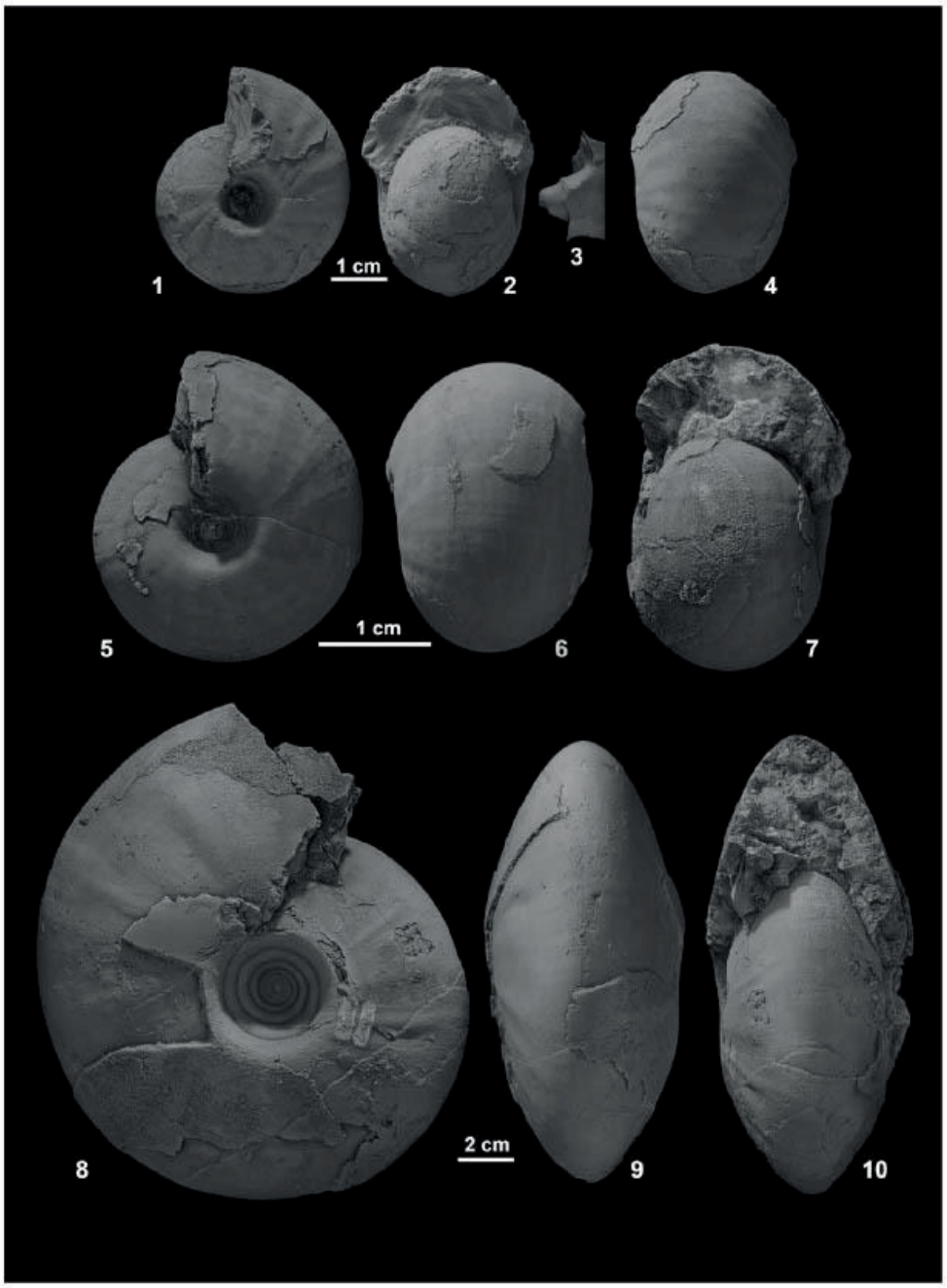

Figure 3. (1–4) *Ptychites wrighti*, from north side of Favret Canyon, Augusta Mountains, Pershing County; (3) cast of deeply incised and funnel-shaped umbilicus, NMMNH 80882. (5–7) *Ptychites guloensis*, Favret Canyon, Augusta Mountains, Pershing County, GSUB C13194. (8–10) *Ptychites gradinarui*, Favret Canyon, Augusta Mountains, Pershing County, GSUB C13196.

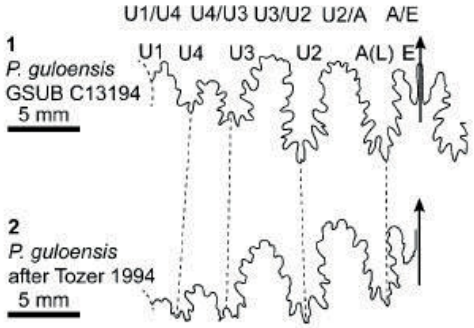

Figure 4. Suture line of *Ptychites guloensis*, (1) GSUB C13194 compared to (2) Tozer (1994, p. 444, fig. 35e). Bracketed letters indicate traditional suture nomenclature.

imprints on the steinkern however reveal that the shell was smooth, bearing some fine growth striae.

The major elements of the suture line of specimen GSUB C13194 (Fig. 4.1) are uniformly large, namely with an U3/U2, U2, A/U2, and an A that are of a similar extent. The A lobe is bifid, with the endings slightly less incised compared to the other major sutural elements. The U2/A tapers towards the aperture. The E/A is slender and less strongly denticulate. The U1/U4 shows a prominent, slender spur. The suture line of GSUB C13194 shows only minor differences to the sutures redrawn from Tozer (1994) (Fig. 4.2). The latter differs by a trifid A lobe that is slightly smaller, a U2/A that is not tapering, and the U1/U4 that lacks a spur.

Materials.—One specimen (GSUB C13196).

Remarks.—Köhler-Lopez and Lehmann (1984) illustrated the ontogenetic development of the suture line of *Aristoptychites*, and thus demonstrated that the traditional nomenclature should be modified in Ptychitidae. In this respect, Tozer (1994, p. 133) refers to "four lateral saddles," these are the U2/A, U3/U2, U4/U3, and U1/U4 of the ontogenetic nomenclature used herein. The diagnosis of the suture line of *P. guloensis* given by Tozer (1994, p. 133) is as follows: "[…] with four lateral saddles, the outer two large and the inner two small. The inner two are depressed in relation to the large saddles. The outer large saddles are not bifid; the inner small saddles weakly bifid." However, this does not characterize the species because the features can be found in other species of *Ptychites* as well. Nevertheless, the Canadian specimen shows typical features of *Ptychites*, such as the rather broad and rounded outline of the U3/U2 and U2/A and the multi point indentations of the lobes. Although we consider the preservation of GSUB C13194 as good, we cannot rule out that the slightly more slender and irregular indentations of the U3/U2 and U2/A and the different shape of the lowermost tip of the A lobe with fairly broad and simple indentations are a matter of preservation.

Ptychites wrighti McLearn, 1946
Figure 3.1–3.4

1946 *Ptychites wrighti*; McLearn, p. 3, pl. 4, fig. 5 [n. s.].
1948 *Ptychites wrighti*; McLearn, p. 12, pl. 4, fig. 5.
1969 *Ptychites wrighti*; McLearn, p. 56, text-fig. 31, pl. 10, fig. 1a–c.
1994 *Ptychites wrighti*; Tozer, p. 134, pl. 48, figs. 3, 4.

Holotype.—According to McLearn (1969), the holotype (GSC 6442) is from the Toad Formation, far up "McTaggart Creek," west slope of Mount Wooliever, Sikanni Chief River valley (GSC loc. 10731), Canada.

Diagnosis.—Small to moderately sized species of *Ptychites* with a rounded to subtriangular venter and a rather narrow umbilicus with an abrupt umbilical shoulder. The conch bears very weak folds and ribs.

Occurrence.—North side of Favret Canyon, Augusta Mountains, Pershing County: NMMNH loc. L 12283, *A. escheri* Subzone, *N. taylori* Zone. According to Tozer (1994), *P. wrighti* also occurs in the middle Anisian, Middle Triassic, *H. minor* Zone?, Toad Formation of north-eastern British Columbia.

Description.—Measurements of the selected specimen are provided in Table 2. Specimen NMMNH 80882 (Fig. 3.1–3.4) is a complete conch with a maximum diameter of 38.74 mm. The pachyconic shell (ww/dm = 0.74) is subinvolute (uw/dm = 0.26) revealing a deeply incised umbilicus (Fig. 3.3) and an abrupt umbilical shoulder. Rounded to subtriangular shoulder. The flanks are covered with very weak, irregular and slightly rursiradiate ribs and folds. The length of the body chamber exceeds one whorl.

Materials.—One specimen (NMMNH 80882).

Remarks.—The diagnosis for this species is newly established here, due to a lack of a former diagnosis. The occurrence of this species seems to be restricted to the open water fauna of the Panthalassic Ocean. The available material does not allow an ontogenetic analysis. The suture line published in McLearn (1969) shows that the sutural elements of this species are

Table 1. Measurements in mm of one specimen of *Ptychites guloensis* Tozer, 1994 collected in the Fossil Hill Member of the Favret Formation at the Muller Canyon locality in the Augusta Mountains, Pershing County, Nevada, USA. For further details on the bed number, see Figure 2 ("Bed No."). uw: maximum umbilical width; ww: maximum whorl width; dm: maximum diameter of shell.

Locality	Specimen	uw	ww	dm	uw/dm	ww/dm
FCE1600	GSUB C13194	5.82	18.33	26.71	0.22	0.69

Table 2. Measurements in mm of one specimen of *Ptychites wrighti* McLearn, 1946 collected by J. Jenks in the Fossil Hill Member of the Favret Formation, Pershing County, Nevada, USA. For further details on the bed number, see Figure 2 ("Bed No."). uw: maximum umbilical width; ww: maximum whorl width; dm: maximum diameter of shell.

Locality	Specimen	uw	ww	dm	uw/dm	ww/dm
L 12283	NMMNH 80882	10.18	28.75	38.74	0.26	0.74

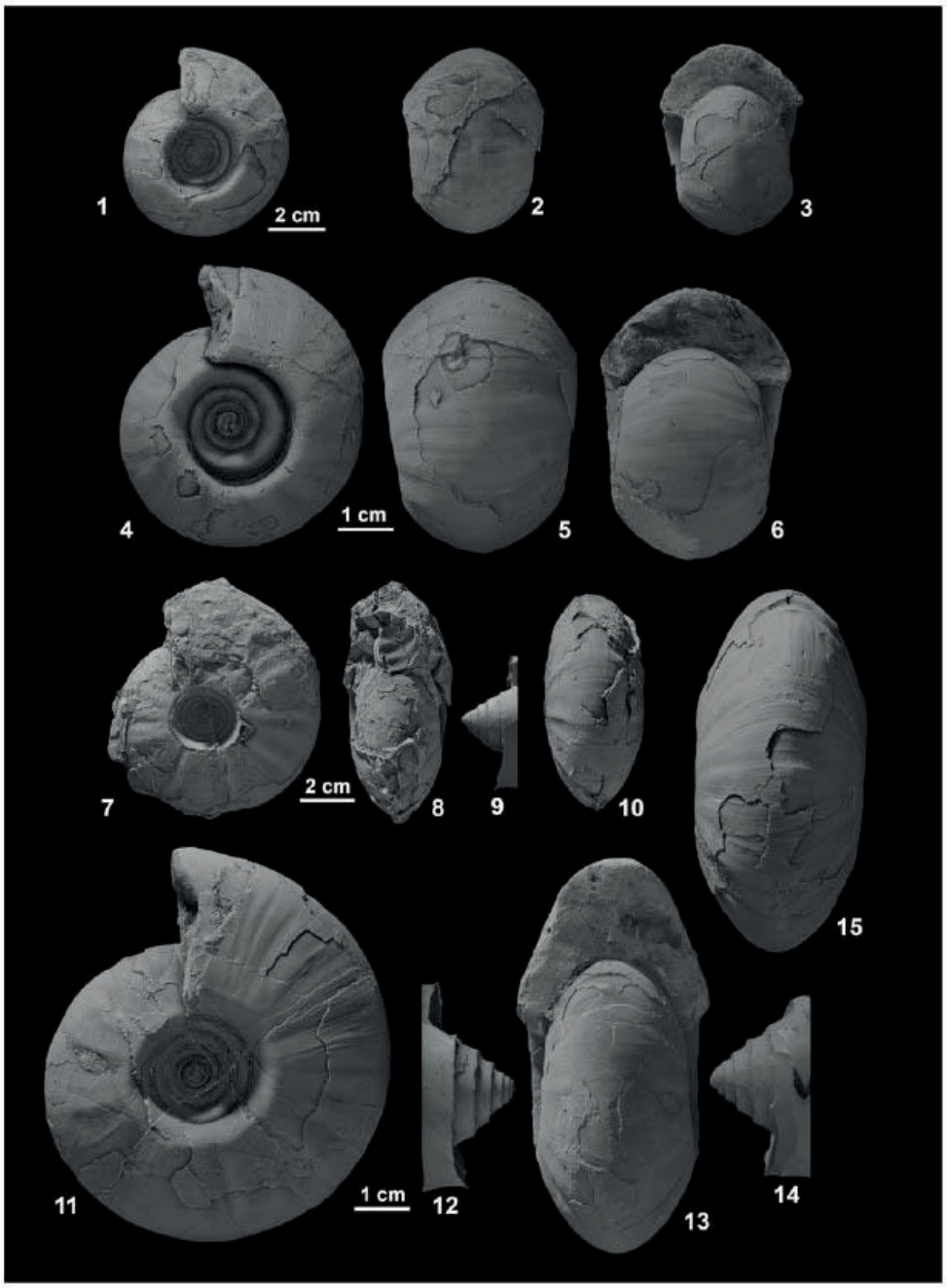

Figure 5. *Ptychites gradinarui* (**1–6**) from Rieber Gulch, Augusta Mountains, Pershing County, (**1–3**) NMMNH 80878, (**4–6**) NMMNH 80879; (**7–14**) from the Wildhorse-McCoy mine area, Churchill County, (**7–10**) GSUB C11443, (**9**) cast of deeply incised and funnel-shaped umbilicus; (**11–14**) NMMNH 80880, (**12, 14**) casts of deeply incised and funnel-shaped umbilicus.

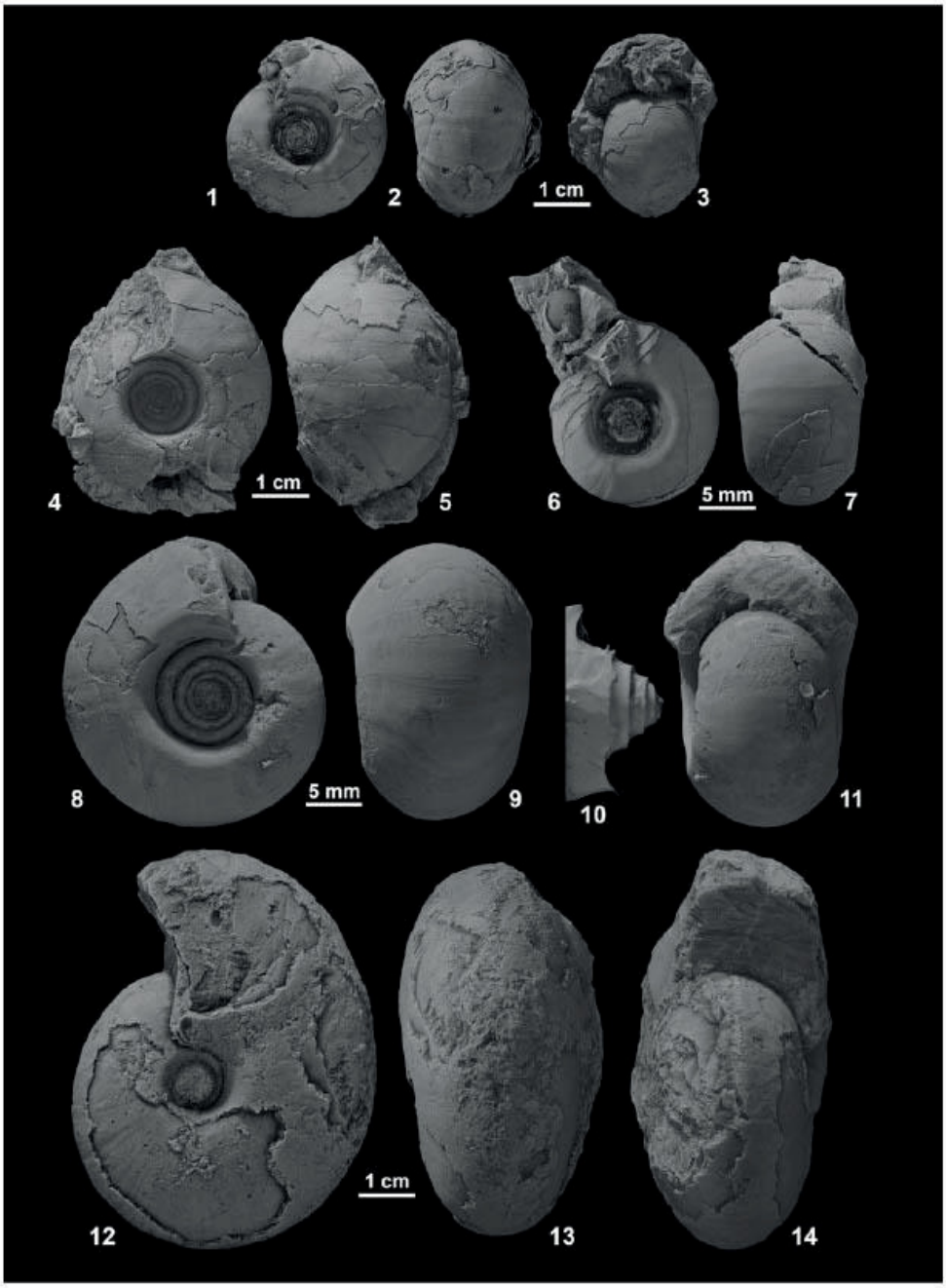

Figure 6. (**1–11**) *Ptychites gradinarui* (**1–5**) from Rieber Gulch, Augusta Mountains, Pershing County, (**1–3**) GSUB C11442, (**4, 5**) GSUB C11441; (**6–11**) from the Wildhorse-McCoy Mine area, Churchill County, (**6, 7**) GSUB C11440, (**8–11**) NMMNH 80877, (**10**) cast of deeply incised and funnel-shaped umbilicus. (**12–14**) *Ptychites densistriatus* from the south side of Favret Canyon, Augusta Mountain, Pershing County, NMMNH 80881.

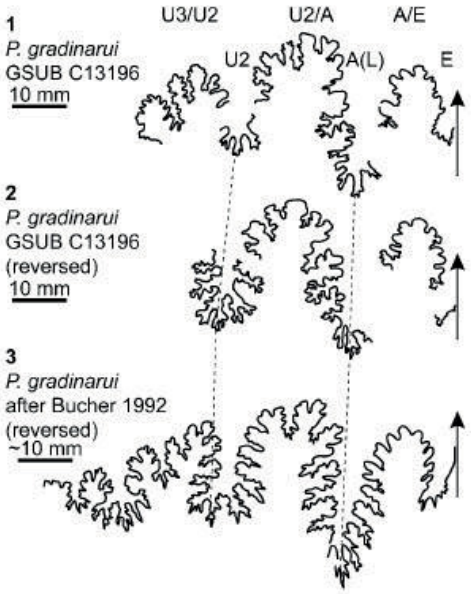

Figure 7. Adult suture of *Ptychites gradinarui*. Bracketed letters indicate traditional suture nomenclature. (1, 2) Suture lines drawn from specimen GSUB C13196, of which (2) is reversed. (3) Reversed suture line redrawn from Bucher, 1992, text-figure 22a.

comparatively strongly denticulate with deep incisions and a rather weak frilling.

Ptychites gradinarui Bucher, 1992
Figures 3.8–3.10, 5, 6.1–6.11, 7, 8

1968 *Ptychites* cf. *P. domatus* (Hauer); Silberling and Tozer, p. 37.
1992 *Ptychites gradinarui*; Bucher, p. 439, pl. 9, figs. 11, 12, pl. 10, figs. 1–4, pl. 11, figs. 21–26, text-fig. 22.
2007 *Ptychites gradinarui*; Jenks et al., p. 36, pl. 18, figs. a, b.

Holotype.—The holotype USNM 448264, the paratypes USNM 448262, USNM 448265–448267, and the plesiotype USNM 448263 are all stored in the collection of the National Museum of Natural History in Washington D.C, USA (Bucher, 1992).

Diagnosis.—Rather large species of *Ptychites* reaching a diameter of 90 mm and in rare cases more than 250 mm (see Bucher, 1992, p. 440). The conch of juvenile specimens is mostly pachyconic. The later ontogenetic stages, however, show two different morphotypes: pachyconic-subevolute (ww/dm ~0.70; uw/dm ~0.40) and discoidal-subinvolute (ww/dm ~0.50; uw/dm ~0.30). Furthermore, the conch bears a smooth ornament of irregular, rectiradiate to slightly falcoid ribs and growth striae. The internal mold of juvenile specimens shows growth constriction.

Occurrence.—Wildhorse-McCoy Mine area, Churchill County: NMMNH locs. L 12281 (*P. fergusoni* Subzone), 12285 and J. Jenks loc. JJ1-04, JJ1-07 (*F. wallacei* Subzone) of the *B. shoshonensis* Zone. Rieber Gulch, Augusta Mountains, Pershing County: NMMNH loc. L 12284 and JJ11-02, *F. wallacei* Subzone, *B. shoshonensis* Zone. Favret Canyon, Augusta Mountains, Pershing County: GSUB loc. FCE1600, *F. ransomei* Subzone, *B. shoshonensis* Zone.

Description.—Measurements of the selected specimens are provided in Table 3. The largest pachyconic (ww/dm = 0.76) and robust specimen (NMMNH 80879; Fig. 5.4–5.6) has a diameter of dm = 66.66 mm. The subevolute to evolute umbilicus (uw/dm = 0.44) is very deeply incised with a steep umbilical wall and a very abrupt umbilical shoulder. The venter is subtriangular. The ornamentation of the conch consists of smooth and irregular, rectiradiate to slightly falcoid ribs, and very fine growth striae. The partly preserved shell of the largest specimen (GSUB C13196; Fig. 3.8–3.10) is very thick (1.5 mm at the venter and >3 mm along the umbilical shoulder).

The partially preserved suture line of GSUB C13196 is illustrated in Figure 7. The umbilical part of the line is missing. The widths of U3/U2, U2, A/U2, A, and A/E of the herein described specimen (Fig. 7.1, 7.2) are comparable to those of the specimen published in Bucher, 1992 (Fig. 7.3 herein). The A lobe is trifid. As with the E/A illustrated in Bucher, 1992, this saddle is slender and less strongly denticulate than the others are. Bucher (1992) did not illustrate the conch of the specimen he analyzed. However, since the whorl height of the specimen indicated is ~80 mm, the specimen must have had a similar conch size to the specimen of this study (whorl height of specimen GSUB C13196: 88.30 mm).

The largest discoidal (ww/dm = 0.46) specimen used for the ontogenetic analysis (GSUB C11443; Fig. 5.7–5.10), has a diameter of dm = 85.62 mm. The subinvolute umbilicus (uw/dm = 0.27) is also very deeply incised (Fig. 5.9). The umbilical wall is a little bit less steep than that of their more robust conspecifics. The venter of the discoidal specimen is subtriangular. The ornamentation, however, equals the robust specimens.

Ontogenetic description.—The ontogenetic development of *P. gradinarui* is illustrated in Figure 8, and the raw data of the analysis are supplied in the Appendix. The whorl expansion rate (WER; Fig. 8.2) shows a triphasic behavior with a strong decrease in the earliest stages and a rather stable intermediate phase. In phase III, the WER increases again, indicating an acceleration of growth.

The values for the whorl width index (WWI) are more scattered than the other series (Fig. 8.3). Nevertheless, a triphasic development of the growth trajectories can be observed. In phase I and II, the conch width index (CWI) and the umbilical width index (UWI) describe opposing parabolas (Fig. 8.4). *Ptychites gradinarui* shows a trend of developing a slightly more pachyconic and less evolute conch in their early stages, resulting in a clock-wise progression (Fig. 8.5). In contrast to UWI, the CWI is a triphasic trajectory. Therefore, at growth stage 8.0, the two indices decouple. Whereas the UWI sticks to the parabolic curve progression, CWI quite abruptly decreases after

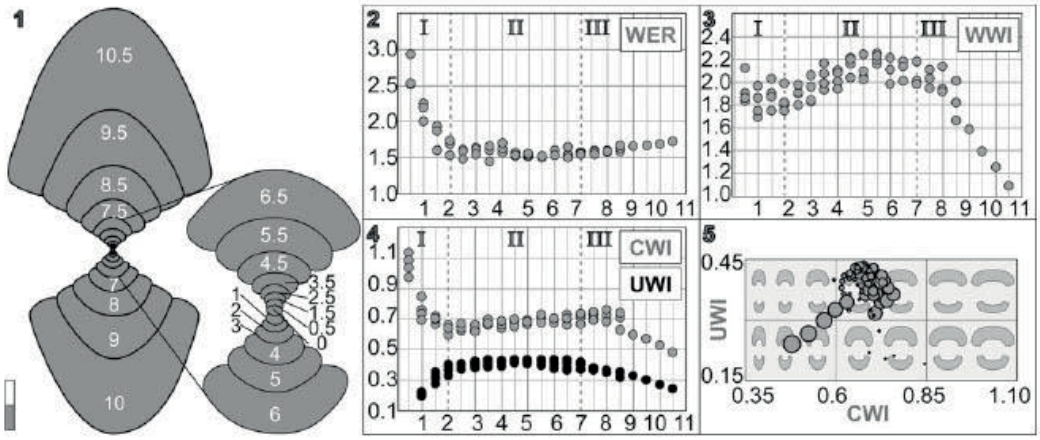

Figure 8. Ontogenetic analysis of *Ptychites gradinarui*. (1) Cross section of the largest discoidal specimen GSUB C11443, scale bar units 5 mm. (2–4) Ontogenetic development of the whorl expansion rate ($WER_n = (dm_n/dm_{n-0.5})^2$), whorl width index ($WWI_n = ww_n/wh_n$), umbilical width index ($UWI_n = uw_n/dm_n$), and the conch width index ($CWI_n = ww_n/dm_n$) plotted against number of half whorls (ontogenetic stages). (5) Ratio between UWI and CWI of the available specimens. Bubble size refers to number of half whorl; the picture in the background shows the shape of the last complete whorl (developed by Korn, 2010). Roman numbers refer to interpretation of different life phases; I: Hatchling, II: Juvenile; III: Subadult–adult; for more detailed explanations see Walton and Korn (2017, p. 713).

whorl 8.0, causing a distinct buckle in the growth trajectories (Fig. 8.5). This means that in later ontogenetic stages, the species develops more discoidal and less evolute conches. Following the notation of Walton and Korn (2017), the morphologic development of *P. gradinarui* is characterized by a C-mode ontogeny.

In general, all the trajectories shown in Figure 8.2–8.5 show a change in direction towards the end of the phase II (growth stage 5.0 to 8.0; roughly corresponds to growth size of 9–27 mm; see also Appendix). These changes in the progression of the trajectories are interpreted to mark the transition from juvenile to adult stages. The analysis of a large pachyconic specimen would allow testing whether the two morphotypes (discoidal and pachyconic, see above) could be explained by sexual dimorphism. If more globous variants of this species show the same ontogenetic trends, at around the same growth stage, this would underpin the hypothesis of sexual dimorphism. However, no appropriate specimen was available.

Table 3. Measurements in mm of selected specimens of *Ptychites gradinarui* Bucher, 1992 collected by J. Jenks and us in the Fossil Hill Member of the Favret Formation, Churchill and Pershing counties, Nevada, USA. For further details on the bed number, see Figure 2 ("Bed No."). uw: maximum umbilical width; ww: maximum whorl width; dm: maximum diameter of shell; (): Fragmented specimens, estimated values; *: specimen used for ontogenetic analysis, cast present.

Locality	Specimen	uw	ww	dm	uw/dm	ww/dm
L 12284	NMMNH 80878	(21.09)	36.75	52.48	0.40	0.70
L 12284	NMMNH 80879	29.32	50.46	66.66	0.44	0.76
L 12284	NMMNH 80880	25.83	34.95	69.62	0.37	0.50
JI11–02	GSUB C11441*	13.07	28.55	(38.27)	0.34	0.75
JI11–02	GSUB C11442*	10.31	23.67	32.48	0.32	0.73
JI1–04	GSUB C11440*	6.00	11.15	15.49	0.39	0.72
JI11–07	GSUB C11443*	22.98	39.81	85.62	0.27	0.46
L12281	NMMNH 80877	10.39	17.53	25.90	0.40	0.68
FCE1600	GSUB C13196	43.49	79.00	177.00	0.25	0.45

Materials.—Nine specimens (NMMNH 80877–80880, GSUB C11440–C11443, GSUB C13196).

Remarks.—The diagnosis for this species is newly established here, due to a lack of a former diagnosis. This species appears to be endemic to Nevada, with its closest ally, *P. sahadeva* Diener, 1895a, from the Himalayan region according to Bucher (1992). Among the material herein, two different morphotypes can be distinguished—a more depressed type with a subtriangular venter and a slightly narrower umbilicus, and a robust variant with very abrupt umbilical shoulders. However, the ornamentation with irregular fine ribs, growth striae, and weak depressions are very similar. Furthermore, smaller specimens herein and the specimens illustrated in Bucher (1992) seem to be intermediate to these two morphotypes. Because the biostratigraphic and geographic ranges of both morphotypes are also overlapping, the two morphotypes were assigned to one species, dimorphism cannot be excluded.

Ptychites densistriatus Bucher, 1992
Figures 6.12–6.14, 9.1–9.3

1992 *Ptychites densistriatus*; Bucher, p. 441, pl. 9, figs. 1–10.

Holotype.—According to Bucher (1992), the holotype (USNM 448261), the paratypes (USNM 448259, 448260), and the plesiotype (USNM 448258) are all stored in the collection of the National Museum of Natural History in Washington D.C., USA.

Diagnosis.—Moderately sized species of *Ptychites* with a subinvolute (uw/dm ~0.25) and discoidal to pachyconic conch

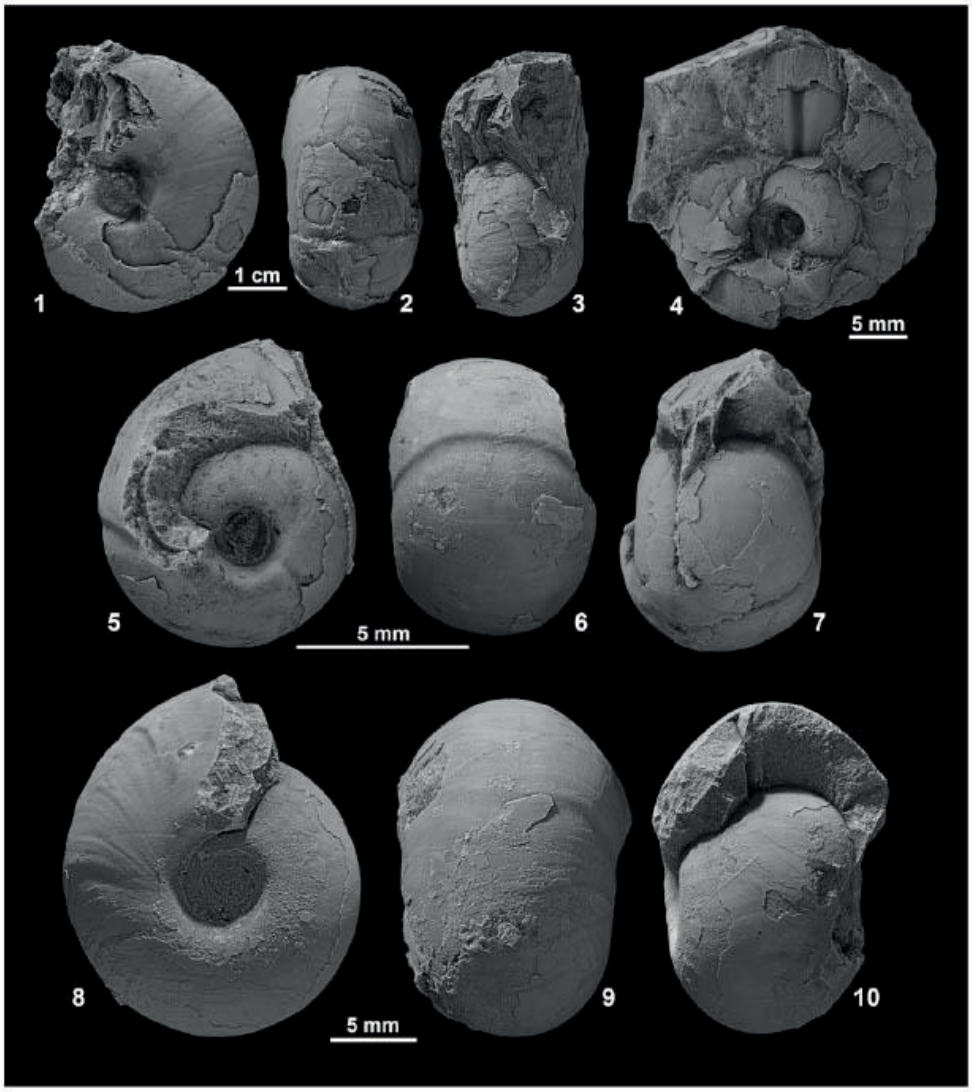

Figure 9. (**1–3**) *Ptychites densistriatus* from Favret Canyon, Pershing County, Nevada, GSUB Cl 1439. (**4–10**) *Ptychites embreei* n. sp. from Muller Canyon, Augusta Mountains, Pershing County, (**4**) GSUB C8273 (paratype), (**5–7**) GSUB C8254, (**8–10**) GSUB C8287 (paratype).

(ww/dm ~0.60). Whereas juvenile specimens are clearly pachyconic, the conch gets more depressed towards later ontogenetic stages. More rounded umbilical shoulder. Smooth shell with an ornament of thick radial growth striae.

Occurrence.—Favret Canyon, Augusta Mountains, Pershing County: NMMNH loc. L 12280, *F. rieberi* Subzone, *B. shoshonensis* Zone.

Description.—Measurements of the selected specimens are provided in Table 4. Specimen NMMNH 80881 (Fig. 6.12–6.14) is a complete conch with a maximum diameter of 53.49 mm. The discoidal to pachyconic shell (ww/dm = 0.60) is subinvolute (uw/dm = 0.24), revealing a deeply incised umbilicus with a steep umbilical wall and a narrowly rounded umbilical shoulder. The specimen is slightly ovoid. Furthermore, the almost smooth surface of the conch only bears smooth growth striae.

Materials.—Two specimens (NMMNH 80881, GSUB C11439).

Remarks.—The diagnosis for this species is newly established here, due to a lack of a former diagnosis. To our knowledge, this species in endemic to Nevada. Preservation of the available material did not allow a sutural and ontogenetic analysis.

Ptychites embreei new species
Figures 9.4–9.10, 10–13

2005 *Ptychites* sp. indet; Monnet and Bucher, p. 49, pl. 23, fig. 9.

Holotype.—GSUB C9453 (Fig. 12), Fossil Hill Member of the Favret Formation, Muller Canyon in the Augusta Mountains, Pershing County, Nevada, USA.

Paratypes.—Five specimens GSUB C8273 (Fig. 9.4), C8287 (Fig. 9.8–9.10), C8289 (Fig. 10.7–10.9), C8280 (Fig. 11.1–11.3), and C9458 (Fig. 11.7–11.9), Fossil Hill Member of the Favret Formation, Muller Canyon in the Augusta Mountains, Pershing County, Nevada, USA.

Diagnosis.—Very small to small-sized and depressed *Ptychites* attaining a diameter <30 mm at maximum. Conch subinvolute to subevolute (uw/dm ~0.29) and pachyconic (ww/dm ~0.73). Smooth surface of shell with a fine ornament of striae. More rounded umbilical shoulder.

Occurrence.—Muller Canyon, Augusta Mountains, Pershing County: GSUB loc. MUC, from *M. spinifer* Subzone, *G. mimetus* Zone to *P. meeki* Subzone, *P. meeki* Zone. McCoy Mine, Churchill County: Loc. HB 2001, *B. cordeyi* Subzone, *G. weitschati* Zone (Monnet and Bucher, 2005, specimen PIMUZ 25361).

Description.—Measurements of the selected specimens are provided in Table 5. The holotype (GSUB C9453; Fig. 12) is a complete specimen with a maximum diameter of 29.77 mm. Because of its large size, compared to other representatives of this new species, it is interpreted as an adult specimen; there are no other criteria for maturity. The pachyconic (ww/dm = 0.61) shell is subevolute (uw/dm = 0.37) and reveals a deeply incised umbilicus with a steep umbilical wall and a distinctive umbilical shoulder. The surface of the shell is smooth and bears a very fine ornament of striae. The venter is perfectly rounded and smooth.

Table 4. Measurements in mm of selected specimens of *Ptychites densistriatus* Bucher, 1992 collected by J. Jenks in the Fossil Hill Member of the Favret Formation. Pershing County, Nevada, USA. For further details on the bed number, see Figure 2 ("Bed No."). uw: maximum umbilical width; ww: maximum whorl width; dm: maximum diameter of shell; (): fragmented specimen, estimated value;**: specimen used for ontogenetic analysis, preservation not sufficient, cast present.

Locality	Specimen	uw	ww	dm	uw/dm	ww/dm
L 12280	NMMNH 80881	12.76	32.02	53.49	0.24	0.60
L 12280	GSUB C11439**	11.26	25.33	(43.03)	0.26	0.59

In general, smaller specimens are subinvolute and slightly more depressed than larger specimens (see Table 5). Furthermore, the umbilical shoulder is more abrupt. The internal molds of some specimens show growth constrictions (C8273, Fig. 9.4; C8254, Fig. 9.5, 9.6; C8287, Fig. 9.9).

Ontogenetic description.—The ontogenetic development of *P. embreei* n. sp. is illustrated in Figure 13, and the raw data of the analysis are supplied in the Appendix. The whorl expansion rate (WER; Fig. 13.2) shows a regular behavior with a strong decrease in the earliest stages, followed by more stable state towards the end of phase II. The slightly higher values of half whorl 7.5 and 8.5 suggest a possible acceleration of growth in later ontogenetic stages.

The values for the whorl width index (WWI; Fig. 13.3) are more scattered than the other series. However, considering the shape of the CWI trajectory (Fig. 13.4) and the more regular WWI of *P. gradinarui* (Fig. 8.3), it can be assumed that the progression of WWI is at least triphasic.

During phase I and II, the trajectories for the conch width index (CWI) and the umbilical width index (UWI) are inverse (Fig. 13.4), indicating a close relationship between these two indices. The development of UWI and CWI is similar to the C-mode ontogeny introduced by Walton and Korn (2017). However, towards later ontogenetic stages, the UWI and CWI are decoupled, which distinguishes *P. embreei* n. sp. from regular C-mode ontogeny. Whereas the conches of early stage *P. embreei* n. sp. are more globous and more involute, in the course of their growth they build slightly more discoidal and more evolute conches, resulting in a counterclockwise progression (Fig. 13.5). The decoupling of the CWI and UWI results in a distinct buckle in the progression. In general, all the trajectories (Fig. 13.2–13.5) that are long enough show a change towards the end of the second phase (growth stage 5.0 to 8.0; roughly corresponds to a growth size of 12–19 mm). These changes in the progression of the trajectories most probably mark the transition from the juvenile to the adult stage.

Etymology.—The species was named in honor of geologist Patrick G. Embree (Orangevale, CA, USA) for his contributions and broad support of the research on the Triassic of Nevada.

Materials.—In total, we collected 38 specimens of *P. embreei* n. sp. in Muller Canyon of the Augusta Mountains, Pershing County, NW Nevada, USA. Two specimens: GSUB C9642, C9643, from bed No. MUC1818; 10 specimens: GSUB C9453, C9455–C9462, C8564, from bed No. MUC2175; one specimen: GSUB C8423, from bed No. MUC2870; 19 specimens: GSUB C8254, C8265, C8267, C8269, C8270, C8272–C8280, C8285–C8287, C8290, from bed No. MUC2980; and six specimens: GSUB C9619, C9621–C9624, C10313; from bed No. MUC3239. The specimen PIMUZ 25361 was illustrated in Monnet and Bucher (2005) and is stored in the original collection of the Paleontological Institute and Museum University of Zurich, Switzerland. For further explanation on the beds see Figure 2.

Remarks.—Specimen PIMUZ 25361, referred to as *Ptychites* sp. indet. by Monnet and Bucher (2005), is regarded as

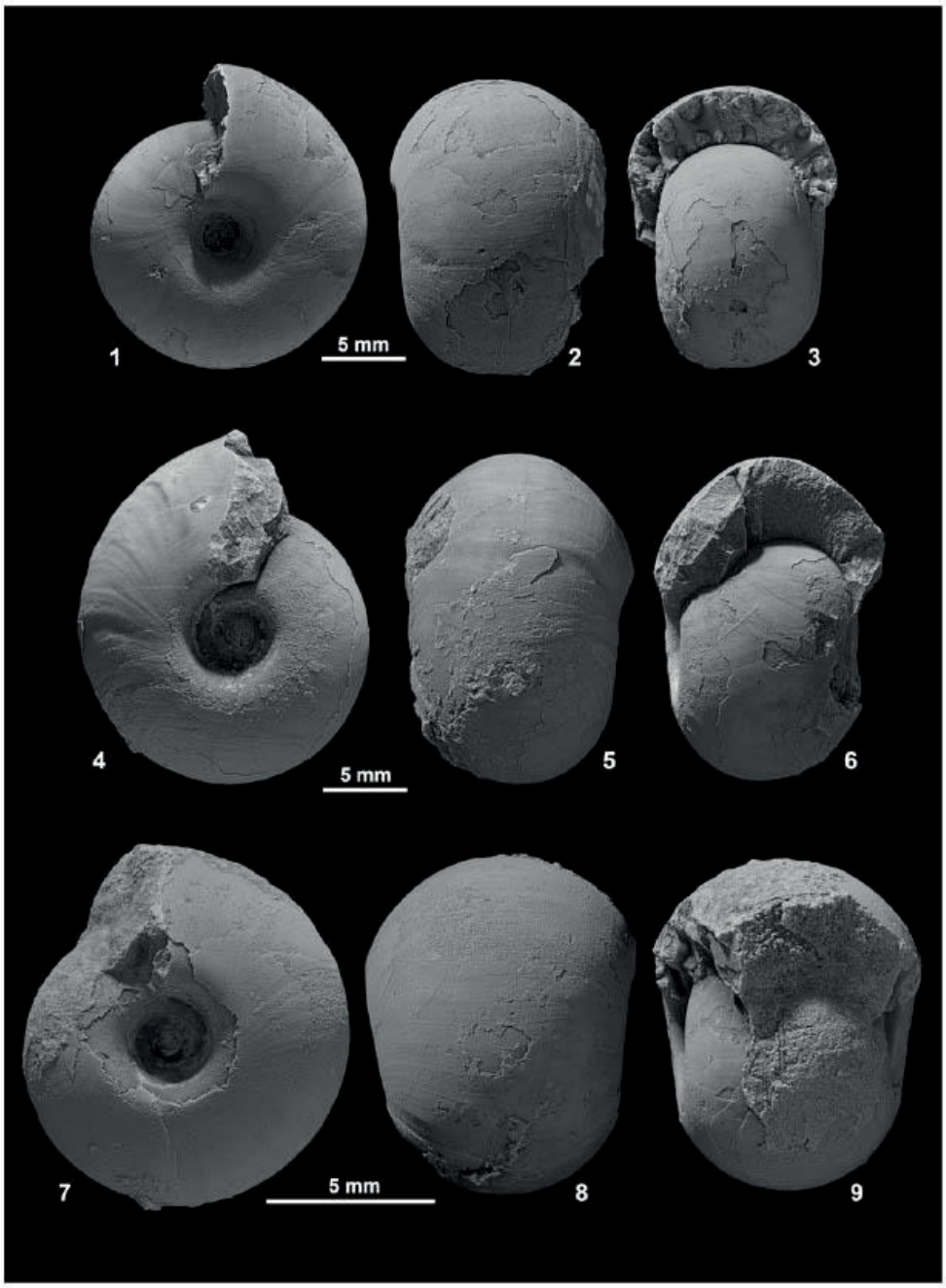

Figure 10. *Ptychites embreei* n. sp. from Muller Canyon, Augusta Mountains, Pershing County. (1–3) GSUB C8272, (4–6) GSUB C10313, (7–9) GSUB C8289 (paratype).

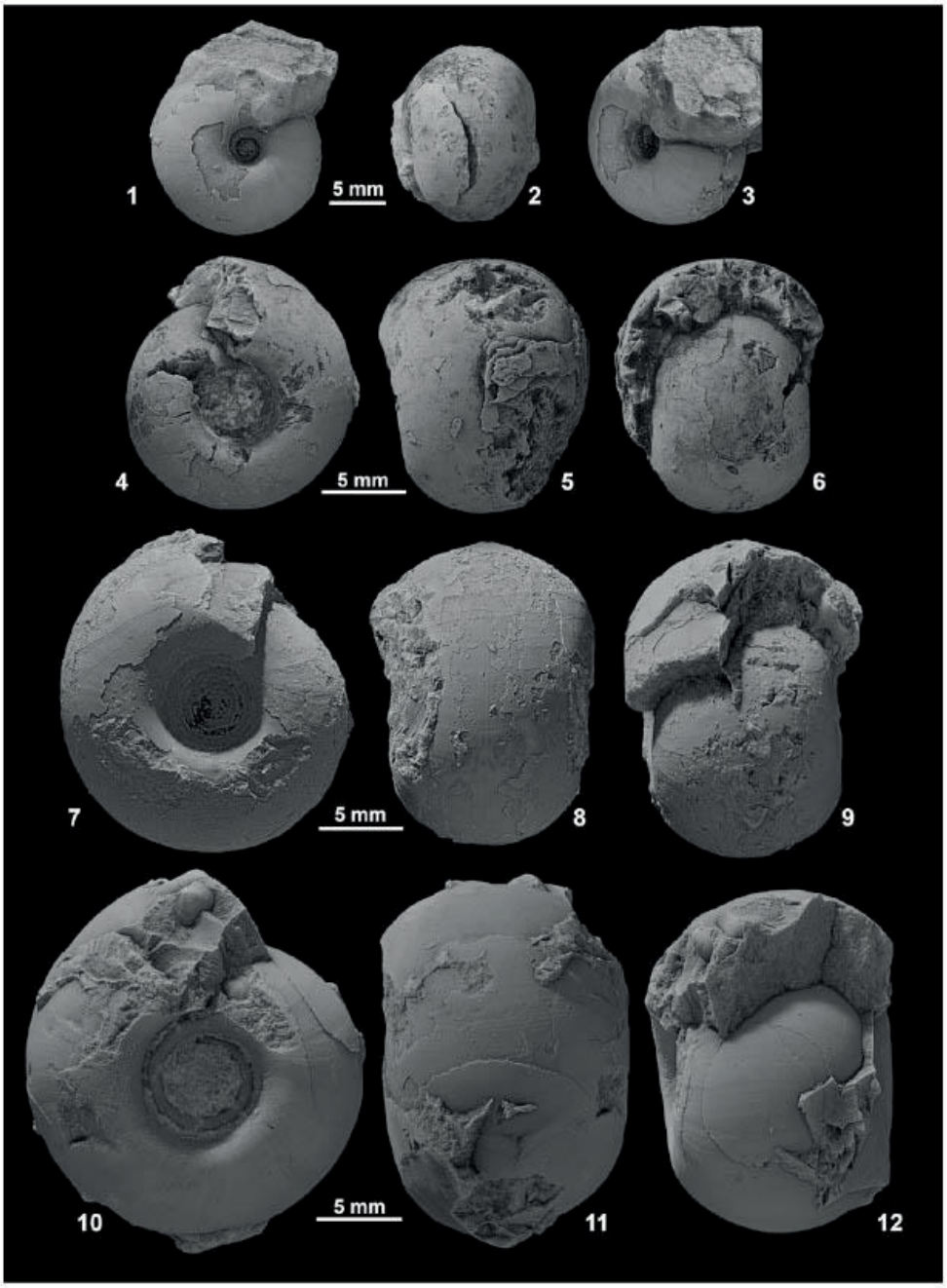

Figure 11. *Prychites embreei* n. sp. from Muller Canyon, Augusta Mountains, Pershing County. (**1–3**) GSUB C8280 (paratype), (**4–6**) GSUB C9458 (paratype), (**7–9**) GSUB C9455, (**10–12**) GSUB C9642.

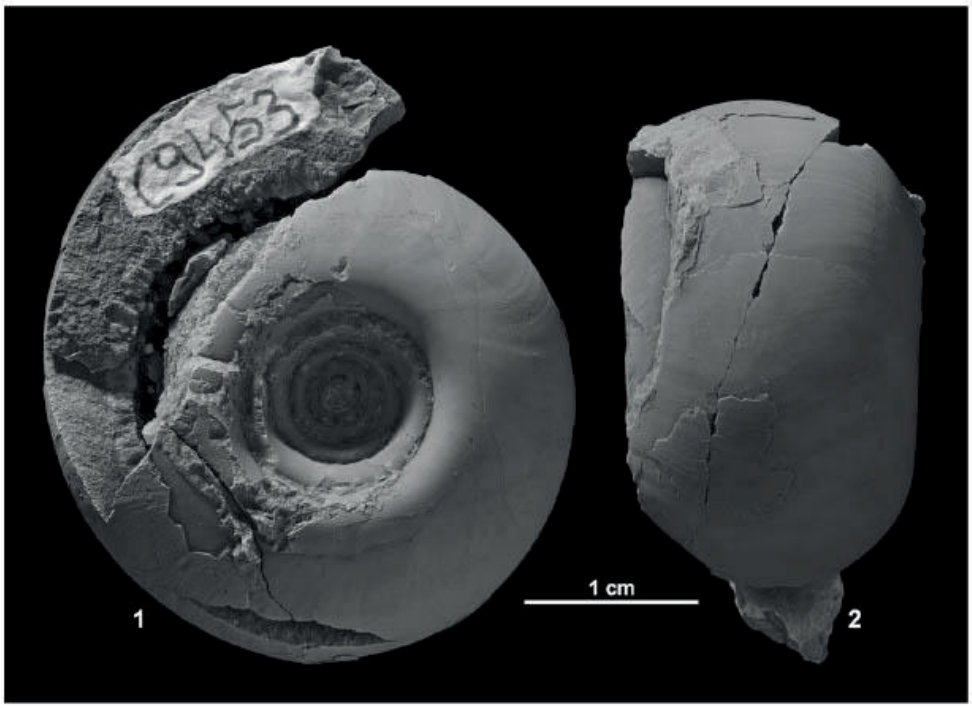

Figure 12. (1, 2) Holotype GSUB C9453 of *Ptychites embreei* n. sp. from Muller Canyon, Augusta Mountains, Pershing County.

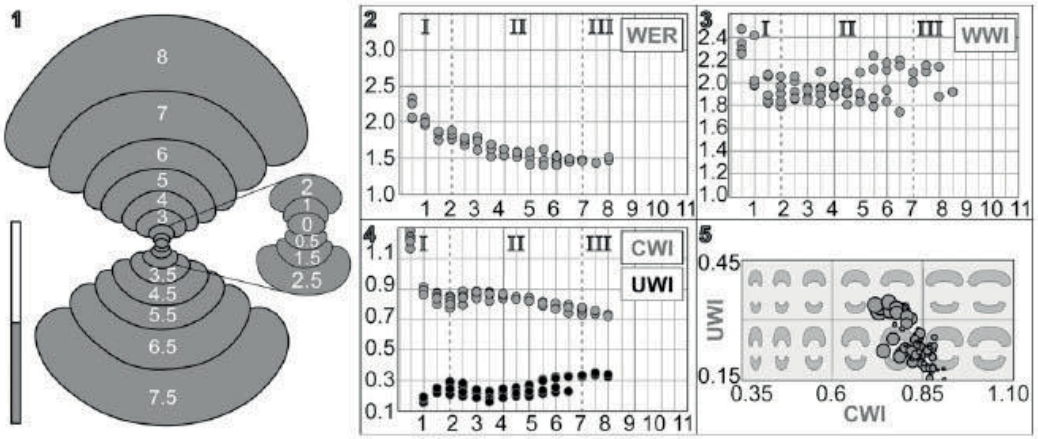

Figure 13. Ontogenetic analysis of *Ptychites embreei* n. sp. (1) Cross section of specimen GSUB C9642, scale bar units 5 mm. (2–4): Ontogenetic development of the whorl expansion rate ($WER_n = (dm_n/dm_{n-0.5})^2$), whorl width index ($WWI_n = ww_n/wh_n$), umbilical width index ($UWI_n = uw_n/dm_n$) and the conch width index ($CWI_n = ww_n/dm_n$) plotted against number of half whorls (ontogenetic stages). (5) Ratio between UWI and CWI of the available specimens. Bubble size refers to number of half whorl; the picture in the background shows the shape of the last complete whorl (developed by Korn, 2010). Roman numbers refer to interpretation of different life phases; I: Hatchling, II: Juvenile; III: Subadult–adult; for more detailed explanations see Walton and Korn (2017).

Table 5. Measurements in mm of selected specimen of *Ptychites embreei* n. sp. collected in the Fossil Hill Member of the Favret Formation at the Muller Canyon locality in the Augusta Mountains. Pershing County. Nevada. USA. Further details on the bed number see Figure 2 ("Bed No."). uw: maximum umbilical width; ww: Maximum whorl width; dm: maximum diameter of shell; (): fragmented specimen, estimated value; *: specimens used for ontogenetic analysis, cast present; **: specimen used for ontogenetic analysis, preservation not sufficient, cast present; H: holotype.

Depth	Specimen	uw	ww	dm	uw/dm	ww/dm
MUC3239	GSUB C10313**	4.84	13.28	18.66	0.26	0.71
MUC2980	GSUB C8287	1.95	8.24	10.95	0.18	0.75
MUC2980	GSUB C8280	3.69	11.80	16.24	0.23	0.73
MUC2980	GSUB C8272*	4.31	13.22	17.74	0.24	0.75
MUC2980	GSUB C8289	2.56	8.10	10.25	0.25	0.79
MUC2980	GSUB C8254	1.8	6.06	7.97	0.23	0.76
MUC2980	GSUB C8276*	1.47	6.20	7.55	0.19	0.82
MUC2870	GSUB C8423*	3.43	8.60	11.29	0.30	0.76
MUC2175	GSUB C9453 H	11.02	18.20	(29.77)	0.37	0.61
MUC2175	GSUB C9455*	5.82	13.63	19.07	0.31	0.71
MUC2175	GSUB C9458	4.53	11.45	14.65	0.31	0.78
MUC1818	GSUB C9642*	6.99	14.76	20.53	0.34	0.72
HB 2001	PIMUZ 25361	2.0	7.1	10.5	0.19	0.68

conspecific with *P. embreei* n. sp. Among the ptychitids of Nevada, *P. embreei* n. sp. covers by far the largest time span. It remains to be clarified whether this is due to biological processes or reflects a bias caused by more intensive sampling associated with this study relative to prior work.

There are two more globular genera occurring in sediments of the same age in Nevada: *Humboldtites* Silberling and Nichols, 1982 and *Proarcestes* Mojsisovics, 1893. Both genera differ from representatives of *P. embreei* n. sp. through their very involute to closed umbilicus and the more compressed shape. Furthermore, their suture lines have much narrower main saddles and a more constricted base.

Mojsisovics (1882, p. 244) divided all species of *Ptychites* in five different groups: P. rugiferi, P. megalodisci, P. subflexuosi, P. opulenti, and P. flexuosi. *Ptychites embreei* n. sp. is included into the group of P. opulenti because it agrees in being predominantly globular. The distinguishing morphologic features of different species of this group are given in Table 6. In summary, representatives of *P. embreei* n sp. differ from other *Ptychites* species mainly in having smaller growth size, the absence of ribs, and the more rounded umbilical shoulder.

The range of intraspecific variability among the material described herein is rather small. The largest differences seem to result from ontogenetic processes, which is also the case with certain Paleozoic ammonoids (e.g., Korn, 2017; Korn et al., 2018), in which the trajectories for CWI and UWI are inverses (Fig. 13.4), indicating a close relationship between these two indices. This means that, in agreement with Buckman's first Rule of Covariation (Westermann, 1966), compression co-occurs with less evolute conches.

Morphospace

In order to analyze the ontogenetic morphospaces of *Ptychites gradinarui* and *P. embreei* n. sp., a principal component analysis was performed (Fig. 14). Despite the low number of available specimens, the ontogenetic morphospaces of the two species are clearly separated in the PCA plot. The first two principal components of the PCA explain ~81.52% (PC 1: 73.76%; PC 2: 7.76%) of the observed variation. The raw data for the analysis are provided in the Appendix.

The first principal component (PC1) is mainly dominated by values of the umbilical width index (UWI) and the conch width index (CWI), which have similar loadings. On principal component 2 (PC2), however, values for the whorl expansion rate (WER) alone feature dominantly. Therefore, the axes of the analysis reflect the following: (1) high PC 1 values express a more depressed and lower values a more compressed conch shape, and (2) high PC 2 values mainly coincide with a higher WER. The right part of the morphospace is thus occupied by more pachyconic, and the left part with rather discoidal conches. Most of the ontogenetic changes are captured within changes of the umbilical diameter and the conch width. Even though *P. gradinarui* generally reaches a much larger growth size, the whorl expansion rate seems to be of minor importance for the distinction of the ontogenetic pathways of these species.

Geographic and stratigraphic occurrence of ptychitids

During the Middle Triassic, representatives of *Ptychites* were widely distributed in the Panthalassic as well as the Tethys Ocean. Here we present a summary of the biostratigraphic distribution of *Ptychites* spp. in the most significant domains (Fig. 15). The different biostratigraphic occurrences of *P. guloensis* in Nevada and British Columbia are possibly biased by a low number of specimens. However, it is apparent that the faunas of Nevada and British Columbia are similar in composition to a certain degree.

Representatives of *Flexoptychites*, closely allied to *Ptychites*, were also described from the isolated Germanic Muschelkalk Sea (e.g., Claus, 1921, 1955; Urlichs and Kurzweil, 1977), which is characterized by an endemic ammonoid fauna. In fact, ptychitids are known from the Lower and the Upper Muschelkalk, probably reflecting that the endemism is higher in the Upper Muschelkalk (see Urlichs and Mundlos, 1985; Kaim and Niedźwiedzki, 1999). However, based on the description and illustrations in the former, it cannot be verified with certainty whether the described specimens really belong to *Ptychites* or closely allied forms. Furthermore, Urlichs and Mundlos (1985) and Balini (1998) doubted that those occurrences were part of a living population and suggested a post-mortem drift of the shells from the Tethys. For those reasons, the Germanic Muschelkalk Basin was not considered in the summary of the biostratigraphical occurrences of ptychitids during the Anisian stage (Fig. 15).

Discussion

Representatives of *Ptychites* can be found in sediments that were deposited in the Panthalassic (e.g., Smith, 1914; McLearn, 1948; Tozer, 1994; Monnet and Bucher, 2005) and Tethyan Oceans (e.g., Diener, 1913; Waterhouse, 1994, 1999, 2002a, b). Due to its almost global distribution, the genus *Ptychites* has been broadly discussed in the literature, but limited research has been done in recent years. Especially the correlation between the Tethyan and Panthalassic faunas still demands further attention. In the Panthalassic realm, the co-occurrence of ptychitids in

Table 6. Morphologic comparison of different species of *Ptychites* of the *P. opulentus* group to the newly introduced species *P. embreei* n. sp. For biostratigraphic and geographic distribution, see Figure 15. U and uw: maximum umbilical width; D and dm: maximum diameter of conch; S.s.: Small specimens; L.s.: Large specimens.

Species	Average conch size	Venter and conch outline	Sculpture	Umbilic: Width	Umbilic: Shape	Adult suture line	Ontogenetic development
Ptychites embreei n. sp.	Small, < 30 mm	Venter perfectly rounded Depressed	Smooth surface, no ribs, fine growth striae S.s. some growth constrictions	S.s. subinvolute: uw/dm < 0.30 L.s. subevolute: uw/dm > 0.30	Distinct, but slightly rounded umbilical shoulder	Unknown	Ontogenetic pathways see Fig. 8
P. gradinarui Bucher, 1992 (p. 439, text-fig. 22, pl. 9, figs. 11, 12, pl. 10, figs. 1–4, pl. 11, figs. 21–26)	Larger	Subtriangular venter L.s. more compressed	L.s. fine ribbing Regular shallow growth constrictions	S.s. more evolute	Umbilical shoulder angular	Four lateral saddles, U2/A largest and highest, A/E high and slender compared to broad U3/U2, A/E lower than U2/A, usually weakly bifid. A lobe deepest lobe. Indentations with irregular fringes.	For comparison of ontogenetic pathway see Figs. 5 and 8, respectively
P. wrighti McLearn, 1946 (p. 3, pl. 4, fig. 5)	Larger	Slightly angular venter More compressed	Slight ribbing	More involute: U/D of holotype is 0.20 (McLearn, 1948)	Umbilical shoulder angular	Unknown	
P. guloensis Tozer, 1994 (p. 133, 444, figs. 35d, e, pl. 58, figs. 1, 2)	Much larger	Similar	Very fine but regular ribbing	More involute	Similar	Four lateral saddles. U2/A most prominent, only slightly larger and higher than U3/U2. A/E high and slender compared to U3/U2. U4/U3 and U1/U4 distinctly smaller than outer saddles, low number of simple indentations. U2 lobe is deepest. Even indentations only, there are no fringes.	
P. densistriatus Bucher, 1992 (p. 440, pl. 9, figs. 1–10)	Larger	Much higher whorl section More compressed and ovoid conch	Similar	S.s. more evolute L.s. more involute	Umbilical shoulder even more rounded	Unknown	
P. trochleaeformis (Lindström, 1865, p. 3, pl. 1, fig. 2)	Much larger (108 mm; Lindström, 1865)	L.s. more compressed	Regular ribbing	More involute: U/D = 20/108 = 0.19 (Lindström, 1865)	Umbilical shoulder angular	Unknown	
P. hamatus Tozer, 1994 (p. 134, pl. 65, figs. 13, 14, pl. 67, fis. 1–4 pl. 71, fig. 2a, b, text-figs. 48d, 50a, 54b)	Larger	L.s. more compressed	Similar	More involute	Umbilical wall less steep Umbilical shoulder more angular	Five lateral saddles, U2/A highest. U2/A, U3/2, U4/U3 almost same breadth, saddles fairly gently reducing in height from U2/A towards umbilical seam. A lobe much deeper than others. Mainly low indentations and only few fringes.	Transition from similar to more compressed shell outline
P. progressus Mojsisovics, 1882 (p. 259, pl. 67, figs. 4, 6)	Larger	More compressed	Regular growth constrictions	Much more involute S.s. uw/dm = 6/38 = 15.8; L.s. uw/dm = 10.67 = 14.9; Mojsisovics, 1882: p. 260	"Stairlike" (terraced) surface of umbilical wall (Mojsisovics, 1882)	Four lateral saddles. U2/A highest, U2/A, U3/2 and U4/U3 almost same breadth, saddles only gently reducing in size from U2/A towards umbilical seam. Center of U4/U3 deeply incised, almost half the height of the saddle. A lobe deepest, but U2 lobes only very slightly shallower. A number of regular fringes.	Transition from more involute to more evolute

Table 6. Continued.

Species	Average conch size	Venter and conch outline	Sculpture	Umbilic: Width	Umbilic: Shape	Adult suture line	Ontogenetic development
P. curvilobatus Diener, 1913 (p. 70, pl. 10, fig. 4)	Much larger (188 mm; Diener, 1913)	Much more compressed	Smooth ribbing	Much more involute	Umbilical wall less steep	Five lateral saddles, U2/A most prominent one, clearly larger than all others. A/E higher and larger compared to U3/U2, with mostly low and indistinct indentations distinguished from other ptychitid sutures discussed. U4/U3 and U1/U4 distinctly lower than outer saddles and U1/U4 with low number of simple indentations only. A lobe clearly deepest and most prominent. Suture line generally irregular, with irregular and regular fringes, low and rounded indentations (?preservational artifact).	
P. opulentus Mojsisovics, 1882 (p. 259, pl. 73, figs. 1–4)	Larger	S.s. conch is wider than high L.s. more compressed	S.s. regular growth constrictions Smooth ribbing	S.s. much narrower (uw/dm = 13/105 = 12.4; Mojsisovics, 1882)	Similar	Five lateral saddles, U2/A most prominent, much larger than others with narrow base compared to others. A/E higher and larger compared to U3/U2, big main indentations. U4/U3 and U1/U4 distinctly smaller than outer saddles, low number of simple indentations. Suture line with low number of irregular fringes. A lobe is clearly the deepest and most prominent lobe.	Transition from way more depressed to more compressed

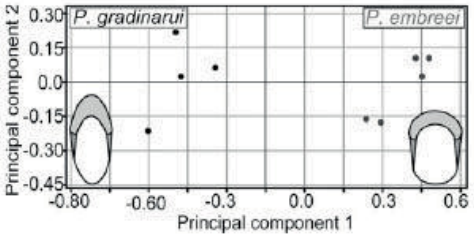

Figure 14. Principal Component Analysis (PCA) of combined ontogenetic stages of all available specimens of *Ptychites gradinarui* and *Ptychites embreei* n. sp. The parameters whorl expansion rate (WER), umbilical width index (UWI), and conch width index (CWI) were used. Every individual is defined by the sum of all parameters of all ontogenetic stages. Black dots *P. gradinarui*, gray dots *P. embreei* n. sp.

Nevada and British Columbia supports the statement of Ji and Bucher (2018) that low- and mid-paleolatitude regions were well connected during the Middle Triassic. This stresses the importance of re-evaluation of the alpha taxonomy of ptychitid species by novel or underexplored methods, as performed in this study.

Ontogenetic analysis.—Ammonoid generic diversity reached its maximum during the Triassic Period (Brayard et al., 2009). At present, few studies have investigated trends in morphological disparity of Triassic ammonoids (Monnet et al., 2015). McGowan (2004, 2005) and Brosse et al. (2013) carried out important foundational research in this field. Although the background data of both studies differ significantly, both come to the same conclusion: the taxonomic diversity and morphologic disparity of Triassic ammonoids are decoupled. However, it is open to debate whether the high diversity is also biased by taxonomic over-splitting (Forey et al., 2004; De Baets et al., 2013) of the ammonoid faunas.

A method, whose potential is far from being fully exploited, is the analysis of ontogenetic trajectories obtained from longitudinal cross-sections. The accretionary growth of ammonoids with conservation of juvenile stages allows the investigation of complete ontogenetic transformations of a set of traits, such as the conch geometry and septal characters (Korn, 2012). Therefore, ontogenetic analyses are an ideal tool to unravel phylogenetic and taxonomic relationships between ammonoid groups (Rieber, 1962). This makes them ideal for the study of evolutionary change in ontogeny through time (Naglik et al., 2015).

Walton and Korn (2017) carried out an extensive comparative ontogenetic analysis of ammonoids within the pachyconic to globular morphospace. They introduced the term C-mode ontogeny, which is by far the most common ontogeny of pachyconic to globular ammonoids. Whereas the herein discussed species *P. gradinarui* shows a C-mode ontogeny, *P. embreei* n. sp. has a different development. In phase I and II, *P. embreei* n. sp. and *P. gradinarui* have opposing trends in their relationships of the CWI and UWI (Figs. 8.5, 13.5). However, both trajectories show a distinct buckle in the curve that marks the decoupling of the UWI and CWI, which is approximately located at an UWI of 0.35 and CWI of 0.70. The change in the direction of the progression marks the onset of the third phase, during which both

	Zone (Nevada, USA)	Subzone (Nevada, USA)	Biostratigraphic distribution of *Ptychites* spp.			
			Nevada, USA Smith, 1914 Silberling & Nichols,1982 Bucher, 1992 Own data	**British Columbia** Tozer, 1994	**Spitsbergen** Weitschat & Lehmann, 1983	**Tethyan realm** Mojsisovics, 1882 Diener, 1913 Waterhouse, 2002a
„early" Ladinian	*Eoprotrachyceras subasperum*			*P. hamatus*		
late Anisian	*Frechites occidentalis*	*P. gabbi*		*P. hamatus* *P. trochleaeformis*	*	
		P. furlongi				
		N. humboldt.				
	Parafrechites meeki	*P. dunni*				
		P. meeki	*P. embreei*		*P. trochleaeformis*	
		F. nevadanus	*P. embreei*			
	Gymnotoceras rotelliformis	*G. blakei*	*P. embreei*	*P. trochleaeformis*		*P. opulentus* *P. progressus* *P. cunninghami* *
		B. vogdesi	*P. embreei*			
	Gymnotoceras mimetus	*M. spinifer*	*P. embreei*			
		D. lawsoni				
	Gymnotoceras weitschati	*R. transiformis*				
		B. cordeyi				
middle Anisian	*Balatonites shoshonensis*	*B. mojsvari*			**	
		P. fergusoni	*P. gradinarui*			
		F. wallacei	*P. gradinarui*			
		F. ransomei	*P. guloensis*			
		F. rieberi	*P. densistriatus*			
	Nevadisculites taylori	*P. tozeri*		*P. guloensis* *P. wrighti*		
		P. praebalat.				
		P. escheri	*P. wrighti*			
		P. spivaki				
		P. nicholsi				

Figure 15. Biostratigraphic distribution of Ptychites spp. The biostratigraphic framework and correlation of Nevada, British Columbia, and the Tethyan realm follows Jenks et al. (2015). For the correlation of Spitsbergen, Harland and Geddes (1997) and Weitschat and Lehmann (1983) were used. Only representatives of Ptychites discussed in this publication are listed in this table. Therefore, empty boxes do not necessarily indicate the absence of all Ptychites spp. * Indicates location of the "Ptychiten Kalke—Ptychites layers" (e.g., Mojsisovics, 1886; Spath, 1921; Gugenberger, 1927; Rosenberg, 1952; Harland and Geddes, 1997). Paleogeographic locations of the localities are provided in Figure 1. ** According to Weitschat (1986, p. 253), the preservation of middle Anisian ammonoids of Spitsbergen is not sufficient for a successful zonation of the area. Crosses mark gaps in the ammonoid biostratigraphic framework.

trajectories behave more or less collinear. According to Walton and Korn (2017), the change in conch morphologies during ontogeny could be caused by the adaptation to different niche types in the different life phases. It is questionable, whether the disparity of these two groups is significant enough to suggest two different modes of life during the earliest life phases. Nevertheless, it is very interesting to note that ptychitids have very distinct ontogenetic developments even at the species level.

In general, there is limited literature on ontogenetic analysis of individual species. However, in their study of heteromorph ammonites of the Early Cretaceous, Hoffmann et al. (2019) used similar multivariate methods as described in this study. Their study proved that the statistical evaluation of ontogenetic trajectories of ammonoids provides useful information about diversity and disparity at species level. Our study verifies that the statistical evaluation of ontogenetic processes is applicable to normally coiled planispiral ammonoid species from the Middle Triassic. Important ontogenetic changes can be visualized using univariate (Figs. 8, 13) and multivariate (Fig. 14) methods. Despite a low number of available specimens, the principal component analysis succeeded in separating the two ontogenetic morphospaces of the two ammonoid groups. This highlights the uniqueness of the ontogenetic trajectories and morphospaces that representatives of this group occupy.

Sutures.—The tapering U2/A saddle and the U1/U4 with a slender spur appear to be unique sutural features among ptychitids. However, due to the lack of specimens for comparison, it remains unclear if this is significant. No further features of the suture line of GSUB C13194, *P. guloensis*, seem to be unique (e.g., bifid endings in the A lobe occur in our material as well as in other specimens referred to the genus; sutures of *P. opulentus* Mojsisovics, 1882 [Qingge et al., 1980]; *Flexoptychites* cf. *cochleatus* [Oppel, 1863] and *P.* cf. *asura* Diener, 1895b [Win, 1991]). Our examination of published suture lines in ptychitids underlines the opinion of Köhler-Lopez and Lehmann (1984, p. 63) that suture lines of ptychitids vary significantly, "much in degree of incision," but

"not in the number of elements." These authors state that the lateral saddle of the very well-investigated species *Aristoptychites kolymensis* Kiparisova, 1937 is always extremely small and narrow. This is true for many specimens of closely related genera and their species as well, but there are exceptions to this rule and thus this cannot be generalized for this group (e.g., *P.* cf. *cochleatus* in Win, 1991). We see no clear relation of sutural features to the conch morphology of ptychitid genera. The suture lines are highly dependent on the growth stage. The very large specimen GSUB C13196 (*P. gradinarui*, Figs. 3.8–3.10, 8) shows clearly more incisions of lobes and saddles than specimens in earlier stages. Specimen GSUB C13194 (*P. guloensis*, Figs. 3.5–3.7, 4) does not show the sutural development and thus we cannot discuss the ontogeny of the suture line of the species based on our material. Nevertheless, the high number of sutural elements at the umbilical seam might indicate a multiplication of elements of the U3 as recorded by Kullmann and Wiedmann (1970). The latter was called a sutural lobe due to its position at the umbilical seam (Wedekind, 1916; "sutural" means umbilical seam in this respect); this term is problematic, though, because it only refers to the position on the shell. Köhler-Lopez and Lehmann (1984) nicely show that the U1 (with multiple subdivisions) can be located at this position as well. Therefore, we agree with Köhler-Lopez and Lehmann (1984) that a U3 developed as a sutural lobe does not characterize Ptychitidae. In fact, the sutures of many species of *Ptychites* and closely allied genera do not show this feature, including *P. compressus* Yabe and Shimizu, 1927; *P. guloensis*; *P. opulentus*; *P. wrighti*; *Discoptychites megalodiscus* (Beyrich, 1967); *Flexoptychites flexuosus* (Mojsisovics, 1882); and *Malletoptychites malletianus* (see Diener, 1895a; Onuki and Bando, 1959; McLearn, 1969; Qingge et al., 1980).

Conclusions

Here we enhance the taxonomic understanding of ptychitids, including a description of *Ptychites embreei* n. sp. from the late Anisian of Nevada. According to the state of the art, this species is the longest-ranging within the group. Furthermore, it fills a gap in the otherwise intensively studied ammonoid fauna of north-western Nevada, USA.

After the Permian/Triassic boundary, Ptychitoidea, Megaphyllitoidea, and Arcestoidea filled the cadicone morphospace (Brosse et al., 2013; De Baets et al., 2016, fig. 7). Despite the wide geographic distribution of ptychitids, they exhibit a remarkably low level of morphological variation within their morphospace. Since all ptychitids have an almost smooth shell, with a subordinate ornamentation only, one of the most important morphological descriptive features of ammonoids (Klug et al., 2015) is not applicable to the group. This means there are narrow limits regarding the shell variability in the cadicone morphospace in the Anisian, with mostly leiostracan forms (smooth shelled ammonoids; Westermann, 1996). However, some features characterizing the species seem to be hidden in a distinct ontogeny (Figs. 8, 13, 14). We emphasize the ontogenetic differences of ptychitids to other Middle Triassic ammonoids of Nevada. Ptychitids, despite their similar morphologies, have unique ontogenetic trajectories, as demonstrated above (Figs. 8, 13). Ontogenetic analyses are therefore an ideal tool to improve the alpha taxonomy of ptychitids.

Since the evaluation of ontogenetic trajectories is a rather descriptive and therefore, to some extent, subjective process, a great potential of this method lies within their statistical quantification and interpretation. This study includes one of the first attempts to quantify the ontogenetic development of individuals using statistical methods. The analysis of the very distinct ontogenetic pathways of ptychitids will serve as an important cornerstone in future studies on the statistical quantification of ontogenetic analyses of ammonoids.

Acknowledgments

First, we thank J. Jenks (Utah, USA) for providing valuable material for this study and his agreement to house these specimens at the New Mexico Museum of Natural History and Science in Albuquerque, USA. N. Ridgwell (Albuquerque, New Mexico, USA) is thanked for transferring the material collected by J. Jenks and its inventory. D. Kuhlmann (Bremen, Germany) did the mechanical preparation of the material collected by our working group and M. Krogmann (Bremen, Germany) is thanked for his broad support in the artwork for this article. Furthermore, we thank C. Anderson for critically reading the manuscript and improving the English. We would also like to express many thanks to C. Schulbert (Erlangen, Germany) and J. Titschack (Bremen, Germany) for testing CT scanning of the material at hand. C. Klug (Zurich, Switzerland) we thank for casting a specimen from the PIMUZ collection. We thank the U.S. Department of the Interior, Bureau of Land Management (BLM, Nevada State office, Winnemucca District) for permission to collect samples in the Wilderness Study Area of the Augusta Mountains, Pershing County. This research received support from the German Science Foundation (DFG), project "Nevammonoidea" (LE 1241/3-1). We thank both reviewers, C. Monnet (Lille) and M. Balini (Milan), for their very useful comments.

References

Balini, M., 1998, Taxonomy, stratigraphy and phylogeny of the new genus *Lanceoptychites* (Ammonoidea, Anisian): Rivista Italiana di Paleontologia e Stratigrafia (Research In Paleontology and Stratigraphy), v. 104, p. 143–166.

Balini, M., Lucas, S.G., Jenks, J.F., and Spielmann, J.A., 2010, Triassic ammonoid biostratigraphy: an overview: Geological Society, London, Special Publications, v. 334, p. 221–262.

Beyrich, E., 1867, Über einige Cephalopoden aus dem Muschelkalk der Alpen und über verwandte Arten: Abhandlungen der Königlichen Akademie der Wissenschaften zu Berlin 1866, p. 105–151.

Brayard, A., Bucher, H., Escarguel, G., Fluteau, F., Bourquin, S., and Galfetti, T., 2006, The Early Triassic ammonoid recovery: paleoclimatic significance of diversity gradients: Palaeogeography, Palaeoclimatology, Palaeoecology, v. 239, p. 374–395.

Brayard, A., Escarguel, G., Bucher, H., Monnet, C., Brühwiler, T., Goudemand, N., Galfetti, T., and Guex, J., 2009, Good genes and good luck: ammonoid diversity and the End-Permian mass extinction: Science, v. 325, p. 1118–1121.

Brosse, M., Brayard, A., Fara, E., and Neige, P., 2013, Ammonoid recovery after the Permian-Triassic mass extinction: a re-exploration of morphological and phylogenetic diversity patterns: Journal of the Geological Society, v. 170, p. 225–236.

Bucher, H., 1992, Ammonoids of the *Shoshonensis* Zone (Middle Anisian, Middle Triassic) from northwestern Nevada (USA): Jahrbuch der Geologischen Bundesanstalt Wien, v. 135, p. 425–465.
Claus, H., 1921, Über *Ptychites* und *Arnoites* aus dem Schaumkalk von Jena: Centralblatt für Mineralogie, Geologie und Paläontologie, v. 1921, p. 120–126.
Claus, H., 1955, Die Kopfflüsser des deutschen Muschelkalkes: Wittenberg, A. Ziemsen, v. 161, 76 p.
De Baets, K., Klug, C., and Monnet, C., 2013, Intraspecific variability through ontogeny in early ammonoids: Paleobiology, v. 39, p. 75–94.
De Baets, K., Hoffmann, R., Sessa, J.A., and Klug, C., 2016, Fossil focus: ammonoids: Palaeontology Online, v. 6, 15 p.
Diener, C., 1895a, The Cephalopoda of the Muschelkalk: Palaeontologia Indica, Memoirs of the Geological Survey of India: Calcutta, Geological Survey Office, v. 15, no. 2, 118 p.
Diener, C., 1895b, Ergebnisse einer geologischen Expedition in den Central-Himalaya von Johar, Hundes und Painkhanda: Denkschriften der mathematisch-naturwissenschaftlichen Classe der kaiserlichen Akademie der Wissenschaften, v. 62, p. 533–608.
Diener, C., 1900, Die triadische Cephalopoden-Fauna der Schiechlinghöhe bei Hallstatt: Beiträge zur Paläontologie und Geologie Österreich-Ungarns und des Orients, v. 13, p. 1–42.
Diener, C., 1907, The fauna of the Himalayan Muschelkalk: Palaeontologia Indica, Memoirs of the Geological Survey of India: Calcutta, Geological Survey Office, v. 15, no. 5, 140 p.
Diener, C., 1913, Triassic Faunæ of Kashmir: Palaeontologia Indica, v. 5, 133 p.
Forey, P.L., Fortey, R.A., Kenrick, P., and Smith, A.B., 2004, Taxonomy and fossils: a critical appraisal: Philosophical Transactions of the Royal Society of London. Series B: Biological Sciences, v. 359, p. 639–653.
Gabb, W.M., 1864, Paleontology of California. Description of the Triassic fossils of California and the adjacent territories: Philadelphia, California Geological Survey, Paleontology, v. 1, p. 17–35.
Gugenberger, O., 1927, Die Cephalopoden des herzegowinischen Ptychiten-Kalkes der Stabljana-Alpe im Volujak-Gebirge: Annalen des Naturhistorischen Museums in Wien, v. 41, p. 97–149.
Haeckel, E.H.P.A., 1899, Kunstformen der Natur: hundert Illustrationstafeln mit beschreibendem Text, allgemeinen Erläuterungen und systematische Übersicht (Band 1), Fünfzig Illustrationstafeln mit beschreibendem Text: Leipzig, Verlag des Bibliographischen Institutes, 169 p.
Haeckel, E.H.P.A., 1900, Kunstformen der Natur: hundert Illustrationstafeln mit beschreibendem Text, allgemeinen Erläuterungen und systematische Übersicht (Band 2), Fünfzig Illustrationstafeln mit beschreibendem Text: Leipzig, Verlag des Bibliographischen Institutes, 231 p.
Hammer, Ø., Harper, D.A., and Ryan, P.D., 2001, PAST: Paleontological Statistics software package for education and data analysis: Palaeontologia Electronica, v. 4(1), 9 p.
Harland, W.B., and Geddes, I., 1997, Chapter 18 Triassic history, *in* Harland, W.B., ed., The Geology of Svalbard: Geological Society, London, Memoirs, v. 17, p. 340–362.
Hauer, F.R., von, 1892, Beiträge zur Kenntnis der Cephalopoden aus der Trias von Bosnien I. Neue Funde aus dem Muschelkalk von Han Bulog bei Sarajevo: Denkschriften der kaiserlichen Akademie der Wissenschaften, v. 59, p. 251–296.
Hoffmann, R., Weinkauf, M.F.G., Wiedenroth, K., Goeddertz, P., and De Baets, K., 2019, Morphological disparity and ontogeny of the endemic heteromorph ammonite genus *Aegocrioceras* (Early Cretaceous, Hauterivian, NW-Germany): Palaeogeography, Palaeoclimatology, Palaeoecology, v. 520, 1–17 p.
Hyatt, A., 1884, Genera of fossil cephalopods: Boston Society of Natural History, Proceedings, v. 22, p. 273–338.
Hyatt, A., and Smith, J.P., 1905, The Triassic cephalopod genera of America: U.S. Geological Survey Professional Paper, v. 40, 394 p.
Jenks, J.F., Spielmann, J.A., and Lucas, S.G., 2007, Triassic ammonoids: a photographic journey, *in* Lucas, S.G., and Spielmann, J.A., eds., Triassic of the American West: New Mexico Museum of Natural History and Science Bulletin, Albuquerque, v. 40, p. 33–80.
Jenks, J.F., Monnet, C., Balini, M., Brayard, A. and Meier, M., 2015, Biostratigraphy of Triassic ammonoids, *in* Klug, C., Korn, D., De Baets, K., Kruta, I., and Mapes, R.H., eds., Ammonoid Paleobiology: From Macroevolution to Paleogeography: Topics in Geobiology, v. 40, p. 329–388.
Ji, C., and Bucher, H., 2018, Anisian (Middle Triassic) ammonoids from British Columbia (Canada): biochronological and palaeobiogeographical implications: Papers in Palaeontology, v. 4, p. 623–642.
Kaim, A., and Niedźwiedzki, R., 1999, Middle Triassic ammonoids from Silesia, Poland: Acta Palaeontologica Polonica, v. 44, p. 93–115.
Kiparisova, L.D., 1937, Fauna triasovykh otlozhenii Sovetskoi Arktiki: Transactions of the Arctic Institute 1937, p. 135–256. [in Russian]
Klug, C., Korn, D., Landman, N., Tanabe, K., De Baets, K., and Naglik, C., 2015, Describing ammonoid conchs, *in* Klug, C., Korn, D., De Baets, K., Kruta, I., and Mapes, R.H., eds., Ammonoid Paleobiology: From Macroevolution to Paleogeography: Topics in Geobiology, v. 43, p. 3–24.
Klug, C., De Baets, K., and Korn, D., 2016, Exploring the limits of morphospace: ontogeny and ecology of late Viséan ammonoids from the Tafilalt, Morocco: Acta Palaeontologica Polonica, v. 61, p. 1–14.
Köhler-Lopez, M., and Lehmann, U., 1984, The Triassic ammonite *Aristoptychites kolymensis* (Kiparisova) from Botneheia, Spitsbergen: Polar Research, v. 2, p. 61–75.
Konstantinov, A.G., 2008, Triassic ammonoids of Northeast Asia: diversity and evolutionary stages: Stratigraphy and Geological Correlation, v. 16, p. 490–502.
Korn, D., 2010, A key for the description of Palaeozoic ammonoids: Fossil Record, v. 13, p. 5–12.
Korn, D., 2012, Quantification of ontogenetic allometry in ammonoids: Evolution & Development, v. 14, p. 501–514.
Korn, D., 2017, The genus *Gonioclymenia* (Ammonoidea; Late Devonian) in Central Europe: Neues Jahrbuch für Geologie und Paläontologie—Abhandlungen, v. 284, p. 258–286.
Korn, D., and Klug, C., 2007, Conch form analysis, variability, morphological disparity, and mode of life of the Frasnian (Late Devonian) ammonoid *Manticoceras* from Coumiac (Montagne Noire, France), *in* Landman, N., Davis, R.A., and Mapes, R.H., eds., Cephalopods Present and Past: New Insights and Fresh Perspectives: Dordrecht, Springer, p. 57–85.
Korn, D., Ebbighausen, V., Bockwinkel, J., and Klug, C., 2003, The A-mode sutural ontogeny in prolecanitid ammonoids: Palaeontology, v. 46, p. 1123–1132.
Korn, D., Price, J.D., and Weyer, D., 2018, The genus *Costaclymenia* in Europe (Ammonoidea, Late Devonian): Neues Jahrbuch für Geologie und Paläontologie—Abhandlungen, v. 287, p. 249–260.
Krystyn, L., 1983, Das Epidaurus-Profil (Griechenland)—Ein Beitrag zur Conodonten-Standardzonierung des tethyalen Ladin und Unterkarn: Schriftenreihe der Erdwissenschaftlichen Kommissionen der Österreichischen Akademie der Wissenschaften, v. 5, p. 231–258.
Krystyn, L., and Mariolakos, I., 1975, Stratigraphie und Tektonik der Halstätter-Kalk-Scholle von Epidauros (Greichenland): Sitzungsberichte der Akademie der Wissenschaften in Wien, Mathematisch-Naturwissenschaftliche Klasse, Abteilung I. Mineralogie, Kristallographie, Botanik, Physiologie der Pflanzen, Zoologie, Paläontologie, Geologie, Physische Geographie und Reisen, v. 184, p. 181–195.
Krystyn, L., Balini, M., and Nicora, A., 2004, Lower and Middle Triassic stage and substage boundaries in Spiti: Albertiana, v. 30, p. 40–53.
Kullmann, J., and Wiedmann, J., 1970, Significance of sutures in phylogeny of Ammonoidea: University of Kansas Paleontological Contributions Paper, v. 47, p. 1–32.
Lindström, G., 1865, Om Trias och Juraförsteningar från Spetsbergen: Kungl. Svenska vetenskapsakademiens handlingar, v. 6, p. 1–20.
Lucas, S.G., 2010, The Triassic chronostratigraphic scale; history and status: Geological Society Special Publications, v. 334, p. 17–39.
McGowan, A.J., 2004, Ammonoid taxonomic and morphologic recovery patterns after the Permian–Triassic: Geology, v. 32, p. 665–668.
McGowan, A.J., 2005, Ammonoid recovery from the Late Permian mass extinction event: Comptes Rendus Palevol, v. 4, p. 517–530.
McLearn, F.H., 1946, A Middle Triassic (Anisian) fauna in Halfway, Sikanni Chief, and Tetsa valleys, northeastern British Columbia: Geological Survey of Canada, v. 46, p. 1–39.
McLearn, F.H., 1948, A Middle Triassic (Anisian) fauna in Halfway, Sikanni Chief, and Tetsa valleys, Northeastern British Columbia, 2nd edition, with supplement, new Middle Triassic ammonoids from northeastern British Columbia: Geological Survey of Canada, v. 46, p. 1–39.
McLearn, F.H., 1969, Middle Triassic (Anisian) ammonoids from northeastern British Columbia and Ellesmere Island: Bulletin Geological Survey of Canada, Ottawa, Department of Energy, Mines and Resources, v. 170, 59 p.
Mojsisovics, E., 1882, Die Cephalopoden der mediterranen Triasprovinz: Wien, Kaiserlich-königliche Geologische Reichsanstalt, v. 10, 322 p.
Mojsisovics, E., 1886, Arktische Triasfaunen. Beiträge zur paläontologischen Charakteristik der arktisch-pacifischen Triasprovinz: Mémoires de l'Académie impériale des sciences de St.-Pétersbourg, v. 7, 160 p.
Mojsisovics, E., 1893, Das Gebirge um Hallstatt, 1. Abtheilung—Die Cephalopoden der Hallstätter Kalke. II. Band: Abhandlungen der Kaiserlich-Königlichen Geologischen Reichsanstalt, v. 6, Hälfte, 835 p.
Monnet, C., and Bucher, H., 2005, New middle and late Anisian (Middle Triassic) ammonoid faunas from Northwestern Nevada (USA): taxonomy and biochronology: Fossils and Strata, v. 52, 121 p.
Monnet, C., Brayard, A., and Brosse, M., 2015, Evolutionary trends of Triassic ammonoids, *in* Klug, C., Korn, D., De Baets, K., Kruta, I., and Mapes, R. H., eds., Ammonoid Paleobiology: From Macroevolution to Paleogeography: Topics in Geobiology, v.44, p. 25–50.
Naglik, C., Monnet, C., Goetz, S., Kolb, C., De Baets, K., Tajika, A., and Klug, C., 2015, Growth trajectories of some major ammonoid sub-clades revealed by serial grinding tomography data: Lethaia, v. 48, p. 29–46.

Neumayr, M., 1875, Die Ammoniten der Kreide und die Systematik der Ammonitiden: Zeitschrift der deutschen geologischen Gesellschaft, v. 27, p. 854–942.
Onuki, Y., and Bando, Y., 1959, On some Triassic ammonites from the Rifu Formation. Stratigraphical and paleontological studies of the Triassic System in the Kitakami Massif, northeastern Japan: Contributions from the Institute of Geology and Paleontology, Tohoku University, v. 50, p. 70–80.
Oppel, A., 1863, Über ostindische Fossilreste aus den secundären Ablagerungen von Spiti und Gnari-Khorsum in Tibet. Beschreibung der von den Herren Adolf, Hermann und Rober Schlagintweit während der Jahre 1854 bis 1857 gesammelten Arten: Palaeontologische Mittheilungen aus dem Museum des Königlich-Bayerischen Staates, v. 1, p. 267–304.
Péron, S., Bourquin, S., Fluteau, F., and Guillocheau, F., 2005, Paleoenvironment reconstructions and climate simulations of the Early Triassic: Impact of the water and sediment supply on the preservation of fluvial systems: Geodinamica Acta, v. 18, p. 431–446.
Pomoni, F.A., and Tselepidis, V., 2013, Lithofacies palaeogeography and biostratigraphy of the lowermost horizons of the Middle Triassic Hallstatt Limestones (Argolis Peninsula, Greece): Journal of Palaeogeography, v. 2, p. 252–274.
Qingge, G., Guoxiong, H., and Yigang, W., 1980, Discovery of the Late Anisian *Paraceratites trinodosus* Fauna (Ammonoidea) from Doilungdeqen, Tibet and its significance: Acta Palaeontologica Sinica, v. 19, p. 343–356.
Renz, C., 1910, Die mesozoischen Faunen Griechenlands: Palaeontographica, v. 58, p. 1–105.
Rieber, H., 1962, Beobachtungen an Ammoniten aus dem Ober-Aalénien (Systematik und Ontogenie): Eclogae Geologicae Helvetiae, v. 55, p. 587–594.
Rosenberg, G., 1952, Vorlage einer Schichtennamentabelle der Nord- und Südalpinen Mitteltrias der Ostalpen: Mitteilungen der Geologischen Gesellschaft in Wien, v. 42–43 (1949–1950), p. 235–247.
Salopek, M., 1911, Über die Cephalopodenfauna der Mittleren Trias von Süddalmatien und Montenegro: Abhandlungen der Königlich Kaiserlichen Geologischen Reichsanstalt, v. 16, p. 1–44.
Silberling, N.J., and Nichols, D.J., 1982, Middle Triassic molluscan fossils of biostratigraphic significance from the Humboldt Range, northwestern Nevada: U.S. Geological Survey Professional Paper, v. 1207, 77 p.
Silberling, N.J., and Tozer, E.T., 1968, Biostratigraphic classification of the marine Triassic in North America: Special Paper Geological Society of America, v. 110, 63 p.
Skrzycki, P., Niedźwiedzki, G., and Tałanda, M., 2018, Dipnoan remains from the Lower-Middle Triassic of the Holy Cross Mountains and northeastern Poland, with remarks on dipnoan palaeobiogeography: Palaeogeography, Palaeoclimatology, Palaeoecology, v. 496, p. 332–345.
Smith, J.P., 1914, The Middle Triassic marine invertebrate faunas of North America: U.S. Geological Survey Professional Paper, v. 83, 254 p.
Spath, L.F., 1921, On ammonites from Spitsbergen: Geological Magazine, v. 58, p. 297–305.
Stoliczka, F., 1865, Geological sections across the Himalaya Mountains from Wangtu bridge on the river Sutlej to Sungdo on the Indus; with an account of the formations in Spiti accompanied by a revision of all known fossils from that district: India Geological Survey Memoirs, v. 5, p. 1–154.
Tozer, E.T., 1971, Triassic time and ammonoids: problems and proposals: Canadian Journal of Earth Sciences, v. 8, p. 989–1031.
Tozer, E.T., 1981, Triassic Ammonoidea: classification, evolution and relationship with Permian and Jurassic forms, *in* House, M.R., and Senior, J.R., eds., The Ammonoidea: The Systematics Association Special Volume, v. 18, p. 65–100.
Tozer, E.T., 1984, The Trias and its ammonoids: the evolution of a time scale: Geological Survey of Canada, Miscellaneous Report, v. 35, 171 p.
Tozer, E.T., 1994, Canadian Triassic ammonoid faunas: Bulletin Geological Survey of Canada, v. 467, 663 p.
Urlichs, M., and Kurzweil, W., 1977, Erstnachweis von *Flexoptychites* (Ammonoidea) aus dem Oberen Muschelkalk (Mitteltrias) Nordwürttembergs: Stuttgarter Beiträge zur Naturkunde. Serie B. Geologie und Paläontologie, v. 253, p. 1–8.
Urlichs, M., and Mundlos, R., 1985, Immigration of cephalopods into the Germanic Muschelkalk Basin and its influence on their suture line, *in* Bayer, U., and Seilacher, A., eds., Lecture Notes in Earth Sciences: Berlin and Heidelberg, Springer, v. 1, p. 221–236.
Vörös, A., 2018, The Upper Anisian ammonoids of the Balaton Highland (Middle Triassic, Hungary): Geologica Hungarica—Series Palaeontologica Table, v. 60, p. 1–241.
Walton, S. A., and Korn, D., 2017, Iterative ontogenetic development of ammonoid conch shapes from the Devonian through to the Jurassic: Palaeontology, v. 60, p. 703–726.
Walton, S.A., and Korn, D., 2018, An ecomorphospace for the Ammonoidea: Paleobiology, v. 44, p. 273–289.
Waterhouse, J.B., 1994, The Early and Middle Triassic ammonoid succession of the Himalayas in western and central Nepal. Part 1. Stratigraphy, Classification and Early Scythian ammonoid systematics: Palaeontographica, v. 232, 83 p.
Waterhouse, J.B., 1999, The Early and Middle Triassic ammonoid succession of the Himalayas in western and central Nepal. Part 5. Systematic studies of the early Anisian: Palaeontographica, v. 255, 84 p.
Waterhouse, J.B., 2002a, The Early and Middle Triassic ammonoid succession of the Himalayas in western and central Nepal. Part 6. Mukut (mostly Anisian) ammonoids from Manang: Palaeontographica, v. 266, p. 121–198.
Waterhouse, J.B., 2002b, The Early and Middle Triassic ammonoid succession of the Himalayas in western and central Nepal. Part 7. Late Anisian ammonoids of the Himalayas in western and central Nepal: Palaeontographica, v. 267, p. 1–118.
Wedekind, R., 1916, Über Lobus, Suturallobus und Inzision: Centralblatt für Mineralogie, Geologie und Paläontologie, v. 1916, p. 185–195.
Weitschat, W., 1986, Phosphatisierte Ammonoideen aus der Mittleren Trias von Central-Spitzbergen: Mitteilungen aus dem Geologisch-Paläontologischen Institute der Universität Hamburg, v. 61, p. 249–279.
Weitschat, W., and Lehmann, U., 1983, Stratigraphy and ammonoids from the Middle Triassic Botneheia Formation (*Daonella* shales) of Spitsbergen: Mitteilungen aus dem Geologisch-Paläontologischen Institut der Universität Hamburg, v. 1983, p. 27–54.
Westermann, G.E.G., 1966, Covariation and taxonomy of the Jurassic ammonite *Sonninia adicra* (Waagen): Neues Jahrbuch für Geologie und Paläontologie, Abhandlungen, v. 124(3), p. 289–312.
Westermann, G.E.G., 1996, Ammonoid life and habit, *in* Landman, N.H., Tanabe, K., and Davis, R.A., eds., Ammonoid Paleobiology: Topics in Geobiology, v. 13, p. 607–707.
Win, Z., 1991, Triassic ammonites from the Plateau Limestone east of Lungyaw and Baukkewzu, Myit-Tha and Ywa-Ngan townships, Myanmar: Georeports, v. 1, p. 75–87.
Yabe, H., and Shimizu, S., 1927, The Triassic fauna of Rifu, near Sendai: The Science Reports of the Tohoku Imperial University, Sendai, Japan, v. 11, p. 101–136.

Appendix

Morphometric data for the available specimens that were measured on the cross-sections and used for the ontogenetic analysis

GSUB Specimen No.	No. of whorl / growth stage	dm [mm]	ww [mm]	wh [mm]	uw [mm]	CWI	UWI	WWI	WER
Cl 1442	8.5	32.44	22.99	12.64	10.31	0.71	0.32	1.82	1.64
	8	25.35	18.35	9.49	8.73	0.72	0.34	1.93	1.60
	7.5	20.03	14.49	7.13	7.23	0.72	0.36	2.03	1.58
	7	15.92	11.35	5.66	5.83	0.71	0.37	2.01	1.56
	6.5	12.74	8.90	4.43	4.81	0.70	0.38	2.01	1.64
	6	9.94	6.92	3.49	3.96	0.70	0.40	1.98	1.61
	5.5	7.84	5.58	2.48	3.27	0.71	0.42	2.25	1.50
	5	6.39	4.37	2.09	2.70	0.68	0.42	2.10	1.54
	4.5	5.15	3.55	1.60	2.21	0.69	0.43	2.21	1.52
	4	4.18	2.67	1.34	1.74	0.64	0.42	2.00	1.63
	3.5	3.28	2.20	1.11	1.37	0.67	0.42	1.99	1.66
	3	2.54	1.58	0.81	1.04	0.62	0.41	1.96	1.61
	2.5	2.00	1.24	0.69	0.73	0.62	0.37	1.80	1.59
	2	1.59	1.01	0.58	0.51	0.64	0.32	1.75	1.74
	1.5	1.21	0.87	0.50	0.33	0.72	0.27	1.75	1.87
	1	0.88	0.75	0.38	0.17	0.85	0.19	1.97	2.00
	0.5	0.62	0.71	0.33		1.14		2.12	2.52
	0	0.39	0.64	0.39					
Cl 1441	8.5	37.10	27.47	13.69	12.98	0.74	0.35	2.01	1.59
	8	29.41	22.31	10.43	10.70	0.76	0.36	2.14	1.58
	7.5	23.43	17.45	8.29	8.91	0.74	0.38	2.11	1.60
	7	18.51	13.59	6.23	7.37	0.73	0.40	2.18	1.58
	6.5	14.72	10.70	4.91	6.06	0.73	0.41	2.18	1.55
	6	11.82	8.29	3.75	5.01	0.70	0.42	2.21	1.53
	5.5	9.55	6.71	3.06	4.11	0.70	0.43	2.19	1.52
	5	7.75	5.35	2.38	3.26	0.69	0.42	2.25	1.52
	4.5	6.29	4.28	2.10	2.59	0.68	0.41	2.03	1.57
	4	5.02	3.32	1.60	2.08	0.66	0.41	2.08	1.57
	3.5	4.01	2.79	1.35	1.60	0.70	0.40	2.07	1.60
	3	3.17	1.95	1.06	1.26	0.62	0.40	1.84	1.63
	2.5	2.48	1.62	0.85	0.99	0.65	0.40	1.91	1.61
	2	1.95	1.16	0.64	0.78	0.60	0.40	1.82	1.69
	1.5	1.50	1.00	0.53	0.53	0.66	0.35	1.87	1.94

Continued.

GSUB Specimen No.	No. of whorl / growth stage	dm [mm]	ww [mm]	wh [mm]	uw [mm]	CWI	UWI	WWI	WER
	1	1.08	0.82	0.44	0.23	0.76	0.21	1.86	2.25
	0.5	0.72	0.78	0.41		1.08		1.90	2.93
	0	0.42	0.75	0.42					
C11443	10.5	84.99	40.76	37.38	20.43	0.48	0.24	1.09	1.72
	10	64.76	33.99	27.17	17.28	0.52	0.27	1.25	1.69
	9.5	49.78	28.30	20.30	14.88	0.57	0.30	1.39	1.66
	9	38.59	23.10	14.60	12.61	0.60	0.33	1.58	1.66
	8.5	29.98	18.91	11.38	10.36	0.63	0.35	1.66	1.67
	8	23.20	15.81	8.24	8.45	0.68	0.36	1.92	1.60
	7.5	18.37	12.69	6.51	6.90	0.69	0.38	1.95	1.55
	7	14.75	9.83	4.96	6.14	0.67	0.42	1.98	1.55
	6.5	11.86	7.82	3.66	5.10	0.66	0.43	2.14	1.50
	6	9.67	6.55	3.11	4.20	0.68	0.43	2.11	1.54
	5.5	7.80	5.27	2.37	3.36	0.68	0.43	2.23	1.53
	5	6.31	4.21	2.08	2.74	0.67	0.43	2.03	1.55
	4.5	5.06	3.29	1.49	2.17	0.65	0.43	2.20	1.53
	4	4.09	2.71	1.40	1.74	0.66	0.43	1.94	1.70
	3.5	3.14	2.07	0.95	1.35	0.66	0.43	2.17	1.45
	3	2.61	1.72	0.83	1.10	0.66	0.42	2.06	1.55
	2.5	2.10	1.33	0.68	0.84	0.64	0.40	1.97	1.48
	2	1.72	1.14	0.57	0.67	0.66	0.39	1.99	1.53
	1.5	1.39	0.97	0.48	0.45	0.70	0.32	2.03	1.60
	1	1.10	0.81	0.46	0.22	0.74	0.20	1.75	2.20
	0.5	0.74	0.77	0.41		1.04		1.86	2.53
	0	0.47	0.70	0.47					
C11440	6.5	15.97	11.23	5.66	5.77	0.70	0.36	1.98	1.58
	6	12.68	8.91	4.53	4.73	0.70	0.37	1.97	1.56
	5.5	10.15	7.39	3.42	3.99	0.73	0.39	2.16	1.54
	5	8.17	5.59	2.73	3.30	0.68	0.40	2.04	1.53
	4.5	6.61	4.60	2.13	2.71	0.70	0.41	2.16	1.51
	4	5.38	3.70	1.76	2.10	0.69	0.39	2.10	1.51
	3.5	4.37	2.93	1.52	1.68	0.67	0.39	1.93	1.59
	3	3.46	2.13	1.17	1.32	0.62	0.38	1.82	1.59
	2.5	2.75	1.85	0.97	1.02	0.67	0.37	1.90	1.67
	2	2.13	1.36	0.75	0.78	0.64	0.36	1.80	1.73
	1.5	1.62	1.14	0.60	0.50	0.70	0.31	1.90	1.65
	1	1.26	0.87	0.52	0.28	0.69	0.22	1.69	2.05
	0.5	0.88	0.86	0.47		0.97		1.83	2.91
	0	0.52	0.72	0.52					
C8272	7	17.65	12.86	7.44	4.10	0.73	0.23	1.73	1.52
	6.5	14.29	10.60	6.10	3.19	0.74	0.22	1.74	1.52
	6	11.59	9.17	5.00	2.52	0.79	0.22	1.83	1.57
	5.5	9.26	7.27	4.07	1.95	0.79	0.21	1.79	1.57
	5	7.40	6.10	3.24	1.47	0.82	0.20	1.88	1.60
	4.5	5.85	4.85	2.69	1.16	0.83	0.20	1.80	1.59
	4	4.64	3.93	2.01	1.00	0.85	0.22	1.96	1.64
	3.5	3.63	3.18	1.63	0.75	0.88	0.21	1.95	1.67
	3	2.81	2.42	1.24	0.61	0.86	0.22	1.95	1.65
	2.5	2.19	1.92	0.96	0.50	0.88	0.23	2.01	1.78
	2	1.64	1.40	0.73	0.39	0.85	0.24	1.90	1.79
	1.5	1.23	1.07	0.52	0.29	0.87	0.24	2.05	1.85
	1	0.90	0.82	0.41	0.14	0.91	0.15	1.99	1.96
	0.5	0.64	0.82	0.35		1.28		2.34	2.30
	0	0.42	0.71	0.42					
C9455	8	18.72	13.64	7.27	6.03	0.73	0.32	1.88	1.47
	7.5	15.46	11.34	5.42	5.13	0.73	0.33	2.09	1.43
	7	12.92	9.82	4.91	4.17	0.76	0.32	2.00	1.48
	6.5	10.62	8.44	3.85	3.46	0.79	0.33	2.19	1.44
	6	8.83	7.00	3.32	2.85	0.79	0.32	2.11	1.46
	5.5	7.31	5.97	2.67	2.22	0.82	0.30	2.24	1.47
	5	6.04	5.05	2.42	1.56	0.84	0.26	2.08	1.51
	4.5	4.92	4.11	2.06	1.15	0.84	0.23	2.00	1.55
	4	3.95	3.33	1.71	0.93	0.84	0.23	1.95	1.54
	3.5	3.19	2.75	1.31	0.72	0.86	0.22	2.09	1.52
	3	2.58	2.16	1.16	0.55	0.84	0.21	1.87	1.61

Continued.

GSUB Specimen No.	No. of whorl / growth stage	dm [mm]	ww [mm]	wh [mm]	uw [mm]	CWI	UWI	WWI	WER
	2.5	2.03	1.79	0.87	0.52	0.88	0.26	2.05	1.70
	2	1.56	1.31	0.64	0.43	0.84	0.28	2.05	1.78
	1.5	1.17	1.02	0.49	0.27	0.87	0.23	2.07	1.75
	1	0.89	0.80	0.41	0.16	0.91	0.18	1.97	1.96
	0.5	0.63	0.79	0.32		1.24		2.47	2.32
	0	0.41	0.64	0.41					
C9642	8	20.50	14.73	7.68	6.94	0.72	0.34	1.92	1.52
	7.5	16.65	12.58	5.88	5.75	0.76	0.35	2.14	1.43
	7	13.91	10.80	5.02	4.60	0.78	0.33	2.15	1.46
	6.5	11.51	8.96	4.30	3.67	0.78	0.32	2.09	1.49
	6	9.44	7.60	3.55	2.93	0.81	0.31	2.14	1.40
	5.5	7.98	6.42	2.96	2.33	0.80	0.29	2.17	1.40
	5	6.75	5.69	2.69	1.80	0.84	0.27	2.11	1.41
	4.5	5.68	4.71	2.26	1.43	0.83	0.25	2.08	1.51
	4	4.62	3.85	1.99	1.11	0.83	0.24	1.93	1.63
	3.5	3.62	2.97	1.52	0.81	0.82	0.22	1.96	1.62
	3	2.84	2.50	1.29	0.67	0.88	0.24	1.94	1.77
	2.5	2.14	1.70	0.88	0.59	0.79	0.28	1.93	1.68
	2	1.65	1.27	0.67	0.48	0.77	0.29	1.91	1.76
	1.5	1.25	1.00	0.51	0.30	0.80	0.24	1.96	1.83
	1	0.92	0.80	0.44	0.16	0.87	0.18	1.82	1.97
	0.5	0.66	0.77	0.32		1.17		2.41	2.05
	0	0.46	0.67	0.46					
C8276	5	7.55	6.20	3.40	1.47	0.82	0.19	1.82	1.59
	4.5	5.98	5.07	2.68	1.14	0.85	0.19	1.89	1.59
	4	4.74	4.06	2.16	0.86	0.86	0.18	1.88	1.63
	3.5	3.72	3.25	1.72	0.65	0.87	0.18	1.89	1.70
	3	2.85	2.50	1.35	0.53	0.88	0.18	1.86	1.80
	2.5	2.13	1.82	0.98	0.41	0.85	0.19	1.85	1.75
	2	1.61	1.32	0.74	0.33	0.82	0.20	1.79	1.82
	1.5	1.19	1.01	0.55	0.25	0.84	0.21	1.84	1.87
	1	0.87	0.78	0.39	0.15	0.89	0.18	1.98	2.05
	0.5	0.61	0.75	0.33		1.23		2.29	2.25
	0	0.41	0.66	0.41					
C8423	6	11.18	8.59	4.44	2.84	0.77	0.25	1.93	1.52
	5.5	9.07	7.26	3.90	2.10	0.80	0.23	1.86	1.62
	5	7.12	5.83	3.07	1.60	0.82	0.22	1.90	1.59
	4.5	5.65	4.69	2.45	1.20	0.83	0.21	1.91	1.58
	4	4.49	3.90	1.99	0.81	0.87	0.18	1.96	1.62
	3.5	3.52	3.06	1.68	0.55	0.87	0.16	1.82	1.69
	3	2.71	2.38	1.29	0.49	0.88	0.18	1.84	1.73
	2.5	2.06	1.73	0.93	0.46	0.84	0.22	1.86	1.78
	2	1.54	1.23	0.67	0.37	0.80	0.24	1.83	1.89
	1.5	1.12	0.94	0.50	0.27	0.84	0.24	1.89	1.87
	1	0.82	0.71	0.35	0.16	0.86	0.19	2.02	2.00
	0.5	0.58	0.71	0.31		1.21		2.25	2.06
	0	0.40	0.65	0.40					

in this study. dm: maximum diameter at respective growth stage (number of half whorl); ww: maximum whorl width (in mm); wh: maximum whorl height (in mm); uw: maximum umbilical width (calculated, in mm); $WER_n = (dm_n/dm_{n-0.5})^2$, whorl expansion rate; $UWI_n = uw_n/dm_n$, umbilical width index; $CWI_n = ww_n/dm_n$, conch width index; $WWI_n = ww_n/wh_n$, whorl width index.

Accepted: 3 April 2020

4.3 Second case study

Ontogeny of highly variable ceratitid ammonoids

from the Anisian (Middle Triassic)

Eva A. Bischof, Nils Schlüter, Dieter Korn, Jens Lehmann

Published in PeerJ

Please cite the following publication as a journal article and not as a thesis chapter:

Bischof EA, Schlüter N, Korn D, and Lehmann J. 2021. Ontogeny of highly variable ceratitid ammonoids from the Anisian (Middle Triassic). PeerJ 9:e10931. 0.7717/peerj.10931. https://peerj.com/articles/10931/

PeerJ

Ontogeny of highly variable ceratitid ammonoids from the Anisian (Middle Triassic)

Eva Alexandra Bischof[1], Nils Schlüter[2], Dieter Korn[2] and Jens Lehmann[1]

[1] Geowissenschaftliche Sammlung, FB5 Geowissenschaften, Universität Bremen, Bremen, Germany
[2] Museum für Naturkunde, Leibniz-Institut für Evolutions-und Biodiversitätsforschung, Berlin, Germany

ABSTRACT

Ammonoids reached their greatest diversity during the Triassic period. In the early Middle Triassic (Anisian) stage, ammonoid diversity was dominated by representatives of the family Ceratitidae. High taxonomic diversity can, however, be decoupled from their morphologic disparity. Due to its high phenotypic variability, the high diversity of ceratitids of the Anisian of Nevada was initially assumed to be caused by artificial over-splitting. This study aims to contribute data to settle this issue by applying geometric morphometrics methods, using landmarks and semi-landmarks, in the study of ontogenetic cross-sections of ammonoids for the first time. The results reveal that alterations in ontogenetic trajectories, linked to heterochronic processes, lead to the morphologic diversification of the species studied herein. Our knowledge, based on these ontogenetic changes, challenge the traditional treatment of species using solely adult characters for their distinction. This study furthermore demonstrates that the high diversity of the Anisian ammonoid assemblages of Nevada based on the traditional nomenclatoric approach is regarded to be reasonably accurate.

Subjects Biodiversity, Evolutionary Studies, Paleontology, Taxonomy, Zoology
Keywords Ammonoidea, Ceratitidae, Anisian, Nevada, Geometric morphometrics, Ontogeny, Phenotypic variation, Beyrichitinae, Paraceratitinae, Fossil Hill Member

Submitted 12 November 2020
Accepted 21 January 2021
Published 2 March 2021

Corresponding author
Eva Alexandra Bischof,
bischof@uni-bremen.de

Academic editor
Brandon Hedrick

Additional Information and Declarations can be found on page 20

DOI 10.7717/peerj.10931

INTRODUCTION

After the Permian-Triassic mass extinction event, ammonoids flourished and spread globally to become an important part of the marine biota (*House, 1993*; *Brosse et al., 2013*; *Brayard & Bucher, 2015*; *Neige, 2015*). They reached their greatest generic diversity of all time in the Triassic Period (*Brayard et al., 2009*; *Whiteside & Ward, 2011*). The diversity peak in the late Anisian is dominated by genera of the family Ceratitidae (*Brayard et al., 2009*; supporting material Fig. S2). Not least due to their wide paleogeographic distribution and high diversity as well as abundance in the fossil record, ammonoids are an excellent biostratigraphic tool. This is especially true for members of the family Ceratitidae *Mojsisovics 1879* after which many North American Anisian biostratigraphic zones and subzones are named (*Jenks et al., 2015*; figs. 13.13, 13.14).

The fossil material used in this study was collected in the late Anisian Fossil Hill Member of the Star Peak Basin in north-western Nevada, USA. The studied successions are considered to be the world's most complete low-paleolatitude successions, yielding

How to cite this article Bischof EA, Schlüter N, Korn D, Lehmann J. 2021. Ontogeny of highly variable ceratitid ammonoids from the Anisian (Middle Triassic). *PeerJ* 9:e10931 http://doi.org/10.7717/peerj.10931

late Anisian ammonoid assemblages (*Monnet & Bucher, 2005*). The first comprehensive taxonomic work on the Anisian ammonoid communities of the famous fossil locality at Fossil Hill in the Humboldt Range was published by *Smith (1914)* in his monograph on the North American Middle Triassic marine invertebrates. According to the taxonomic practice of his time, he described or listed a total of 110 ammonoid species from Fossil Hill. More recently, *Silberling & Nichols (1982)*, *Bucher (1992)* and *Monnet & Bucher (2005)* refined the original alpha taxonomy and the biostratigraphy with contemporaneous methods and reduced the number to 81 valid species (*Brosse et al., 2013*). However, it is important to note that succeeding assemblages show a progressive shift in morphology; therefore, the cutoff between contiguous species is essentially arbitrary (*Silberling, 1962*; *Silberling & Nichols, 1982*). This challenges the taxonomic concept and sheds new light on diversity patterns in general. An increasing number of studies suggest that the seemingly high diversity could in some cases be artificially inflated by taxonomic over-splitting (i.e., *Kennedy & Cobban, 1976*; *Forey et al., 2004*; *De Baets, Klug & Monnet, 2013*; *Knauss & Yacobucci, 2014*; *De Baets et al., 2015*). Furthermore, taxonomic diversity and morphological disparity of Triassic ammonoids were probably decoupled (*McGowan, 2004*; *McGowan, 2005*; *Brosse et al., 2013*). At present, only a few studies have investigated trends in morphological disparity of Triassic ammonoids (*Monnet, Brayard & Brosse, 2015*).

Previous studies have proven that—particularly due to their accretionary planispiral conch growth with conservation of previous growth stages—ammonoids offer a high-resolution data set for ontogenetic, developmental and also taxonomic studies. While the study of conch ontogeny has a long history in the study of Paleozoic ammonoids (e.g., *Korn & Klug, 2007*; *Korn, 2010*; *Monnet, De Baets & Klug, 2011*; *Naglik et al., 2015*), it was only rarely examined on Mesozoic ammonoids (e.g., *Rieber, 1962*; *Tajika et al., 2015*; *Bischof & Lehmann, 2020*). So far, the morphology and ontogeny of ammonoids was mainly assessed using descriptive, comparative or traditional morphometric methods (linear measurements). In his classic work of *1966*, *Raup* introduced traditional geometric parameters for the description of coiled conch morphospace. These "Raupian parameters" were subsequently refined by *Korn & Klug (2003)*, *Korn & Klug (2007)*, *Korn (2010)*, *Klug et al. (2015a)* and *Klug et al. (2015b)*. However, the shapes of discoidal ammonoids often differ through their characteristic ways of ventral arching and presence or absence of a keel. Both characteristics can hardly be described with linear measurements (*Neige, 1999*). Therefore, the use of traditional morphometric methods might be limited when it comes to distinguishing ceratitid species.

For the first time, the morphology and ontogeny of whorl profiles of the late Anisian ceratitids were analyzed using landmark- and semilandmarks-based geometric morphometric methods (GMM) instead of linear measurements (traditional morphometrics). This is reasoned in the tremendous advantages of GMM over the latter; landmarks and semi-landmarks cover shape variations of complete morphologies, which are sometimes not to be recognized or overseen with linear measurements of traditional morphometrics methods (*Neige, 1999*). In addition, GMM allow the analysis of shape and size separately (*Hammer & Harper, 2005*; *Zelditch, Swiderski & Sheets, 2012*;

Polly & Motz, 2016) and do not introduce artifactual patterns of covariation (*Gerber, 2017*), which is often the case when proportions are studied.

The literature on geometric morphometric analyses (landmark-based approaches and Fourier analysis) of molluscs is rather scarce. Although important pioneering works exist, the previous studies are of limited use in an ontogenetic context because they all focus either on the shape of the whole conch or on single (isolated) ontogenetic stages (landmarks: e.g., *Johnston, Tabachnick & Bookstein, 1991*; *Neige & Dommergues, 1995*; *Reyment & Kennedy, 1998*; *Stone, 1998*; *Neige, 1999*; *Reyment, 2003*; *Van Bocxlaer & Schultheiß, 2010*; *Knauss & Yacobucci, 2014*; Fourier analysis: e.g., *Courville & Crônier, 2005*; *Simon, Korn & Koenemann, 2010*; *Simon, Korn & Koenemann, 2011*; *Korn & Klug, 2012*; *Klein & Korn, 2014*).

In order to evaluate the hitherto used taxonomic scheme, ontogenetic patterns within the family Ceratitidae and their changes over time were investigated. Working with ontogenetic cross-sections allows the estimation of the relative age of the whorls, which adds an extra dimension to the analysis. The tools presented here are intended to complement traditional descriptions and to evaluate and quantify their results. This study should serve as a general motivation to conduct GMM studies on invertebrates with accretionary planispiral growth.

MATERIALS & METHODS

Geological setting

The ammonoid material derives from the Fossil Hill Member of Fossil Hill in the Humboldt Range and Muller Canyon in the Augusta Mountains (Pershing County), north-western Nevada, USA (Fig. 1) and is stored in the Geosciences Collection of the University of Bremen (GSUB), Germany. The material from the Wilderness Study Area of the Augusta Mountains, Pershing County was collected with permission of the US Department of the Interior, Bureau of Land Management (BLM, Nevada State office, Winnemucca District). The Fossil Hill Member is a succession of alternating layers of mudstone with lenticular limestone and calcareous siltstone beds (see Fig. 2). The rich and diverse fossil content consists primarily of halobiid bivalves and ammonoids. Detailed geological and stratigraphic descriptions were published by *Nichols & Silberling (1977)*, *Silberling & Nichols (1982)* and *Monnet & Bucher (2005)*.

Studied specimens

The fossil material comprises 72 ammonoid specimens of the family of Ceratitidae (*Mojsisovics, 1879*). These represent twelve species in seven genera (Fig. 2, Table 1) that either belong to the subfamily Beyrichitinae (*Spath, 1934*) or Paraceratitinae (*Silberling, 1962*). Most of the studied species show high intraspecific variation with overlapping morphologies (see Table 1 and Figs. 3–5). Members of these genera (*Gymnotoceras*, *Frechites* and *Parafrechites* in particular) are sometimes hard to differentiate. They mainly differ in the ventral conch outline, ornamentation, adult ribbing and maximum growth size. The younger the individuals are, the greater the similarities. Despite their complicated taxonomy, all selected species are index fossils of the late Anisian Fossil Hill Member (see Fig. 2). It was assumed that the individual species have similar coiling rates (i.e., the

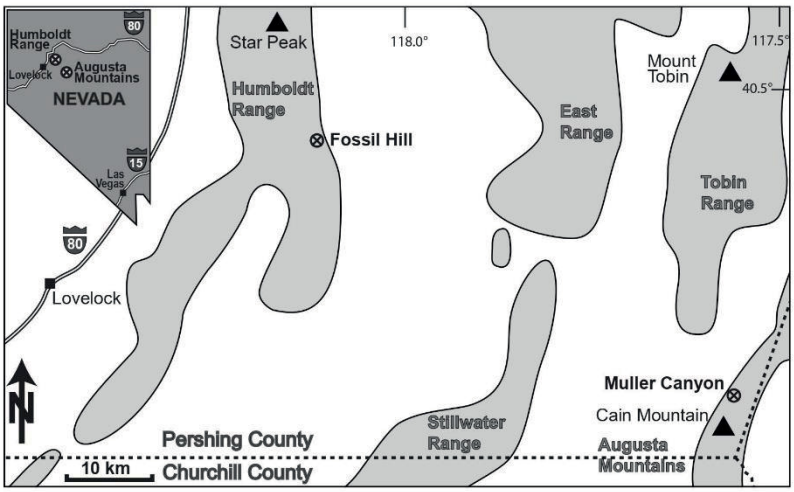

Figure 1 **Location of the study area in NW Nevada, USA. The Fossil Hill and the Muller Canyon localities are marked. Figure adapted from *Bischof & Lehmann (2020)*, Fig. 1.**
Full-size DOI: 10.7717/peerj.10931/fig-1

individual species develop the same number of whorls in the course of their life). The total number of volutions developed by the species varies between five and a half and seven (see Table 1—Total number of volutions).

Preparation and data acquisition

We prepared high-precision cross-sections intersecting the protoconch of each specimen, following the methods by *Korn (2010)*, *Klug et al. (2015a)* and *Klug et al. (2015b)*. Subsequently, we scanned the polished surfaces in high resolution with a flat screen scanner to ensure that all pictures have the same scale. Thereafter, the scan images were digitized. CT scan images of Anisian ammonoids from Nevada do not provide sufficient contrast of the internal structures for a reliable analysis (*Bischof & Lehmann, 2020*).

Based on the digitized cross-sections, we performed a 2D landmark-based geometric morphometrics analysis. The landmarks were retrieved in tpsDig2 v.2.31 (*Rohlf, 2010*). Sixteen landmarks were digitized per half whorl (i.e., whorl stage), which resulted in 176 landmarks per specimen (16 landmarks on 11 half whorls; Fig. 6). This set of landmarks consists of two single (1, 2) and 7 pairs of landmarks (3–16), of which eight are sliding semi-landmarks. Whereas landmarks are discrete anatomical loci (i.e., point of highest curvature of venter), sliding semi-landmarks are placed along a curve (or a surface) between two landmarks in a way that best describes the curvatures of the outline. In a second step, an algorithmic approach optimizes the approximation of the outline (*Zelditch, Swiderski & Sheets, 2012*).

In order to omit missing values in subsequent analyses, the data set was limited to whorl stage number 5.5. From a methodological point of view, it is more practical to rotate

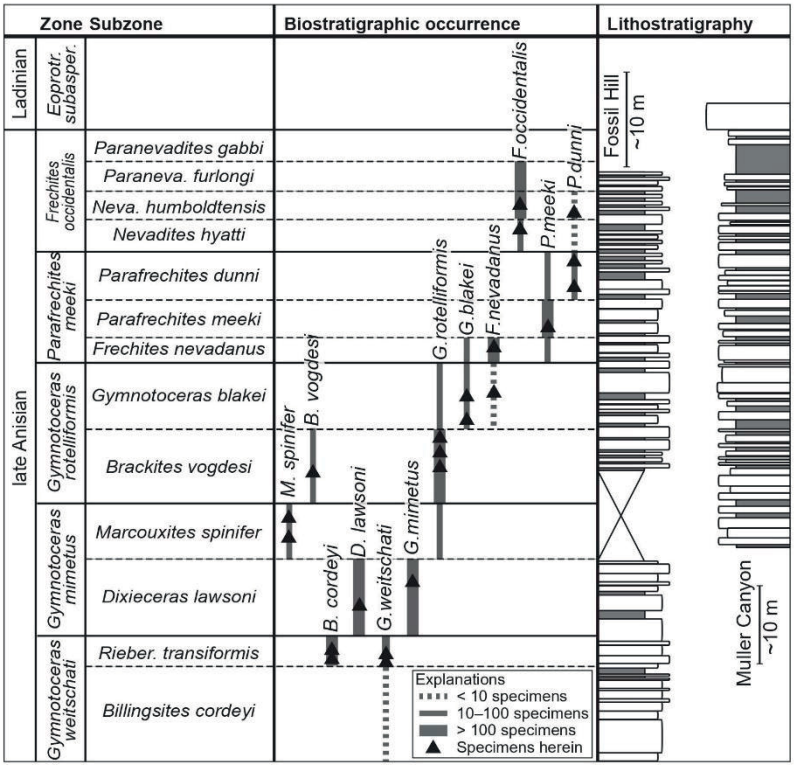

Figure 2 **Biostratigraphic distribution of fossil material and synoptic lithostratigraphic sections of the outcrops in the Muller Canyon and Fossil Hill area. Stratigraphic section of Muller Canyon adapted from *Bischof & Lehmann (2020)*, Fig. 2.** Gray areas in stratigraphic column: Calcareous siltstone; white areas: lenticular limestone, box width refers to weathering profile.

Full-size DOI: 10.7717/peerj.10931/fig-2

the shells by 90° compared to conventional illustrations (cf. *Stridsberg, 1990*) into a lying position. Since ammonoid conchs are spiral-shaped, each whorl is cut in two parts when preparing the cross sections (see Fig. 6). The half whorls on the left side of the protoconch have odd numbers ("odd whorls"; here 0.5–5.5) and those on the right side have even numbers ("even whorls"; here 1.0–5.0"). Homologous landmarks were set in accordance to the axial plane.

Calculation of procrustes shape

All geometric morphometric analyses were carried out using the R software v 3.6.3. (*R Core Team, 2020*) packages *Morpho* v2.8 (*Schlager, 2017*), *geomorph* v3.3.1. (*Adams et al., 2020*) and *RRPP* v0.6.0 (*Collyer & Adams, 2018*; *Collyer & Adams, 2020*). Plots were drawn with the R package ggplot2 (*Wickham, 2016*). Using the *Morpho::procSym* function, the 2D

Table 1 Morphological comparison of the species in focus. For biostratigraphic distribution see Fig. 2.

Species	*N*	Total number of volutions	Venter and conch outline	Sculpture	Dmax [mm]	U/D	W/D	Figure herein
Beyrichitinae *Spath, 1934*								
Billingsites cordeyi Monnet & Bucher, 2005	6	6—6.5	Slightly angular ventral shoulder	Falcoid, prorsiradiate ribs, sometimes branched	34.3	min: 0.17	min: 0.28 max: 0.35	3A–D
			Very weak developed keel	Nodes at branching points		max: 0.24		
Dixieceras lawsoni (*Smith, 1914*)	10	6—7	Stout, discoidal outline	Falcoid, prorsiradiate ribs, sometimes branched	57.7	min: 0.19	min: 0.23 max: 0.44	3I–L
			Rounded ventral shoulders	Umbilical thickening of whorls		max: 0.25		
Frechites nevadanus (*Mojsisovics, 1888*)	6	5.5—6	Subrectangular outline	Strong, falcoid, prorsiradiate ribs, sometimes branched	28.9	min: 0.29	min: 0.39 max: 0.46	3M–P
			Clearly developed keel	Adults: Pronounced tubercles at lower flank		max: 0.37		
Frechites occidentalis (*Smith, 1914*)	7	6—7	Angular ventral shoulder	Strong, slightly prorsiradiate ribs, some rare tubercles	42.6	min: 0.24	min: 0.38 max: 0.43	4I–L
			Sometimes very weak developed keel	Towards maturity ribbing fades		max: 0.27		
Gymnotoceras blakei (*Gabb, 1864*)	5	5.5—6	Discoidal outline	Falcoid, prorsiradiate, unbranched ribs	37.8	min: 0.15	min: 0.30 max: 0.38	4A–D
			Rounded ventral shoulders, weak keel	Towards maturity fading ribs and megastriae		max: 0.28		
Gymnotoceras mimetus Monnet & Bucher, 2005	9	6—6.5	Discoidal to subrectangular outline	Megastriae and weak falcoid, prorsiradiate ribs, slightly swelling towards umbilicus	43.0	min: 0.14	min: 0.29 max: 0.40	5K–N
			Rounded ventral shoulders, no keel			max: 0.22		
Gymnotoceras rotelliformis (*Meek, 1877*)	6	6	Stout discoidal outline, very weak keel	Regular, slightly prorsiradiate ribs	34.3	min: 0.17	min: 0.32 max: 0.38	4M–P
			Rounded ventral shoulders	Towards maturity ribbing slightly fades		max: 0.26		

(*continued on next page*)

Table 1 (*continued*)

Species	N	Total number of volutions	Venter and conch outline	Sculpture	Dmax [mm]	U/D	W/D	Figure herein
Gymnotoceras weitschati Monnet & Bucher, 2005	3	6	Compressed, discoidal outline	Megastriae and weak falcoid, prorsiradiate ribs, slightly swelling towards umbilicus	28.4	min: 0.17	min: 0.29 max: 0.33	5A–E
			Perfectly rounded shoulders, no keel			max: 0.20		
Parafrechites dunni (Smith, 1914)	5	5.5—6.5	Stout discoidal outline, sometimes keel	Regular but weak, slightly prorsiradiate ribs	35.2	min: 0.18	min: 0.31 max: 0.42	4E–H
			Rounded to subangular ventral shoulders	Towards maturity ribbing slightly fades		max: 0.20		
Parafrechites meeki (Mojsisovics, 1888)	5	5.5—6	Subrectangular outline	Strong and regular, falcoid, prorsiradiate ribs, sometimes branched	32.1	min: 0.22	min: 0.34 max: 0.41	5O–R
			Strong keel, subangular shoulders			max: 0.27		
Paraceratitinae Silberling, 1962								
Brackites vogdesi (Smith, 1904)	4	6—7	Subrectangular outline, slightly rounded shoulders	Regular, falcoid, branched, prorsiradiate ribs	29.6	min: 0.28	min: 0.35 max: 0.37	3E–H
			Tubercles at branching point		max: 0.37			
Marcouxites spinifer (Smith, 1914)	6	5.5—6	Subrectangular outline, angular shoulder	Strong and regular, falcoid, prorsiradiate ribs	25.8	min: 0.26	min: 0.38 max: 0.42	5F–J
			Clearly developed keel	Tubercles and spines at branching point		max: 0.36		

Notes.
N, Number of specimens; U, maximum umbilical diameter; W, maximum whorl width; D, maximum diameter of conch.
Measurement values and ratios based on material herein. More detailed information on the studied species was published by Silberling & Nichols (1982) and Monnet & Bucher (2005).

landmark coordinates were subjected to a full generalized Procrustes alignment (GPA). The semilandmarks were slid minimizing Procrustes distance. The full Procrustes fit standardizes size, orientation and position, leaving only the Procrustes shape coordinates (Bookstein, 1991, chap. 7.1, p. 258–270; Hammer & Harper, 2005; Zelditch, Swiderski & Sheets, 2012). Since the "odd" and "even" whorls cannot be made congruent by any of these operations (i.e., alignment, translation, rotation), all "even" whorls were manually mirrored before the GPA.

The individual whorls were regarded as different structures of the ammonoid conch. Therefore, the GPA was performed separately for every whorl. The *procSym*

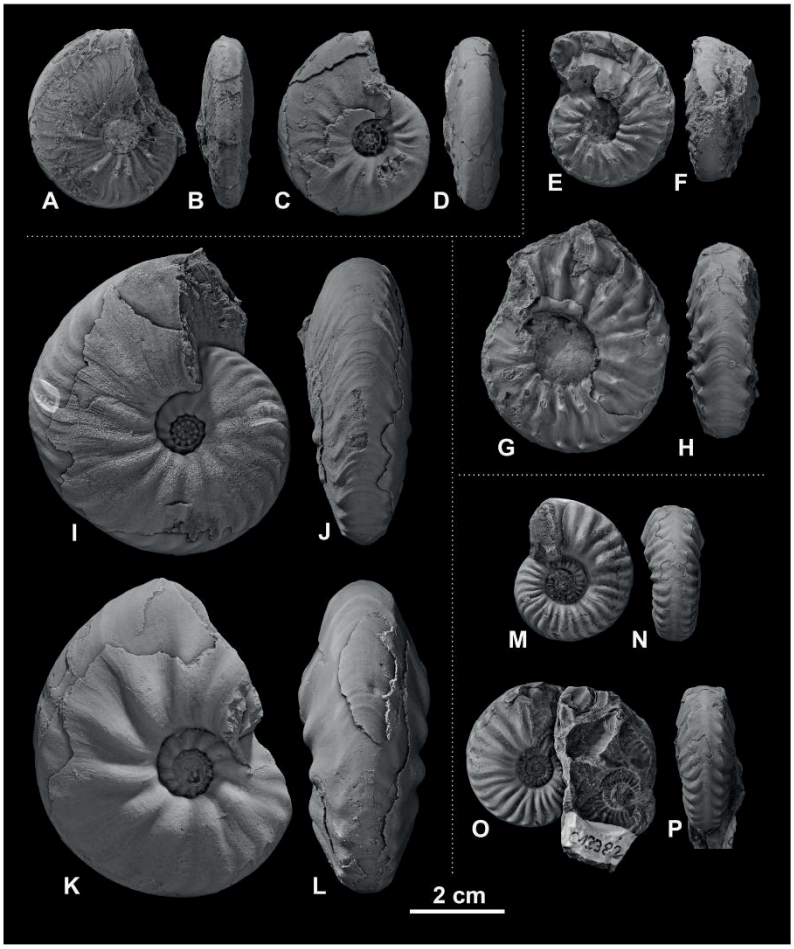

Figure 3 Ceratitid ammonoids from the Anisian (Middle Triassic) Fossil Hill Member of NW Nevada, USA. (A–D) *Billingsites cordeyi* (*Monnet & Bucher, 2005*), (A, B) GSUB C11082, (C, D) GSUB C11517; (E–H) *Brackites vogdesi* (*Smith, 1904*), (E, F) GSUB C11649, (G, H) GSUB C11646; (I–L) *Dixieceras lawsoni* (*Smith, 1914*), (I, J) GSUB C13801, (K, L) GSUB C13805; (M–P) *Frechites nevadanus* (*Mojsisovics, 1888*), (M, N) GSUB C12377, (O, P) GSUB C12382.

Full-size DOI: 10.7717/peerj.10931/fig-3

function performs Procrustes superimposition including sliding of semi-landmarks on curves and accounts for the symmetry of the object. Subsequently, the R function *geomorph::combine.subsets* was used to normalize the configurations of all whorl stages to unit centroid size or with a customized weighting (see "Developmental morphospaces"). The centroid size (CS) is regarded as a proxy for the size of the whorls and equals the

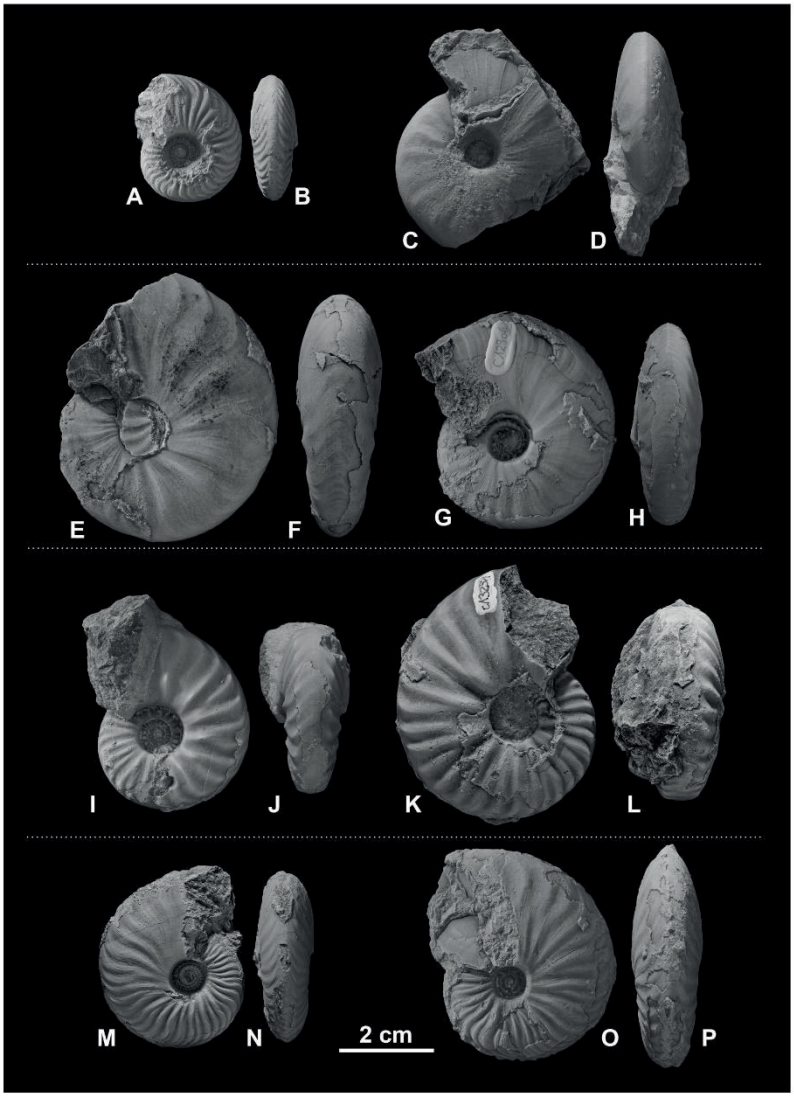

Figure 4 **Ceratitid ammonoids from the Anisian (Middle Triassic) Fossil Hill Member of NW Nevada, USA.** (A–D) *Gymnotoceras blakei* (*Gabb, 1864*), (A, B) GSUB C12243, (C, D) GSUB C12264; (E–H) *Parafrechites dunni* (*Smith, 1914*), (E, F) GSUB C9946 (G, H) GSUB C12906; (I–L) *Frechites occidentalis* (*Smith, 1914*), (I, J) GSUB C8998, (K, L) GSUB C13251; (M–P) *Gymnotoceras rotelliformis* (*Meek, 1877*), (M, N) GSUB C11594, (O, P) GSUB C11702.

Full-size DOI: 10.7717/peerj.10931/fig-4

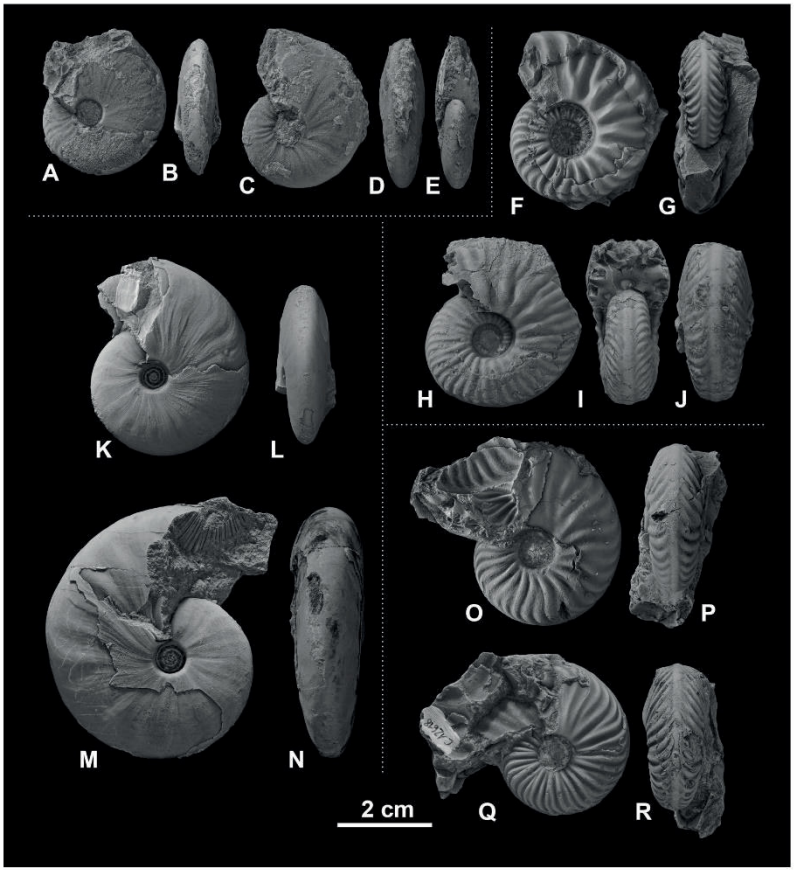

Figure 5 Ceratitid ammonoids from the Anisian (Middle Triassic) Fossil Hill Member of NW Nevada, USA. (A–E) *Gymnotoceras weitschati* (*Monnet & Bucher, 2005*), (A, B) GSUB C11111, (C–E) GSUB C11158; (F–J) *Marcouxites spinifer* (*Smith, 1914*), (F, G) GSUB C10050, (H–J) GSUB C10137; (K–N) *Gymnotoceras mimetus* (*Monnet & Bucher, 2005*), (K, L) GSUB C15005, (M, N) GSUB C13811; (O–R) *Parafrechites meeki* (*Mojsisovics, 1888*), (O, P) GSUB C12534, (Q, R) GSUB C12618.
Full-size DOI: 10.7717/peerj.10931/fig-5

square root of the summed squared distances of each landmark from the centroid of the landmark configuration before the GPA (*Zelditch, Swiderski & Sheets, 2012*). The function *geomorph::combine.subsets* was originally introduced to combine different parts of a body (e.g., heads and tails; *Collyer, Davis & Adams, 2020*).

To visualize the multivariate data in two-dimensional morphospaces, we ran a Principal Component Analysis (PCA) on the aligned Procrustes shape coordinates using the R

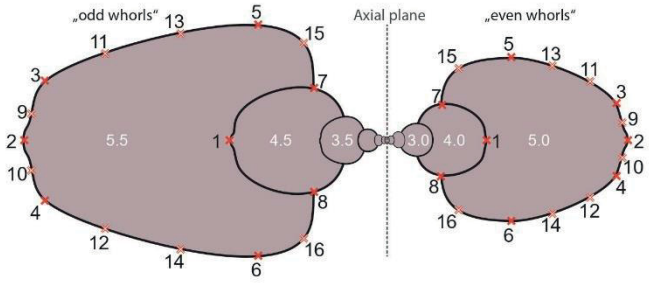

Figure 6 Digitized sketch of high-precision cross-section of an ammonoid specimen meeting the initial chamber (protoconch) with position of landmarks on last two half whorls. Filled crosses: fixed landmarks; empty crosses: sliding landmarks; black numbers: numbers. Definition of fixed landmarks: (1) venter of preceding whorl; (2) venter of whorl; (3) and (4) ventral shoulder or point of highest curvature; (5) and (6) maximum width; (7) and (8) Umbilical seam.

Full-size DOI: 10.7717/peerj.10931/fig-6

function *stats*::*prcomp*. Thereby we used two different types of visualization: Ontogenetic trajectory spaces and developmental morphospaces.

Ontogenetic trajectory spaces

It is well-known that ammonoids have a very characteristic but also complex ontogenetic development (e.g., *Klug, 2001*). To visualize the ontogenetic development of ammonoids, there are different types of morphospaces. Ontogenetic trajectory spaces (originally called ontogenetic morphospaces), as defined by *Bischof & Lehmann (2020)*, p.2), illustrate the differences in total ontogenetic development of individuals. They show the data in an artificial state of combined morphologies of different ontogenetic stages. To calculate an ontogenetic trajectory space, all Procrustes shapes (i.e., whorls) of an individual are re-assembled before running the Principal Component Analysis. This means that, in an ontogenetic trajectory space, the ontogenetic trajectory of every individual is reduced to a single data point. Ontogenetic trajectory spaces are a tool to examine if the ontogenetic pathways of individuals differ, but they do not show how the trajectories vary. To test whether ontogenetic trajectories statistically differ between species, a multivariate analysis of variance (MANOVA) using the R function *stats*::*manova* was applied.

Developmental morphospaces

Developmental morphospaces as defined by *Eble* (*2003*, p. 40) are morphospaces that directly contain developmental information. In terms of this study, this means that every individual dot in the morphospace reflects a specific ontogenetic stage (i.e., half whorl) of an individual. By connecting all points of an individual, its ontogenetic trajectory can be obtained. In contrast to ontogenetic trajectory spaces, developmental morphospaces show how individual whorls differ from each other.

General Procrustes Analysis (GPA) removes all information about size from a given set of data leaving only the pure shape coordinates. However, as can be seen in Fig. 6, size differences between different whorl stages are tremendous. If normalized to unit centroid

size (i.e., non-weighted morphospace), the earliest whorls of ammonoids therefore get enormously enlarged and the last whorls scaled down. In general, deviations (measurement uncertainties as well as actual morphological variation) are increased for the initial whorls and reduced for older whorl stages. Therefore, a second morphospace with weighted Procrustes shape coordinates was calculated. Thereby, the logarithmic centroid size ($\log_{10}$CS) of all configurations of a whorl stage were normalized to the proportional centroid size of the respective stage to the sum of all whorl stages ($\log_{10}$ $CS_{whorl\ i}/\sum \log_{10}$ CS_{whorls}). The principal components of the PCA on the weighted shapes were called wPC (weighted principal components).

If the relative $\log_{10}$CS is used to normalize the centroid size of the configurations, this approach is extremely similar to a Relative Warp Principal Component Analysis (RW-PCA; size-shape space) after *Mitteroecker et al. (2004)*. To calculate a RW-PCA the shape matrix of a configuration is augmented by an additional column containing information about the $\log_{10}$CS of the configurations. Whereas the R function *geomorph::combine.subsets* scales every configuration accordingly, the size information in the RW-shape matrices are stored in the additional variable. The resulting RW size-shape space can be analyzed with an ordinary PCA. Typically, RW size-shapes spaces are strongly dominated by the $\log_{10}$CS and PC1 therefore often accounts for more than 90% of the variation. If proportional $\log_{10}$CS-values ($\log_{10}CS_{configuration\ i}/\sum \log_{10}CS_{configurations}$) are used, the analysis is less dominated by size, but the eigenvalues are very similar to the ones of the weighted PCA (wPCA). For simplicity the R function was used here.

Because weighting does not change the shapes itself, weighted and non-weighted developmental morphospaces look very similar. The main difference is the placement of the individual configurations within the morphospace. Whether weighted or non-weighted shape coordinates should be used, depends on what the analysis is intended to show. A summary of the three different approaches how to combine landmark configurations can be found in Table 2.

To model the shapes at the maximum and minimum PC-values, the R function *GeometricMorphometricsMix::reversePCA* (*Fruciano, 2019*) was used. The function is designed to recalculate artificial Procrustes shape variables from the extreme PC-values in a morphospace. The thin-plate spline deformation grids were calculated using the R function *geomorph::plotRefToTarget*.

Trajectory analysis

In morphometric studies, ontogenetic trajectories represent a series of measurement values of different ontogenetic stages of an individual or a group, called longitudinal data (*Klingenberg, 1998*). To quantify the differences of the ontogenetic trajectories of the individual species, the R function *RRPP::trajectory.analysis* with 999 iterations was used. The function calculates a linear model with at least one categorical interaction variable (here: Shape ~ Species * WhorlStage) and assesses differences in path distance (magnitude differences, length of trajectories), trajectory shape and the angle between the individual trajectories (trajectory correlation) (*Collyer & Adams, 2013*).

Table 2 Comparison of most important characteristics of weighted and non-weighted approaches to combine landmark configurations.

Shape variables	Effect on shape data set	Advantages	Disadvantages
Non-weighted (wPCA)	• Minimizes shape difference between all configurations of all o.s.	• No perturbation of original dataset	• Overestimation of deviations of earliest/small earliest/smallest o.s. and underestimation of latest/largest o.s.
Weighted (wPCA)	• Adds allometric/size information to analysis	• More complicated computation than other methods	• Domination of size (less than in RW-PCA)
	• Maximizes shape differences between o.s.	• Deviations of earliest/smallest o.s. less overestimated and of latest/large o.s. less underestimated	• Partial loss of objectivity
	• Minimizes shape differences within an o.s.		• May suppress potential true variation in earliest o.s.
			• Slight perturbation of original data set (creation of arbitrary covariances)
Shape-size space (RW-PCA)	• Adds allometric/size information to analysis	• Easy to compute	• Extreme domination of size
	•Every configuration is scaled individually according to their centroid size	• Intuitive	• Strong perturbation of original data set, cannot be used for most subsequent analyses

Notes.
o.s., ontogenetic stages (i.e., whorls).

If weighted shape-coordinates were used, the artificial size-shape relationship could overlay true differences between the trajectories. Therefore, only non-weighted shape coordinates were analyzed in the trajectory analysis.

RESULTS

Ontogenetic trajectory spaces

Ontogenetic trajectory spaces are means to visualize whether or not the ontogenetic development of two or more individuals differs. The first three components (PCs) of the Principal Component Analysis (PCA) on the shape coordinates with combined ontogenetic stages of an individual account for 58.3% ($PC_1 = 38.3\%$, $PC_2 = 13.4\%$, $PC_3 = 6.6\%$) of the total variation. Especially considering that there are a total of 352 primary components (x and y coordinates of 176 landmarks), but only 72 specimens, this result can be regarded as satisfactory. The convex hulls of the ontogenetic trajectory space of most species reveal a large overlap (Fig. 7). Nevertheless, ontogenetic trajectory spaces differ significantly between species (MANOVA: Pillai's trace $= 9.8962$; $\sim F\ (1, 11) = 1.6437$, $p < 0.001$).

Since PC1 accounts for 38.3% of the total variation, the most important characteristic is the position of the individuals on the x-axis. In fact, there are certain species that primarily have negative PC1 values (*B. vogdesi*, *F. nevadanus*, *F. occidentalis*, *M. spinifer*, *P. meeki*) and some that are more restricted to positive PC1 values (*G. blakei*, *G. mimetus*, *G. rotelliformis*, *G. weitschati*, *P. dunni*). *B. cordeyi* and *D. lawsoni*, both cover a wider range of different PC1 values, but are generally restricted to negative PC2 and positive PC3 values.

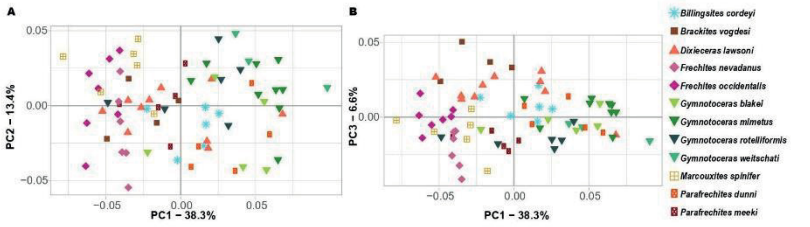

Figure 7 **Ontogenetic morphospace of all species analyzed. (A) Principal Component 1 and 2; (B) Principal component 1 and 3.**

Full-size DOI: 10.7717/peerj.10931/fig-7

Non-weighted developmental morphospace occupation

The first three components of the PCA on the non-weighted shape space account for 93.8% ($PC_1 = 78.5\%$, $PC_2 = 11.5\%$, $PC_3 = 3.1\%$) of the total variation. The PCA plot (Fig. 8) of PC1 and PC2 shows that the whorls of early ontogenetic stages cover the lower left quadrant of the morphospace (negative PC1 and PC2 values), which characterizes extremely depressed, broad whorls with a flat venter (Fig. 9A). The center of the morphospace (PC1 equals 0 and PC2 is positive) is occupied by intermediate growth stages (juveniles), which have a more quadratic outline with an only slightly triangular venter (Fig. 9B). The lower right quadrant (high PC1 and low PC2 values) is associated with the latest ontogenetic stages (adults). Towards maturity, the whorls increase mainly in height and have a clearly triangular venter and sometimes a keel (Figs. 9C and 10). Overall, there are two extreme adult shapes: Type (A) describes rather depressed, stout conchs with only a slight overlap with the preceding whorl and are associated with much shorter ontogenetic trajectories. Type (B) describes compressed conchs with a clearly triangular venter and a higher degree of overlap and are associated with longer ontogenetic trajectories. For the assignment of the species to the two types see Table 3.

The developmental morphospace of beyrichitine and paraceratitine ammonoids comprises three basic shape stages, which are not separated by sharp borders (Fig. 9): (1) Earliest whorls: broad and very flat; (2) Juveniles: more rounded and depressed; (3) Adults: mostly high and compressed whorls. Since type A species stop their development at more rounded and depressed whorls, their adult whorls resemble the juvenile stages of type B (Fig. 10).

Ontogenetic trajectories in the non-weighted developmental morphospace

The ontogenetic trajectories of species in the non-weighted developmental morphospace share many similarities: They all have similar directions of propagation and a slight parabolic shape (Fig. 8). The variation detected by the trajectory analysis (R function *RRPP::trajectory.analysis*) revealed significant differences in trajectory length (path distance), trajectory shape and trajectory slope between most species (File S1, summarized results below).

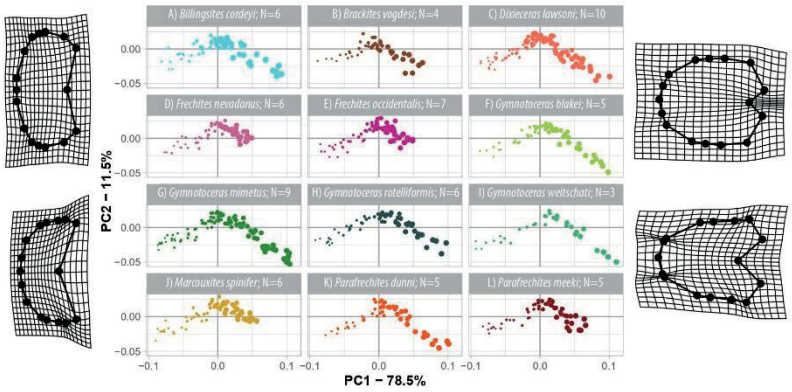

Figure 8 **Developmental morphospace with PCA of Procrustes shape variables. Point size refers to whorl stage. Deformation grids of the mean shape to the modeled shapes of the extreme values for PC1 and PC2.**

Full-size DOI: 10.7717/peerj.10931/fig-8

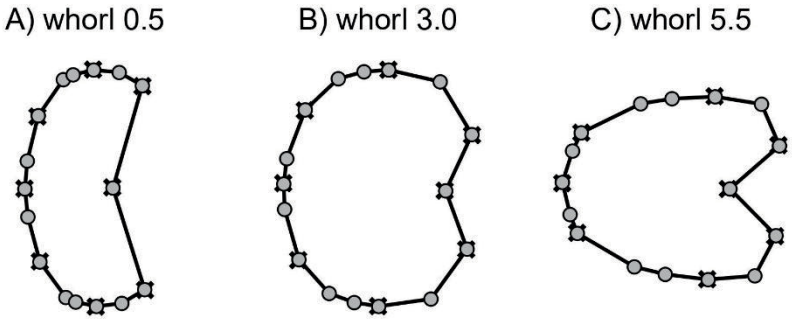

Figure 9 **Mean shapes of whorl stages 0.5, 3.0 and 5.5.** Fixed landmarks are marked with a cross.

Full-size DOI: 10.7717/peerj.10931/fig-9

Members of the type A ontogeny have smaller magnitudes of shape change and different trajectory shapes than members from type B ontogeny (path distances A: 0.2005–0.0225; B: 0.2276–0.2778). For the assignment of the species to the two types see Table 3. Only pairwise differences of the path distance and the trajectory shape between type A and type B species are statistically significant (magnitude of shape change: 17/66 possible pairs; trajectory shape: 16/66 possible pairs).

Most species have statistically significant pairwise differences in trajectory slope (57/66 possible pairs). Species of all pairs with non-significant pairwise *p*-values are in the same ontogenetic group (i.e., both belong to type A or B). The trajectories of the nine pairs with non-significant differences in slope, have non-significant magnitudes and shapes also.

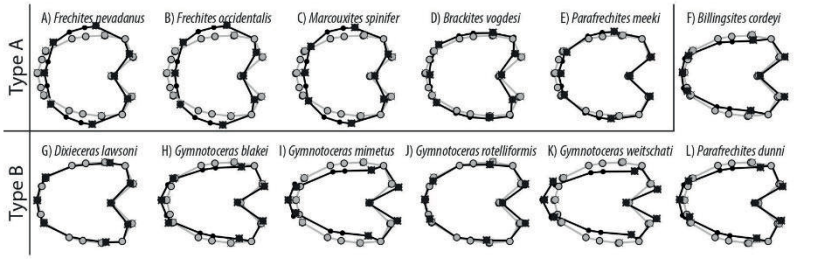

Figure 10 TPS spline of mean shape of whorl 5.5 of all species in this study (grey) plotted against the mean shape of whorl 5.5 of the respective species (black). Fixed landmarks are marked with a cross.
Full-size DOI: 10.7717/peerj.10931/fig-10

Table 3 Summary and explanation on the three different ontogenetic types. Heterochronic terms as defined by *McNamara (2012)*.

Type	Species	Heterochrony	Adult whorl shapes
A1	*F. nevadanus* *F. occidentalis* *M. spinifer* *B. vogdesi* *P. meeki* *B. cordeyi*	Paedomorph	Depressed, stout conches, only slight overlap with preceding whorl
B	*D. lawsoni* *G. blakei* *G. mimetus* *G. rotelliformis* *G. weitschati* *P. dunni*	Peramorph (Acceleration)	Compressed conches, more pronounced venter, more overlap with preceding whorl

However, none of the species that share a common slope have overlapping biostratigraphic ranges.

Weighted developmental morphospace occupation

The first three components of the PCA on the weighted shape space account for 94.8% ($wPC_1 = 85.8\%$, $wPC_2 = 7\%$, $wPC_3 = 3.0\%$) of the total variation. In comparison to the regular PCA, the wPCA is—by definition—more strongly controlled by the centroid size of the configurations, which is mainly expressed by the domination of PC1.

Similar to the regular PCA plot (Fig. 8), the wPCA morphospace (Fig. 11) can be divided into three main parts: (1) The extremely depressed earliest whorls cover the lower left quadrant (low PC1 and PC2 values); (2) the center of the plot (PC1 equals 0, PC2 positive) is occupied by the more depressed whorls of juveniles and (3) adult whorls are associated with positive PC1 values. In contrast to the PCA, the wPCA reveals a more distinct separation of the type A and type B groups of adult whorls (see Table 3). Representatives of the more depressed type B clearly occupy the lower right quadrant (positive PC1 and

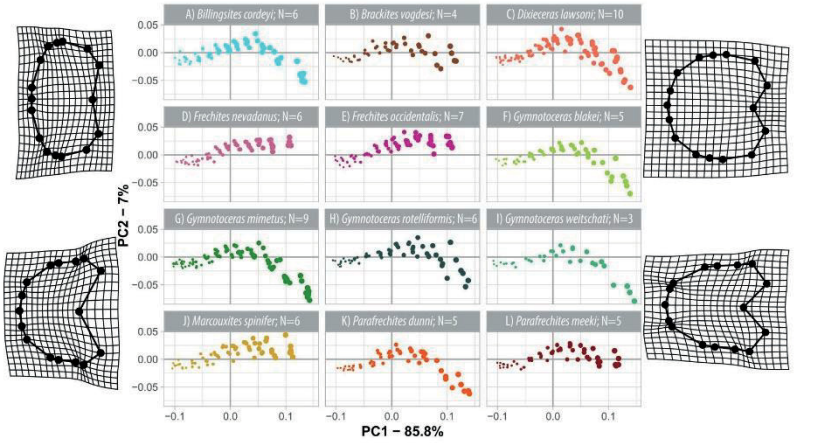

Figure 11 **Developmental morphospace with PCA of weighted Procrustes shape variables. Point size refers to number of whorl stage. Deformation grids of the mean shape to the modeled shapes of the extreme values for PC1 and PC2.**

Full-size DOI: 10.7717/peerj.10931/fig-11

negative PC2 values). This division into type A and B can also be seen in the mean shapes of the whorl 5.5 of the respective species (Fig. 10).

DISCUSSION

Members of the family Ceratitidae show high intraspecific variation and strongly overlapping morphospaces (Table 1, Figs. 3, 4 and 5). The ornamentation, which is often regarded as essential for the description of Mesozoic ammonoid groups (*Klug et al., 2015*; *Klug et al., 2015b*), is not a unique characteristic among the family Ceratitidae. A better feature to delineate the ceratitids studied here appears to be the shape of the whorl section. The latter, however, cannot be quantified adequately by traditional morphometric methods (*Neige, 1999*). Accordingly, the utility of conventional taxonomic and morphological methods is limited in this regard. Here, we utilize landmarks and semi-landmarks on ontogenetic cross-sections. Since previous geometric morphometric studies on mollusks all focus either on conch shape or on single (isolated) ontogenetic stages (landmarks: e.g., *Johnston, Tabachnick & Bookstein, 1991*; *Neige & Dommergues, 1995*; *Reyment & Kennedy, 1998*; *Stone, 1998*; *Neige, 1999*; *Reyment, 2003*; *Van Bocxlaer & Schultheiß, 2010*; *Knauss & Yacobucci, 2014*; Fourier analysis: e.g., *Courville & Crônier, 2005*; *Simon, Korn & Koenemann, 2010*; *Simon, Korn & Koenemann, 2011*; *Korn & Klug, 2012*; *Klein & Korn, 2014*) they cannot be regarded as ontogenetic studies. This study, investigates the use of geometric morphometric methods (GMM) with respect to their usefulness in ontogenetic developmental studies and taxonomic descriptions.

Ontogenetic patterns in Ceratitidae

The ontogenetic trajectories of the studied species comprise the biphasic development from strongly depressed to weakly depressed to compressed whorl profiles (Figs. 8–11). It is commonly accepted that sudden changes in ontogenetic allometry often mark the onset of sexual maturity (i.e., *Kullmann & Scheuch, 1970*; *Klug, 2001*; *Klug et al., 2015a*; *Klug et al., 2015b*).

The studied species can be divided into two main ontogenetic groups: Type (A) Truncated trajectories that are associated with depressed adult whorls; type (B) longer, complete trajectories that lead to a compressed adult whorl shape. The process of lengthening and shortening of the trajectories (i.e., related to changes in rate and timing of the development) account for the ontogenetic differentiation of the species in focus. This contrasts a previous traditional morphometric analysis by *Bischof & Lehmann (2020)* of ptychitids, which revealed that the spherocone-cadicone morphospace is much more distinct. The highly ontogenetically differentiated genus *Ptychites* directly differed through characteristic ontogenetic trajectories.

While precise temporal growth rates of ammonoids are unknown (*Lécuyer & Bucher, 2006*; *Knauss & Yacobucci, 2014*), a basic assumption herein was that the individual species have similar coiling rates (i.e., the individual species develop the same number of whorls in the course of their life). Modified rate/timing of shape change from any ancestor to any descendent within an evolutionary framework is called heterochrony (*Zelditch, Swiderski & Sheets, 2012*, p. 317). Between type A and type B species, interspecific variation of the species in focus arises from an acceleration, a special case of peramorphosis; (for discussion of this term, see *Alberch et al., 1979*; *McNamara, 2012*) that allows type B species to occupy an extended portion of the morphospace characterized by more compressed whorls. Therefore, the studied ceratitids do not primarily differ in shape, but rather in the timing of the development of individual shapes. Heterochrony as a mechanism in macroevolution is known to be a key driving factor in phenotypic diversification (e.g., *Gould, 1977*; *Alberch et al., 1979*; *McKinney & McNamara, 1991*; *Gerber, Neige & Eble, 2007*; *Gerber, 2011*; *Korn et al., 2013*; *Knauss & Yacobucci, 2014*). The quantification of patterns of morphologic disparity and the relationship between size and shape (i.e., heterochrony) will be the subject of future studies.

Anisian ammonoid diversity

It is widely agreed that ammonoid diversity reached its maximum during the Triassic period (*House, 1993*; *Brayard et al., 2009*; *Whiteside & Ward, 2011*). Thereby, the late Anisian ammonoid diversity peak was dominated by members of the family Ceratitidae (*Brayard et al., 2009*; supporting material Fig. S2). However, there are a growing number of studies critically questioning diversity peaks by arguing that—to some extent—the high diversity might be artificially inflated by taxonomic over-splitting (*Forey et al., 2004*; *De Baets, Klug & Monnet, 2013*; *Knauss & Yacobucci, 2014*).

The results obtained here do justice to the general opinion that ontogenetic trajectories can be a powerful tool to describe (e.g., *Korn & Klug, 2007*) and discriminate ammonoid species (e.g., *Rieber, 1962*; *Bischof & Lehmann, 2020*): The newly introduced methods

succeeded in statistically discriminating the ontogenetic pathways of the pre-defined ceratitid species. Based on this analysis, the high diversity of the Anisian ammonoid assemblages of Nevada appears not to be artificially inflated and the alpha taxonomy is regarded to be adequate. However, the high morphological resemblances of the investigated species cannot be denied. Therefore, this study supports the main idea of *McGowan (2004)*, *McGowan (2005)* and *Brosse et al. (2013)* that taxonomic diversity and morphological disparity need not necessarily be closely linked.

It is important to be aware of the fact that GMM carry no direct biological information. They help to understand if and how configurations differ, but not what the underlying mechanisms for their morphological development are. In the complex discoidal morphospace landmark-based approaches have proven to be useful to evaluate a priori defined taxonomic groups. Nevertheless, geometric morphometric methods cannot be considered as being a phylogenetic or taxonomic tool per se. But they certainly represent an improvement and valuable supplement to traditional methods.

Why it is worth the effort

There is no doubt that preparation and analysis of ontogenetic cross sections involves a lot of work (*Korn, 2012*). However, geometric morphometric methods (GMMs) open the door to a new world of objectified, statistically quantifiable descriptions. For example, in the case of the fauna described herein, conventional descriptions and traditional morphometric methods did not succeed to differentiate species adequately. Landmarks and semi-landmarks, however, make it possible to statistically quantify shape variations of entire morphologies (*Neige, 1999*) and allow the analysis of shape and size separately (*Hammer & Harper, 2005*).

The high resolution of the ontogenetic trajectories of the herein studied material was achieved owing to the accretionary planispiral growth of ammonoids with conservation of previous growth stages (*Korn, 2012*), which adds an intuitive, relative time-component to the ontogenetic analysis. Even though it is likely that small-scale ontogenetic changes are overlooked at a measurement density of one measurement per 180 degrees, it can be assumed that no major developmental steps were skipped (*Tajika & Klug, 2020*). Leaving out complete ontogenetic stages would most likely prevent the recognition of ontogenetic processes such as heterochrony. If, for example, only the earliest and latest stages of the ceratitid development were analyzed, representatives of type A and type B would differ fundamentally. The accretionary growth of many ammonoid conchs therefore not only adds an individual time component to the analysis, but more importantly ensures that no major developmental steps have been overlooked. This reinforces the general opinion that ontogenetic trajectories of ammonoids are a powerful tool to study evolutionary processes.

CONCLUSIONS

The Anisian ammonoid diversity peak was dominated by the family Ceratitidae (*Brayard et al., 2009*; supporting material Fig. S2). However, the investigated ceratitid species show high intraspecific variation and sometimes completely overlapping morphospaces. Using conventional methods, ceratitids are often difficult to distinguish. It was therefore assumed

that the high Anisian diversity in Nevada might be artificially inflated by taxonomic over-splitting.

Using a landmark-based geometric morphometric approach, this study succeeded in differentiating the ontogenetic growth of the pre-defined taxonomic entities in the fossil material from the late Anisian Fossil Hill Member in Nevada, USA. Based on the findings of this study, the high Anisian ammonoid diversity in western North America appears not to be unreasonably inflated. In this context, this study furthermore supports the hypothesis that taxonomic diversity and morphologic disparity of Triassic ammonoids were decoupled (*Brosse et al., 2013*; *McGowan, 2004*; *McGowan, 2005*). The largest interspecific differences of ceratitids are the result of alterations of the ontogenetic trajectories that are likely linked to heterochronic processes (i.e., differences in timing of ontogenetic changes). This means that the individual species of this group are not solely defined by the morphology they attain at a certain growth stage, but rather by the sum and timing of all of their ontogenetic stages. The statistical quantification of the relationship between size and shape (i.e., heterochrony) will be the subject of future studies. These processes make an ad hoc distinction of the different species particularly challenging.

For a reliable traditional taxonomic identification of the species herein, it is necessary to have several individuals (*Silberling, 1962*) with different ages of the same species from the same stratum. It has furthermore proven to be essential to analyze morphological variation of ceratitids not only between species but also across different ontogenetic stages. Therefore, the significance of ontogenetic studies on ammonoids with regard to taxonomic implications cannot be dismissed. The geometric morphometric methods introduced herein represent a big leap towards more quantitative and objective taxonomic descriptions of ammonoids.

ACKNOWLEDGEMENTS

We would like to thank D Kuhlmann (now Messel, Germany) as former technician of the Geowissenschaftliche Sammlung Bremen for mechanical preparation of the material collected by our working group. M Krogmann (Bremen, Germany) is thanked for his broad support in the artwork for this article. We are indebted to K Boos for statistical support and the introduction to the R software. P Embree (Orangevale, CA, USA) is thanked for broad support, including organization of field-campaigns, scientific information and the permission to collect on his private property. Our gratitude goes to the reviewers Christian Klug and Kenneth De Baets and the editor Brandon Hedrick for their corrections and suggestions that greatly improved the manuscript.

ADDITIONAL INFORMATION AND DECLARATIONS

Funding

This research received support from the German Science Foundation (DFG), project "Nevammonoidea" (LE 1241/3-1). The funders had no role in study design, data collection and analysis, decision to publish, or preparation of the manuscript.

Grant Disclosures

The following grant information was disclosed by the authors:
German Science Foundation (DFG), project "Nevammonoidea": LE 1241/3-1.

Competing Interests

The authors declare there are no competing interests.

Author Contributions

- Eva Alexandra Bischof conceived and designed the experiments, performed the experiments, analyzed the data, prepared figures and/or tables, authored or reviewed drafts of the paper, preparation of fossil specimens, and approved the final draft.
- Nils Schlüter conceived and designed the experiments, performed the experiments, analyzed the data, authored or reviewed drafts of the paper, and approved the final draft.
- Dieter Korn conceived and designed the experiments, authored or reviewed drafts of the paper, preparation of fossil specimens, and approved the final draft.
- Jens Lehmann conceived and designed the experiments, authored or reviewed drafts of the paper, and approved the final draft.

Field Study Permissions

The following information was supplied relating to field study approvals (i.e., approving body and any reference numbers):

The U.S. Department of the Interior, Bureau of Land Management (BLM, Nevada State office, Winnemucca District) gave permission to collect samples in the Wilderness Study Area of the Augusta Mountains, Pershing County.

Data Availability

The following information was supplied regarding data availability:

Data and code are available in the Supplemental Files.

Supplemental Information

Supplemental information for this article can be found online at http://dx.doi.org/10.7717/peerj.10931#supplemental-information.

REFERENCES

Adams DC, Collyer ML, Kaliontzopoulou A, Baken E. 2020. Geomorph: software for geometric morphometric analyses. R package version 3.2.1. *Available at https://cran.r-project.org/package=geomorph*.

Alberch P, Gould SJ, Oster GF, Wake DB. 1979. Size and shape in ontogeny and phylogeny. *Paleobiology* **5**:296–317 DOI 10.1017/S0094837300006588.

Bischof EA, Lehmann J. 2020. Ontogenetic analysis of Anisian (Middle Triassic) ptychitid ammonoids from Nevada, USA. *Journal of Paleontology* **94**:829–851 DOI 10.1017/jpa.2020.25.

Bookstein F. 1991. *Morphometric tools for landmark data: geometry and biology*. New York: Cambridge Univ. Press, 435.

Brayard A, Bucher H. 2015. Permian-triassic extinctions and rediversifications. In: Klug C, Korn D, De Baets K, Kruta I, Mapes RH, eds. *Topics in geobiology*. Dordrecht: Springer, 465–473.

Brayard A, Escarguel G, Bucher H, Monnet C, Brühwiler T, Goudemand N, Galfetti T, Guex J. 2009. Good genes and good luck: ammonoid diversity and the End-Permian mass extinction. *Science* **325**:1118–1121 DOI 10.1126/science.1174638.

Brosse M, Brayard A, Fara E, Neige P. 2013. Ammonoid recovery after the Permian–Triassic mass extinction: a re-exploration of morphological and phylogenetic diversity patterns. *Journal of the Geological Society* **170**:225–236 DOI 10.1144/jgs2012-084.

Bucher H. 1992. Ammonoids of the *Shoshonensis* Zone (Middle Anisian, Middle Triassic) from northwestern Nevada (USA). *Jahrbuch der Geologischen Bundesanstalt Wien* **135**:425–465.

Collyer ML, Adams DC. 2013. Phenotypic trajectory analysis: comparison of shape change patterns in evolution and ecology. *Hystrix* **24**:75–83.

Collyer ML, Adams DC. 2018. RRPP: an R package for fitting linear models to high-dimensional data using residual randomization. *Methods in Ecology and Evolution* **9**:1772–1779 DOI 10.1111/2041-210X.13029.

Collyer ML, Adams DC. 2020. RRPP: linear model evaluation with randomized residuals in a permutation procedure. *Available at https://cran.r-project.org/web/packages/RRPP*.

Collyer ML, Davis MA, Adams DC. 2020. Making heads or tails of combined landmark configurations in geometric morphometric data. *Evolutionary Biology* **47**:1–13 DOI 10.1007/s11692-020-09492-z.

Courville P, Crônier C. 2005. Diversity or disparity in the Jurassic (Upper Callovian) genus Kosmoceras (ammonitina): a morphometric approach. *Journal of Paleontology* **79**:944–953 DOI 10.1666/0022-3360(2005)079[0944:DODITJ]2.0.CO;2.

De Baets K, Bert D, Hoffmann R, Monnet C, Yacobucci MM, Klug C. 2015. Ammonoid intraspecific variability. In: Klug C, Korn D, De Baets K, Kruta I, Mapes RH, eds. *Topics in geobiology*. Dordrecht: Springer, 359–426.

De Baets K, Klug C, Monnet C. 2013. Intraspecific variability through ontogeny in early ammonoids. *Paleobiology* **39**:75–94 DOI 10.1666/0094-8373-39.1.75.

Eble GJ. 2003. Developmental morphospaces and evolution. In: Crutchfield JP, Schuster PM, eds. *Santa Fe institute studies on the sciences of complexity*. Oxford University Press, 33–63.

Forey PL, Fortey RA, Kenrick P, Smith AB. 2004. Taxonomy and fossils: a critical appraisal. *Philosophical Transactions of the Royal Society of London Series B* **359**:639–653 DOI 10.1098/rstb.2003.1453.

Fruciano C. 2019. Geometric morphometrics mix: miscellaneous functions useful for geometric morphometrics. R package version 0.0.7.9000.

Gabb WM. 1864. *Paleontology of California. Description of the Triassic fossils of California and the adjacent territories.* Philadelphia: California Geological Survey, Paleontology, 17–35.

Gerber S. 2011. Comparing the differential filling of morphospace and allometric space through time: the morphological and developmental dynamics of Early Jurassic ammonoids. *Paleobiology* **37**:369–382 DOI 10.1666/10005.1.

Gerber S. 2017. The geometry of morphospaces: lessons from the classic Raup shell coiling model. *Biological Reviews* **92**:1142–1155 DOI 10.1111/brv.12276.

Gerber S, Neige P, Eble GJ. 2007. Combining ontogenetic and evolutionary scales of morphological disparity: a study of early Jurassic ammonites. *Evolution & Development* **9**:472–482 DOI 10.1111/j.1525-142X.2007.00185.x.

Gould SJ. 1977. *Ontogeny and phylogeny*. Cambridge, Massachusetts: Harvard University Press, 1–501.

Hammer Ø, Harper D. 2005. *Paleontological data analysis*. Second Edition. Cambridge: Blackwell, 1–368.

House MR. 1993. Fluctuations in ammonoid evolution and possible environmental controls. In: House MR, ed. *Systematics association special volume*. Oxford: Clarendon Press, 13–34.

Jenks JF, Monnet C, Balini M, Brayard A, Meier M. 2015. Biostratigraphy of Triassic ammonoids. In: Klug C, Korn D, De Baets K, Kruta I, Mapes RH, eds. *Topics in geobiology*. Dordrecht: Springer, 329–388.

Johnston MR, Tabachnick RE, Bookstein FL. 1991. Landmark-based morphometrics of spiral accretionary growth. *Paleobiology* **17**:19–36 DOI 10.1017/S0094837300010320.

Kennedy WJ, Cobban WA. 1976. Aspects of ammonite biology, biogeography, and biostratigraphy. *Special Papers in Palaeontology* **17**:1–94.

Klein C, Korn D. 2014. A morphometric approach to conch ontogeny of Cymaclymenia and related genera (Ammonoidea, Late Devonian). *Mitteilungen aus dem Museum für Naturkunde in Berlin Fossil Record* **17**:1–32.

Klingenberg CP. 1998. Heterochrony and allometry: the analysis of evolutionary change in ontogeny. *Biological Reviews* **73**:79–123.

Klug C. 2001. Life-cycles of some devonian ammonoids. *Lethaia* **34**:215–233 DOI 10.1080/002411601316981179.

Klug C, Korn D, Landman N, Tanabe K, De Baets K, Naglik C. 2015a. Describing ammonoid conchs. In: Klug C, Korn D, De Baets K, Kruta I, Mapes RH, eds. *Topics in geobiology*. Dordrecht: Springer, 30–24.

Klug C, Zatoń M, Parent H, Hostettler B, Tajika A. 2015b. Mature modifications and sexual dimorphism. In: Klug C, Korn D, De Baets K, Kruta I, Mapes RH, eds. *Topics in geobiology*. Dordrecht: Springer, 253–320.

Knauss MJ, Yacobucci MM. 2014. Geographic Information Systems technology as a morphometric tool for quantifying morphological variation in an ammonoid clade. *Palaeontologia Electronica* **17**:1–27.

Korn D. 2010. A key for the description of Palaeozoic ammonoids. *Fossil Record* **13**:5–12 DOI 10.1002/mmng.200900008.

Korn D. 2012. Quantification of ontogenetic allometry in ammonoids. *Evolution & Development* **14**:501–514 DOI 10.1111/ede.12003.

Korn D, Bockwinkel J, Ebbighausen V, Walton SA. 2013. Rare representatives in the ammonoid fauna from Büdesheim (Cephalopoda, Eifel, Late Devonian) and the role of heterochrony. *Neues Jahrbuch für Geologie und Paläontologie-Abhandlungen* **269**:111–124 DOI 10.1127/0077-7749/2013/0337.

Korn D, Klug C. 2003. Morphological pathways in the evolution of Early and Middle Devonian ammonoids. *Paleobiology* **29**:329–348 DOI 10.1666/0094-8373(2003)029<0329:MPITEO>2.0.CO;2.

Korn D, Klug C. 2007. In: Landman N, Davis RA, Mapes RH, eds. *Conch form analysis, variability, morphological disparity, and mode of life of the Frasnian (Late Devonian) ammonoid Manticoceras from Coumiac (Montagne Noire, France)*. Dordrecht: Springer, 57–85.

Korn D, Klug C. 2012. *Palaeozoic ammonoids–diversity and development of conch morphology. Earth and life.* Springer, 491–534.

Kullmann J, Scheuch J. 1970. Wachstums-Änderungen in der Ontogenese paläozoischer Ammonoideen. *Lethaia* **3**:397–412 DOI 10.1111/j.1502-3931.1970.tb00831.x.

Lécuyer C, Bucher H. 2006. Stable isotope compositions of a late Jurassic ammonite shell: a record of seasonal surface water temperatures in the southern hemisphere? *eEarth Discussions* **1**:1–19 DOI 10.5194/eed-1-1-2006.

McGowan AJ. 2004. Ammonoid taxonomic and morphologic recovery patterns after the Permian–Triassic. *Geology* **32**:665–668 DOI 10.1130/G20462.1.

McGowan AJ. 2005. Ammonoid recovery from the Late Permian mass extinction event. *Comptes Rendus Palevol* **4**:517–530 DOI 10.1016/j.crpv.2005.02.004.

McKinney ML, McNamara KG. 1991. Heterochrony. In: *The evolution of ontogeny*. New York: Springer Science+Business Media, LLC, 1–437.

McNamara KJ. 2012. Heterochrony: the evolution of development. *Evolution: Education and Outreach* **5**:203–218.

Meek FB. 1877. In: King C, ed. *Part I. Palæontology*. Washington: Government Printing Office, 1–197.

Mitteroecker P, Gunz P, Bernhard M, Schaefer K, Bookstein FL. 2004. Comparison of cranial ontogenetic trajectories among great apes and humans. *Journal of Human Evolution* **46**:679–698 DOI 10.1016/j.jhevol.2004.03.006.

Mojsisovics EV. 1879. Vorläufige kurze Übersicht der Ammoniten-Gattungen der mediterranen und juvavischen Trias. *Verhandlungen der Kaiserlich-Königlichen Geologischen Reichsanstalt Wien* **1879**:113–143.

Mojsisovics EV. 1888. *Über einige japanische Trias-Fossilien*. Vienna: Alfred Holder, K.K. Hof- und Universtitäts-Buchhändler, 163–178.

Monnet C, Brayard A, Brosse M. 2015. Evolutionary trends of Triassic ammonoids. In: Klug C, Korn D, De Baets K, Kruta I, Mapes RH, eds. *Topics in geobiology*. Dordrecht: Springer, 25–50.

Monnet C, Bucher H. 2005. New Middle and Late Anisian (Middle Triassic) ammonoid faunas from Northwestern Nevada (USA): taxonomy and biochronology. *Fossils and Strata* **52**:1–121.

Monnet C, De Baets K, Klug C. 2011. Parallel evolution controlled by adaptation and covariation in ammonoid cephalopods. *BMC Evolutionary Biology* **11(115)**:1–21 DOI 10.1186/1471-2148-11-1.

Naglik C, Monnet C, Goetz S, Kolb C, De Baets K, Tajika A, Klug C. 2015. Growth trajectories of some major ammonoid sub-clades revealed by serial grinding tomography data. *Lethaia* **48**:29–46 DOI 10.1111/let.12085.

Neige P. 1999. The use of landmarks to describe ammonite shape. In: Olóriz F, Rodríguez-Tovar FJ, eds. *Advancing research an living and fossil cepha/opods.* New York: Kluwer Academic/Plenum, 263–272.

Neige P. 2015. *Events of increased biodiversity: evolutionary radiations in the fossil record.* London & Oxford: ISTE Press Elsevier, 1–152.

Neige P, Dommergues J-L. 1995. Morphometrics and phenetic versus cladistic analysis of the early Harpoceratinae (Pliensbachian ammonites). *Neues Jahrbuch für Geologie und Paläontologie, Abhandlungen* **196**:411–438.

Nichols KM, Silberling NJ. 1977. Stratigraphy and depositional history of the Star Peak Group (Triassic), northwestern Nevada. *Special Paper Geological Society of America* **178**:1–73 DOI 10.1130/SPE178-p1.

Polly PD, Motz GJ. 2016. Patterns and processes in morphospace: geometric morphometrics of three-dimensional objects. *The Paleontological Society Papers* **22**:71–99 DOI 10.1017/scs.2017.9.

R Core Team. 2020. *R: a language and environment for statistical computing.* Vienna: R Foundation for Statistical Computing.

Raup DM. 1966. Geometric analysis of shell coiling: general problems. *Journal of Paleontology* **40**:1178–1190.

Reyment RA. 2003. Morphometric analysis of variability in the shell of some Nigerian Turonian (Cretaceous) ammonites. *Cretaceous Research* **24**:789–803 DOI 10.1016/j.cretres.2003.09.002.

Reyment RA, Kennedy WJ. 1998. Taxonomic recognition of species of *Neogastroplites* (Ammonoidea, Cenomanian) by geometric morphometric methods. *Cretaceous Research* **19**:25–42 DOI 10.1006/cres.1997.0094.

Rieber H. 1962. Beobachtungen an ammoniten aus dem ober-Aalénien (Systematik und Ontogenie). *Eclogae Geologicae Helvetiae* **55**:587–594.

Rohlf F. 2010. TPSDig2: a program for landmark development and analysis. *Available at http://life.bio.sunysb.edu/morph* (accessed on 30 January 2018).

Schlager S. 2017. In: Zheng G, Li S, Székely G, eds. *Morpho and Rvcg—shape analysis in R: R-Packages for geometric morphometrics, shape analysis and surface manipulations.* San Diego: Academic Press, 217–256.

Silberling NJ. 1962. Stratigraphic distribution of Middle Triassic ammonites at Fossil Hill, Humboldt Range, Nevada. *Journal of Paleontology* **36**:153–160.

Silberling NJ, Nichols DJ. 1982. Middle Triassic molluscan fossils of biostratigraphic significance from the Humboldt Range, northwestern Nevada. US Geological Survey Professional Paper. 1–77.

Simon MS, Korn D, Koenemann S. 2010. Disparity fluctuations in Jurassic ammonoids by means of conch geometry. *Palaeogeography, Palaeoclimatology, Palaeoecology* **292**:520–531 DOI 10.1016/j.palaeo.2010.04.023.

Simon MS, Korn D, Koenemann S. 2011. Temporal patterns in disparity and diversity of the Jurassic ammonoids of southern Germany. *Fossil Record* **14**:77–94 DOI 10.1002/mmng.201000016.

Smith JP. 1904. The comparative stratigraphy of the marine Trias of western America. San Francisco: California Academy of Sciences, 323–430.

Smith JP. 1914. *The Middle Triassic marine invertebrate faunas of North America*. Washington, D.C.: US Government Printing Office, 1–254.

Spath LF. 1934. *Catalogue of the fossil Cephalopoda in the British Museum (Natural History): Part IV the ammonoidea of the trias.* London: British Museum of Natural History, 1–521.

Stone JR. 1998. Landmark based thin plate spline relative warp analysis of gastropod shells. *Systematic Biology* **47**:254–263 DOI 10.1080/106351598260905.

Stridsberg S. 1990. Orientation of cephalopod shells in illustrations. *Palaeontology* **33**:243–248.

Tajika A, Klug C. 2020. How many ontogenetic points are needed to accurately describe the ontogeny of a cephalopod conch? A case study of the modern nautilid *Nautilus pompilius*. *PeerJ* **8**:e8849 DOI 10.7717/peerj.8849.

Tajika A, Morimoto N, Wani R, Naglik C, Klug C. 2015. Intraspecific variation of phragmocone chamber volumes throughout ontogeny in the modern nautilid Nautilus and the Jurassic ammonite Normannites. *PeerJ* **3**:e1306 DOI 10.7717/peerj.1306.

Van Bocxlaer B, Schultheiß R. 2010. Comparison of morphometric techniques for shapes with few homologous landmarks based on machine-learning approaches to biological discrimination. *Paleobiology* **36**:497–515 DOI 10.1666/08068.1.

Whiteside JH, Ward PD. 2011. Ammonoid diversity and disparity track episodes of chaotic carbon cycling during the early Mesozoic. *Geology* **39**:99–102 DOI 10.1130/G31401.1.

Wickham H. 2016. *ggplot2: elegant graphics for data analysis.* New York: Springer.

Zelditch ML, Swiderski DL, Sheets HD. 2012. *Geometric morphometrics for biologists: a primer*. Second Edition. London, Waltham & San Diego: Academic Press, 1–478.

4.4 Third case study

Morphologic disparity and ontogenetic allometry of beyrichitine ammonoids

(unpublished manuscript)

Eva A. Bischof, Nils Schlüter, Jens Lehmann

To be submitted to PlosOne

Morphologic disparity and ontogenetic allometry of beyrichitine ammonoids

(unpublished manuscript)

Eva A. Bischof[1], Nils Schlüter[2], Jens Lehmann[1]

[1] Geowissenschaftliche Sammlung, Fachbereich Geowissenschaften, Universität Bremen, Leobener Strasse 8, 28357 Bremen, Germany
[2] Naturhistorisches Forschungsinstitut, Museum für Naturkunde, Humboldt-Universität zu Berlin, Invalidenstraße 43, 10115 Berlin, Germany

Corresponding author:
Eva Bischof[1]
Geowissenschaftliche Sammlung, Leobener Strasse 8, 28359 Bremen, Germany
Email address: eva.bischof@hotmail.com

Abstract

The high taxonomic diversity of Anisian (Middle Triassic) beyrichitine ammonoids of NV Nevada is decoupled from their relatively low morphologic disparity. Depending on the exact definition, morphologic disparity of a data set is a direct consequence of the sum of all ontogenetic changes. In the past, however, the interplay of both morphological processes has only rarely been addressed.

Using geometric morphometric methods, this study aims at a quantification of allometric processes and the morphologic disparity of beyrichitine ammonoids. The multivariate statistical analysis revealed that the morphologic disparity within and between the studied species seems to be the result of deviations in the ontogenetic allometric growth pattern (i.e. heterochrony). During deposition of the stratigraphic sequence, a general progressive pedomorphism (juvenilization) was observed. The intraspecific variability pattern coincides with the total interspecific morphologic disparity of the analyzed species. The comparison of ontogenetic allometric patterns and changes in morphologic disparity are likely to refine our understanding of the intrinsic factors influencing the speciation of this group.

Keywords: Geometric morphometrics, heterochrony, allometry, ontogeny, morphologic disparity, morphospace, Beyrichitinae, Anisian, Nevada

4.4.1 Introduction

Analysis of morphology and ontogeny are the source for evolutionary and developmental studies in deep time. Since the late 20th century, developmental concepts such as heterochrony (e.g., Gould 1977; Alberch et al. 1979; McNamara 1990; McKinney & McNamara 1991; Klingenberg 1998; Zelditch et al. 2012) and morphological disparity or inter- and intraspecific variation (e.g., Gould 1991; Foote 1997; Eble 2000; Ciampaglio et al. 2001) have proven to be an invaluable source of information complementing taxonomic approaches (Eble 2000; Gerber et al. 2008; Bischof et al. 2021) and enriching our knowledge of evolutionary dynamics (Foote 1997; McNamara & McKinney 2005; Gerber et al. 2008; Gerber 2011). If intraspecific variation is regarded as differences between ontogenetic end points, it can be argued that the total amount of disparity is a direct consequence of heterochrony *sensu* Alberch 1979 (McNamara & McKinney 2005). Knowledge of the ontogenetic trajectories is therefore a prerequisite for enlarging our understanding of macroevolutionary development (Gerber et al. 2008). However, despite their close relationship, morphologic disparity patterns have been relatively rarely addressed in the context of heterochronic analyses (e.g., Eble 1998; Eble 2000, 2002, 2003; Zelditch et al. 2003; McNamara & McKinney 2005; Crônier 2013).

In general, heterochrony is defined as change in timing (age) or rate (size) of development relative to the ancestor (McNamara 2012). However, changes in rate and timing of ontogenetic events can, by definition, only be determined where the age of compared individuals is known (McKinney & McNamara 1991; chap. 2). Particularly in paleontology, exact growth rates are often not known (Lécuyer & Bucher 2006; Knauss & Yacobucci 2014). In ammonoids the accretionary growth with preservation of previous chambers, adds a relative time component to the analysis (i.e. the more whorls an individual has, the older it must be). Here it was assumed that the analyzed species have similar coiling rates (i.e., the individual species develop the same number of whorls in the course of their life). Where growth rate is similar between two groups, allometric relationships may reflect true heterochronies (McKinney & McNamara 1991; chap. 2). In general, ammonoids are ideal model organisms to study ontogenetic change, intraspecific variability, and macroevolutionary patterns (Seilacher 1988; Bucher et al. 1996; Landman et al. 1996; Monnet et al. 2011). That is reasoned in their wide paleogeographic distribution, high preservation potential and high taxonomic diversity and morphological disparity (Korn 2012).

Previous research has shown that late Anisian (Middle Triassic) ammonoid assemblages of the Fossil Hill Member in NV Nevada are well suited as morphological case studies (Bischof et al. 2021). The ammonoids are very abundant and well preserved almost throughout the member. In addition, the continuous thin-layered calcareous successions were deposited in a rather stable and calm paleoenvironment (Lehmann et al. in prep.). During the depositional period of the Fossil Hill Member no

major paleoenvironmental shifts were detected. Therefore, the sequences allow to trace morphological change of the species on a high-resolution stratigraphical scale.

Previous geometric morphometric analyses on the Anisian family Ceratitidae Mojsisovics, 1879 of Nevada revealed that members of this group cover a wide range of taxonomic diversity, which, however, is associated with rather low levels of morphologic disparity (Bischof et al. 2021). Quantification of morphological disparity and ontogenetic allometry would provide further insight into the evolutionary history of these species. However, by defitinition, phylogenetic information is crucial in determining heterochronic changes among taxa (McKinney & McNamara 1991; chap. 2). To our knowledge, for ceratitid ammonoids there is no phylogenetic framework available. For the analyses herein, we therefore focused on more closely related species of the subfamily Beyrichitinae Spath, 1934. The continuous successive stratigraphic sections of the Fossil Hill Member of NV Nevada allow to trace the development of individual species of this subfamily.

In this study, we used a landmark-based geometric morphometric approach including a suite of multivariate statistical tests to study morphological change through ontogeny of beyrichitine ammonoids. This is done in order to analyze heterochronic processes and compare the intra- and interspecific developmental patterns of these species. First, we analyzed ontogenetic allometric trajectories and compared the individual pattern to each other at the species level. Furthermore, we investigated whether intra- and interspecific variability patterns of whorl shape can be noticed among all studied species. The analysis of such patterns might reveal important evolutionary mechanisms in the diversification of this clade. In a second step, we contrasted the concept of heterochrony and morphologic disparity in order to assess their interlinkage.

4.4.2 Material & methods

Fossil material

For this study 46 specimens representing a total of eight species of the genera *Gymnotoceras* Hyatt 1877, *Frechites* Smith 1932 and *Parafrechites* Silberling & Nichols 1982 were analyzed. These three genera all belong to the subfamily Beyrichitinae Spath, 1934. The selected species are the most characteristic ammonoids of the late Anisian Fossil Hill Member of NW Nevada, USA. All specimens were collected at the Fossil Hill of the Humboldt Range and in the Muller Canyon of the Augusta Mountains (Pershing County), north-western Nevada, USA. The material is stored in the Geosciences Collection of the University of Bremen (GSUB), Germany. More information on the meta data of the fossil material (i.e. geological framework, biostratigraphy, morphologic comparison, data acquisition) can be found in Bischof et al. (2021).

Members of the three genera in focus are morphologically similar (Bischof et al. 2021; figs. 3–5). The studied species belong to the discoidal morphospace and mainly differ through characteristic ways of ventral arching and some gradual differences in ribbing (Fig. 1). Bischof et al. (2021) have shown that all species follow the same ontogenetic pathway from very depressed to compressed whorls. However, while some species complete the entire path, some stop their development at an earlier ontogenetic stage. This study therefore examines the closely related species in more detail and quantifies the allometric differences between them.

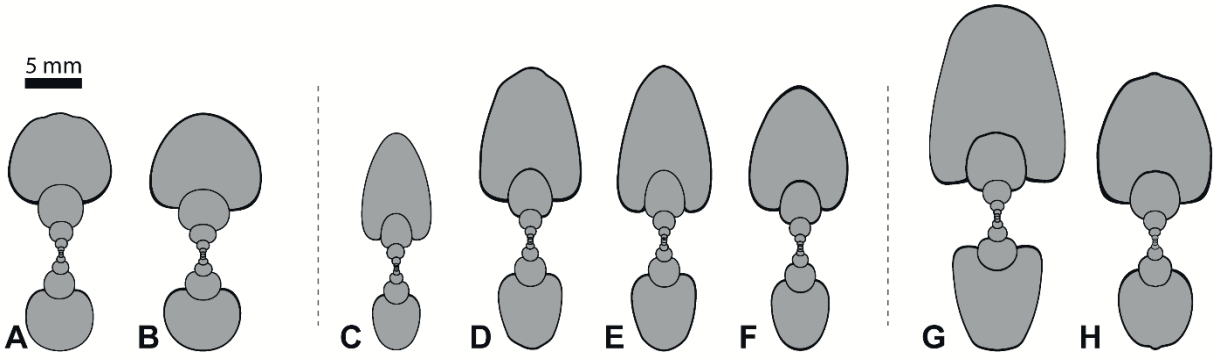

Fig. 1. Cross sections of the analyzed ammonoid species of the late Anisian Fossil Hill Member of NW Nevada, USA; all × 1.5. (A) *Frechites nevadanus*, GSUB C12377. (B) *Frechites nevadanus*, GSUB C13250. (C) *Gymnotoceras weitschati*, GSUB C14190. (D) *Gymnotoceras blakei*, GSUB C12243. (E) *Gymnotoceras mimetus*, GSUB C13814. (F) *Gymnotoceras rotelliformis*, GSUB 11594. (G) *Parafrechites dunni*, GSUB C9356. (H) *Parafrechites meeki*, GSUB C12536.

Data acquisition

The underlying shape data of this study represents an excerpt of the data of Bischof et al. (2021). The landmarks were retrieved using tpsDig2 v.2.31 (Rohlf 2010). Every half whorl is a separate configuration, which is represented by 16 landmarks (Fig. 2). The set of landmarks consists of two unpaired (1, 2) and seven pairs of landmarks (3–16), of which eight are sliding semi-landmarks. To omit missing values in subsequent analyses, the data set was limited to 11 half volutions (i.e., half whorl or growth stage number 5.5). Therefore, every specimen is represented by a total of 176 landmarks (16 landmarks on 11 half whorls).

Geometric morphometric analysis

The exact appearance of any morphospace depends on the shapes which are being analyzed. Therefore, only the raw data of Bischof et al. (2021) were used and the basic geometric morphometric analysis was repeated as briefly summarized below in this sub-section. All geometric morphometric analyses were done using the R software v 3.6.3. (R CoreTeam 2020) including the R packages *Morpho* v2.8 (Schlager 2017), *geomorph* v3.3.1. (Adams et al. 2020) and *RRPP* v0.6.0 (Collyer & Adams 2018; Collyer et al. 2020).

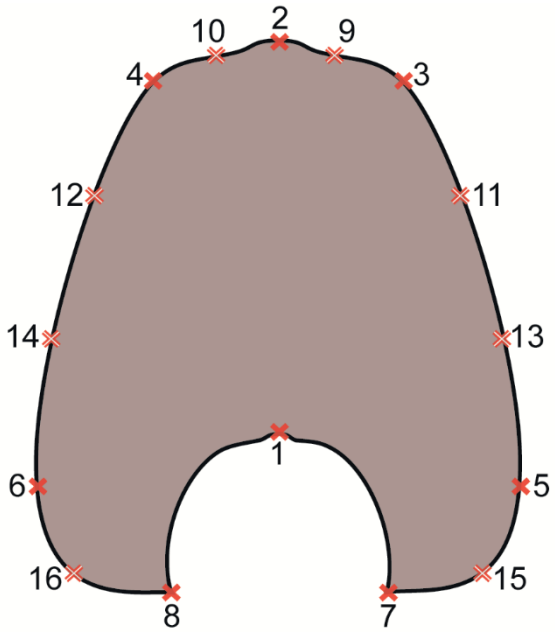

Figure 2. Digitized sketch of high-precision cross-section of an ammonoid whorl with position of landmarks. Filled crosses: fixed landmarks; empty crosses: sliding landmarks; black numbers: number of landmark. Definition of fixed landmarks: 1) venter of preceding whorl; 2) venter of whorl; 3 and 4) ventral shoulder or point of highest curvature; 5 and 6) maximum width; 7 and 8) Umbilical seam.

In a first step the 2D landmark coordinates were subjected to a full generalized Procrustes alignment (GPA) using the *Morpho*::*procSym* function. The full Procrustes fit standardizes size, orientation and position, leaving only the Procrustes shape coordinates (Hammer & Harper 2005). Subsequently, the R function *geomorph*::*combine.subsets* was used to standardize all configurations of all growth stages to unit centroid size (log_{10}CS; un-weighted Procrustes shapes) Centroid size is regarded as a proxy for the size of the whorls and equals the square root of the summed squared distances of each landmark from the centroid of the landmark configuration before the GPA (Zelditch et al. 2012). For the calculation of the two-dimensional morphospace we then ran a principal component analysis (PCA) on the aligned un-weighted Procrustes shape coordinates.

To illustrate morphologic variation an ontogenetic trajectory space and a developmental morphospace were calculated. In an ontogenetic trajectory space, the ontogenetic trajectory of every individual is reduced to a single data point (Bischof & Lehmann 2020; Bischof et al. 2021, formerly called ontogenetic morphospaces). The difference of allometric spaces *sensu* Gerber et al. (2008) to trajectory spaces is that the first use allometric trajectories of the size-shape space instead of ontogenetic trajectories. Whereas ontogenetic trajectory spaces are a tool to examine if the ontogenetic pathways of individuals differ, developmental morphospaces *sensu* Eble (2003, p. 40) describe how trajectories

vary. In the context of this study this means that every individual dot in the developmental morphospace is represented by a specific ontogenetic stage (i.e. half whorl) of an individual (Bischof et al. 2021). The extreme shapes of the developmental morphospace, were calculated with the R function *GeometricMorphometricsMix*::*reversePCA* (Fruciano 2019) and for the computation of the thin-plate spline deformation grids the R function geomorph::plotRefToTarget was used. All scatterplots were drawn with the R package ggplot2 (Wickham 2016).

Ontogenetic allometry

Depending on the scientific context, there are various, closely related biological and evolutionary developmental (evo-devo) terms that can be associated to studies of the size-shape space: Allometry (e.g. Klingenberg 1996; Gerber et al. 2008; Mitteroecker et al. 2013), allometric space (e.g. Gerber et al. 2008; Gerber 2011) or simply heterochrony (e.g. Alberch et al. 1979; McKinney & McNamara 1991; McNamara 2012). To unravel patterns in the ontogenetic development of individuals and the phylogenetic variation between taxa, the size-shape relationship was analyzed here. In this study the allometric space was calculated with a regression analysis of the log-transformed size on the values of the first primary component (PC1) of each species (PCshape ~ $\log_{10}$CS*Group) using the R function *geomorph::procD.lm* with 999 iterations and Sum of Squares type I. To quantify the relationship between Procrustes shape variables and a predictor (here log-transformed centroid size) the function fits a linear model to the Procrustes data and creates a size-shape space. A significant association between size and shape for particular species rejects the null hypothesis of isometry (no change in shape during growth) and reveals the influence of allometry.

Quantification of allometric trajectories

To quantify interspecific and intergeneric allometric relationships, we performed a homogeneity of slopes (HOS; R function *RRPP*::*pairwise*) test and a phenotypic trajectory analysis (R function *RRPP*::*trajectory*.*analysis* with 999 iterations). Both functions test for differences in the slope angle and length of the shape-size relationship to quantify the amount of shape variation, which is explained by size. More details on these procedures can be found in Esquerré et al. (2017, p. 2832).

Allometry is associated with changes during growth with age by definition. Since the age of fossil specimens can only hardly be determined, size and whorl number are used here as a proxy for age. Whereas the HOS test regards size as a continuous variable (i.e. $\log_{10}$size), the *trajectory.analysis* function depends on at least one categorical interaction variable (i.e. number of whorl) as a proxy for size. Therefore, the above computed allometric model (PCshape ~ $\log_{10}$CS*Group) was used in the HOS test and in the trajectory analysis a linear model including the whorl number (PCshape ~ Group * WhorlStage) was used. In general, differences in slope angles and maximum centroid size can be the

result of heterochronic processes. For the terminology for heterochrony we follow the concept of Alberch et al. (1979) which is nicely illustrated in McNamara (2012).

Morphologic disparity

To examine whether intraspecific variability differs amongst growth stages, we used the R function *geomorph::morphol.disparity*. Intraspecific variance is calculated in an analogous manner to morphological disparity (Zelditch et al. 2012). The function calculates absolute differences in Procrustes variances of specified groups and tests for pairwise differences in Procrustes variances between these groups while accounting for group size. The statistical significance of the calculated Procrustes variances between the different growth stages was assessed using a randomized residual permutation test with 999 iterations.

It is very important to note that only discontinuous predictors (i.e. whorls) can be used here. In case a continuous predictor such as $\log_{10}$CS is used, the function *morphol.disparity* uses the overall mean of all configurations. It is also essential to make the distinction between intraspecific (range of variation of a within a species) and interspecific variability (difference of a characteristic between species).

4.4.3 Results

Ontogenetic and developmental morphospaces

The ontogenetic (Fig. 3) and developmental (Fig. 4) morphospace of beyrichitine ammonoids do not substantially differ from the ceratitid morphospaces that were described in Bischof et al. (2021). The first three components (PCs) of the Principal Component Analysis (PCA) on the data set with joint configurations (i.e. ontogenetic trajectory spaces, Fig. 3) account for 63.5 % (PC_1 = 43.7 %, PC_2 = 15.6 %, PC_3 = 4.2 %) of the total variation. Since most of the variation is explained by the first component, the placement of the species along PC1 is the most important characteristic. Whereas the genus *Frechites* occupies the left side (low PC 1-values), in the central and right part of the diagram *Gymnotoceras* and *Parafrechites* intermingle to some extent. This distribution is a first indication that the ontogenetic trajectories have taxonomic significance.

The developmental morphospace (Fig. 4) shows the same three basic ontogenetic phases as described in Bischof et al. (2021): (1) Earliest whorls are flattened and occupy the lower left quadrant (negative PC1 and PC2 values; Fig. 5 A); (2) the depressed whorls of juveniles cover the central area of plot (PC1 = 0; PC2 slightly positive; Fig. 5 B); (3) adults have more compressed and stout whorls, right side of the diagram (positive PC1 and negative PC2 values; Fig. 5 C). The first three components of the

PCA of all growth stages of the specimens as separate configurations (i.e. developmental morphospace) account for 93.8 % (PC_1 = 80.1 %, PC_2 = 10.7 %, PC_3 = 3.0 %) of the total variation.

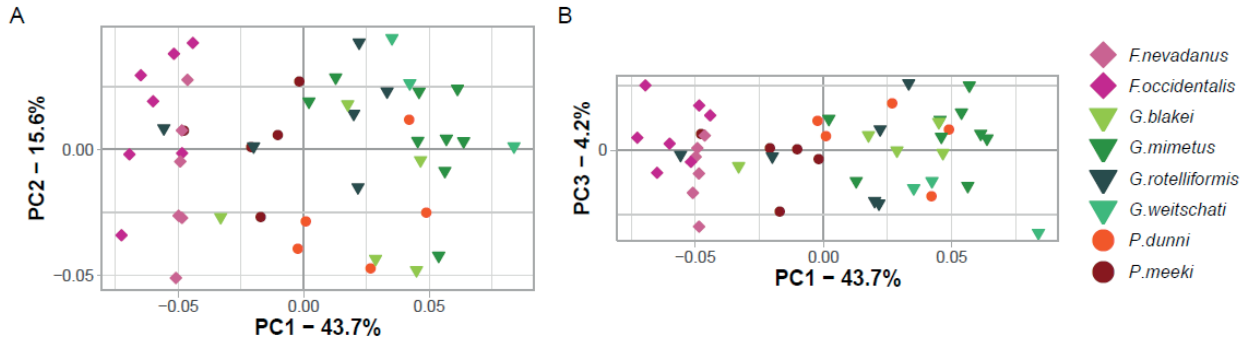

Fig. 3. PCA plots of ontogenetic trajectory space of all species of **A)** Principal Component 1 and 2; **B)** Principal component 1 and 3.

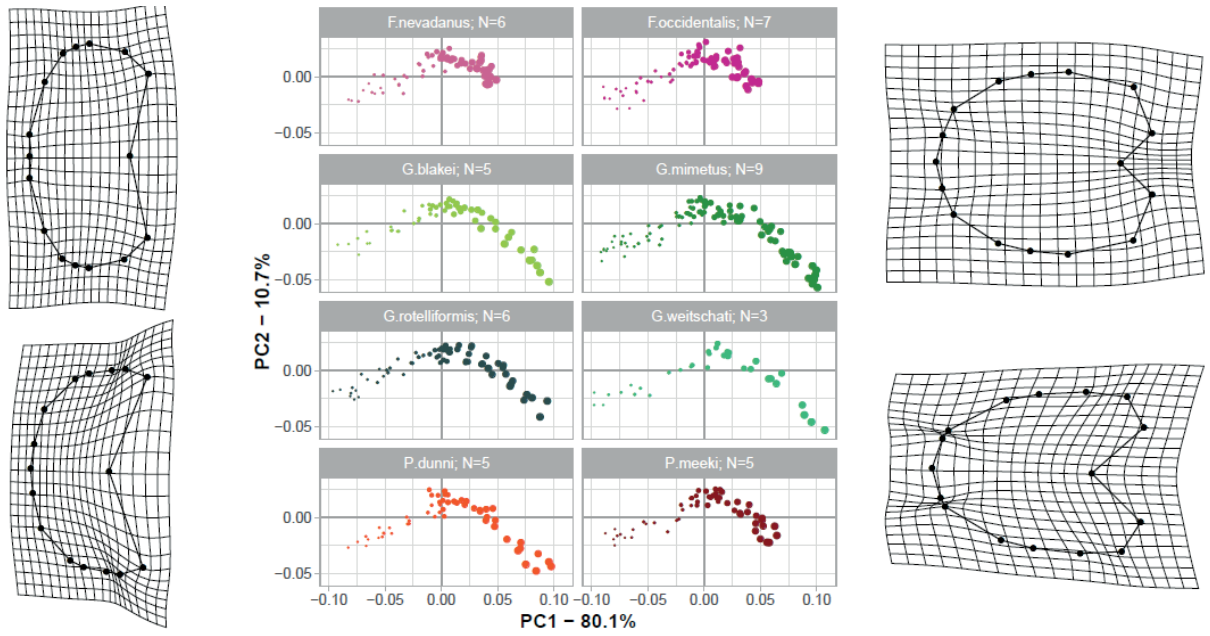

Fig. 4. Developmental morphospace with PCA of un-weighted Procrustes shape variables. Point size refers to growth stage. Deformation grids show the transformation of the mean shape to the modeled shapes of the extreme values for PC1 and PC2.

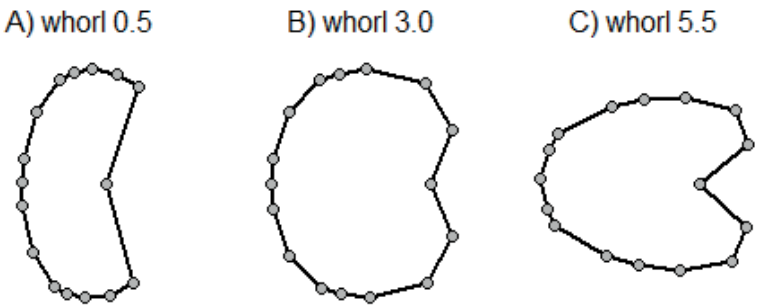

Fig. 5. Mean shapes of growth stages **A)** 0.5, **B)** 3.0 and **C)** 5.5.

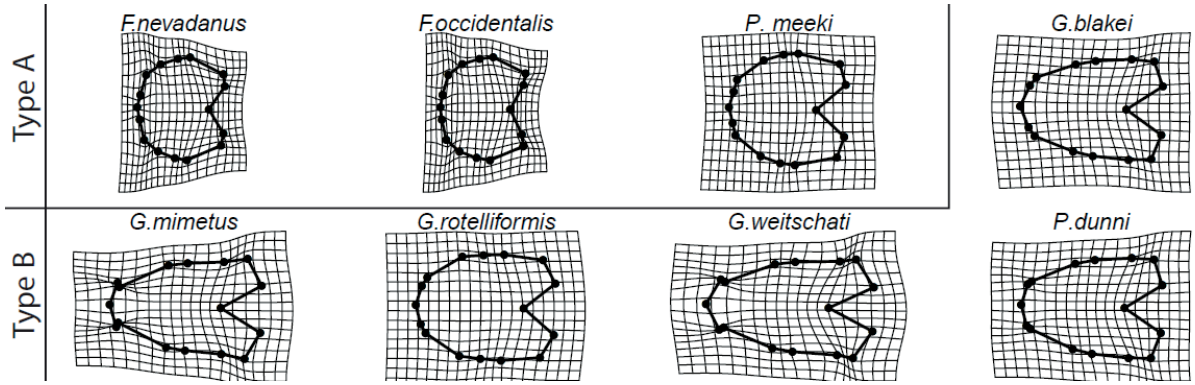

Fig. 6. TPS spline of mean shape of whorl 5.5 of all species in this study (grey) plotted against the mean shape of whorl 5.5 of the respective species (black).

Since the herein studied species show Type A and Type B ontogenetic trajectories (for a discussion on types see Bischof et al. 2021), there are two extreme adult shapes (Fig. 6): Type A) rather depressed, stout conches that do not overlap much the preceding whorl and are associated with much shorter ontogenetic trajectories (*F. nevadanus*, *F. occidentalis*, *P. meeki)*, and Type B) compressed conches with a more pronounced venter and a higher degree of overlap with the preceding whorl (*G. blakei*, *G. mimetus*, *G. rotelliformis*, *G. weitschati*, *P. dunni*).

Examining ontogenetic allometry: Regression model

Whorl shape is influenced by the centroid size, the group (species and/or genus) and the interaction of the two (R function *geomorph::procD.lm*; Table 1). This indicates that there is an ontogenetic allometric (and not isometric) pattern present and the allometric slopes differ amongst species and genus. The full model (PCshape ~ $\log_{10}$CS * species; Table 1) describes the shape significantly better

than the reduced model (PCshape ~ log_{10}CS; additional file 1). Therefore, the full model was used for further analysis.

Table 1. Analysis of variance table obtained from the Procrustes ANOVA (R function RRPP::lm.rrpp) of the full model (PCshape~ log10CS *group) on the species and genus level: Df: Degrees of freedom; SS: Sum of squares; MS: mean squares; R^2: coefficient of determination; Z: Effect sizes (Z) based on F distributions; Pr(>F): p-value of F statistics.

Species	Df	SS	MS	R^2	F	Z	Pr(>F)
log.size	1	0.98264	0.98264	0.70889	1463.5398	7.2528	0.001
species	7	0.02765	0.00395	0.01995	5.8834	6.1831	0.001
log.size:species	7	0.04689	0.00670	0.03383	9.9769	7.7669	0.001
Residuals	490	0.32899	0.00067	0.23734			
Total	505	1.38617					

Genus	Df	SS	MS	R^2	F	Z	Pr(>F)
log.size	1	0.98264	0.98264	0.70889	1401.3677	7.2141	0.001
genus	2	0.01675	0.00837	0.01208	11.9416	4.9199	0.001
log.size:genus	2	0.03619	0.01809	0.02611	25.8034	6.4041	0.001
Residuals	500	0.3506	0.0007	0.25293			
Total	505	1.38617					

The fitted values of the linear regression model were plotted against the log_{10}CS (Fig. 7). Differences in slopes of the ontogenetic allometric trajectories are caused by changes in ontogenetic allometric patterns. There is not much variation in shape of whorl 0.5 between the individual species (Figs. 5, 7), but the range of different shapes of whorl 5.5 is more complex (Figs. 6, 7). The species *G. weitschati* displays a much smaller y-intercept (Fig. Reg) than all other species. However, with three specimens this species had the smallest sample size (Fig. 4) and therefore also less statistical power.

Evaluation and quantification of allometric slopes

Allometric slopes differ among species (Fig. 7) and genera as well. For the statistical quantification of the allometric trajectories an allometric trajectory analysis (R function *RRPP*::*trajectory.analysis*) and a homogeneity of slopes test (HOS; R function *RRPP::pairwise*) were performed. Pairwise comparison of allometric trajectories revealed that all genera and most species have significantly different pairwise slopes (direction of shape change) in at least one of the two test procedures (see additional

file 2). Three species pairs did not reveal statistically significant slopes in either of the two tests (*G. blakei-P. dunni*, *G. weitschati-G. mimetus* and *G. weitschati-G. rotelliformis*). The members of the non-significant pairs all belong to type B.

Whereas the minimal centroid size does not vary much between the individual species, there is more variability in later ontogenetic stages. In general type A species attain smaller maximum (centroid) sizes than type B species. Accordingly, the prevailing heterochronic process from type B to type A can be regarded as a neoteny (pedomorphosis).

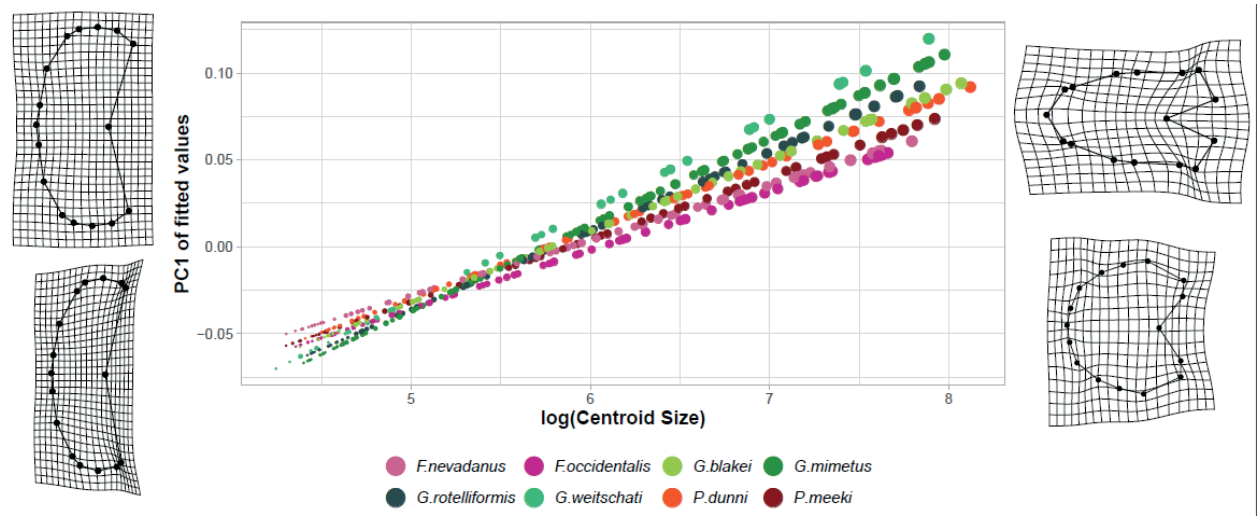

Fig. 7. Ontogenetic allometric trajectories with fitted values of the linear regression model plotted against $\log_{10}$CS. Point size refers to growth stage. TPS splines of Procrustes shapes for extreme regression values against the mean shapes of respective growth stage. The values of the y-intercept and the slopes of all species can be found in Table 2.

Intraspecific variability and morphological disparity during ontogeny

A general pattern in the levels of intraspecific Procrustes variance (Fig. 8 A) among the whorls can be observed in all investigated species: a faint decrease of relative variability occurs after the first whorl (0.5), with a general slight increase after whorl stage 1.5 or 2.0. The taxa *F. nevadanus*, *F. occidentalis* and *P. meeki*, have a relatively homogenous pattern with no significant differences among the whorls in the levels of Procrustes variance. In *G. weitschati*, *G. mimetus, G. blakei*, *G. rotelliformis* and *P. dunni*, in contrast, the Procrustes variance of whorl 5.5 is approximately doubled to tripled compared to previous whorls (see. Fig. 8 A for visual comparison, additional file 3 for data). Whereas the Procrustes variance of whorls 0 to 5.0 of *G. blakei*, *G. rotelliformis* and *P. dunni*, are again relatively homogenous,

as in above mentioned species, *G. mimetus and G. weitschati* are the only species that have a second significant minima of variance between the whorl stage 3.0 and 5.5.

Table 2. Intercept and slopes of linear model of fitted shape values on centroid size. Stratigraphic order from 1=old to 8=young.

Species	Ontog. Type	Stratigraphic order	y-Intercept	Regression slope
G. weitschati	B	1	-0.2914	0.05211
G. mimetus	B	2	-0.2852	0.04963
G. rotelliformis	B	3	-0.2626	0.04529
G. blakei	B	4	-0.2374	0.04107
P. dunni	B	7	-0.2247	0.039
P. meeki	A	6	-0.2119	0.03603
F. occidentalis	A	8	-0.2042	0.03372
F. nevadanus	A	5	-0.1867	0.03175

The total variance of the respective whorls (Fig. 8 B) of the investigated species is relatively homogenous among whorls 0.5–5, with a relatively small drop from whorl 0.5 to whorl 1.5. The variance of following whorls is generally increased again, though, admittedly, no significant differences among whorls 0.5 – whorl 5 can be reported; only whorl 5.5 with the most elevated level of Procrustes variance differs significantly to previous whorls.

The total intraspecific morphologic disparity (Fig. 8 C) in stratigraphic order shows a downward trend from old to young. Especially within the evolutionary line of the genus *Gymnotoceras* the morphologic disparity is constantly decreasing.

4.4.4 Discussion

In this study, ontogenetic allometric trajectories and intraspecific variability patterns of ammonoids were quantified for the first time using geometric morphometric methods. The methods used represents an extension of the methods previously introduced by Bischof et al. (2021). The analysis of the evolutionary patterns revealed that the analyzed species do not really differ through morphological shapes that are developed *per se*, but rather through their individual developmental rates, i.e. heterochrony (Figs. 4, 8). This is confirmed by differences in ontogenetic (Fig. 3) and allometric ontogenetic

trajectories (Fig. 7) among species. The ontogenetic development of the species in focus are characterized by several changes in morphologic disparity (Fig. 8) and developmental rate or "timing" of whorl outline (Fig. 7; Table 1). These findings go in line with previous research on ceratitid ammonoids by Bischof et al. (2021).

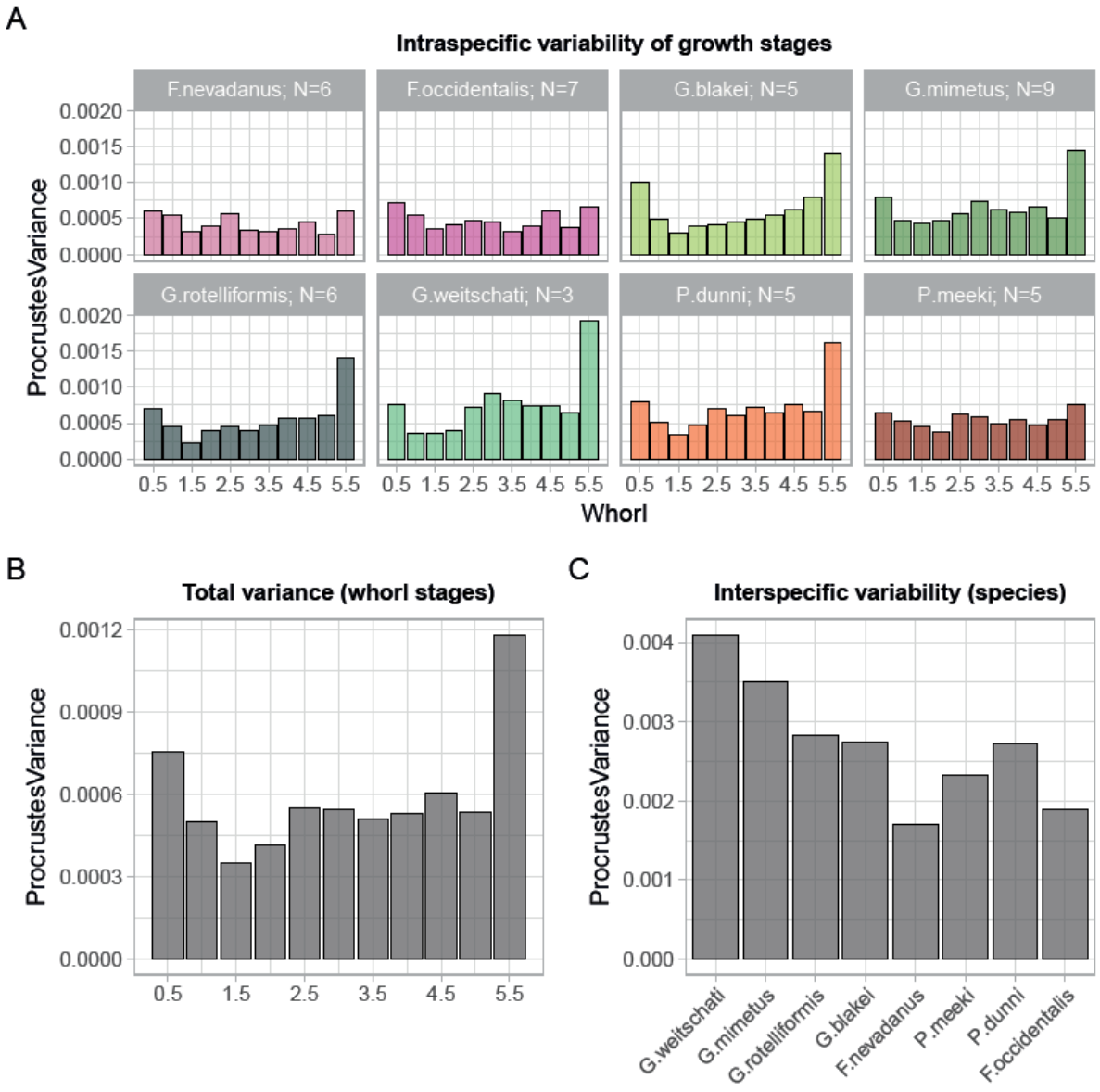

Fig. 8. A) Intraspecific variability patterns. Contribution of individual whorls of species to intraspecific morphologic disparity. The x axis shows the growth stages from 0.5 to 5.5. **B)** Total Procrustes variance of all species at specific growth stages. The x axis shows the growth stages from 0.5 to 5.5. **C)** Contribution of species to overall morphologic disparity. Species are ordered in stratigraphic order from left-old to right-young.

Patterns in ontogenetic allometry

The ontogenetic development of the species and genera in focus are characterized by changes in developmental rate or "timing" of whorl shape (Fig. 7; Table 1), which manifests itself in an almost constant decrease of the allometric slope in stratigraphic order (Table 2). In general, adult representatives of stratigraphically younger species resemble juveniles of stratigraphically older individuals, i.e. pedomorphosis or juvenilization (Gould 1977, p. 209; Alberch et al. 1979; McKinney & McNamara 1991, p. 14).

Due to their small size (+/- 0.4 mm) the earliest whorls are more difficult to measure than later and larger ontogenetic stages. However, more importantly, this large difference implies also that the relative measurement error associated with the earliest (smaller) ontogenetic stages is much larger (Bischof et al. 2021). Such measurement inaccuracies have a greater influence on the y-intercept (more strongly influenced by shape at origin) than on the slope of the allometric trajectories (reflects interplay of all shapes during ontogeny). Therefore, it is suggested that pre- and/or post-replacement of the allometric trajectories was induced by measurement inaccuracies. The full ontogenetic sequence of the studied specimens, as already described by Bischof et al. (2021), includes the transition from flat to depressed to compressed whorls. Thereby the studied species can be divided in two main ontogenetic groups: B) longer trajectories that refer to an elongated adult whorl shape (*G. blakei*, *G. mimetus*, *G. rotelliformis*, *G. weitschati*, *P. dunni*), and A) truncated trajectories that are caused by "juvenilized" (pedomorphic), rather rounded and stout adult whorls (*F. nevadanus*, *F. occidentalis*, *P. meeki*). Regarding the quantification of allometric heterochrony the following three main statements can be made: (1) The pairwise difference in slope of the individual species and genera are statistically significant. (2) The evolutionary lineage of *Gymnotoceras* lineage is characterized by a progressive decrease in allometric slope, i.e. neoteny (pedomorphosis). (3) The smaller allometric slope of Type A species compared to Type B species is indicative for neoteny (resulting in pedomorphosis).

Paleobiologists argue that certain heterochronic changes would be adaptively favored in particular environments (Yacobucci 2015). Thereby, more stable environments can rather be associated with slowed down growth of the pedomorphic development (Neoteny) (Gould 1977, chap. 8; McKinney & McNamara 1991, chap. 4). The relatively calm and stable paleoenvironment under which the successions of the Fossil Hill Member were deposited (Lehmann et al. in prep.) do not challenge this picture.

Intraspecific variability and morphological disparity

Two unequivocal patterns of intraspecific variability during ontogeny can be recognized among the studied species (Fig. 8). The first pattern is characterized by homogeneous levels of Procrustes variance among the whorls and can be detected in *F. nevadanus*, *F. occidentalis* and *P. meeki*

(ontogenetic type A). The ontogenetic trajectories of these species are shorter (Fig. PCA), i.e. reflect pedomorphic development. The second pattern shows a significantly increased level of Procrustes variance in the last whorl (whorl 5.5). The latter pattern is particularly seen in ontogenetic type B species: *G. weitschati*, G. *blakei*, *G. rotelliformis*, *G. mimetus* and *P. dunni*. Similar developmental patterns were detected by Gerber et al. (2007; tab. 2; fig. 6) that described significant higher levels of variance of adult hildoceratid ammonoids than their corresponding juveniles. By applying a traditional morphometric approach, Hoffmann et al. (2019) studied intraspecific variation during the ontogeny in ammonoids, resulting in no clear patterns in variation. The differences in study design hinder a close comparison of their study with ours.

In general, there is no clear-cut pattern in the variability during ontogeny in ammonoids. Studies report ontogenies for instance with a decrease in variability from oldest to youngest stages and vice versa (McNamara & McKinney 2005; De Baets et al. 2015). The intraspecific variability patterns of the studied species can be explained by their ontogenetic developmental grouping rather than by their taxonomic assignment. Particularly within the evolutionary line of the genus *Gymnotoceras* the total Procrustes variance (Fig. 8 C) is characterized by a progressive decrease in stratigraphic order (from old to young).

In case of the studied material elevated levels of morphologic disparity coincide with the occurrence of the three “extreme” shapes (flat – depressed – compressed; Fig. 5). When transitions between developmental stages are accompanied by abrupt changes (critical points or ‘‘Knickpunkte’’; Kullmann & Scheuch 1970; Kant & Kullmann 1973), developmental disparity patterns are likely to be polyphasic as well (Gerber et al. 2007).

It is remarkable that in the intraspecific variability of particularly the ontogenetic type B group group (Fig. 8A; *G. weitschati*, *G. blakei*, *G. rotelliformis*, *G. mimetus* and *P. dunni*) a pattern is revealed which coincides with the total interspecific morphologic disparity of the analyzed species (Fig 8B). The variance of the latest whorl (5.5) is significantly elevated, in comparison to the remaining whorls, in either both, morphologic disparity and intraspecific variability, patterns. Accordingly, the shape of whorl 5.5, which yields the highest disparity in the analyzed species, has also the highest level of intraspecific variability. This might indicate weakened developmental constraints that promote disparity in the shape of the latest whorl among the analyzed beyrichitine ammonoids. Similar observations were made in species of the Late Cretaceous echinoid *Micraster* (Schlüter & Wiese 2018).

4.4.5 Conclusion

Even though heterochronic processes are possible factors responsible for morphologic disparity, the interplay of heterochrony and morphological disparity has only rarely been addressed (McNamara & McKinney 2005). In this study heterochronic relationships and morphologic disparity of ammonoids were quantified using geometric morphometric methods on ontogenetic cross-sections for the first time. Comparisons of disparity, when combined with multivariate statistical analyses of ontogenetic allometric trajectories, help to quantitatively assess the role of development in shaping morphospace occupation and adult disparity (Gerber et al. 2008).

The geometric morphometric analysis of this study revealed that intraspecific variability patterns of the studied species are only roughly linked to their taxonomic classification; rather it is explained by their individual ontogenetic developmental grouping. Therefore, intra- and interspecific morphologic disparity in beyrichitines seems to be the result of perturbations of the allometric growth pattern (i.e. heterochrony). There is evidence that more stable environments can generally rather be associated with slowed down growth of pedomorphic development, i.e. neoteny (Gould 1977, chap. 8; McKinney & McNamara 1991, chap. 4). This suggests that the rather calm and stable environment of the Fossil Hill Member (Lehmann et al. in prep.) favored pedomorphic processes, which is reflected by the continuously decreasing allometric slopes (Fig. 7) of the species studied here.

The comparison of ontogenetic allometry patterns and changes in morphologic disparity are likely to refine our understanding of the intrinsic factors influencing the speciation of this group. Even if the methods introduced herein might not supply the full causal explanation on the diversity and disparity patterns observed, they offer additional insights into the macroevolutionary processes in ammonoids. This study therefore underlines the importance of using quantitative multivariate analyses to properly assess the role of ontogenetic processes in shaping morphologic disparity across species.

References (of chapter 4.4 only)

Adams DC, Collyer ML, and A. K. 2020. Geomorph: Software for geometric morphometric analyses. R package version 3.2.1. https://cran.r-project.org/package=geomorph.

Alberch P, Gould SJ, Oster GF, and Wake DB. 1979. Size and shape in ontogeny and phylogeny. *Paleobiology* 5:296-317.

Bucher H, Landman NH, Klofak SM, and Guex J. 1996. Mode and rate of growth in ammonoids. In: Landman NH, Tanabe K, and Davis RA, eds. *Topics in Geobiology*. New York: Plenum, 407-461.

Ciampaglio CN, Kemp M, and McShea DW. 2001. Detecting changes in morphospace occupation patterns in the fossil record: characterization and analysis of measures of disparity. *Paleobiology* 27:695-715.

Collyer ML, and Adams DC. 2018. RRPP: An R package for fitting linear models to high-dimensional data using residual randomization. *Methods in Ecology and Evolution* 9:1772-1779.

Collyer ML, Davis MA, and Adams DC. 2020. Making heads or tails of combined landmark configurations in geometric morphometric data. *Evolutionary Biology*:1-13.
Crônier C. 2013. Morphological disparity and developmental patterning: contribution of phacopid trilobites. *Palaeontology* 56:1263-1271.
De Baets K, Bert D, Hoffmann R, Monnet C, Yacobucci MM, and Klug C. 2015. Ammonoid intraspecific variability. In: Klug C, Korn D, De Baets K, Kruta I, and Mapes RH, eds. *Topics in Geobiology*. Dordrecht: Springer, 359-426.
De Baets K, Klug C, and Monnet C. 2013. Intraspecific variability through ontogeny in early ammonoids. *Paleobiology* 39:75-94. 10.1666/0094-8373-39.1.75
Dworkin I. 2005. CHAPTER 8 - Canalization, Cryptic Variation, and Developmental Buffering: A Critical Examination and Analytical Perspective. In: Hallgrímsson B, and Hall BK, eds. *Variation*. Burlington: Academic Press, 131-158.
Eble GJ. 1998. The role of development in evolutionary radiations. In: McKinney M, and Drake J, eds. *Biodiversity dynamics: Turnover of populations, taxa, and communities*, 132-161.
Eble GJ. 2000. Contrasting evolutionary flexibility in sister groups: disparity and diversity in Mesozoic atelostomate echinoids. *Paleobiology* 26:56-79.
Eble GJ. 2002. Multivariate approaches to development and evolution. In: Minugh-Purvis N, and McNamara KG, eds.: The Johns Hopkins University Press, 51-78.
Eble GJ. 2003. Developmental morphospaces and evolution. In: Crutchfield JP, and Schuster PM, eds. *Santa Fe Institute Studies on the Sciences of Complexity*: Oxford University Press, 33-63.
Esquerré D, Sherratt E, and Keogh JS. 2017. Evolution of extreme ontogenetic allometric diversity and heterochrony in pythons, a clade of giant and dwarf snakes. *Evolution* 71:2829-2844.
Foote M. 1997. The Evolution of Morphological Diversity. *Annual Review of Ecology and Systematics* 28:129-152. 10.1146/annurev.ecolsys.28.1.129
Fruciano C. 2019. GeometricMorphometricsMix: Miscellaneous functions useful for geometric morphometrics. R package version 0.0.7.9000.
Gerber S. 2011. Comparing the differential filling of morphospace and allometric space through time: the morphological and developmental dynamics of Early Jurassic ammonoids. *Paleobiology* 37:369-382.
Gerber S, Eble GJ, and Neige P. 2008. Allometric space and allometric disparity: a developmental perspective in the macroevolutionary analysis of morphological disparity. *Evolution* 62:1450-1457. 10.1111/j.1558-5646.2008.00370.x
Gerber S, Neige P, and Eble GJ. 2007. Combining ontogenetic and evolutionary scales of morphological disparity: a study of early Jurassic ammonites. *Evolution & Development* 9:472-482.
Gould SJ. 1977. Ontogeny and phylogeny. Cambridge, Massachusetts: Harvard University Press. p 501.
Gould SJ. 1991. The disparity of the Burgess Shale arthropod fauna and the limits of cladistic analysis: why we must strive to quantify morphospace. *Paleobiology*:411-423.
Hammer Ø, and Harper D. 2005. Paleontological data analysis. 2 ed. Cambridge: Blackwell. p 368.
Hoffmann R, Weinkauf MFG, Wiedenroth K, Goeddertz P, and De Baets K. 2019. Morphological disparity and ontogeny of the endemic heteromorph ammonite genus Aegocrioceras (Early Cretaceous, Hauterivian, NW-Germany). *Palaeogeography, Palaeoclimatology, Palaeoecology* 520:1-17. https://doi.org/10.1016/j.palaeo.2019.01.020
Hunt G. 2004. Phenotypic variation in fossil samples: modeling the consequences of time-averaging. *Paleobiology* 30:426-443.
Hyatt A. 1877. Part I. Palæontology. In: Meek FB, ed. *Report of the US Geological Exploration of the 40th Parallel*. Washington: US Government Printing Office, 110-111.
Kant R, and Kullmann J. 1973. "Knickpunkte" im allometrischen Wachstum von Cephalopoden-Gehäusen. *Neues Jahrbuch für Geologie und Paläontologie, Abhandlungen* 142:97-114.
Klingenberg CP. 1996. Multivariate allometry. In: F. ML, M. C, A. L, P. NGJ, and E. SD, eds. New York: Plenum Press, 23-49.

Klingenberg CP. 1998. Heterochrony and allometry: the analysis of evolutionary change in ontogeny. *Biological Reviews* 73:79-123.

Knauss MJ, and Yacobucci MM. 2014. Geographic Information Systems technology as a morphometric tool for quantifying morphological variation in an ammonoid clade. *Palaeontologia Electronica* 17:1-27.

Korn D. 2012. Quantification of ontogenetic allometry in ammonoids. *Evolution & Development* 14:501-514. doi:10.1111/ede.12003

Kullmann J, and Scheuch J. 1970. Wachstums-Änderungen in der Ontogenese paläozoischer Ammonoideen. *Lethaia* 3:397-412.

Landman NH, Tanabe K, and Shigeta Y. 1996. Ammonoid embryonic development. In: Landman NH, Tanabe K, and Davis RA, eds. *Topics in Geobiology*. New York: Plenum, 343-405.

Lécuyer C, and Bucher H. 2006. Stable isotope compositions of a late Jurassic ammonite shell: a record of seasonal surface water temperatures in the southern hemisphere? *eEarth Discussions* 1:1-19.

McKinney ML, and McNamara KG. 1991. Heterochrony. The Evolution of Ontogeny. New York: Springer Science+Business Media, LLC. p XXI+437.

McNamara KJ. 1990. Heterochrony. In: Briggs DEG, and Crowther PR, eds. Oxford-London-Edinburgh-Boston-Melbourne: Blackwell, 111-119.

McNamara KJ. 2012. Heterochrony: the evolution of development. *Evolution: Education and Outreach* 5:203-218.

McNamara KJ, and McKinney ML. 2005. Heterochrony, disparity, and macroevolution. *Paleobiology* 31:17-26.

Mitteroecker P, Gunz P, Windhager S, and Schaefer K. 2013. A brief review of shape, form, and allometry in geometric morphometrics, with applications to human facial morphology. *Hystrix, the Italian Journal of Mammalogy* 24:59-66.

Mojsisovics Ev. 1879. Vorläufige kurze Übersicht der Ammoniten-Gattungen der mediterranen und juvavischen Trias. *Verhandlungen der Kaiserlich-Königlichen Geologischen Reichsanstalt Wien* 1879:133-143.

Monnet C, De Baets K, and Klug C. 2011. Parallel evolution controlled by adaptation and covariation in ammonoid cephalopods. *BMC Evolutionary Biology* 11 (115):1-21. 10.1186/1471-2148-11-115

Rohlf F. 2010. TPSDig2: A program for landmark development and analysisAvailable at: http://life.bio.sunysb.edu/morph (accessed at January 30, 2018)).

Schlager S. 2017. Morpho and Rvcg – Shape Analysis in R: R-Packages for Geometric Morphometrics, Shape Analysis and Surface Manipulations. In: Zheng G, Li S, and Székely G, eds. San Diego: Academic Press, 217-256.

Schlüter N, and Wiese F. 2018. The variable echinoid *Micraster woodi* sp. nov. – Trait variability patterns in a taxonomic nightmare. *Cretaceous Research* 87:194-205. https://doi.org/10.1016/j.cretres.2017.05.019

Seilacher A. 1988. Why are nautiloid and ammonite sutures so different ? *Neues Jahrbuch für Geologie und Paläontologie, Abhandlungen* 177:41-69.

Silberling NJ, and Nichols KM. 1982. Middle Triassic molluscan fossils of biostratigraphic significance from the Humboldt Range, northwestern Nevada. *US Geological Survey Professional Paper*.

Smith JP. 1932. Lower Triassic Ammonoids of North America. Washington: United States Government Printing Office. p iv+199.

Spath LF. 1934. Catalogue of the fossil Cephalopoda in the British Museum (Natural History): Part IV The Ammonoidea of the Trias. London: British Museum of Natural History. p 521.

Tajika A, and Klug C. 2020. How many ontogenetic points are needed to accurately describe the ontogeny of a cephalopod conch? A case study of the modern nautilid *Nautilus pompilius*. *PeerJ* 8:e8849. 10.7717/peerj.8849

Team RC. 2020. R: A Language and Environment for Statistical Computing. Version 3.6.3. Vienna, Austria: R Foundation for Statistical Computing.

Webster M. 2019. Morphological homeostasis in the fossil record. *Seminars in Cell & Developmental Biology* 88:91-104. https://doi.org/10.1016/j.semcdb.2018.05.016

Wickham H. 2016. *ggplot2: elegant graphics for data analysis*. New York: Springer.

Yacobucci MM. 2015. Macroevolution and paleobiogeography of Jurassic-Cretaceous Ammonoids. In: Klug C, Korn D, De Baets K, Kruta I, and Mapes RH, eds. *Topics in Geobiology*. Dordrecht: Springer, 189-228.

Zelditch M, Sheets HD, and Fink W. 2003. The ontogenetic dynamics of shape disparity. *Paleobiology*:139–156. 10.1666/0094-8373(2003)029<0139:TODOSD>2.0.CO;2

Zelditch ML, Swiderski DL, and Sheets HD. 2012. Geometric morphometrics for biologists: a primer. 2 ed. London, Waltham & San Diego: Academic Press. p 478.

4.5 Additional case study

Palaeoenvironment of the Fossil Hill Member (Middle Triassic) in Nevada, USA

(manuscript in progress)

Jens Lehmann, Eva Bischof, Thomas Lis, Martin Sander, Patrick G. Embree

Palaeoenvironment of the Fossil Hill Member (Middle Triassic, Anisian), Nevada, USA

(manuscript in progress)

Jens Lehmann[1], Eva Bischof[1], Thomas Lis[1], Martin Sander[2] & Patrick G. Embree[3]

[1] Geosciences Collection, FB Geosciences, University of Bremen, Klagenfurter Strasse 4, 28357 Bremen, Germany

[2]Steinmann Institute, Paleontology, University of Bonn, Nußallee 8, 53115 Bonn, Germany

[3]Resource Exploration and Drilling, LLC; 8834 Central Avenue, CA 95662 Orangevale, California, USA

Abstract

Carbonatic successions of the Late Anisian in northern Nevada (USA) are lithologically fairly monotonous successions with a fossil record investigated since the 19th century. Shells of ammonoids and halobiid bivalves are abundant in these strata and thus subject to studies of early palaeontologists, as well as its ichthyosaurs that give insights into the early evolution of this group. Nevertheless, most studies based on material collected under insufficient stratigraphic control and thus we re-investigated the classical Fossil Hill site in the Humboldt Range in Nevada (USA) as well as in the neighboured Augusta Mountains. Extensive trenching allowed a detailed investigation of the measured sections, its microfacies and palaeontological content. This is including the analysis of the occurrence patterns of several thousand invertebrate fossils (mainly ammonoids). The depositional realm is generally reconstructed as a steep shelf-ramp of moderate depth. The Fossil Hill site is a succession deposited in a more dynamic depositional setting compared to the Augusta Mountain succession “as indicated by quite a few changes in microfacies. This includes episodes of higher water energy as indicated by packstones and tephra layers including the newly defined Red Bed interval. In contrast, the much more expanded Augusta Mountain succession is dominated by less frequent changes in carbonate microfacies and a predominance of wackestones that indicate a rather calm depositional regime.

The abundant halobiid bivalves are autochthonous/parautothonous, indicating at least episodically well-oxygenated conditions. A post-mortem settlement of ammonoid shells by oysters indicate that the oxygenation was at least episodically sufficient for benthic life. This agrees with the occurrence of gastropods as well as an agglutinating benthic foraminifera fauna that is low-diversity though.

4.5.1 Introduction

As an aftermath of the Permian/Triassic boundary crisis the carbonate system changed dramatically - almost certainly reflecting a large-scale shift in ocean chemistry that lasted at least for most of the Early Triassic (Baud et al., 2007). The resulting non-skeletal carbonate factory of the Lower Triassic was slowly started again (Baud and Richoz, 2004; Baud et al., 2007). Novel Triassic taxa performed few new ecosystem functions compared to middle Permian taxa and thus probably did not fill into new ecospaces as broadly suggested earlier (Dineen et al., 2019). This might be a reason why- at least in some areas - the recovery of complex communities was less delayed (Brayard et al., 2011). This view is not necessarily contradictory to the traditional opinion that the recovery of protozoans, metazoans, the diversification of animals with skeletons and particularly reefs, was delayed until the Middle Triassic (Hallam, 1991; Schubert and Bottjer, 1995; Flügel and Kiessling, 2002; Pruss and Bottjer, 2005; Weidlich, 2007; Payne et al., 2011), but it shows that the organismic response to the event follows a complex pattern. In fact, examples of a lowered diversity in the early to middle Triassic interval are not necessarily connected with the aftermath of the Permian/Triassic crisis. Locally limited ecological complexity is shown to have been induced by tectonic movements for example (Mercedes-Martín and Buatois, 2021), but when compared to coeval open marine settings this can be interpreted as opportunistic colonization in a restricted, shallow water facies belt. For this reason, it is important to understand the facies patterns and palaeoenvironmental development of the wider recovery interval of the early and middle Triassic on a global scale and at different bathymetric positions.

Here we focus to reconstruct the biofacies of the open water ecosystems at the eastern rim of the Panthalassan ocean in modern Nevada (Fig. 1). This is important because we need to understand the facies patterns of this bathymetric setting in this area that has been in focus

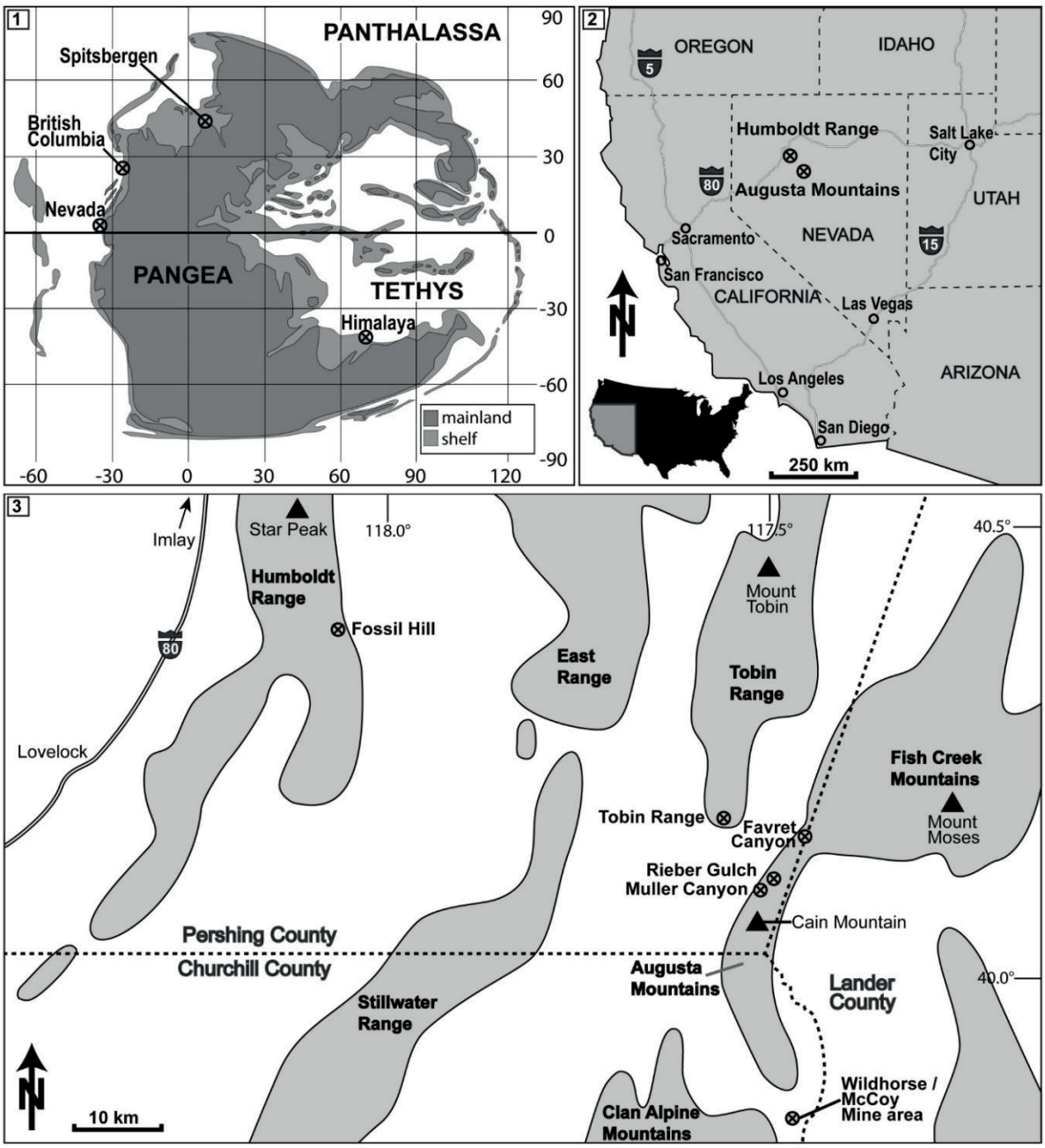

Fig. 1. (1) Global palaeogeographic reconstruction for the Middle Triassic, following Péron et al. (2005), Brayard et al. (2006) and Skrzycki et al. (2018), with some globally important successions. **(2)** Position of the working-areas in the Humboldt Range and Augusta Mountains within western North America. **(3)** Position of the measured sections of the Fossil Hill Member obtained during field-work and other prominent sites in this respect.

for palaeontological research for a long time already, but that has not been understood in terms of many palaeoenvironmental and palaeoecological aspects. Palaeontological research on the Triassic of Nevada was particularly focussing on marine reptiles (Leidy, 1868; Merriam, 1908; Sander et al., 1994 ; Sander et al., 1997; Schmitz et al., 2004) and

ammonoids (Smith, 1914; , 1932; Silberling and Nichols, 1982; Bucher, 1992; Monnet et al., 2010; Bischof and Lehmann, 2020). Ammonoids were unequivocally a very important part of the food web, but beyond these the Nevada occurrences allow the study of a time interval and its fauna of the initial phase of the Mesozoic Marine Revolution (MMR), the full reorganisation of predator-prey relationships after the Permian/Triassic extinction event according to the concept developed by Vermeij (1977). Processes and the development of marine benthic invertebrates with respect to the MMR are becoming better proved recently (Tackett and Bottjer, 2012), but we know little about the development of predator-prey relationships of nektonic organisms and its palaeoenvironmental background. This is important, however, since particularly the Anisian is identified as comprise the onset of several predatory taxa that are significant throughout the Mesozoic (Harper, 2003). Anisian sediments of Nevada can provide a deep insight into these questions and here we contribute by analysing microfacies, microfossil samples and selected macrofossils. They have been deposited on the deeper shelf/slope of a submarine Back-Arc setting at the Mesozoic continental margin of North America (Wyld, 2000, 2002 ; Ingersoll, 2008; LaMaskin et al., 2011) and did comprise turbiditic and hemipelagic to carbonatic sediments (Saleeby et al., 1992). As an ecosystem representing a fully developed food web after the environmental stress by the Permian/Triassic event this (Fröbisch et al., 2013), but still during the initial MMR, a facies analysis constitutes a relevant topic from our view. The framework of the sedimentation is steered by the global condition of the huge Panthalassa and Tethys oceans well connected, with a mega-monsoon belt along the equator (Parrish, 1993; Preto et al., 2010; Ogg et al., 2020).

In this framework, we analyse the succession of late Anisian carbonates of the Star Peak/Luning Basin belonging to two different Formations, Prida- and Favret Formation in the present study. Each of them contains the Fossil Hill Member, but despite an identical name both are regarded as different sedimentary bodies (Wyld, 2000). One focus of this paper is on parts of the the Fossil Hill Member of the Prida Formation at its type locality at Fossil

Hill in the Humboldt Range. This is the first study based on freshly made trenches and thus enabling detailed measured sections at this deeply eroded outcrop. Former studies were mostly referring to sets of outcropping beds, most of the succession remained covered and its lithology and fossil content of the gaps were interpolated based on picked

up and loose material. We also focus on the succession of the Fossil Hill Member of the Favret Formation in Pershing County, Augusta Mountains. In this part of Nevada morphological elevations are higher, with steep erosional slopes, and thus we were able to measure and sample continuous detailed sections without digging trenches. The successions mentioned cover a time interval of roughly estimated almost three million years according to the latest international time scale (Ogg et al., 2020), based on a correlation of the ammonoid standard zonation mainly based on the Mediterranean realm (Jenks et al., 2015). This paper also documents the stratigraphy for of some vertebrate fossils, among these some relevant material including a type described by Schmitz et al. (2004). Here the stratigraphical context of each of these published specimens are documented for the first time.

Previous work

The Fossil Hill Member (middle and late Anisian) consists of alternating layers of calcareous siltstone and mudstone with lenticular limestone. The rich fauna of the succession primarily consists of halobiid bivalves and ammonoids. Ceratitids are quite abundant and diverse throughout the member. The biostratigraphically important ammonoid faunas of the Humboldt Range were previously described in the 19th and early 20th century (Gabb, 1864; Hyatt and Smith, 1905; Smith, 1914). Recently, Silberling and Nichols, 1982 and Monnet and Bucher, 2005 refined the biostratigraphy of the succession. The Fossil Hill locality became, however, most famous by findings of marine reptiles, mainly ichthyosaurs, starting with Leidy (1868). They are described as accumulated and also better preserved compared to Californian fossils at Fossil Hill and at the neighbouring Saurian Hill (Merriam, 1908). This monograph is part of a series of papers by Merriam and co-authors exploiting this remarkable occurrence (Merriam, 1905, 1906, 1910; Merriam and Bryant, 1911a, b). This work is based on historically well-recognized field-work in 1905, joined and financed by Annie Montague Alexander (https://ucmp.berkeley.edu/about-ucmp/history-of-ucmp/annie-alexander/; accessed February 21, 2021; Anonymous, 1980). Recent work on vertebrates from this site is on Lower Triassic fossils (Kelley et al., 2016). Despite these extensive palaeontological studies very little work has been done on the rocks itself. A couple of thin section of Anisian age have been figured by Horowitz and Potter (1971).

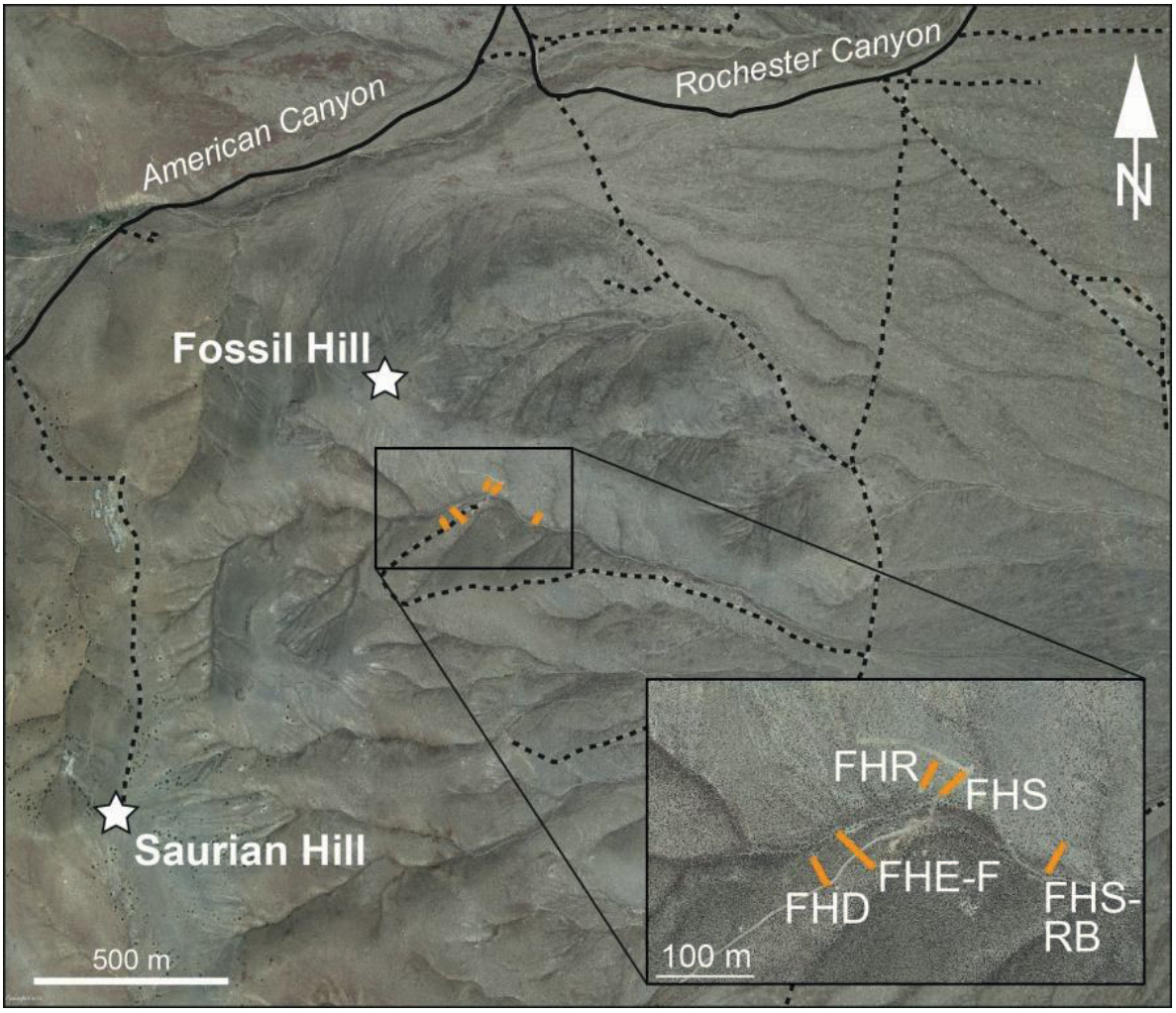

Fig. 2. Location of the measured section at Fossil Hill. Humboldt Range, Nevada. Stars indicate peaks of mountains, roads in italics. Map modified after Google (2021).

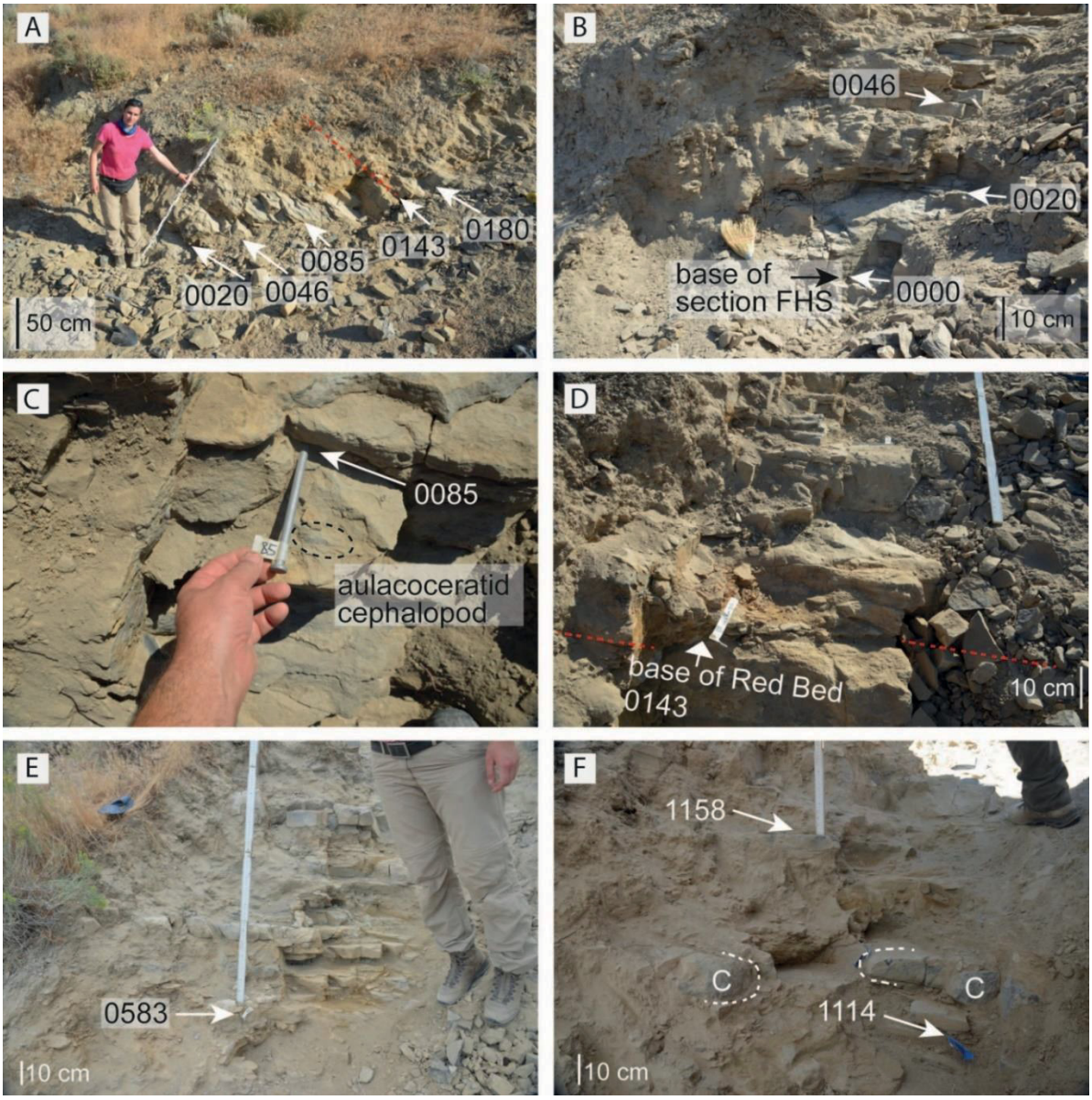

Fig. 3. Documentation of field-work at Fossil Hill, Humboldt Range, section FHS, trench 2017. **(A)** Lowermost part of the measured section. **(B)** Detail of base of the FHS section. C: Semipermanent field-markers indicating position section meter 0.85, and fragment of an aulacoceratid cephalopod in situ at section meter0.80. **(D)** Base of Red Bed, a reddish weathering succession of the FHS section, at section meter 1.43. **(E)** Succession above section meter 5.83, showing a succession of the upper part of the Red Bed interval. **(F)** Discontinuous carbonate concretions (c) in the upper part of the FHS section.

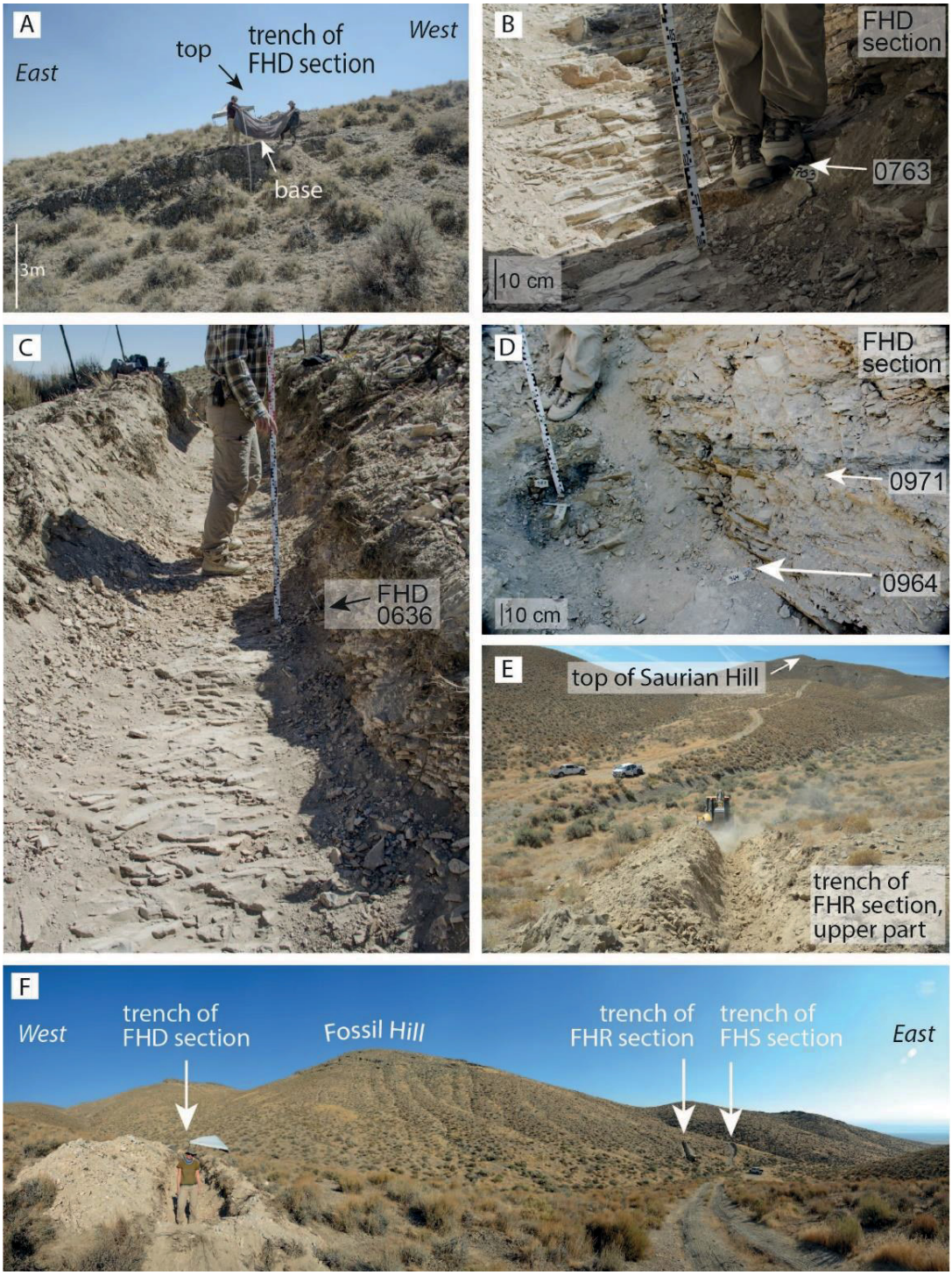

Fig. 4. Documentation of field-work at Fossil Hill, Humboldt Range, sections FHD and FHS, trenched 2018. **(A)** Base of the measured section FHD, starting at the southeasternmost limit of a low but prominent limestone cliff. **(B)** Detail of FHD trench at section meter 7.63. **(C)** Trench around section meter 6.36. **(D)** Succession of the FHD succession, note the darker claystone above section meter 9.71. **(E)** Southeast view from the upper limit of the FHS trench, in the center of the picture a backhoe used for the works is visible. **(F)** Panoramic view with Fossil Hill in the center and position of trenches FHD, FHR and FHS.

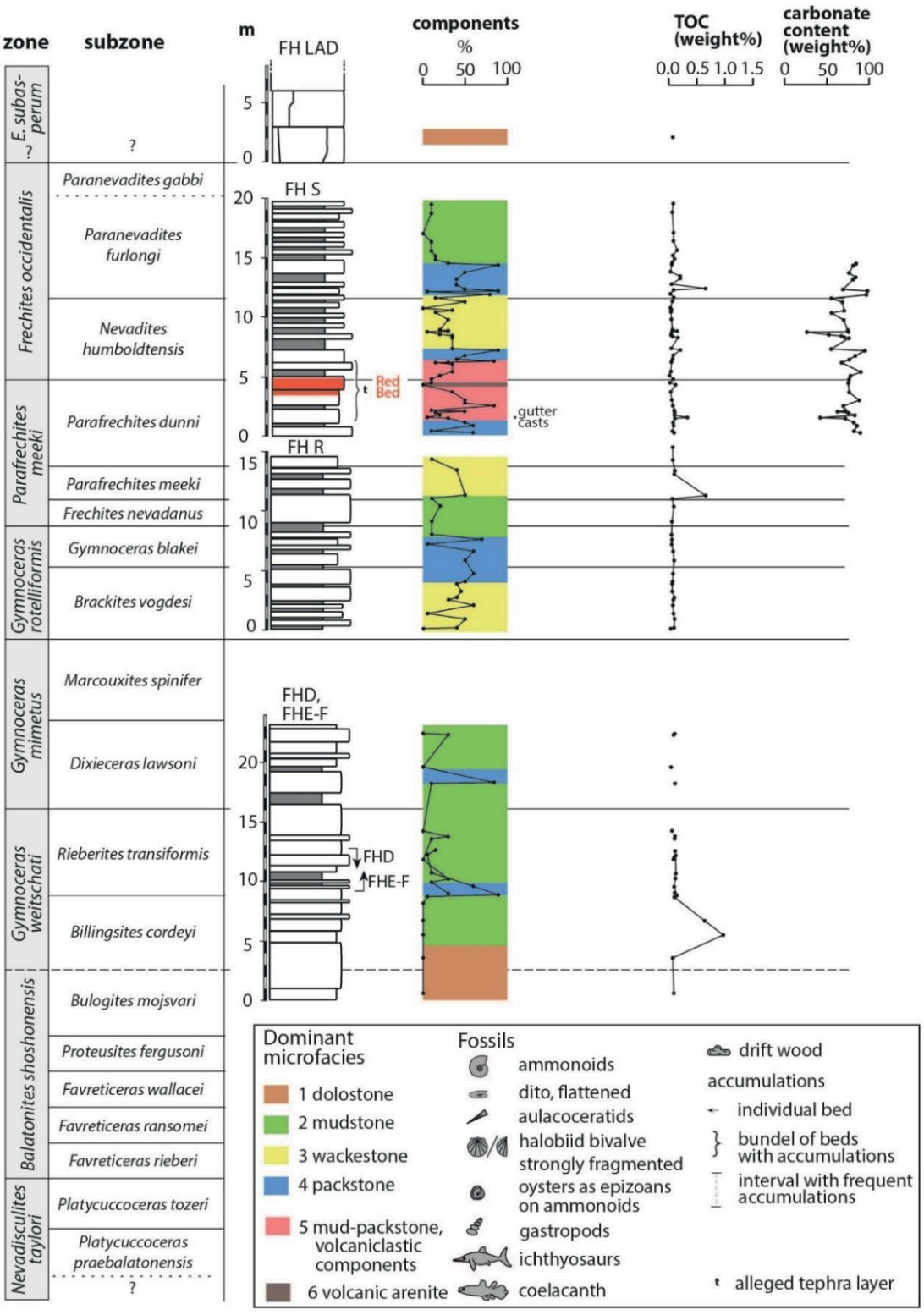

Fig. 5. Measured sections at the Fossil Hill locality, Humboldt Range, with biostratigraphical dating based on ammonoids (own data), following former zonal- and subzonal schemes by Smith (1914), Silberling and Nichols (1982), Bucher (1992), Monnet and Bucher (2005), with modifications by Jenks et al. (2015) and microfacies. Note that the lithological columns indicate the prevailing lithology, since it was idealised due to the scale of this overview figure.

4.5.2 Localities, methods and conventions

The field-work for this study was performed by a group of each three respectively four members of the Geosciences Collection of the University of Bremen (Germany) in 2017 and 2018. We visited the classical Fossil Hill site in the Humboldt Range, north-western Nevada, USA as well as Muller and Favret Canyons in the Augusta Mountains (Pershing County) (Fig. 1).

Fossil Hill. At Fossil Hill several sections of the Fossil Hill Member was unearthed by using a backhoe by the owner of the property, geologist P. Embree (Figs. 2-4). Later these trenches were renaturated. Due to this machinery work it was possible to reveal a total number of five individual sections with a different thickness in great detail. These are – from the base to the top: FCE (20.65 m), FHD (12.27 m), FHEF (13.40 m), FHR (15.31 m), FHSRB (2.29 m) and FHS (19.46 m). They were logged and rock as well as fossil samples were taken. A part of these secions are overlapping (Fig. 5). Subsequently a synthetic log was composed from the very detailed field observations.

Augusta Mountains. At the Augusta Mountains a complete section of the upper portion of the Fossil Hill Member of the Favret Formation (late Anisian), and the lowermost part of the early Ladinian Home Station Member of the Augusta Mountain Formation, was meticulously documented and measured (Figs. 6 and 7). This constitutes our main section in this area, with a

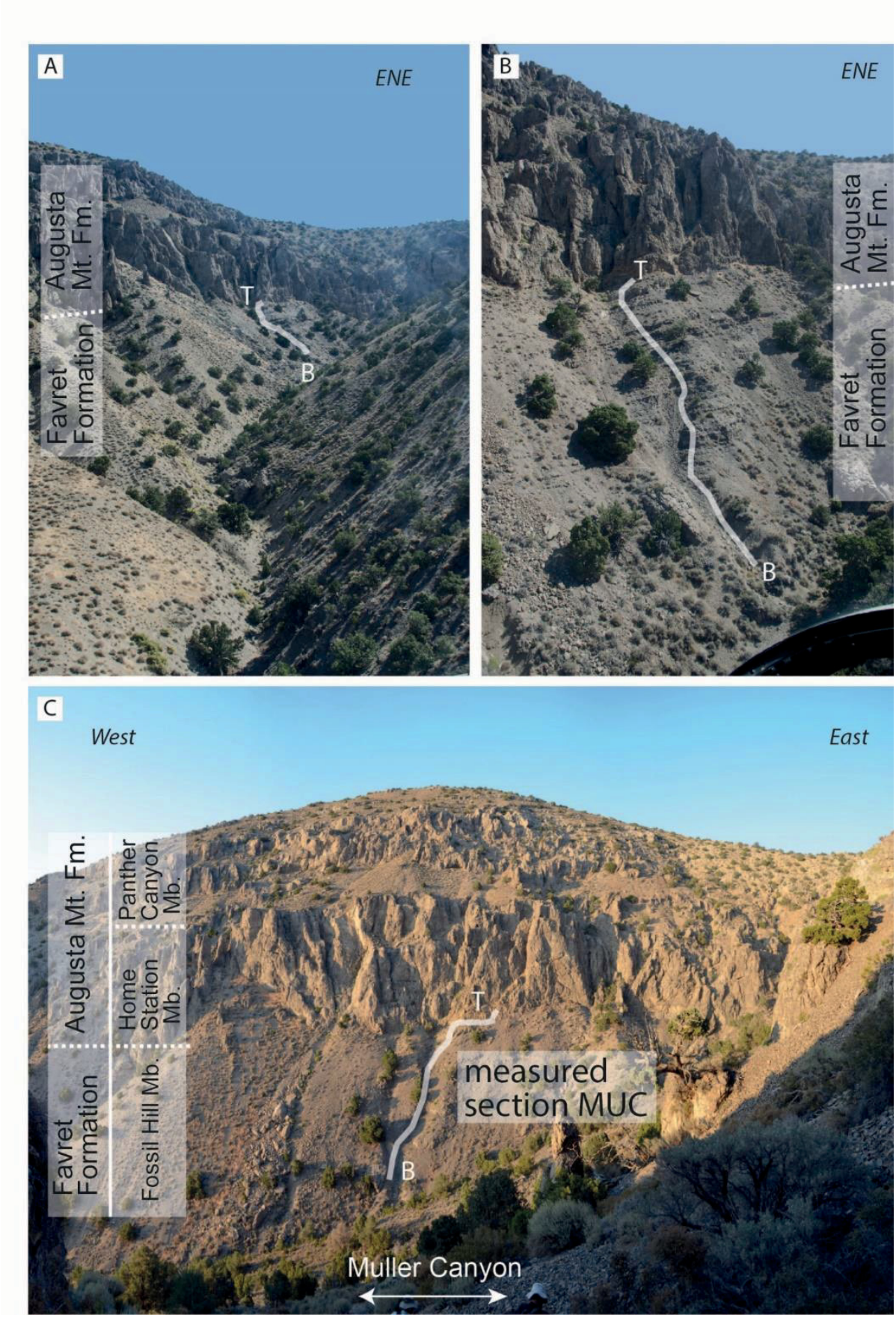
A
ENE
Augusta Mt. Fm.
Favret Formation
T
B
B
ENE
Augusta Mt. Fm.
Favret Formation
T
B
C
West
East
Augusta Mt. Fm.
Panther Canyon Mb.
Home Station Mb.
Favret Formation
Fossil Hill Mb.
T
measured section MUC
B
Muller Canyon

Fig. 6. Location of the measured MUC section in Muller Canyon, Augusta Mountains. **(A)** View from a helicopter from the central part of the canyon towards the eastern end of Muller Canyon. T=Top and B=Base of the measured section. **(B)** Same as A, but view close to the eastern end of Muller Canyon. **(C)** View from the slope of the mountains of the southern rim of Muller Canyon to the north. Mt.=Mountain, Mb.=Member.

total length of about 56 m. Since the locality is part of Muller Canyon and thus the section was abbreviated MUC. The MUC section consists of exactly 56.9 section meters that were available for study without any gap (Fig. 8). Logging was started at the base located at N40°02'29.1'',

W117°33'00.2'' in the Favret Formation (Fossil Hill Member), following the best outcrop conditions to the foot of the cliff forming Home Station Member of the Augusta Mountain Formation (Fig. 8). To retain the option to measure further downwards numbering started with sample number 1000 during initial field-work, later this turned out to be impossible. Of the totally logged almost 56.09 m only the about 3.5m topmost meter belong to the Home Station Member, the boundary between the Favret Formation and the Augusta Mountain Formation is at section meter 55.53. Logging further downwards from the base of section MUC was impossible from the logistic point of view, but a shorter section of almost 21 m of the middle Anisian lower part of the Fossil Hill Member has been documented in the same way as MUC. This section is located in the neighboured Favret Canyon (Fig. 1.3) and is abbreviated FCE.

Since the topography is very steep, there was no need to move a lot of overburden in contrast to the Fossil Hill locality. In the Augusta Mountain trenching work was performed gentle, restricted to parts of the succession covered by a thin layer of debris only and in general work has been done by hand and under care since it is a Wilderness Study Area and the use of any machinery is forbidden. The rock in the Augusta Mountains is distinctly less weathered compared to Fossil Hill and thus the detailed logging of measured section was easier because of less rock dust and debris. Recognizing fossils in the field was also easier under these circumstances.

Microfacies. The microfacies of a total of 186 thin sections have been described and analysed for this study, the sample abbreviations MUC (Muller Canyon) and FCE (Favret

Canyon east section= originate from the Augusta Mountains, respectively samples FHD, FHEF, FHR, FHS, FLAD from Fossil Hill.

Their identification is based on the classical classification by Dunham (1962). In case of a few thin section specimens energy dispersive x-ray spectroscopy has been applied. For each section biogene components (mainly ostracods, ammonoids, radiolarian, bivalves) and inorganic components (quartz grains, pyrite) have been counted in a semiquantitative approach, preservational mode and sorting were also noted. The frequency distribution has been captured in 5% steps, using the charts by Flügel (2010, electronic enclosure). Qualitative analysis ended up with identifying microfacies types (abbreviated MF in the following). Microfossils

identifications are based on Horowitz and Potter (1971), MacPhie et al. (1993), Adams and Mac Kenzie (2001) and Ulmer-Scholle et al. (2015).

Energy dispersive X-ray spectroscopy (EDX) has been done for the microproblematics and vesicular particles probably of volcanic origin.

We refer to fossils stored in the Geosciences Collection of the University of Bremen, Federal State of Bremen, Germany (GSUB) and the Cincinnati Museum Center, Museum of Natural History and Science, Cincinnati, Ohio, USA (CMC).

4.5.3 Sections

Fossil Hill

FHD section. The base of the FHD reaches into the middle Anisian Lower Member (Balatonites shoshonensis Zone, Bulogites mojsvari Subzone) which is characterised by thick-bedded, grey weathering limestone with bed thicknesses of 30-40 cm.

Section FHD revealed only a sparse record of macrofossil in the field with ammonoids in section meters FHD 845, 920 and 1085 only. Daonellid bivalves have been traced only at three levels (section meters FHD 841, 946 and 1075), only in the topmost layers daonellids are abundant (FHD 1210-1225).

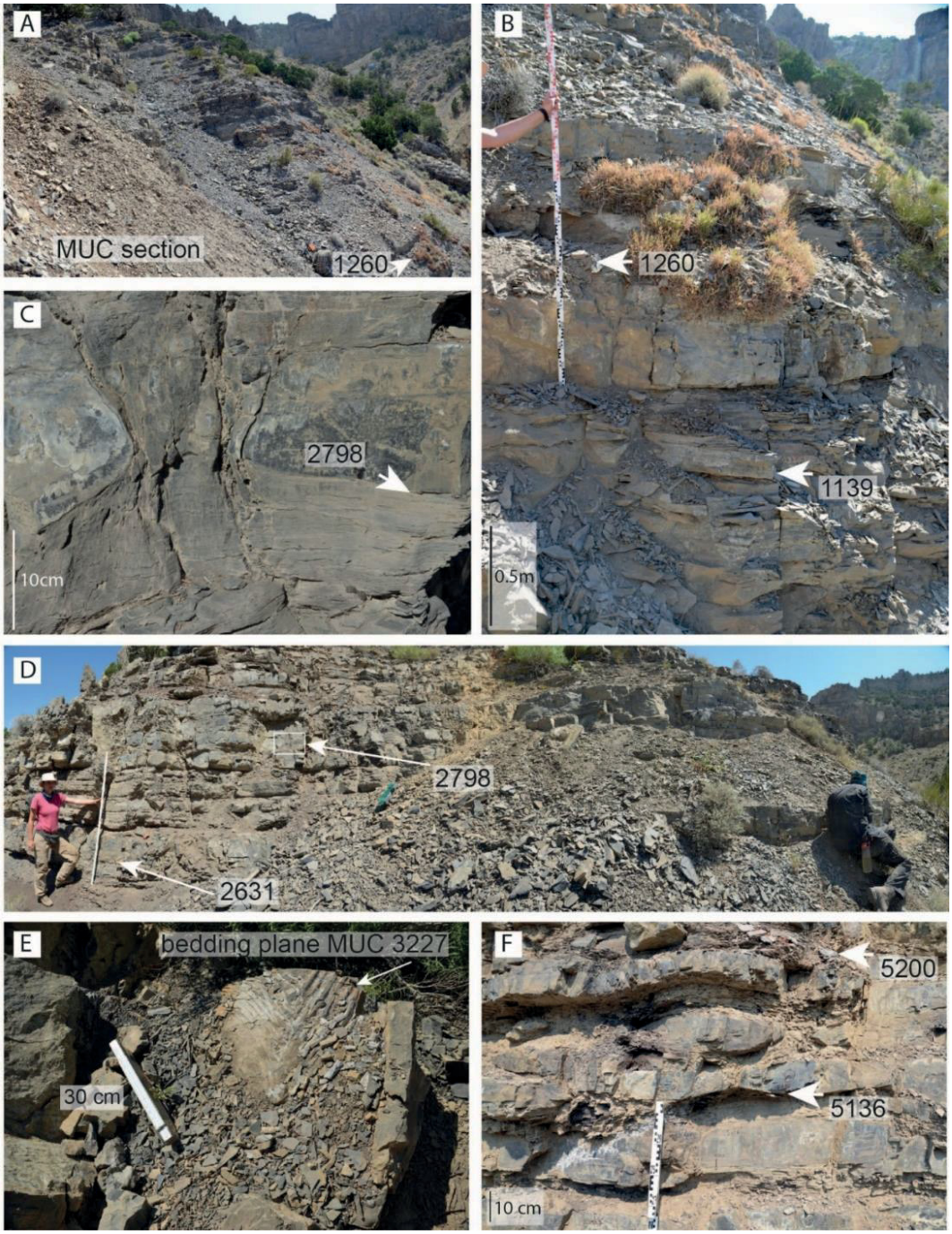

Fig. 7: Documentation of field-work at the MUC section in the Augusta Mountains. **(A)** Based of MUC section, sitting person for scale. **(B)** An alternation of calcareous, laminated siltstone with subordinate limestone beds is characterizing the lower part of the section. **(C)** Example of a discontinuous limestone bed with clearly softer calcareous siltstone in between the concretionary-like carbonate bodies. **(D)** Middle part of the MUC section with continuous limestone beds in the calcareous siltstone and abundant bivalves especially in the upper beds. **(E)** Weathered out partial ichthyosaur skeleton on bedding plane MUC 3227, showing fragmentary ribs. **(F)** Higher part of MUC section with lenticular mudstone lenses and generally irregular bedding planes. Note that sample counting started with 1000 at this site, because the option to measure further downwards was left open at the very start of field-work.

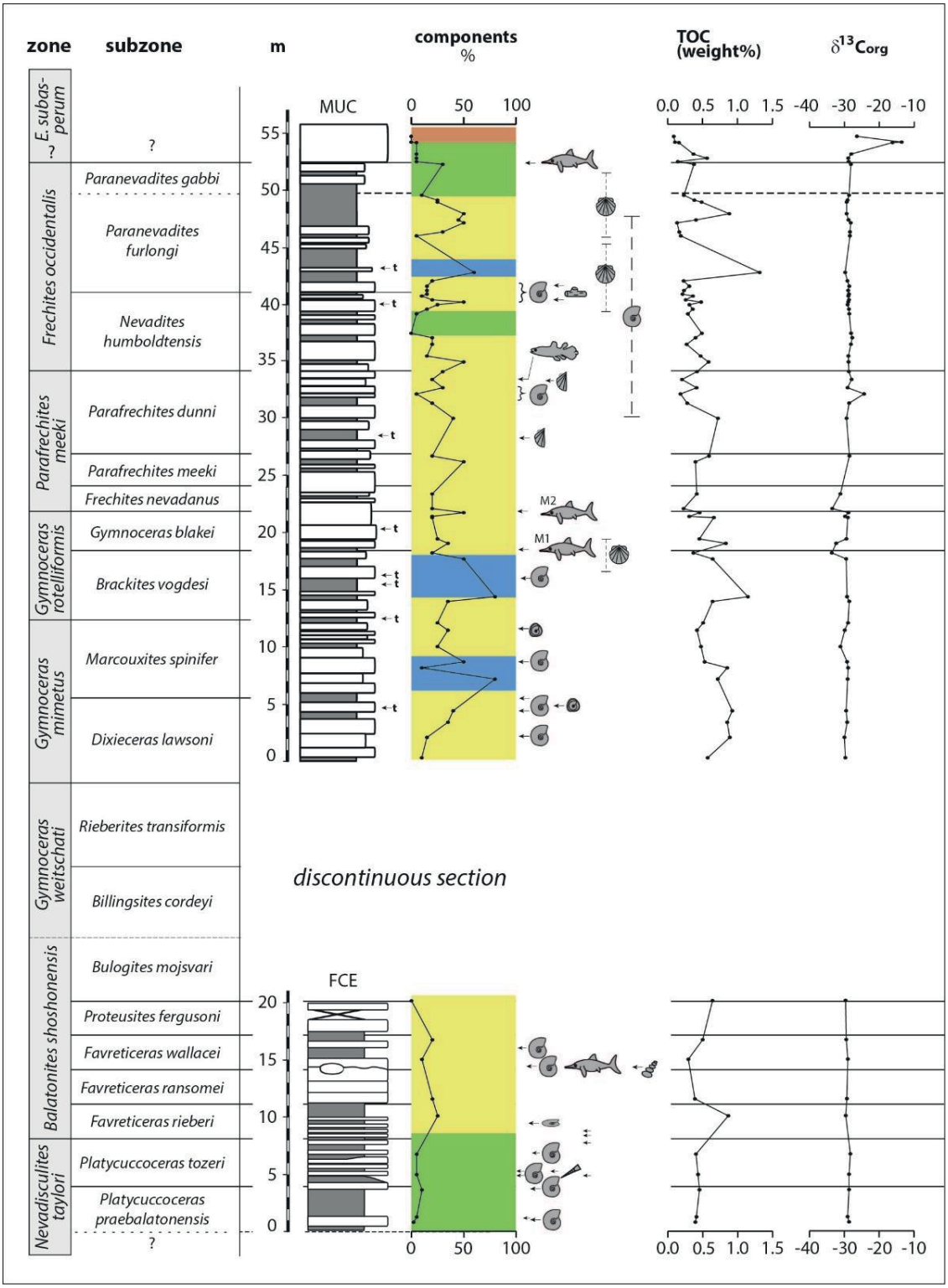

Fig. 8: Measured sections at the Augusta Mountains and its microfacies; references for biostratigraphical dating see Fig. 5. Note that the lithological columns indicate the prevailing lithology, since it was idealised due to the scale of this overview figure. M1: Level of the holotype of *Mixosaurus nordenskioeldii*, M2: Level of a mixosaurid trunk (Schmitz et al. 2004, CMC VP 7276) and a large rib cage figured here as Fig. 7E. Legend see Fig. 5.

FHE-F section. At first sections FHE and FHF were trenched separately, later it was possible to unearth the connection with the help of machinery and to unify both as section FHE-F. Many of the individual beds show lamination, this is particularly true for the siltstones.

The upper part of the FHE-F section is barren of any macrofossils. Ammonoids only occur at section meter FHE-F 0125 and daonellid bivalves occur mainly in four short intervals (each 20-30 cm in total thickness) in the lower part, where the latter are partly accumulated. The directly succeeding FHF section is tectonically strongly influenced, the disturbance strongly mask the fossil record. Nevertheless, six ammonoid horizons are found that are spread across the section and the daonellid bivalves are preferably occur in the upper part of FHE-F. A striking mass occurrence is the ammonoid placer in bed FHF 310 with more than 800 ammonoids (amongst others 300 specimens of *Dixieceras lawsoni*, >200 *Gymnotoceras mimetus*, >200 *Longobardites zsigmondyi*; partly used by Bischof et al. (2021: figs. 3I-L, 5K-N).

FHR section. Many of the individual beds show lamination, this is particularly true for the siltstones. Several limonitic layers were found between the interval from FHR 650 to 1160 and one in 1390.

In section FHR there is an almost continuous record of ammonoids and bivalves, while trenching we found only a couple of up to 1.5 m gaps where no fossils of these two macrofossil groups were recorded. Compared to other sections this site yielded many beds with aulacoceratid cephalopods (FHR 0165, 0398, 0979, 0870, 0980, 1355). Remarkable is the occurrence of small pieces of wood (sample horizon FHR 755).

FHS section. The FHS section consists of alternations of siltstones (a few centimeters in thickness up to 80 cm in thickness) and limestones up to half a meter in thickness. Many of the individual beds show lamination, this is particularly true for the siltstones. There are a few strongly varying limestone beds in the upper third of the section and a couple of concretionary beds at the base. The most striking interval is a sandy limestone interval of reddish weathering colours in between about section meter 360 and 480. The previously informally term Red Bed is herein introduced for this interval. FHS-RB is a 2.5 m section

approximately 25 m in the West of section FHS in a dried up river bed. The measured section FHS-RB did not reveal many fossils.

Ammonoids continuously occur throughout the FHS section for its lower three quarters, a particularly rich record of fossils is recorded from sample horizons 750 to 950. In the upper quarter there are only a few horizons containing ammonoids. Nicely preserved ammonoids were only found in sample horizons FHS 133 and 155.The FHS section is the only section with a large number of horizons (24 in total) yielding aulcacoceratid cephalopods. In four of these aulococeratids are abundant (FHS 65, 93, 242, 6945). Daonellid bivalves are accumulated at around section meters FHS 108 (strongly fragmented), 720, 1037; in general, they are not uncommon between FHS 617 and 1220.

Augusta Mountains

FCE section. Section FCE is 20.5 m in thickness, the single beds are up to about 2m in thickness and only very few beds are thinner than several dm. Its lower half consist mainly of calcareous siltstones, and the upper half predominantly of limestones, some beds show lamination, this is particularly true for the siltstones. Compared to MUC (see below) the bedding planes are very even, there is only a short interval (section meter 6.0 to 6.5 m) with concretions, and a single limestone bed that is strongly varying in thickness.

The section FCE contains occasionally ammonites in a few beds (section meter FCE 105, 115,380, 500, 570, 700, completely flattened in 945). A striking occurrence is an ammonite accumulation in section meter 1445 and the ammonoid placer in bed 1600 (partly used by Bischof and Lehmann 2020: fig. 3.8-10). The accumulation at FCE 1445 is apparently due to a current shadow, since it is directly associated with a partial ichthyosaur skeleton that consists at least of a huge skull. Additionally, aulacoceratid cephalopods come from section meterFCE 570. Daonellid bivalves occur in the lower half of the section only (sample horizon FCE 500, 785, 835, 875). Three gastropods are recorded from sample horizon FCE 1445.

MUC section. The almost 57 section meters of the MUC succession mainly consist of calcareous siltstones with intercalated limestone beds, with many of the individual beds show lamination or fine bedding what is particularly true for the less resistant beds. Many of the beds thicker than 1 m and thus contrasting the generally thinner bedding observed

at Fossil Hill. Some limestones beds show considerable variability in thickness, with single beds varying between about 12 cm and 50 cm. The latter is the case for the bed around section meter 22 that is associated with a large ichthyosaur skeleton and thus a context is likely, but not obvious for all cases of these variations in bed thickness. Calcareous concretions are missing in the upper and lower 5 m of the section, otherwise they are occasionally intercalated, but only common in the intervals around section meters 38 and 42. Several less indurated and thin layers are interpreted as tephra layers, however, until not having analysed these geochemically we treat them as allegedly of volcanic origin (sample horizons MUC 1472, 2274, 2595,2673, 3100, 3900, 5100, 5420).

Ammonoids are accumulated in 23 beds of the MUC section according to our results. In the lower 30 m there are only very few accumulations traceable, but above up to section meter 48 there are many individual beds with ammonoid accumulations (particularly sample horizon 4150-4350 and 5118-5290). Above section meter 48 no layers with ammonoid accumulations can be found anymore. Daonellid bivalves occur throughout the succession and they are present in almost every bed in several intervals (sample horizon MUC 2659-2991, 5024-5532, 5710-6147). Most shells are broken and fragmented to some extent. Striking sample horizon with respect to daonellids are MUC 5450, with specimens that are very large compared to those from the other beds of the succession and there are two layers with packed and strongly fragmented daonellids (3829, 4424). Besides daonellids, occasionally oysters of the genus *Liostrea* are encountered in the Muller Canyon section. Some of these bivalves display nice examples of xenomorphic growth of the oyster shells, recorded from sample horizons 1495 and 2175 (Fig. 10). This describes a morphology of the right shell that is paused through the soft-body of the oyster from the substrate the specimen has been attached to with its left valve (Stenzel, 1971). In the cases of GSUB L9074 and GSUB C9398 the substrate were unequivocally ceratitic ammonoid shells and due to the xenomorphic nature an obscure

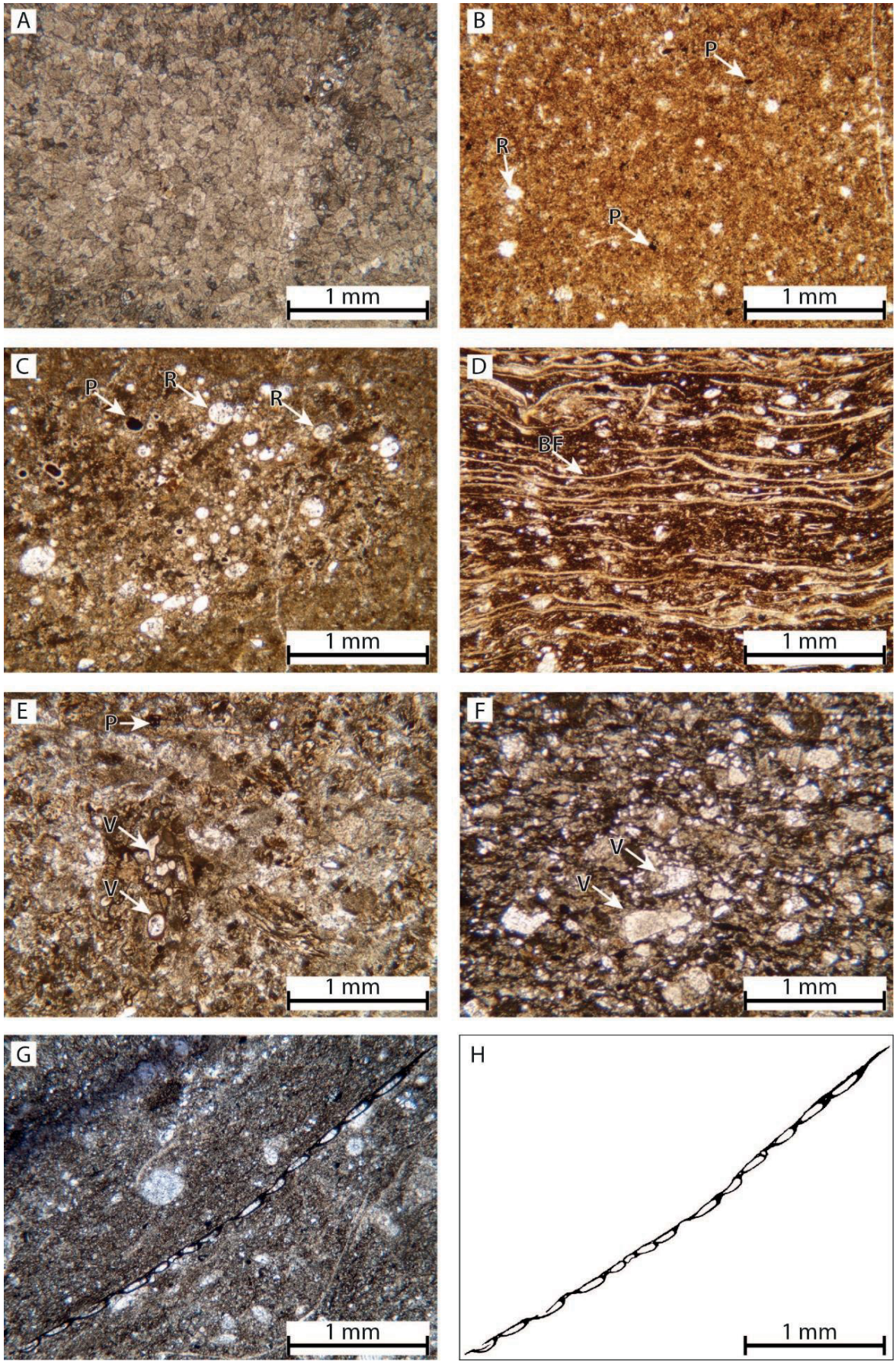
A
1 mm
B
P
R
P
1 mm
C
P
R
R
1 mm
D
BF
1 mm
E
P
V
V
1 mm
F
V
V
1 mm
G
1 mm
H
1 mm

Fig. 9: Thin sections from various localities in NV Nevada, origin indicated. **(A)** Microfacies type 1, Dolostone with sugar-grained granular structure (MUC 6657). **(B)** Microfacies type 2, Micritic mudstone. Micritic microstructure with single radiolarians and thin-shelled bivalve fragments (FCE 80). **(C)** Microfacies type 3, Micritic wackestone with radiolarians (FHS 190). **(D)** Microfacies type 4, Packstone. Bivalve filaments in micritic matrix (MUC 2471). **(E)** Microfacies type 5, Mud-Packstone with volcaniclastic components (FHS 615). **(F)** Microfacies type 6, Volcanic arenite. Carbonaceous matrix with fragmented particles of possible volcanoclastic origin (FHS 425). **(G-H)** microfossil of unknown affinity from microfacies type 3, micritic Wackestone. Original photograph **(G)** and sketch **(H)** of microfossil of unknown affinity in thin section (MUC 2236). For distribution of the different types of microfacies in the investigated sequences, see Figures 5 and 8. Legend: BF: Bivalve filament; P: pyrite; R: radiolarians; V: volcanic particle.

copy of the overgrown ammonoid is seen. Wood fragments were found in sample horizon MUC 5120 to 5270.

Vertebrates have been found in a few layers only. Coelacanth fish remains (level of sample horizon MUC 4424; on display at the Museum of Natural History of Science in Cincinnati, Ohio, USA) as well as ichthyosaurs are rare. An ichthyosaur skull collected in 1996 originates from sample horizon MUC 2850, it is the holotype of *Mixosaurus nordenskioeldii* Schmitz et al. (2004). This is specimen CMC VP 7275 of Schmitz et al. (2004). In contrast to these

authors, that referred referred to their find as probably from the Parafrechites meeki zone, we place this at the base of the Gymnotoceras blakei Zone (Fig. 8). A large ichthyosaur thorax depicted here *in situ* in the field (Fig. 7) is from sample horizon MUC 3227. From the same level MUC 3227 a mixosaurid trunk that is lacking the skull and the tail, and that was also described by Schmitz et al (2004; specimen CMC VP 7276). The original biostratigraphical information (Schmitz et al. 2004) is also revised here from probably P. meeki zone to G. blakei Zone. Some additional minor ichthyosaur remains have been discovered during our field-work in the year 2018 in sample horizon MUC 6245.

Microfacies. (*incomplete paragraph, work in progress*) The portion of biogene components in the thin sections from the Augusta Mountains (samples MUC, FCE) is varying, but most sections show a portion of 20% and less common of 5% and 50% (Fig. 8). Thin sections with portions higher than 50% of biogene components are rare. In case of the thin sections from

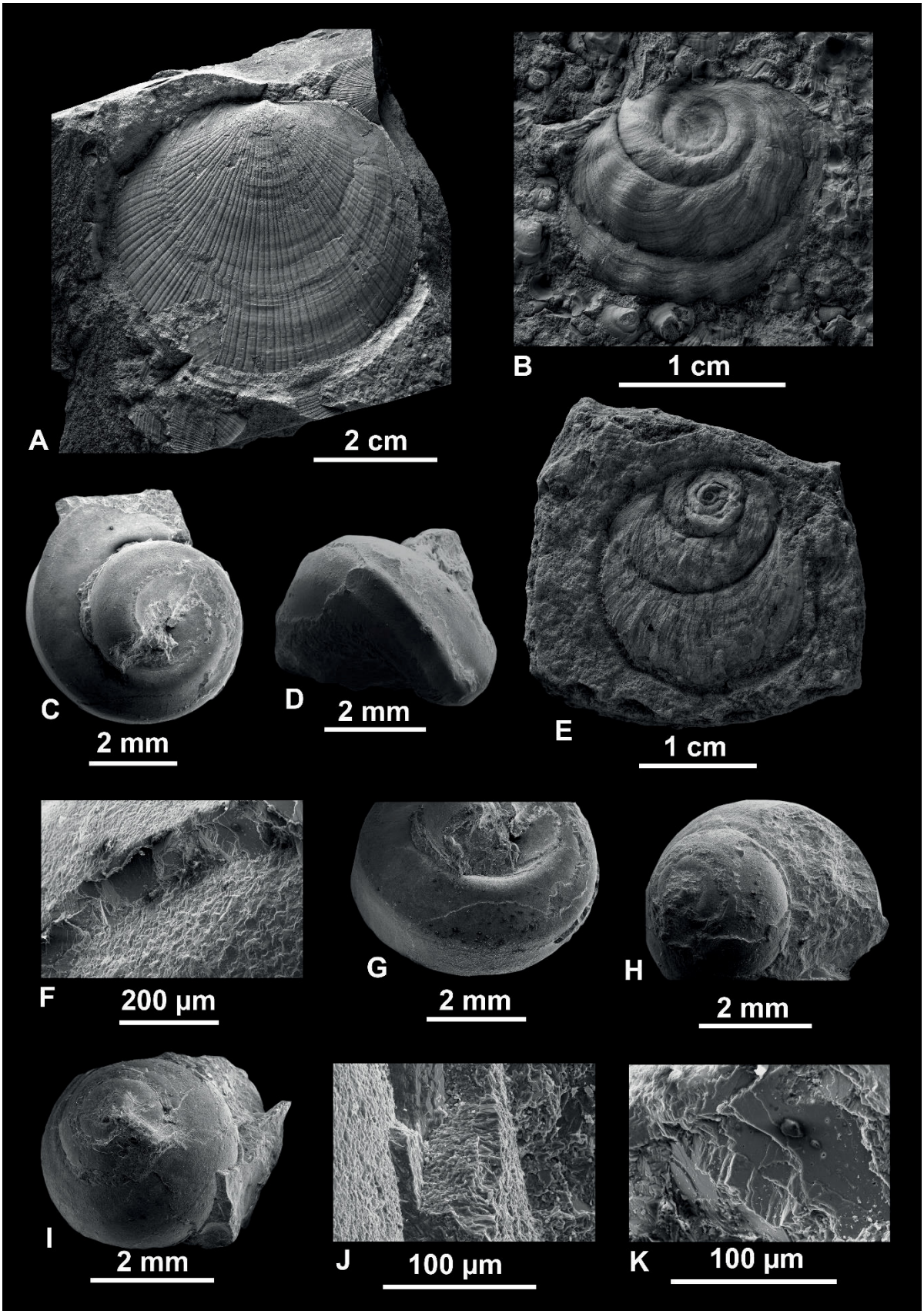
A
2 cm
B
1 cm
C
2 mm
D
2 mm
E
1 cm
F
200 µm
G
2 mm
H
2 mm
I
2 mm
J
100 µm
K
100 µm

Fig. 10: Fossils from the late Anisian Muller Canyon section. A: Halobiid bivalve, GSUB L9084, sample horizon MUC 5064. B: Examples of xenomorphic ornament of oyster shells, *Liostrea* sp., after ceratitic ammonoid shells, sample horizon MUC 2175; GSUB L9074, associated with GSUB C9398 on a rock slab. C: Gastropod from the late Anisian Muller Canyon section, sample horizon FCE 1445, GSUB G10577. D: Same, GSUB G10579. E: Same as B, GSUB L9073, sample horizon MUC 1495. F: Ultrastructure of the internal-mould-shell transition depicted as D. G: Side view of C. H-K: Same as C, specimen G10578, with J showing an overview of the wall structure and K showing details of it.

Fossil Hill (samples FHD, FHEF, FHR, FHS, FLAD) the portions of biogene components are similar, but here amounts of biogene components higher than 50% are found more often (Fig. 5).

Based on the total of 186 thin sections six facies types have been identified, five can be distinguished based on the classification of carbonate rocks and one is a volcanic arenite (Fig. 9). Regarding the biogenic component of the carbonates bivalve filaments are lined up following the bedding-plane. Usually bivalve filaments are the most common biogenic components, but in MF type 4 occassionally ammonoid shells prevail and bivalves are less abundant than usually – with about the same number of ostracods (FHD 846; Fig. 9). All radiolarians (MF type 2 and 3) belong to the order Spumellaria. The quartz grains in MF type 2 and 3 belong to silt and sand size classes.

Pyrite crystals in MF type 2 and 3 are of different size and can be either accumulated in thin layers or are dispersed. The angular/subangular volcaniclastic components in MF type 5 are well-distinguishable from the matrix, often with dark rim, the rim of the circular/oval vesicles are filled with secondary minerals and are also often accentuated by dark rims.

4.5.4 Discussion

(incomplete paragraph, work in progress)

The working area exposes Anisian sediments deposited at a gentle continental slope or steeper shelf ramp at a moderate depth of possibly around 200 m paleowaterdepth in a fully marine environment. This bathymetric position is evident by an association of frequent ammonoids, aulacoceratids, bivalves, and occasionally ichthyosaurs and fishes, a mostly moderate destruction of invertebrate shells by palaeocurrents. Most fossils, particularly the bivalves, show less destruction and therefore can be regarded as

authothonous or paraautochtonous. Many of the limestone beds are either pinching out on the outcrop scale, are discontinuous, or are - more rarely - lense-shaped (Fig. 3F, 7C, 7F). Some, but not all of these sedimentary bodies, can be attributed to gutter cast or scour trough fillings as is evident e.g. by shell coquinas (e.g. MUC 5257, MUC 5265).

Many of the individual beds show lamination, this is particularly true for the siltstones. Although fully anoxic conditions appears unlikely based on these observations the paleoenvironmental background needs to be discussed in the following with keeping in mind the question of the ancient marine oxygen level.

The succession measured in the Augusta Mountains is more expanded in total thickness compared to Fossil Hill (Fig. 5 and 8). Since the general faunal content and the carbonate microfacies is very similar, but individual beds are much thinner at Fossil Hill the latter might have been deposited on a submarine swell or height, whereas the Augusta Mountains succession

represents a basin deposit. There is little direct hint on an influence from the hinterland. We encountered some small pieces of drift wood in sample horizon FHR 755, in the G. blakei Subzone of the G. rotelliformis Zone of the FHR section at Fossil Hill. At the Augusta Mountains more common plant remains is encountered at least in a single level supposedly in the G. weitschati or in the B. shoshonensis Zone, from the gap below our measured Muller Canyon section. There are also a couple of smaller drift wood pieces from the sample horizons MUC 5120 to 5270 (Fig. 8), representing the middle part of the F. occidentalis Zone.

The investigated Anisian (Middle Triassic) sequences of Nevada proof an unfavorable to hostile benthic paleoenvironment with suboxic-dysoxic conditions and episodic oxygenation. The macrofossil association is clearly dominated by ammonoids and daonellids. As the finely laminated rocks of the investigated sequences show no signs for a turbiditic nature or other mass movement processes, the daonellids are interpreted to reflect the (para-)autochthonous biocoenose (Schatz, 2000, 2005). Earlier a pseudoplanktonic to nektonic mode of life was assumed in the past due to unfavorable conditions of the bottom-water i.e., De Capoa Bonardi, 1969; Rieber, 1968. Our study supports more recent views suggesting a benthic-epibenthic lifestyle (i.e., Del Piero et al., 2020; Duff, 1975; Etter, 1996; Schatz, 2000, 2005), mainly because of the lack of suitable transport media. A few wood samples found in the investigated sequences only cannot be associated with

daonellids. A suggested water depth of more than 200 m below the photic zone, rules out an attachment of daonellids to algae as well. Additionally, the absence of byssus glands, suggests that daonellid could not have been attached to floats (Schatz, 2005).

According to Schatz (2000, 2005), daonellids underwent a series of transformations to adapt to the hostile environment on the soft ocean floor. At low pH values, which are typical of dysoxic areas, calcite secretion is much more energy-intensive (Rhoads and Morse, 1971). Therefore, the development of thinner and calcitic shells (instead of the heavier aragonite) is regarded as an important adaptation to the dysoxic bottom waters Schatz, 2000. Additionally, the flat, subcircular shells (Fig. 10) lead to a high surface-to-volume ratio that helped daonellids to "float" on the soft sediment "snow-shoe strategy"; Schatz, 2000, 2005.

The evidence of ammonoid shells overgrown by the oyster *Liostrea* from the Muller Canyon section is a phenomenon well-known from the late Mesozoic (Lewy, 1972; Spaeth, 1985;

Lehmann and Wippich, 1995). Similar finds are known from the early Triassic already (Hautmann et al., 2017), but these are cases of *in vivo* settlement of epizoan oysters on much larger ammonoid shells. In the present case, the oysters are about as big as their shell substrate, indicating that the oyster must have grown on empty shells on the seafloor. This post-mortem settlement indicates that the oxygenation was at least episodically sufficient for benthic life. This also agrees with a few small gastropods found in sample horizon FCE 1445 of the Favret Canyon section (GSUB G10577, G105778, G105779; Fig. 10).

The large quantity of ammonoid material being available in this study is regarded as promising for reconstructing predator-prey relationships: with ammonoids as prey, but also vice versa, with ammonites as predators. In fact, changes in predation pressure respectively in the type of predator-prey relationships are directly readable from quantitative and qualitative paleopathological analyses (e.g. Keupp and Ilg, 1994, Mapes and Chaffin, 2003). A demersal life style made ammonoids more open to injury by benthic predators, particularly by crustaceans, as suggested for example by Keupp and Ilg (1992, 1994), but triangular bite marks could indicate other cephalopods as predators. For the Triassic a case studies on a collection of 148 pathological specimens of two *Dieneroceras* species from the early Triassic of Nevada (Keupp 2012: fig. 48) indicate most healed

injuries at 70° (with 0 at the upper limit of the aperture and 100 at the lower) attributed to U-shaped, allegedly fish bites, and a lower maximum at 30° attributed to V-shaped bites. Despite investigating 7809 specimens from the Middle Triassic, covering 53 different species, we found only a low number of specimens with pathologies. This agrees with the general observation that the frequency of repair scars is lower in the Triassic compared to the Jurassic and Cretaceous, an aspect of the increasing escalation by the "Mesozoic Marine Revolution" (Kerr and Kelley, 2015). Nevertheless, we strongly assume that the low number of pathologies in our succession indicates that most species were preferably species of the open-water and that there was a comparatively low number of preferably demersal forms.

On the ammonoid as prey side, the Triassic of Nevada contains *Omphalosaurus*, an early ichthyosaur with specialized crushing jaws, that is a highly eligible candidate to prey on ammonites. Although ammonoids occupy a position low in the food web compared to marine reptiles, and thus it is very likely that the later did prey on them, the evidence is still weak for the whole Mesozoic (Odunze and Mapes, 2013). Presumably it would be much more difficult to find evidence for this predation, because the shells would have been mostly completely crushed after an attack and thus it is difficult to distinguish this from post-mortem mechanical damage of empty shells.

4.5.5 Conclusions

(incomplete paragraph, work in progress)

The paleoenvironment for the Fossil Hill Member Anisian (Middle Triassic) can be described as deposited under generally calm depositional conditions. At Fossil Hill the succession was deposited in a more dynamic depositional setting compared to the Augusta Mountain succession. Nevertheless, at both working areas small-scale changes of the biofacies were present, ruled by episodic dysoxic or oxygen-depleted conditions on the sea floor. The conditions were hostile and unfavorable most of the time as evident by a mono- or paucispecific fauna reflecting a biocoenoses of an authochtonous to parautochthonous nature.

The important marine reptile fossils described earlier by Schmitz et al. (2004) were referred in this paper as probably from the Parafrechites meeki zone. Based on the

biostratigraphical data obtained from the field-work for this paper we place these fossils lower in the ammonoid zonal sequence of the late Anisian, namely into the Gymnotoceras blakei Zone.

Acknowledgements

We are grateful for the financial help of booster club of the Geowissenschaftliche Sammlung, Bremen, to finance the use of a backhoe at Fossil Hill. D. Kuhlmann (now Messel, Germany) and M. Krogmann (Bremen, Germany) is thanked for their broad technical support and for joining field-work. We thank the U.S. Department of the Interior, Bureau of Land Management (BLM, Nevada State office, Winnemucca District) for permission to collect samples in the Wilderness Study Area of the Augusta Mountains, Pershing County. This research received support from the German Science Foundation (DFG), project "Nevammonoidea" (LE 1241/3-1). We thank both reviewers, # (#) and # (#), for their very useful comments. A. Munnecke (Erlangen), F. Schlagintweit (Munich) and B. Senowbari-Daryan (Erlangen) are thanked for the interpretation of problematic microfossils encountered in our thin sections.

References (of chapter 4.5 only)

Adams, A.E., Mac Kenzie, W.S., 2001. A colour atlas of carbonate sediments and rocks under the microscope, Manson Publishing, New York, pp. 1-180.

Anonymous, 1980. Annie Alexander — the intrepid collector. PG&E Progress 57(7).

Baud, A., Richoz, S., 2004. The Lower Triassic microbialites and precipitates: environmental control, distribution in space and time, Microbialites and microbial communities in sedimentary systems, Workshop, Paris. 6 September 2004, ASF Publication 46, Paris, 6, pp. 15-17.

Baud, A., Richoz, S., Pruss, S., 2007. The lower Triassic anachronistic carbonate facies in space and time. Global and Planetary Change 55(1), 81-89.

Bischof, E.A., Lehmann, J., 2020. Ontogenetic analysis of Anisian (Middle Triassic) ptychitid ammonoids from Nevada, USA. Journal of Paleontology 94, 829-851.

Bischof, E.A., Schlüter, N., Korn, D., Lehmann, J., 2021. Ontogeny of highly variable ceratitid ammonoids from the Anisian (Middle Triassic). PeerJ(9:e10931), 1-28.

Brayard, A., Bucher, H., Escarguel, G., Fluteau, F., Bourquin, S., Galfetti, T., 2006. The Early Triassic ammonoid recovery: Paleoclimatic significance of diversity gradients. Palaeogeography, Palaeoclimatology, Palaeoecology 239(3–4), 374-395.

Brayard, A., Vennin, E., Olivier, N., Bylund, K.G., Jenks, J., Stephen, D.A., Bucher, H., Hofmann, R., Goudemand, N., Escarguel, G., 2011. Transient metazoan reefs in the aftermath of the end-Permian mass extinction. Nature Geoscience 4(10), 693-697.

Bucher, H., 1992. Ammonoids of the Hyatti Zone (Middle Anisian, Middle Triassic) and the Anisian transgression in the Star Peak Group (northwestern Nevada). Palaeontographica A 223, 137-166.

De Capoa Bonardi, P., 1969. La Daonelle e Halobie della serie calcareo-silico-marnosa della Lucania (Apenino Meridionale). Studio paleontologico e biostratifico. Memoria della Societá Naturalia in Napoli v.78, 1-127.

Del Piero, N., Rigaud, S., Takahashi, S., Poulton, S.W., Martini, R., 2020. Unravelling the paleoecology of flat clams: New insights from an Upper Triassic halobiid bivalve. Global and Planetary Change 190, 103-195.

Dineen, A.A., Roopnarine, P.D., Fraiser, M.L., 2019. Ecological continuity and transformation after the Permo-Triassic mass extinction in northeastern Panthalassa. Biology Letters 15(3), 20180902.

Duff, K., 1975. Palaeoecology of a bituminous shale: the Lower Oxford Clay of Central England. Palaeontology 18, 443-482.

Dunham, R.J., 1962. Classification of carbonate rocks according to depositional texture, in: Ham, W.E. (Ed.), Classification of carbonate Rocks, Memoirs of the American Association of Petroleum Geologists, Tulsa, pp. 108-121.

Etter, W., 1996. Pseudoplanktonic and benthic invertebrates in the Middle Jurassic Opalinum Clay, northern Switzerland. Palaeogeography, Palaeoclimatology, Palaeoecology 126(3-4), 325-341.

Flügel, E., 2010. Microfacies of carbonate rocks: Analysis, interpretation and application, Springer, Berlin, pp. 1-984.

Flügel, E., Kiessling, W., 2002. Patterns of Phanerozoic reef crises, in: Kiessling, W., Flügel, E., Golonka, J. (Eds.), Phanerozoic Reef Patterns, SEPM Special Publication. SEPM Society for Sedimentary Geology, Tulsa, 72, pp. 691-733.

Fröbisch, N.B., Fröbisch, J., Sander, P.M., Schmitz, L., Rieppel, O., 2013. Macropredatory ichthyosaur from the Middle Triassic and the origin of modern trophic networks. Proceedings of the National Academy of Sciences of the United States of America 110(4), 1393-1397.

Gabb, W.M., 1864. Paleontology of California. Description of the Triassic fossils of California and the adjacent territories, 1. California Geological Survey, Paleontology, Philadelphia, pp. 1-17-35.

Google, 2020. Google Earth. Screenshot - Lebanon, p. 2020.2008.2024.

Hallam, A., 1991. Why was there a delayed radiation after the end-palaeozoic extinctions? Historical Biology 5, 257-262.

Harper, E.M., 2003. The Mesozoic marine revolution, in: Kelley, P.H., Kowalewski, M., Hansen, T.A. (Eds.), Predator-prey interactions in the fossil record, Topics in Geobiology. Kluwer Academic/Plenum Publishers, New York, Boston, Dordrecht, London, Moscow, 20, pp. 433-455.

Hautmann, M., Ware, D., Bucher, H., 2017. Geologically oldest oysters were epizoans on Early Triassic ammonoids. Journal of Molluscan Studies 83(3), 253-260.

Horowitz, A.S., Potter, P.E., 1971. Introductory Petrography of Fossils, Springer, Berlin, pp. 1-XIV + 302.

Hyatt, A., Smith, J.P., 1905. The Triassic cephalopod genera of America. Govt. Print. Off.

Ingersoll, R.V., 2008. Subduction-related sedimentary basins of the USA cordillera, in: Miall, A.D. (Ed.), Sedimentary Basins of the World. Elsevier, Amsterdam, 5, pp. 395-428.

Jenks, J.F., Monnet, C., Balini, M., Brayard, A., Meier, M., 2015. Biostratigraphy of Triassic ammonoids, in: Klug, C., Korn, D., De Baets, K., Kruta, I., Mapes, R.H. (Eds.), Ammonoid Paleobiology: From macroevolution to paleogeography, Topics in Geobiology. Springer, Dordrecht, 44, pp. 329-388.

Kelley, N.P., Motani, R., Embree, P.G., Orchard, M.J., 2016. A new Lower Triassic ichthyopterygian assemblage from Fossil Hill, Nevada. PeerJ 4:e1626, 1-16.

Kerr, J.P., Kelley, P.H., 2015. Assessing the influence of escalation during the Mesozoic Marine Revolution: Shell breakage and adaptation against enemies in Mesozoic ammonites. Palaeogeography, Palaeoclimatology, Palaeoecology 440, 632-646.

Keupp, H., 2012. Atlas zur Paläopathologie der Cephalopoden. Berliner Paläobiologische Abhandlungen 12, 1-390.

Keupp, H., Ilg, A., 1992. Paläopathologie der Ammonitenfauna aus dem Obercallovium der Normandie und ihre palökologische Interpretation. Berliner geowissenschaftliche Abhandlungen E 3, 171-189.

Keupp, H., Ilg, A., 1994. Paläopathologische Nachlese zur Ammoniten-Fauna aus dem Ober-Callovium der Normandie. Berliner Geowissenschaftliche Abhandlungen E 13, 321-327.

LaMaskin, T.A., Vervoort, J.D., Dorsey, R.J., Wright, J.E., 2011. Early Mesozoic paleogeography and tectonic evolution of the western United States: Insights from detrital zircon U-Pb geochronology, Blue Mountains Province, northeastern Oregon. Geological Society of America Bulletin 123(9-10), 1939-1965.

Lehmann, J., Wippich, M.G.E., 1995. Oyster attachment scar preservation of the late Maastrichtian ammonite *Hoploscaphites constrictus*. Acta Palaeontologica Polonica 40(4), 437-440.

Leidy, J., 1868. Notice of some reptilian remains from Nevada. Proceedings of the Academy of Natural Sciences of Philadelphia 109, 177-178.

Lewy, Z., 1972. Xenomorphic growth in ostreids. Lethaia 5, 347-352.

MacPhie, J., Doyle, M., Allen, R.L., 1993. Volcanic textures: a guide to the interpretation of textures in volcanic rocks, Centre for Ore Deposit and Exploration Studies, University of Tasmania, Hobart, pp. 1-X+198.

Mapes, R.H., Chaffin, D.T., 2003. Predation on cephalopods. A general overview with a case study from the Upper Carboniferous of Texas, in: Kelley, P.H., Kowalewski, M., Hansen, T.A. (Eds.), Predator-prey interactions in the fossil record, Topics in Geobiology. Kluwer Academic/Plenum Publishers, New York, Boston, Dordrecht, London, Moscow, 20, pp. 177-213.

Mercedes-Martín, R., Buatois, L.A., 2021. Microbialites and trace fossils from a Middle Triassic restricted carbonate ramp in the Catalan Basin, Spain: evaluating environmental and evolutionary controls in an epicontinental setting. Lethaia 54(1), 4-25.

Merriam, J.C., 1905. A primitive ichthyosaurian limb from the Middle Triassic of Nevada. University of California Publications, Bulletin of the Department of Geology 4(2), 33-38.

Merriam, J.C., 1906. Preliminary note on a new marine reptile from the Middle Triassic of Nevada. University of California Publications, Bulletin of the Department of Geology 5(5), 75-79.

Merriam, J.C., 1908. Triassic Ichthyosauria, with special reference to the American forms. Memoirs of the University of California 1(1), 1-155.

Merriam, J.C., 1910. The skull and dentition of a primitive ichthyosaurian from the Middle Triassic. University of California Publications, Bulletin of the Department of Geology 5(24), 381-390.

Merriam, J.C., Bryant, H.C., 1911a. Notes on the dentition of *Omphalosaurus*. University of California Publications, Bulletin of the Department of Geology 6(14), 329-332.

Merriam, J.C., Bryant, H.C., 1911b. Preliminary note on a new marine reptile from the Middle Triassic of Nevada. University of California Publications, Bulletin of the Department of Geology 5(5), 75-79.

Monnet, C., Bucher, H., 2005. New Middle and Late Anisian (Middle Triassic) ammonoid faunas from Northwestern Nevada (USA): Taxonomy and biochronology. Fossils and Strata 52, 1-121.

Monnet, C., Bucher, H., Wasmer, M., Guex, J., 2010. Revision of the genus *Acrochordiceras* Hyatt, 1877 (Ammonoidea, Middle Triassic): morphology, biometry, biostratigraphy and intra-specific variability. Palaeontology 53(5), 961-996.

Odunze, S., Mapes, R.H., 2013. Nearly circular, oval and irregular holes in Cretaceous ammonoids from Nigeria. Lethaia 46(3), 409-415.

Ogg, J.G., Chen, Z.Q., Orchard, M.J., Jiang, H.S., 2020. Chapter 25 - The Triassic Period, in: Gradstein, F.M., Ogg, J.G., Schmitz, M.D., Ogg, G.M. (Eds.), Geologic Time Scale 2020. Elsevier, pp. 903-953.

Parrish, J.T., 1993. Climate of the Supercontinent Pangea. The Journal of Geology 101(2), 215-233.

Payne, J.L., Summers, M., Rego, B.L., Altiner, D., Wei, J., Yu, M., Lehrmann, D.J., 2011. Early and Middle Triassic trends in diversity, evenness, and size of foraminifers on a carbonate

platform in south China: implications for tempo and mode of biotic recovery from the end-Permian mass extinction. Paleobiology 37(3), 409-425.
Péron, S., Bourquin, S., Fluteau, F., Guillocheau, F., 2005. Paleoenvironment reconstructions and climate simulations of the Early Triassic: Impact of the water and sediment supply on the preservation of fluvial systems. Geodinamica Acta 18(6), 431-446.
Preto, N., Kustatscher, E., Wignall, P.B., 2010. Triassic climates — State of the art and perspectives. Palaeogeography, Palaeoclimatology, Palaeoecology 290(1), 1-10.
Pruss, S.B., Bottjer, D.J., 2005. The reorganization of reef communities following the end-Permian mass extinction. Comptes Rendus Palevol 4(6), 553-568.
Rhoads, D.C., Morse, J.W., 1971. Evolutionary and ecologic significance of oxygen-deficient marine basins. Lethaia 4(4), 413-428.
Rieber, H., 1968. Die Artgruppe der *Daonella elongata* Mojs. aus der Grenzbitumenzone der mittleren Trias des Monte San Giorgio (Kt. Tessin, Schweiz). Paläontologische Zeitschrift 42(1/2), 33-61.
Saleeby, J.B., Busby-Spera, C., Oldow, J.S., Dunne, G.C., Wright, J.E., Cowan, D.S., Walker, N.W., Allmendinger, R.W., 1992. Early Mesozoic tectonic evolution of the western U.S. Cordillera, in: Burchfiel, B.C., Lipman, P.W., Zoback, M.L. (Eds.), The Cordilleran Orogen. Geological Society of America, Boulder, pp. 107-168.
Sander, M.P., Rieppel, O.C., Bucher, H., 1997. A new pistosaurid (Reptilia: Sauropterygia) from the Middle Triassic of Nevada and its implications for the origin of the plesiosaurs. Journal of Vertebrate Paleontology 17(3), 526-533.
Sander, P.M., Rieppel, O.C., Bucher, H., 1994. New marine vertebrate fauna from the Middle Triassic of Nevada. Journal of Paleontology 68(3), 676-680.
Schatz, W., 2000. Taxonomie, Paläoökologie und biostratigraphische Anwendung der Daonellen (Bivalvia) aus der Mitteltrias Europas.University of Zurich, p. 313.
Schatz, W., 2005. Palaeoecology of the Triassic black shale bivalve *Daonella*—new insights into an old controversy. Palaeogeography, Palaeoclimatology, Palaeoecology 216(3–4), 189-201.
Schmitz, L., Sander, M.P., Storrs, G.W., Rieppel, O., 2004. New Mixosauridae (Ichthyosauria) from the Middle Triassic of the Augusta Moutains (Nevada, USA) and their implications for mixosaur taxonomy. Palaeontographica Abteilung A 270(4-6), 133-162.
Schubert, J.K., Bottjer, D.J., 1995. Aftermath of the Permian-Triassic mass extinction event: Paleoecology of Lower Triassic carbonates in the western USA. Palaeogeography, Palaeoclimatology, Palaeoecology 116(1), 1-39.
Silberling, N.J., Nichols, D.J., 1982. Middle Triassic molluscan fossils of biostratigraphic significance from the Humboldt Range, northwestern Nevada. U.S. Geological Survey Professional Paper.
Skrzycki, P., Niedźwiedzki, G., Tałanda, M., 2018. Dipnoan remains from the Lower-Middle Triassic of the Holy Cross Mountains and northeastern Poland, with remarks on dipnoan palaeobiogeography. Palaeogeography, Palaeoclimatology, Palaeoecology 496, 332-345.
Smith, J.P., 1914. The Middle Triassic marine invertebrate faunas of North America, Professional Papers U.S. Geological Survey 83. Washington, pp. 1-254.
Smith, J.P., 1932. Lower Triassic Ammonoids of North America, U.S. Geological Survey Professional Papers 167. United States Government Printing Office, Washington, pp. 1-iv+199.
Spaeth, C., 1985. Aufwuchs und xenomorphe Skulptur bei *Aetostreon latissimum* (Lamarck) (Ostreidae) aus dem Hauterivium von Helgoland. Mitteilungen aus dem Geologisch-Paläontologischen Institute der Universität Hamburg 59, 57-70.
Stenzel, H.B., 1971. Oysters, Treatise on invertebrate paleontology. Part N. Mollusca 6, Bivalvia 3. Geological Society of America and University of Kansas Press, Boulder & Lawrence, pp. N953–N1224.
Tackett, L.S., Bottjer, D.J., 2012. Faunal succession of Norian (Late Triassic) level-bottom benthos in the Lombardian basin: Implications for the timing, rate, and nature of the early Mesozoic Marine Revolution. Palaios 27(8), 585-593.

Ulmer-Scholle, D.S., Scholle, P.A., Schieber, J., Raine, R.J., 2015. A color guide to the petrography of sandstones, siltstones, shales and associated rocks. American Association of Petroleum Geologists, Tulsa, p. 526.

Vermeij, G.J., 1977. The Mesozoic Marine Revolution: Evidence from snails, predators and grazers. Paleobiology 3(3), 245-258.

Weidlich, O., 2007. PTB mass extinction and earliest Triassic recovery overlooked? New evidence for a marine origin of Lower Triassic mixed carbonate–siliciclastic sediments (Rogenstein Member), Germany. Palaeogeography, Palaeoclimatology, Palaeoecology 252(1), 259-269.

Wyld, S.J., 2000. Triassic evolution of the arc and backarc of northwest Nevada, and evidence for extensional tectonism. Geological Society of America Special Papers 347, 185-207.

Wyld, S.J., 2002. Structural evolution of a Mesozoic backarc fold-and-thrust belt in the U.S. Cordillera: New evidence from northern Nevada. GSA Bulletin 114(11), 1452-1468.

5 Final conclusions

As outlined in chapter 2, this thesis can be subdivided into three main research topics: (1) Palaeoenvironmental reconstruction, (2) ammonoid species associations, and (3) ammonoid morphology. The following discussion examines how the specific research goals were addressed in this thesis (chapters 5.1–5.3) and how these three aspects influence each other (chapter 5.4).

5.1 Palaeoenvironmental reconstruction

How stable was the palaeoenvironment during the deposition of the Fossil Hill Member?

The beginning and the end of the Triassic are each defined by major mass extinctions (Fig. 1.3-1 herein; Brayard & Bucher 2015). While the ecosystem in the Lower Triassic was recovering, the Upper Triassic was already affected by further, but smaller extinctions. In the Middle Triassic, we can therefore observe less constrained ammonoid evolution beyond the scope of lethal conditions of a mass extinction. Despite the long history of biostratigraphic research, the evolution of Triassic ammonoids still remains poorly studied (Monnet et al. 2015).

The very diverse Anisian and lower Ladinian ammonoid assemblages in NW Nevada are among the world's most famous of Triassic age (Silberling & Nichols 1982; Monnet & Bucher 2005b). It is generally agreed upon that palaeoenvironmental changes are a key driving force for evolutionary and morphologic change (Yacobucci 2015). In order to find an explanation for the high Anisian diversity, the Fossil Hill Member was thoroughly investigated for palaeoenvironmental shifts. Therefore, the bio- and lithostratigraphy including geochemical proxies ($\delta^{13}C$, TOC) were analysed.

The investigated sequences all consist of alternating layers of calcareous siltstone and mudstone with lenticular limestone (chapter 4.5, Appendix 1). The finely laminated and fine-grained sediment indicate deposition below the storm wave base and thus more than 200 m water depth. The few pieces of wood that were found in the sequences suggest some proximity and connection to the shoreline of Pangaea. The bottom water (or at least the sediment-water interface) was dysoxic to anoxic with oxygenated water above (Schatz 2000, 2005). The rather hostile environment allowed only little to no benthic fauna. Small-scale environmental changes most likely occurred in relation to short-term oxygenation of the bottom waters (chapter 4.5). This is supported by the occurrence of abundant and partially well-preserved mono- to paucispecific bivalve assemblages that prove the–at least temporary–dense occupation of the habitat.

Our study found no evidence of major palaeoenvironmental shifts driving evolutionary change of ammonoids. In the absence of external forces such as palaeoenvironmental and predatory pressure, it can be concluded that the evolutionary changes must have been driven by intrinsic factors from within

the ammonoids population. This demonstrated the need for a more detailed morphologic analysis, which will be discussed in more detail in the following chapters.

5.2 Ammonoid associations

Are there any taxonomic patterns or major shifts in biostratigraphic distribution of ammonoid associations?

5.2.1 Biostratigraphic distribution

The almost continuously fossiliferous Fossil Hill Member offers a unique opportunity for detailed studies of the changes within ammonoid populations through time; and gives considerable insights into the evolution and taxonomy of these fossils (Silberling & Nichols 1982). There are numerous studies on the Anisian ammonoid assemblages from NW Nevada, USA (i.e. Silberling & Nichols 1982; Bucher 1988, 1989, 1991, 1992a, b, 1994; Monnet & Bucher 2005a, b; Jenks et al. 2007; Monnet et al. 2010; Ji & Bucher 2018). In the present thesis, observations of the upper and lower parts of the Fossil Hill Member were combined into one study for the first time. In the course of this study, a total of 53 different species that are housed into 32 genera and 15 families were detected (Fig. 4.3-1). Overall, the observed biostratigraphic distribution pattern (Fig. 3.4-1) is in agreement with the biostratigraphy published by Silberling & Nichols (1982) and Monnet & Bucher (2005b). Within the Fossil Hill Member, no substantial shifts in ammonoid species association were detected (Fig. 3.4-1). Overall the investigated sequence can be subdivided in three different main parts (Tab. 5.2-1).

5.2.2 Alphataxonomy

The basic work on the biostratigraphic species distribution has revealed the complexity of the alphataxonomy of the involved species. In many cases, arguments over biostratigraphy commonly reduce to arguments over taxonomy (Lucas 2010). As it is quite common, new ammonoid species in Nevada were frequently described based on a stratophenetic view (Yacobucci 2015). Thereby, the species are initially distinguished by their stratigraphic occurrence, with a subsequent identification of diagnostic anatomical features for those groupings (Donovan 1994). The stratophenetic approach makes the alphataxonomy of these species particularly challenging (Yacobucci 2015).

Tab. 5.2-1. Summary of three main groups of ammonoid associations of Fossil Hill Member in Nevada, USA. Figure 3.4-1 shows the biostratigraphic distributions of the ammonoid species in the member.

Biostratigraphic zones	Dominant species / groups	Prevailing morphologies
Frechites occidentalis *Parafrechites meeki*	Almost balanced ratio between Beyrichitinae, Paraceratitinae, Longobartinae,	Rather balanced ratio of discoidal to spherical and oxyconic morphologies. Particularly Paraceratitinae generally with tubercles and spines.
Gymnotoceras rotelliformis *Gymnotoceras mimetus* *Gymnotoceras weitschati*	*Gymnotoceras* (Beyrichitinae)	Discoidal conches, mostly rather smooth shells or falcoid ribs
Balatonites shoshonensis *Nevadisculites taylori*	*Acrochordiceras* (Acrochordiceratidae)	Rather balanced ratio of discoidal, spherical and oxyconic morphologies

Even though smaller shifts in species association occur, the member, which covers a depositional period of about 4 Ma (chapter 4.5), can be considered as one composite unit. As expected from the literature (Brayard et al. 2009b; supporting material fig. S2), the high ammonoid diversity in the Fossil Hill Member was mainly dominated by genera of the family Ceratitidae Mojsisovics, 1879. Particularly the evolutionary lineage of Beyrichitinae Spath 1934 is characterised by progressive shifts in morphology rather than abrupt changes, as originally stated by Silberling (1962). Subsequently this was rejected by Silberling & Nichols (1980, 1982). In the context of this thesis, I would like to emphasize that stratigraphically successive beyrichitine ammonoid assemblages do commonly show a progressive and gradual shift in morphology confirming the initial assumption by Silberling (1962). Therefore, species separation of this group is necessarily arbitrary to some extent (Silberling 1962). It might, however, not be adequate to generalize this finding or to extend it to all Anisian ammonoids.

In the study of ammonoids, the greatest difficulties often centre on the definition and delimitation of the species as the fundamental unit of classification (Donovan 1994). Considered superficially, the Anisian ammonoids of Nevada show a very high disparity with well-defined morphologies. Therefore, the taxonomy of the species does not seem to be very complex at first. However, a closer look reveals that many species exhibit high intraspecific variability hindering a clear distinction of individual species. These difficulties are particularly common among representatives of the family Ceratitidae Mojsisovics 1879. This is mainly caused by the stratophenetic classification of the species in their original taxonomic descriptions. Therefore, it is especially important to apply a more objective and quantitative approach to original species descriptions (Rouget et al. 2004; Neige et al. 2007; Yacobucci 2015). In chapter 5.3 of this thesis, this was addressed by complementing traditional descriptions with Traditional and Geometric Morphometric Methods.

5.3 Ammonoid morphology

What are the main factors influencing morphologic change in Anisian ceratitid ammonoids of Nevada, USA?

The continuous stratigraphic sections of the Fossil Hill Member in NW Nevada allow to trace changes of morphologies through time. For the observation of many evolutionary processes - such as heterochrony - a close phylogenetic relationship between species is essential (McKinney & McNamara 1991; chap. 2). Therefore, the abundant and diverse family Ceratitidae Mojsisovics 1879 and subfamily Beyrichitinae Spath 1934 were chosen for further morphologic analyses.

For the evaluation and quantification of morphologic changes of ammonoids three different morphologic approaches were used: (1) Linear measurements, (2) Raupian parameters of Traditional Morphometrics methods, (3) Geometric Morphometric methods (GMM) using landmark data. Linear measurements and the derived Raupian parameters are a very straightforward tool for a basic description of ammonoids. Ceratitid ammonoids, however, often differ through their characteristic ways of ventral arching and presence or absence of a keel, which can hardly be described with linear measurements (Neige 1999). In chapter 4.3 of this thesis a more detailed discussion on the advantages of GMM over the latter can be found. The main advantage lies within the much higher flexibility of landmark data.

The observed patterns in ontogenetic allometry and intra- and interspecific variability of beyrichitine species are closely linked to one another. Morphologic disparity, which is a measure of the latter, seems to be the result of perturbations of the allometric growth pattern (i.e. heterochrony). However, none of the morphometric approaches used in chapter 4.2–4.4. revealed the presence of dominant, directional evolutionary processes. This is interpreted to be the result of the generally stable palaeoenvironment and therefore only a limited amount of environmental pressure (Chap. 4.5). The geometric morphometric approach revealed that paedomorphic development seems to be more common within the evolutionary line of ceratitid ammonoids than peramorphic development. In fact, this observation supports the common view that paedomorphosis is the dominant evolutionary process in stable environments (Gould 1977, chap. 8; McKinney & McNamara 1991, chap. 4).

Whereas the evolutionary lineage of *Gymnotoceras* is characterised by a progressive decrease in allometric slope (i.e. “juvenilisation”), the changes in the other, younger genera rather suggest a progressive peramorphosis (i.e. “overmaturation”). This would suggest a paradigm shift between the *Gymnotoceras rotelliformis* and *Parafrechites meeki* zones. However, based on the current data, this hypothesis is highly speculative. To underpin this assumption, additional fossil specimens would be needed to collect more data.

5.4 Overarching conclusions

The overarching aim of this thesis is to broaden our understanding of evolutionary and developmental processes of ammonoids. Ammonoid diversity but also disparity is controlled by both "internal" biological processes (e.g. developmental flexibility, intraspecific variability, heterochronic processes) and "external" environmental factors controlling habitat space and geographic distributions (e.g. sea level cycles, tectonic shifts, oceanographic conditions, and climate change) (Yacobucci 2015). Therefore, a synthetic and quantitative approach to the macroevolution and palaeobiogeography of ammonoids is essential to understand the evolutionary dynamics of this highly remarkable group of animals (Yacobucci 2015).

The Fossil Hill Member is characterised by drastic facies changes at the base and top. However, during its deposition, no major palaeoenvironmental shifts were detected. The investigated sequences proof of a generally stable, but nevertheless hostile palaeoenvironment of the Middle Triassic ecosystem with dysoxic to anoxic bottom-waters. Small-scale environmental changes most likely occurred in relation to short-term oxygenation of the ocean floor (chapter 4.5). The occurrence of abundant and partially well-preserved bivalve assemblages prove the–at least temporary–dense occupation of the habitat.

We could not identify a dominating environmental factor driving the evolution of the studied ammonoids in one direction. The observed evolutionary trends within Ceratitidae seem to be driven by intrinsic factors rather than by adaptation to the few small-scale palaeoenvironmental changes. Within the family Ceratitidae, paedomorphosis seems to be more common than peramorphosis. The biologic meaning of the observed evolutionary pattern currently remains elusive.

6 Outlook

This doctoral thesis represents an integrated approach to develop a better understanding of processes influencing morphologic change in ammonoids. Particularly the Geometric Morphometric analyses using R programming has proven to be a fruitful area of research. The Geometric Morphometric methods introduced here represent a major step towards more comprehensive and quantitative species descriptions. However, despite the contributions of this study, the application of Geometric Morphometric methods on ammonoids remains challenging and further methodological work is undoubtedly needed. The following three paragraphs summarise additional research questions and issues that deserve more attention.

1) Acquisition of additional morphometric data

I am confident that the heterochronic processes observed in the Geometric Morphometric Analysis of this work reflect true biological processes. Nevertheless, it cannot be denied that the statistical power is rather low in some cases. It is however very important to always keep in mind what is being analysed. For example, the R function *geomorph::morphol.disparity* accounts for group size. Therefore, overall morphologic variability is not strongly dependent on how many individuals of a single species are analysed. Individual outliers can potentially distort the amount of total variability in a dataset. Proportionally, however, no significant deviations are to be expected. However, caution is required when statistical statements are made about individual whorl stages. Even though statistical functions usually take the sample size into account, random deviations may be overestimated.

A completely different approach to improve Geometric Morphometric analyses is the use of CT scanning. The disadvantage of CT scanning is that this method is very expensive. On the other hand, as a non-destructive method, it can be obtained from any sample, e.g. also from historical specimens. Unfortunately, it was impossible to produce useful CT scanning images of the fossils of the Anisian Fossil Hill Member due to a lack of contrast (chapter 5.2 and 5.3). Had it been successful, the geometric analysis would have been possible at a much finer resolution. However, Tajika & Klug (2020) stated that a resolution of 180° is usually sufficient for capturing the main development steps.

2) Geochemistry and absolute age model

The geological and geochemical part of the thesis would benefit from a more targeted and detailed geochemical analysis. Particularly the less competent calcareous mudstone could be sampled in greater detail. However, from a geochemical point of view, the rocks at the Fossil Hill locality are too heavily weathered for a reliable analysis (chapter 4.5). The thicker and less weathered sequences in

the Augusta Mountains, on the other hand, still yield a high potential. Especially the irregularly occurring alleged tephra layers should be sampled and examined thoroughly. Zircon dating would open the gate to a much more precise age model. This is potentially very important for estimating the sedimentation rate and evolutionary rates of organisms.

3) Widen the scope of the geometric morphometric analysis

It was always the intention to focus mainly on Anisian ammonoids from Nevada because of their good preservation and the opportunity to collect large sample series. Therefore, it was appropriate that the analytical tools of this thesis were tailored to a small-scale analysis with a rather narrow scope. Obviously, it would be particularly interesting to explore the applicability of these methods in the context of a wider scope. Potential for future studies therefore lies in a universalisation of the Geometric Morphometric methods introduced here. Additionally, a standardised system to compare different morphotypes (i.e. discoidal, pachyconic, globular, spindle-shaped) would allow statements about the total morphologic disparity of larger and more diverse ammonoid assemblages.

In this analysis, whorl cross sections were compared with one another only. It would be particularly interesting to check whether these could be combined with other characteristics such as conch shape, conch size or umbilical width. From a methodological point of view, the R function *geomorph*::*combine.subsets* (Adams et al. 2020) would be particularly helpful in this respect.

Anisian ammonoids from Nevada are associated with a rather calm and stable palaeoenvironment at a palaeodepth well below the stormwave base. The comparison of evolutionary and developmental characteristics of ammonoid assemblages from other sites – that have been exposed to more palaeoenvironmental perturbations, e.g. more shallow water conditions, but distinct third order sea level change – would reveal more insights on the role of palaeoenvironmental pressure on morphology.

References

Adams DC, Collyer ML, and A. K. 2020. Geomorph: Software for geometric morphometric analyses. R package version 3.2.1. https://cran.r-project.org/package=geomorph.

Alberch P, Gould SJ, Oster GF, and Wake DB. 1979. Size and shape in ontogeny and phylogeny. *Palaeobiology* 5:296-317.

Arias C. 2008. Palaeoceanography and biogeography in the Early Jurassic Panthalassa and Tethys Oceans. *Gondwana Research* 14:306-315. https://doi.org/10.1016/j.gr.2008.03.004

Balini M, Lucas SG, Jenks JF, and Spielmann JA. 2010. Triassic ammonoid biostratigraphy: an overview. *Geological Society, London, Special Publications* 334:221-262. 10.1144/sp334.10

Barnosky AD, Matzke N, Tomiya S, Wogan GOU, Swartz B, Quental TB, Marshall C, McGuire JL, Lindsey EL, Maguire KC, Mersey B, and Ferrer EA. 2011. Has the Earth's sixth mass extinction already arrived? *Nature* 471:51-57.

Benton MJ. 1995. Diversification and extinction in the history of life. *Science* 268:52-58.

Bischof EA, and Lehmann J. 2020. Ontogenetic analysis of Anisian (Middle Triassic) ptychitid ammonoids from Nevada, USA. *Journal of Palaeontology* 94:829-851. 10.1017/jpa.2020.25

Brayard A, and Bucher H. 2015. Permian-Triassic extinctions and rediversifications. In: Klug C, Korn D, De Baets K, Kruta I, and Mapes RH, eds. *Topics in Geobiology*. Dordrecht: Springer, 465-473.

Brayard A, Escarguel G, Bucher H, and Brühwiler T. 2009a. Smithian and Spathian (Early Triassic) ammonoid assemblages from terranes: Palaeoceanographic and palaeogeographic implications. *Journal of Asian Earth Sciences* 36:420-433. https://doi.org/10.1016/j.jseaes.2008.05.004

Brayard A, Escarguel G, Bucher H, Monnet C, Brühwiler T, Goudemand N, Galfetti T, and Guex J. 2009b. Good genes and good luck: Ammonoid diversity and the End-Permian mass extinction. *Science* 325:1118-1121. 10.1126/science.1174638

Brayard A, Escarguel G, Monnet C, Jenks JF, and Bucher H. 2015. Biogeography of Triassic ammonoids. In: Klug C, Korn D, De Baets K, Kruta I, and Mapes RH, eds. *Topics in Geobiology*. Dordrecht: Springer, 163-187.

Brosse M, Brayard A, Fara E, and Neige P. 2013. Ammonoid recovery after the Permian–Triassic mass extinction: a re-exploration of morphological and phylogenetic diversity patterns. *Journal of the Geological Society* 170:225-236. 10.1144/jgs2012-084

Brueckner HK, and Snyder WS. 1985. Structure of the Havallah sequence, Golconda allochthon, Nevada: Evidence for prolonged evolution in an accretionary prism. *Geological Society of America Bulletin* 96:1113-1130.

Bucher H. 1988. A new Middle Anisian (Middle Triassic) ammonoid zone from northwestern Nevada (USA). *Eclogae Geologicae Helvetiae* 81:723-762.

Bucher H. 1989. Lower Anisian Ammonoids from the northern Humboldt Range (northwestern Nevada, USA) and their bearing upon the Lower-Middle Triassic Boundary. *Eclogae Geologicae Helvetiae* 82:945-1002.

Bucher H. 1991. New Ammonoids from the Taylori zone (middle Anisian, middle Triassic) from Northwestern Nevada (USA). In: Guex J, and Baud A, eds. *Memoires de Geologie (Lausanne)*. Lausanne, 1-8.

Bucher H. 1992a. Ammonoids of the Hyatti Zone (Middle Anisian, Middle Triassic) and the Anisian transgression in the Star Peak Group (northwestern Nevada). *Palaeontographica* 223:137-166.

Bucher H. 1992b. Ammonoids of the *Shoshonensis* Zone (Middle Anisian, Middle Triassic) from northwestern Nevada (USA). *Jahrbuch der Geologischen Bundesanstalt Wien* 135:425-465.

Bucher H. 1994. New ammonoids of the Taylori Zone (Middle Anisian, Middle Triassic) from western Nevada (USA). In: Guex J, and Baud A, eds. *Mémoires de Géologie*. Lausanne, 1-8.

Cameron EN. 1939. Geology and mineralization of the northeastern Humboldt Range, Nevada. *Bulletin of the Geological Society of America* 50:563-634.

Close RA, Benson RBJ, Saupe EE, Clapham ME, and Butler RJ. 2020. The spatial structure of Phanerozoic marine animal diversity. *Science* 368:420. 10.1126/science.aay8309

Decourten FL, and Biggar N. 2017. Roadside geology of Nevada. Missoula: Mountain Press Publishing Company. p 406.

Donovan DT. 1994. History of classification of Mesozoic ammonites. *Journal of the Geological Society* 151:1035-1040.

Dunham RJ. 1962. Classification of carbonate rocks according to depositional textures. *American Association of Petroleum Geologists Memoir* 1:108-121.

Engeser T. 1996. The position of the Ammonoidea within the Cephalopoda. In: Landman NH, Tanabe K, and Davis RA, eds. *Topics in Geobiology*. New York: Plenum, 3-19.

Erwin DH. 1994. The Permo-Triassic extinction. *Nature* 367:231-236. 10.1038/367231a0

Ferguson H, Muller S, and Roberts R. 1951. Geology of the Winnemucca quadrangle, Nevada. *US Geological Survey Map GQ-11*.

Fiero B. 2009. Geology of the Great Basin. Reno & Las Vegas: University of Nevada Press. p 239.

Folk RL. 1962. Spectral subdivision of limestone types. *American Association of Petroleum Geologists Memoir* 1:62-84.

Gabb WM. 1864. Palaeontology of California. Description of the Triassic fossils of California and the adjacent territories. Philadelphia: California Geological Survey, Palaeontology. p 17-35.

Gerber S. 2011. Comparing the differential filling of morphospace and allometric space through time: the morphological and developmental dynamics of Early Jurassic ammonoids. *Palaeobiology* 37:369-382.

Gerber S, Neige P, and Eble GJ. 2007. Combining ontogenetic and evolutionary scales of morphological disparity: a study of early Jurassic ammonites. *Evolution & Development* 9:472-482.

Gould SJ. 1977. Ontogeny and phylogeny. Cambridge, Massachusetts: Harvard University Press. p 501.

Gould SJ. 1988. The uses of heterochrony. In: McKinney ML, ed. *Topics in Geobiology*. New York: Springer Science + Business Media, LLC, 1-13.

Gradstein FM. 2020. Chapter 3 - Evolution and Biostratigraphy. In: Gradstein FM, Ogg JG, Schmitz MD, and Ogg GM, eds. *Geologic Time Scale 2020*: Elsevier, 35-137.

Hoffmann R, Weinkauf MFG, Wiedenroth K, Goeddertz P, and De Baets K. 2019. Morphological disparity and ontogeny of the endemic heteromorph ammonite genus Aegocrioceras (Early Cretaceous, Hauterivian, NW-Germany). *Palaeogeography, Palaeoclimatology, Palaeoecology* 520:1-17. https://doi.org/10.1016/j.palaeo.2019.01.020

Hyatt A, and Smith JP. 1905. *The Triassic cephalopod genera of America*: US Government Printing Office.

Ingersoll RV. 2008. Subduction-related sedimentary basins of the USA Cordillera. *Sedimentary basins of the world* 5:395-428.

Ingersoll RV. 2019. Subduction-Related Sedimentary Basins of the US Cordillera. *The Sedimentary Basins of the United States and Canada*: Elsevier, 477-510.

Jenks JF, Monnet C, Balini M, Brayard A, and Meier M. 2015. Biostratigraphy of Triassic ammonoids. In: Klug C, Korn D, De Baets K, Kruta I, and Mapes RH, eds. *Topics in Geobiology*. Dordrecht: Springer, 329-388.

Jenks JF, Spielmann JA, and Lucas SG. 2007. Triassic ammonoids: A photographic journey. In: Lucas SG, and Spielmann JA, eds. *New Mexico Museum of Natural History and Science Bulletin*. Albuquerque, 33-80.

Ji C, and Bucher H. 2018. Anisian (Middle Triassic) ammonoids from British Columbia (Canada): biochronological and palaeobiogeographical implications. *Papers in Palaeontology* 4:623-642. 10.1002/spp2.1222

King C. 1878. Systematic geology: Report of the US Geological Exploration of the Fortieth Parallel: Engineering Department. United States Geological Exploration of the 40th Parallel: US Government Printing Office. p 1-803.

Klingenberg CP. 1998. Heterochrony and allometry: the analysis of evolutionary change in ontogeny. *Biological Reviews* 73:79-123.

Klug C, Korn D, De Baets K, Kruta I, and Mapes R. 2015a. Ammonoid Palaeobiology: From Anatomy to Ecology.

Klug C, Korn D, De Baets K, Kruta I, and Mapes R. 2015b. Ammonoid Palaeobiology: From Macroevolution to Palaeogeography.

Klug C, Kröger B, Vinther J, Fuchs D, and De Baets K. 2015c. Ancestry, origin and early evolution of Ammonoids. In: Klug C, Korn D, De Baets K, Kruta I, and Mapes RH, eds. *Topics in Geobiology*. Dordrecht: Springer, 3-24.

Korn D. 2012. Quantification of ontogenetic allometry in ammonoids. *Evolution & Development* 14:501-514. doi:10.1111/ede.12003

Korn D, Klug C, and Walton SA. 2015. Taxonomic diversity and morphological disparity of Palaeozoic ammonoids. In: Klug C, Korn D, De Baets K, Kruta I, and Mapes RH, eds. *Topics in Geobiology*. Dordrecht: Springer, 431-464.

Kröger B, Vinther J, and Fuchs D. 2011. Cephalopod origin and evolution: A congruent picture emerging from fossils, development and molecules. *BioEssays* 33:602-613. 10.1002/bies.201100001

Landman NH, Tanabe K, and Davis RA. 1996a. Ammonoid Palaeobiology. Topics in Geobiology. New York: Plenum. p 857.

Landman NH, Tanabe K, and Shigeta Y. 1996b. Ammonoid embryonic development. In: Landman NH, Tanabe K, and Davis RA, eds. *Topics in Geobiology*. New York: Plenum, 343-405.

Lehmann U. 1990. Ammonoideen - Leben zwischen Skylla und Charybdis. In: Erben HK, Hillmer G, and Ristedt H, editors. Stuttgart: Enke. p 1-257.

Lucas SG. 2010. The Triassic chronostratigraphic scale; history and status. *Geological Society Special Publications* 334:17-39.

Mayr E. 1949. *Systematics and the origin of species: from the viewpoints of a zoologist*.

McKinney ML, and McNamara KG. 1991. Heterochrony. The Evolution of Ontogeny. New York: Springer Science+Business Media, LLC. p XXI+437.

McNamara KJ. 2012. Heterochrony: the evolution of development. *Evolution: Education and Outreach* 5:203-218.

Meek FB. 1877. Part I. Palæontology. In: King C, editor. Washington: Government Printing Office. p 1-197.

Mojsisovics E, Waagen W, and Diener C. 1895. Entwurf einer Gliederung der pelagischen Sedimente des Trias-Systems. *Sitzungsberichte der kaiserlichen Akademie der Wissenschaften in Wien, Mathematisch-naturwissenschaftliche Klasse, Abteilung 1* 104:1271-1302.

Mojsisovics Ev. 1879. Vorläufige kurze Übersicht der Ammoniten-Gattungen der mediterranen und juvavischen Trias. *Verhandlungen der Kaiserlich-Königlichen Geologischen Reichsanstalt Wien* 1879:133-143.

Monnet C, Brayard A, and Brosse M. 2015. Evolutionary trends of Triassic ammonoids. In: Klug C, Korn D, De Baets K, Kruta I, and Mapes RH, eds. *Topics in Geobiology*. Dordrecht: Springer, 25-50.

Monnet C, and Bucher H. 2005a. Anisian (Middle Triassic) ammonoids from North America: quantitative biochronology and biodiversity. *Stratigraphy* 2:281-296.

Monnet C, and Bucher H. 2005b. New Middle and Late Anisian (Middle Triassic) ammonoid faunas from Northwestern Nevada (USA): Taxonomy and biochronology. *Fossils and Strata* 52:1-121.

Monnet C, Bucher H, Wasmer M, and Guex J. 2010. Revision of the genus *Acrochordiceras* Hyatt, 1877 (Ammonoidea, Middle Triassic): morphology, biometry, biostratigraphy and intra-specific variability. *Palaeontology* 53:961-996. 10.1111/j.1475-4983.2010.00956.x

Naglik C, Monnet C, Goetz S, Kolb C, De Baets K, Tajika A, and Klug C. 2015. Growth trajectories of some major ammonoid sub-clades revealed by serial grinding tomography data. *Lethaia* 48:29-46. 10.1111/let.12085

Neige P. 1999. The use of landmarks to describe ammonite shape. In: Olóriz F, and Rodríguez-Tovar FJ, eds. *Advancing Research an Living and Fossil Cepha/opods*. New York: Kluwer Academic/Plenum, 263-272.

Neige P, Rouget I, and Moyne S. 2007. Phylogenetic practices among scholars of fossil cephalopods, with special reference to cladistics. In: Landman NH, Davis RA, and Mapes RH, eds. New York: Springer, 3-14.

Nichols KM, and Silberling NJ. 1977. Stratigraphy and depositional history of the Star Peak Group (Triassic), northwestern Nevada. *Special Paper Geological Society of America* 178:1-73.

Ogg JG, Chen ZQ, Orchard MJ, and Jiang HS. 2020. Chapter 25 - The Triassic Period. In: Gradstein FM, Ogg JG, Schmitz MD, and Ogg GM, eds. *Geologic Time Scale 2020*: Elsevier, 903-953.

Parrish JT. 1993. Climate of the Supercontinent Pangea. *The Journal of Geology* 101:215-233.

Péron S, Bourquin S, Fluteau F, and Guillocheau F. 2005. Palaeoenvironment reconstructions and climate simulations of the Early Triassic: Impact of the water and sediment supply on the preservation of fluvial systems. *Geodinamica Acta* 18:431-446. 10.3166/ga.18.431-446

Preto N, Kustatscher E, and Wignall PB. 2010. Triassic climates — State of the art and perspectives. *Palaeogeography, Palaeoclimatology, Palaeoecology* 290:1-10. https://doi.org/10.1016/j.palaeo.2010.03.015

Price JG. 2002. Geology of Nevada. In: Castor SB, Papke KG, and Meeuwig RO, eds. *Nevada Bureau of Mines and Geology Special Publication*.

Raup DM. 1966. Geometric analysis of shell coiling: general problems. *Journal of Palaeontology* 40:1178-1190.

Raup DM, and Sepkoski JJJ. 1986. Periodic extinction of families and genera. *Science* 231:833-836.

Rieber H. 1962. Beobachtungen an Ammoniten aus dem Ober-Aalénien (Systematik und Ontogenie). *Eclogae Geologicae Helvetiae* 55:587-594.

Rogers JJW, and Santosh M. 2003. Supercontinents in Earth History. *Gondwana Research* 6:357-368. https://doi.org/10.1016/S1342-937X(05)70993-X

Rouget I, Neige P, and Dommergues J-L. 2004. Ammonites phylogenetic analysis: state of the art and new prospects. *Bulletin de la Société Géologique de France* 175:507-512. 10.2113/175.5.507

Sahney S, and Benton MJ. 2008. Recovery from the most profound mass extinction of all time. *Proceedings: Biological Sciences* 275:759-765.

Schatz W. 2000. Taxonomie, Paläoökologie und biostratigraphische Anwendung der Daonellen (Bivalvia) aus der Mitteltrias Europas PhD. University of Zurich.

Schatz W. 2005. Palaeoecology of the Triassic black shale bivalve *Daonella*—new insights into an old controversy. *Palaeogeography, Palaeoclimatology, Palaeoecology* 216:189-201. http://dx.doi.org/10.1016/j.palaeo.2004.11.002

Sepkoski JJJ. 1984. A kinetic model of Phanerozoic taxonomic diversity. III. Post-Palaeozoic families and mass extinctions. *Palaeobiology* 10:246-267.

Silberling N, and Wallace R. 1967. Geologic map of the Imlay quadrangle, Pershing County, Nevada. *US Geological Survey Map GQ-666*.

Silberling NJ. 1962. Stratigraphic distribution of Middle Triassic ammonites at Fossil Hill, Humboldt Range, Nevada. *Journal of Palaeontology* 36:153-160.

Silberling NJ, and Nichols KM. 1980. Phylogenetic patterns among Middle Triassic ammonites. *Revista Italiana di Palaeontologia e Stratigrafia* 85:737-740.

Silberling NJ, and Nichols KM. 1982. Middle Triassic molluscan fossils of biostratigraphic significance from the Humboldt Range, northwestern Nevada. *US Geological Survey Professional Paper*.

Silberling NJ, and Tozer ET. 1968. Biostratigraphic classification of the marine Triassic in North America. *Special Paper Geological Society of America* 110:1-63.

Silberling NJ, and Wallace RE. 1969. Stratigraphy of the Star Peak Group (Triassic) and overlying lower Mesozoic rocks, Humboldt Range, Nevada. *US Geological Survey Professional Paper* 592:1-50.

Skrzycki P, Niedźwiedzki G, and Tałanda M. 2018. Dipnoan remains from the Lower-Middle Triassic of the Holy Cross Mountains and northeastern Poland, with remarks on dipnoan

palaeobiogeography. *Palaeogeography, Palaeoclimatology, Palaeoecology* 496:332-345. https://doi.org/10.1016/j.palaeo.2018.01.049

Smith JP. 1914. The Middle Triassic marine invertebrate faunas of North America. Washington: US Government Printing Office. p 254.

Spath LF. 1934. Catalogue of the fossil Cephalopoda in the British Museum (Natural History): Part IV The Ammonoidea of the Trias. London: British Museum of Natural History. p 521.

Tajika A, and Klug C. 2020. How many ontogenetic points are needed to accurately describe the ontogeny of a cephalopod conch? A case study of the modern nautilid *Nautilus pompilius*. *PeerJ* 8:e8849. 10.7717/peerj.8849

Totman Parrish J. 1999. Pangaea und das Klima der Trias. In: Hauschke N, and Wilde V, eds. Munich: Dr. Friedrich Pfeil, 37-42.

UCMP History. (n.d.). 1905 Saurian Expedition. *Available at https://ucmp.berkeley.edu/about-ucmp/history-of-ucmp/saurian-expedition-1905/* (accessed 21.01.2021.

Wyld SJ. 2000. Triassic evolution of the arc and backarc of northwest Nevada, and evidence for extensional tectonism. *Geological Society of America Special Papers* 347:185-207. 10.1130/0-8137-2347-7.185

Yacobucci MM. 2015. Macroevolution and palaeobiogeography of Jurassic-Cretaceous Ammonoids. In: Klug C, Korn D, De Baets K, Kruta I, and Mapes RH, eds. *Topics in Geobiology*. Dordrecht: Springer, 189-228.

Zakharov YD, and Mousavi Abnavi N. 2013. The ammonoid recovery after the end-Permian mass extinction: Evidence from the Iran-Transcaucasia area, Siberia, Primorye, and Kazakhstan. *Acta Palaeontologica Polonica* 58:127-147. 10.4202/app.2011.0054

Zakharov YD, and Popov AM. 2014. Recovery of brachiopod and ammonoid faunas following the End-Permian crisis: Additional evidence from the lower Triassic of the Russian Far East and Kazakhstan. *Journal of Earth Science* 25:1-44. 10.1007/s12583-014-0398-6

Zelditch ML, Swiderski DL, and Sheets HD. 2012. Geometric morphometrics for biologists: a primer. 2 ed. London, Waltham & San Diego: Academic Press. p 478.

Acknowledgements

This project was financed by the German Science Foundation (DFG; project “Nevammonoidea”, LE 1241/3-1 and received a lot of academic, financial and infrastructural support from the University of Bremen, the MARUM, Center for Marine Environmental Sciences, and GLOMAR - Bremen Graduate School for Marine Sciences.

First and foremost, I want to thank my supervisor Jens Lehmann for giving me the chance to work on this fascinating project. He also provided me the support and freedom to develop my scientific skills in the framework of this project. Many thanks go also to Marco Balini (Milan) for taking the position as second reviewer of this thesis. Jochen Kuss, Charlotte Decker, and Angelina Füllberg are thanked for attending my defence as examining committee members.

I would like to thank Bernhard Hostettler and Ursula Menkveld-Gfeller for motivating me to do a PhD. They were one of the most important people on my professional journey so far. Without their kindness of heart and support, I might never have dared to follow this path. They fully captured me with their own fascination for the subject. I might also not be where I am today if my parents Beda and Christina Bischof had not raised me to be a strong and independent woman with the world open to her with all its opportunities and possibilities.

Pat Embree (Orangevale, CA, USA) is thanked for permission to do field-work on his private property on the Fossil Hill of the Humboldt Range in NW Nevada, USA and his infrastructural support. I also had many discussions with other colleagues. In particular I would like to thank Nils Schlüter (Berlin), Romain Jattiot (Bremen), Dieter Korn (Berlin), Karin Boos (Oldenburg), and Jim Jenks (West Jordan, UT, USA). Special gratitude goes to Nils for being my sparring partner in Geometric Morphometrics and to Nils and Romain for reviewing this thesis. Their comments greatly improved this manuscript and, even more importantly, increased my confidence in it. Imhof is warmly thanked for helping me to translate the summary into Bernese dialect. Clearly, his Bernese pronunciation is way better than mine.

Henning Kuhnert, Birgit Meyer, Marco Klann, and Rüdiger Stein (all Bremen) were of great help with the Geochemical analysis. Petra Witte and Wolfgang Bach helped with the Scanning Electron Microscope (SEM). Jarrid Tschaikowsky, Isabel Schröder, Olawale Oluwafemi, Thomas Lis (all Bremen) helped with the preparation of the palaeontological and geochemical analysis. I furthermore appreciated technical support by Martin Krogmann, David Kuhlmann, Anne Hübner, and Ralf Bätzel (Bremen).

Martin Krogmann and David Kuhlmann, I would furthermore also like to thank for their endless support as co-workers but even more importantly as friends. I really enjoyed working with the extended GSUB-Team consisting of Jens, Martin, Romain, David but also Werner, Jürgen, Andy and in the

broader sense Allan as well. They all carry just the right amount of craziness in them, which is exactly why I was so happy to have them around.

In the course of the last years I have spent so many hours with peers discussing, laughing and joking but also whining and complaining. But special thank goes to the “(SUPPORT)”-group. Mareike, Jule, Charlotte and Runa: You rock! Special gratitude goes to Runa for reviewing this thesis. Additionally, I would also like to thank everybody else that made my time here in Bremen such a wonderful experience. Even though they had no direct scientific influence, they were of great moral support. Here I would like to mention in particular (order of appearance): Martin, Lutz, Christiane, Bente, David, Tascha and Tim, all Pastorentöcher, Gabi Charlotte and Fabi, Jule and Renja, and Uli and all other climactivists. You made Bremen a home for us!

And finally, the biggest and fattest thank you goes to my fiancé Matthias Bächli, who voluntarily followed me into the new and also scary world of the unknown. From the very beginning he accompanied me on my journey and together we have built a new life in our own little universe.

APPENDIX

Appendix 1 Lithostratigraphic Sections

Legend:

Lithologies


Siltstone


Calcareous siltstone


Very calcareous siltstone


Lime mudstone


Dolomitic limestone


Tectonic overprint

Components


Sand


Frag. of echinoderms


Woods


Drainage structure

Fossil Content


Ammonoids


Aulacocerate


Daonella

Vertebrates


Nautiloid


Brachiopod


Fragmented fossils

Samples


Rock sample taken

Spyke for orientation (fotographs)


Loose rock sample

Favret Canyon - Eva I (FCE)
Photos: Some
Length: 20.65 m

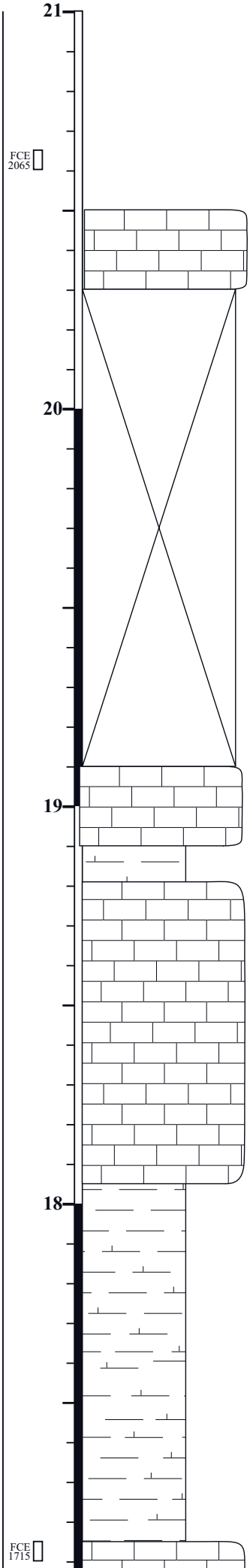

lime mudstone

not explored (channel above seating area)

lime mudstone

siltstone

lime mudstone, thin-layered

siltstone

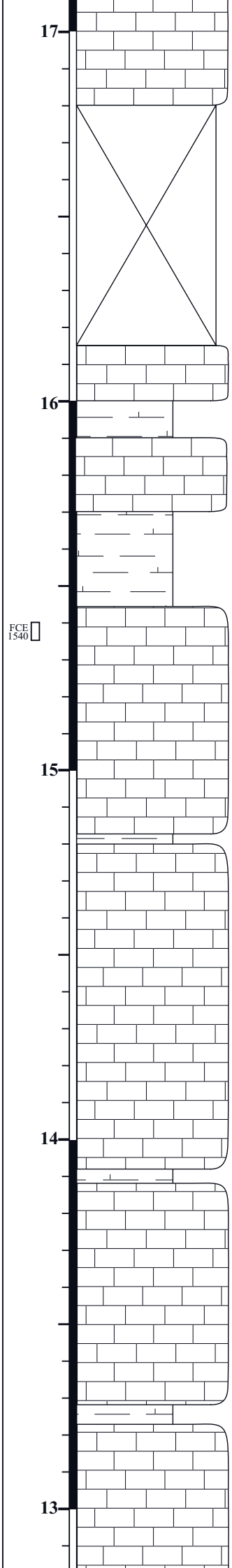

lime mudstone

not explored (seating area above Ichthyosaur Eva I)

lime mudstone
1600: fossil placer

1600

silstone

lime mudstone

siltstone

1445

1445

ICHTHYOSAUR (Eva I), high abundance of ammonoids

more than 4.00 m of concretionary lime mudstones intercalating with siltstones. Strong lateral variations. The individual stones have a lumpy appearance. Wavy top of every individual rock.

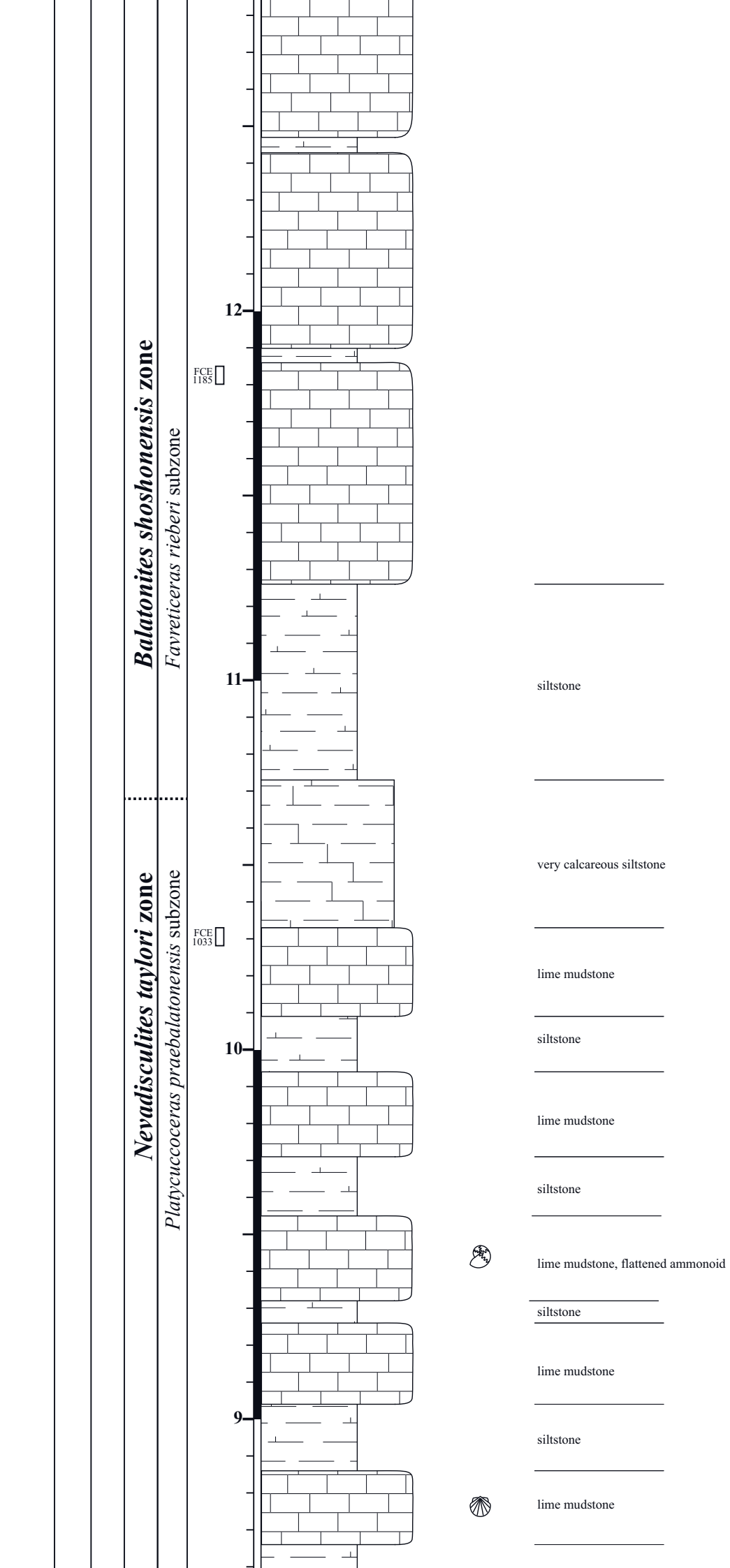
Balatonites shoshonensis zone
Favreticeras rieberi subzone
Nevadiscultites taylori zone
Platycuccoceras praebalatonensis subzone
12
11
10
9
FCE 1185
FCE 1033
siltstone
very calcareous siltstone
lime mudstone
siltstone
lime mudstone
siltstone
lime mudstone, flattened ammonoid
siltstone
lime mudstone
siltstone
lime mudstone

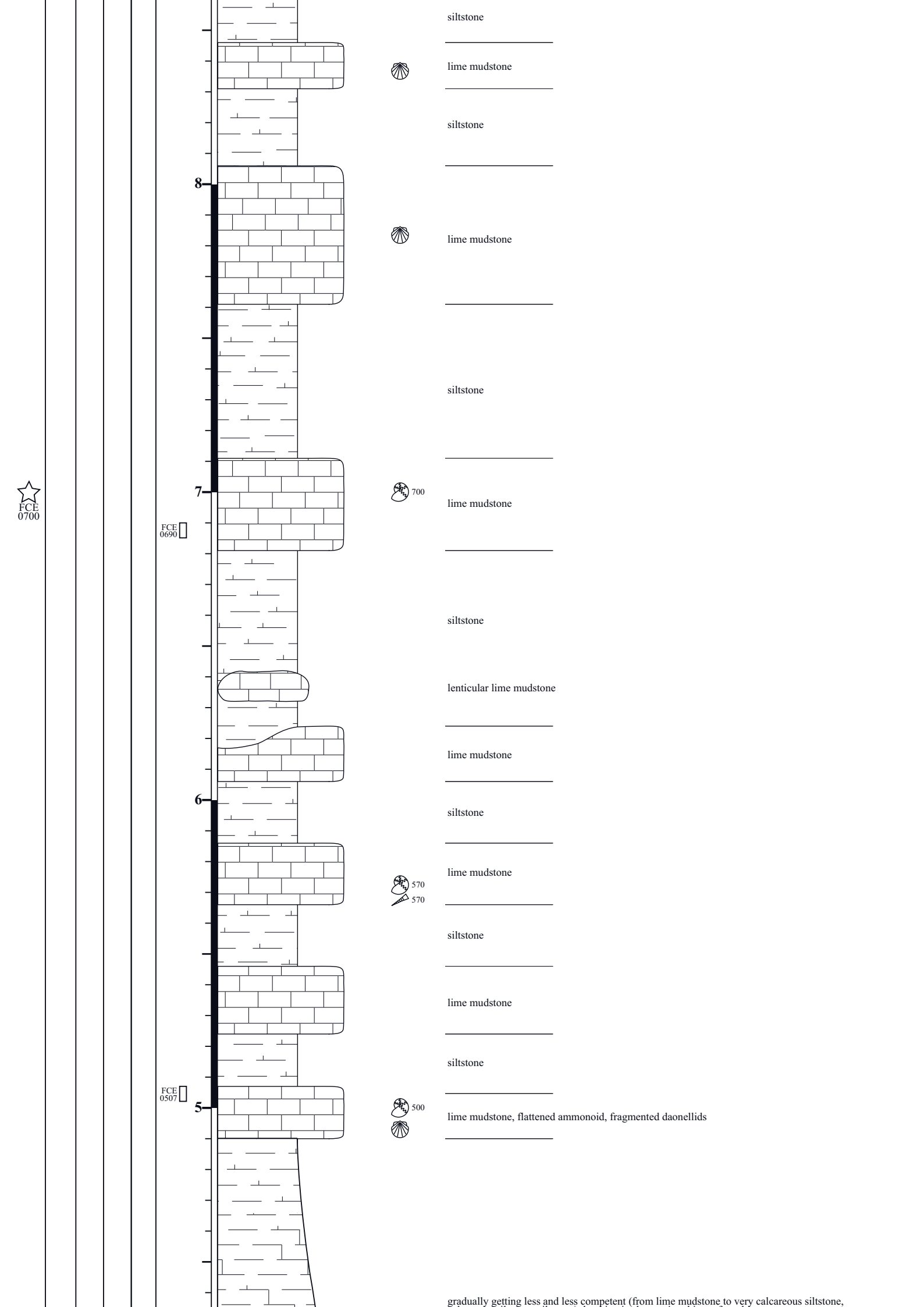
siltstone
lime mudstone
siltstone
8
lime mudstone
siltstone
FCE
0700
7
700
lime mudstone
FCE
0690
siltstone
lenticular lime mudstone
lime mudstone
6
siltstone
lime mudstone
570
570
siltstone
lime mudstone
siltstone
FCE
0507
5
500
lime mudstone, flattened ammonoid, fragmented daonellids
gradually getting less and less competent (from lime mudstone to very calcareous siltstone,

late Anisian

Fossil Hill Member

FCE 0380

FCE 0370

FCE 0127

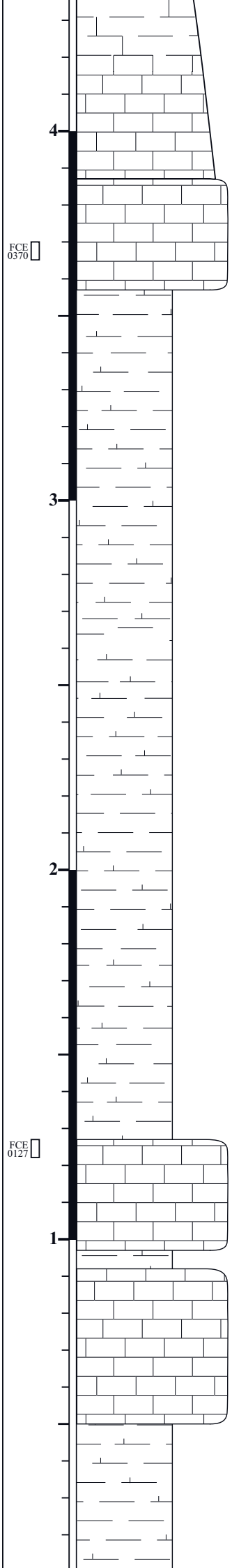

380

115

calcareous siltstone, siltstone), layering is also getting thinner from base to top

lime mudstone

siltstone

lime mudstone

siltstone

lime mudstone

siltstone

base not explored

stage
member
zone
subzone
samples
scale [m]
spikes
fossils

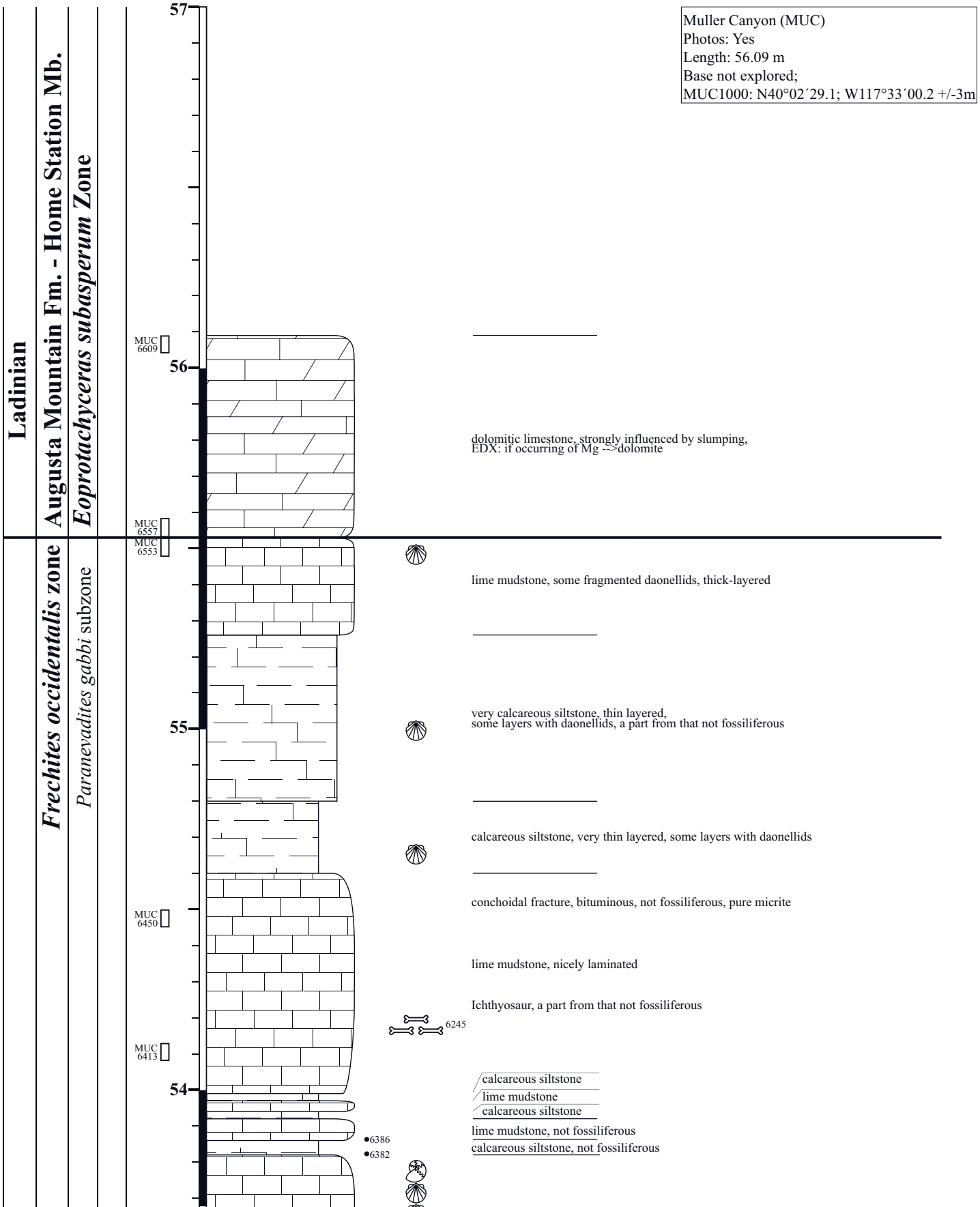
Ladinian
Augusta Mountain Fm. - Home Station Mb.
Eoprotachyceras subasperum Zone
Frechites occidentalis zone
Paranevadites gabbi subzone
Muller Canyon (MUC)
Photos: Yes
Length: 56.09 m
Base not explored;
MUC1000: N40°02´29.1; W117°33´00.2 +/-3m
57
56
55
54
MUC 6609
MUC 6557
MUC 6553
MUC 6450
MUC 6413
6245
6386
6382
dolomitic limestone, strongly influenced by slumping,
EDX: if occurring of Mg -->dolomite
lime mudstone, some fragmented daonellids, thick-layered
very calcareous siltstone, thin layered,
some layers with daonellids, a part from that not fossiliferous
calcareous siltstone, very thin layered, some layers with daonellids
conchoidal fracture, bituminous, not fossiliferous, pure micrite
lime mudstone, nicely laminated
Ichthyosaur, a part from that not fossiliferous
calcareous siltstone
lime mudstone
calcareous siltstone
lime mudstone, not fossiliferous
calcareous siltstone, not fossiliferous

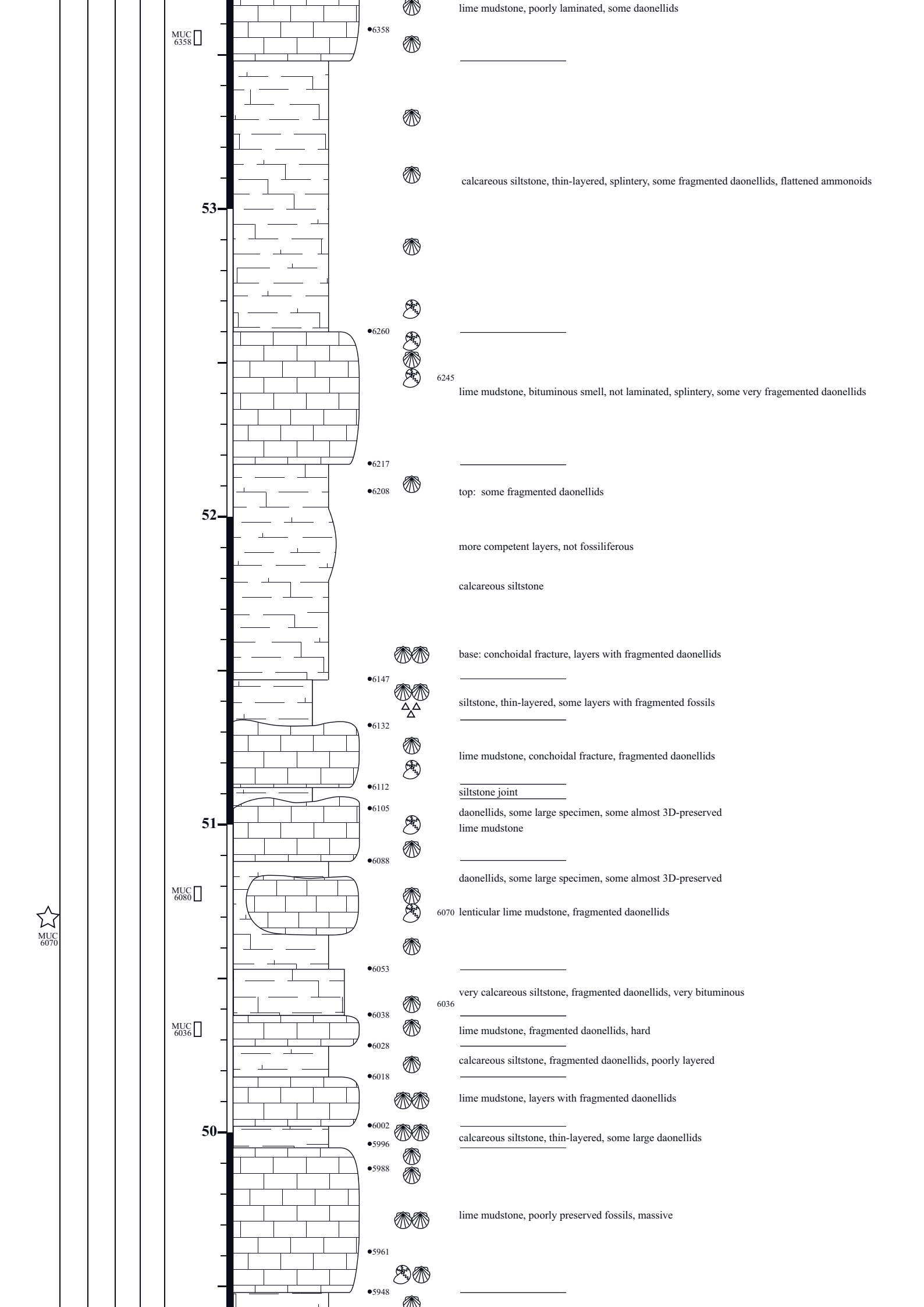
lime mudstone, poorly laminated, some daonellids
MUC 6358
6358
calcareous siltstone, thin-layered, splintery, some fragmented daonellids, flattened ammonoids
53
6260
6245
lime mudstone, bituminous smell, not laminated, splintery, some very fragemented daonellids
6217
6208
top: some fragmented daonellids
52
more competent layers, not fossiliferous
calcareous siltstone
base: conchoidal fracture, layers with fragmented daonellids
6147
siltstone, thin-layered, some layers with fragmented fossils
6132
lime mudstone, conchoidal fracture, fragmented daonellids
6112
siltstone joint
6105
daonellids, some large specimen, some almost 3D-preserved
51
lime mudstone
6088
daonellids, some large specimen, some almost 3D-preserved
MUC 6080
6070
lenticular lime mudstone, fragmented daonellids
MUC 6070
6053
very calcareous siltstone, fragmented daonellids, very bituminous
6036
6038
MUC 6036
lime mudstone, fragmented daonellids, hard
6028
calcareous siltstone, fragmented daonellids, poorly layered
6018
lime mudstone, layers with fragmented daonellids
6002
50
calcareous siltstone, thin-layered, some large daonellids
5996
5988
lime mudstone, poorly preserved fossils, massive
5961
5948

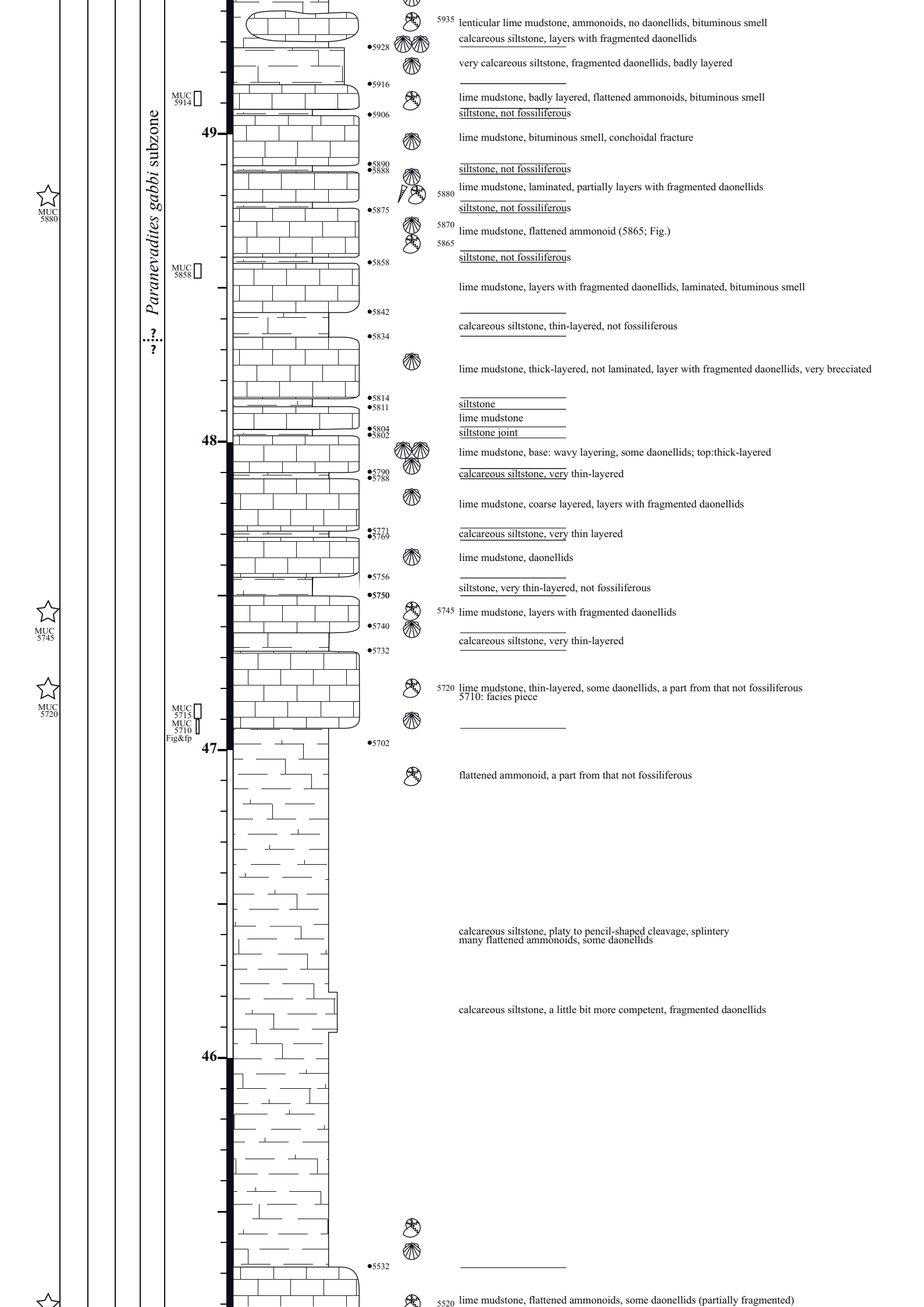
Paranevadites gabbi subzone
MUC 5880
MUC 5745
MUC 5720
MUC 5914
MUC 5858
MUC 5715
MUC 5710
Fig&fp
49
48
47
46
5935
lenticular lime mudstone, ammonoids, no daonellids, bituminous smell
5928
calcareous siltstone, layers with fragmented daonellids
very calcareous siltstone, fragmented daonellids, badly layered
5916
lime mudstone, badly layered, flattened ammonoids, bituminous smell
5906
siltstone, not fossiliferous
lime mudstone, bituminous smell, conchoidal fracture
5890
5888
siltstone, not fossiliferous
5880
lime mudstone, laminated, partially layers with fragmented daonellids
5875
siltstone, not fossiliferous
5870
lime mudstone, flattened ammonoid (5865; Fig.)
5865
siltstone, not fossiliferous
5858
lime mudstone, layers with fragmented daonellids, laminated, bituminous smell
5842
calcareous siltstone, thin-layered, not fossiliferous
5834
lime mudstone, thick-layered, not laminated, layer with fragmented daonellids, very brecciated
5814
siltstone
5811
lime mudstone
5804
siltstone joint
5802
lime mudstone, base: wavy layering, some daonellids; top:thick-layered
5790
calcareous siltstone, very thin-layered
5788
lime mudstone, coarse layered, layers with fragmented daonellids
5771
calcareous siltstone, very thin layered
5769
lime mudstone, daonellids
5756
siltstone, very thin-layered, not fossiliferous
5750
5745
lime mudstone, layers with fragmented daonellids
5740
calcareous siltstone, very thin-layered
5732
5720
lime mudstone, thin-layered, some daonellids, a part from that not fossiliferous
5710: facies piece
5702
flattened ammonoid, a part from that not fossiliferous
calcareous siltstone, platy to pencil-shaped cleavage, splintery
many flattened ammonoids, some daonellids
calcareous siltstone, a little bit more competent, fragmented daonellids
5532
5520
lime mudstone, flattened ammonoids, some daonellids (partially fragmented)

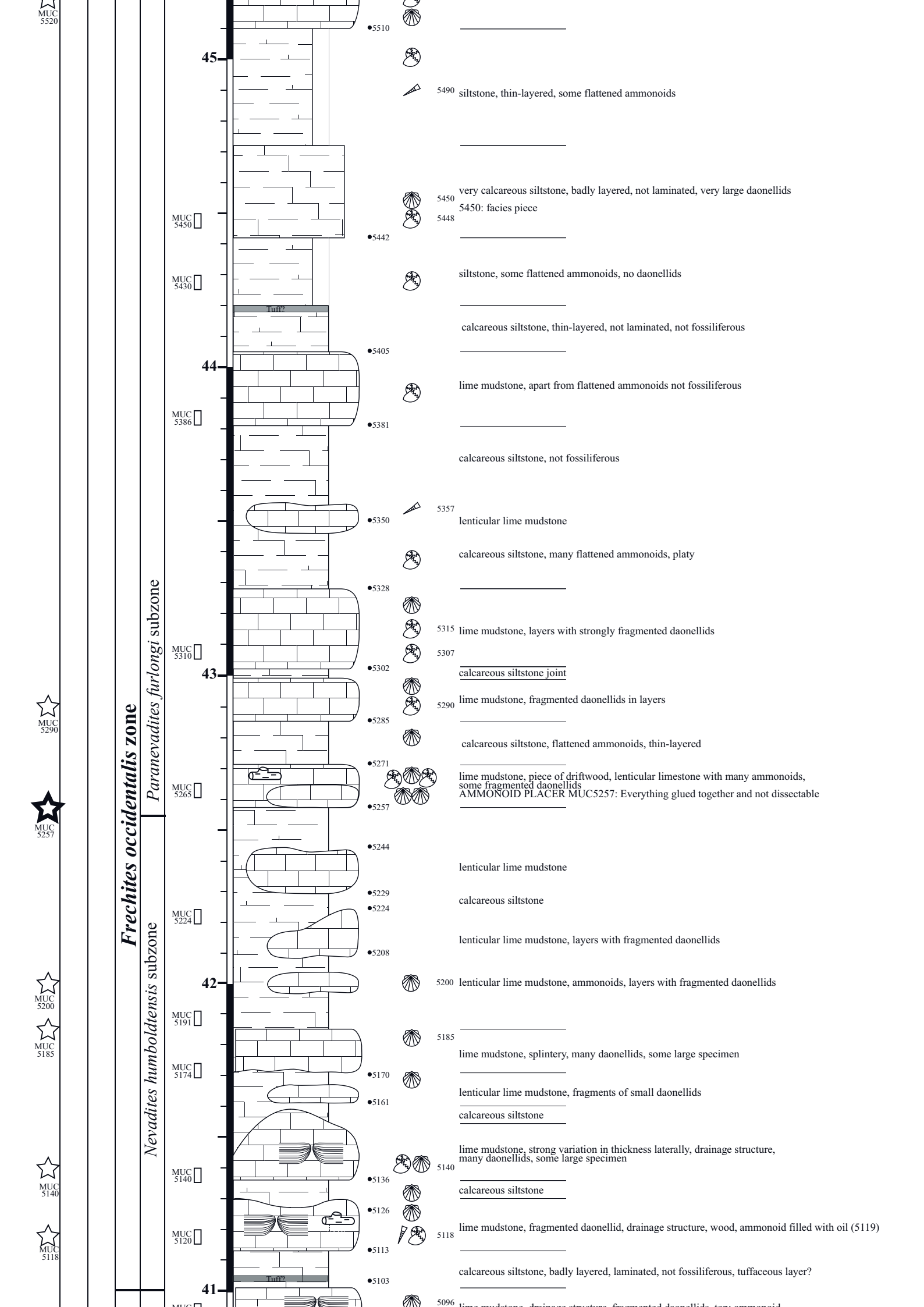
MUC 5520
45
5510
5490
siltstone, thin-layered, some flattened ammonoids
very calcareous siltstone, badly layered, not laminated, very large daonellids
5450
5448
5450: facies piece
MUC 5450
5442
MUC 5430
siltstone, some flattened ammonoids, no daonellids
Tuff?
calcareous siltstone, thin-layered, not laminated, not fossiliferous
5405
44
lime mudstone, apart from flattened ammonoids not fossiliferous
MUC 5386
5381
calcareous siltstone, not fossiliferous
5357
5350
lenticular lime mudstone
calcareous siltstone, many flattened ammonoids, platy
5328
5315
lime mudstone, layers with strongly fragmented daonellids
MUC 5310
5307
5302
calcareous siltstone joint
43
MUC 5290
5290
lime mudstone, fragmented daonellids in layers
5285
calcareous siltstone, flattened ammonoids, thin-layered
5271
MUC 5265
lime mudstone, piece of driftwood, lenticular limestone with many ammonoids, some fragmented daonellids
AMMONOID PLACER MUC5257: Everything glued together and not dissectable
5257
MUC 5257
5244
lenticular lime mudstone
5229
calcareous siltstone
5224
MUC 5224
lenticular lime mudstone, layers with fragmented daonellids
5208
42
MUC 5200
5200
lenticular lime mudstone, ammonoids, layers with fragmented daonellids
MUC 5191
MUC 5185
5185
lime mudstone, splintery, many daonellids, some large specimen
MUC 5174
5170
lenticular lime mudstone, fragments of small daonellids
5161
calcareous siltstone
lime mudstone, strong variation in thickness laterally, drainage structure, many daonellids, some large specimen
MUC 5140
5140
5136
calcareous siltstone
MUC 5140
5126
MUC 5120
5118
lime mudstone, fragmented daonellid, drainage structure, wood, ammonoid filled with oil (5119)
MUC 5118
5113
calcareous siltstone, badly layered, laminated, not fossiliferous, tuffaceous layer?
Tuff?
5103
41
5096
Frechites occidentalis zone
Paranevadites furlongi subzone
Nevadites humboldtensis subzone

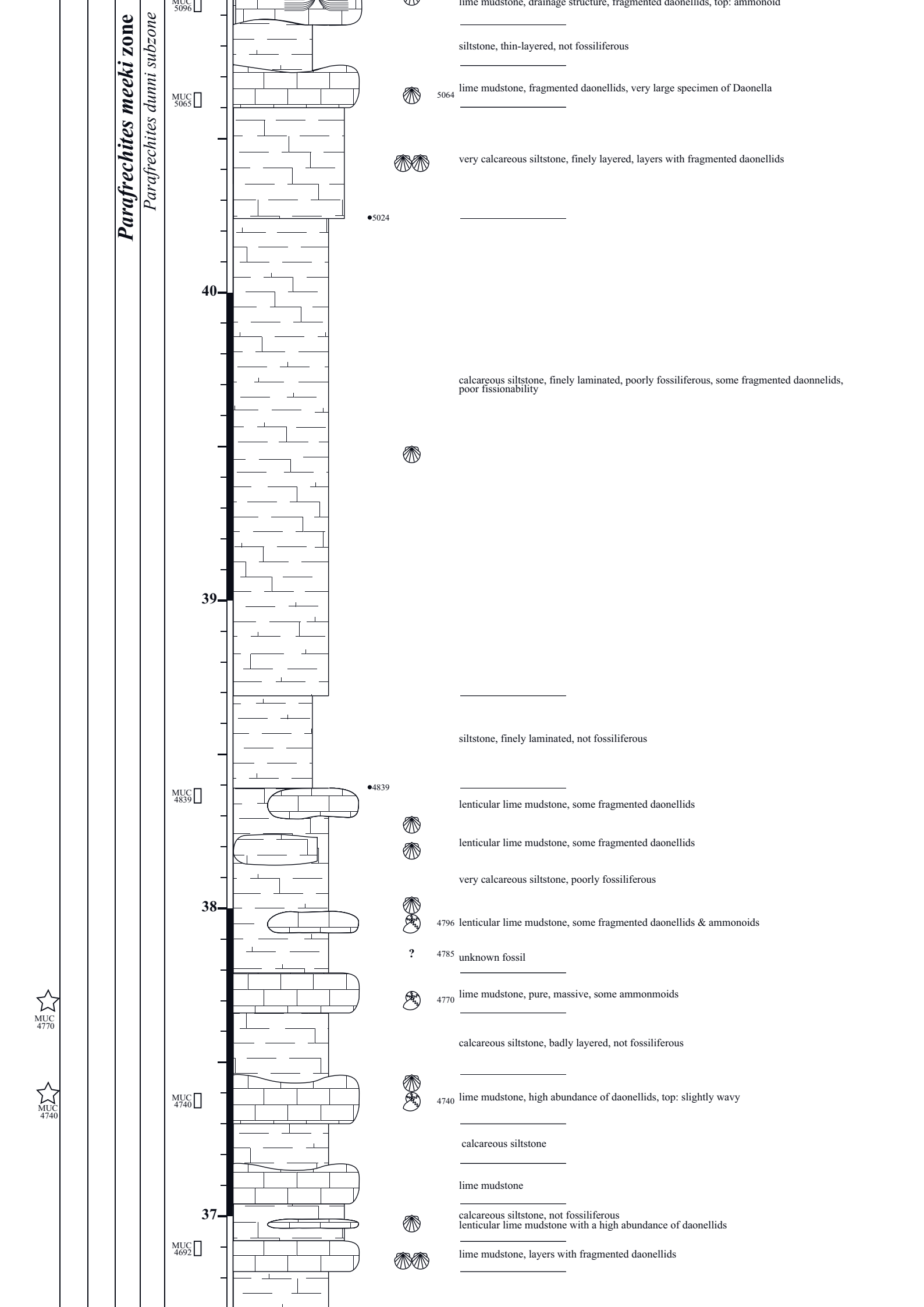
Parafrechites meeki zone
Parafrechites dunni subzone
MUC 5096
lime mudstone, drainage structure, fragmented daonellids, top: ammonoid
siltstone, thin-layered, not fossiliferous
MUC 5065
5064
lime mudstone, fragmented daonellids, very large specimen of Daonella
very calcareous siltstone, finely layered, layers with fragmented daonellids
5024
40
calcareous siltstone, finely laminated, poorly fossiliferous, some fragmented daonnelids, poor fissionability
39
siltstone, finely laminated, not fossiliferous
4839
MUC 4839
lenticular lime mudstone, some fragmented daonellids
lenticular lime mudstone, some fragmented daonellids
very calcareous siltstone, poorly fossiliferous
38
4796
lenticular lime mudstone, some fragmented daonellids & ammonoids
?
4785
unknown fossil
MUC 4770
4770
lime mudstone, pure, massive, some ammonmoids
calcareous siltstone, badly layered, not fossiliferous
MUC 4740
4740
lime mudstone, high abundance of daonellids, top: slightly wavy
calcareous siltstone
lime mudstone
37
calcareous siltstone, not fossiliferous
lenticular lime mudstone with a high abundance of daonellids
MUC 4692
lime mudstone, layers with fragmented daonellids

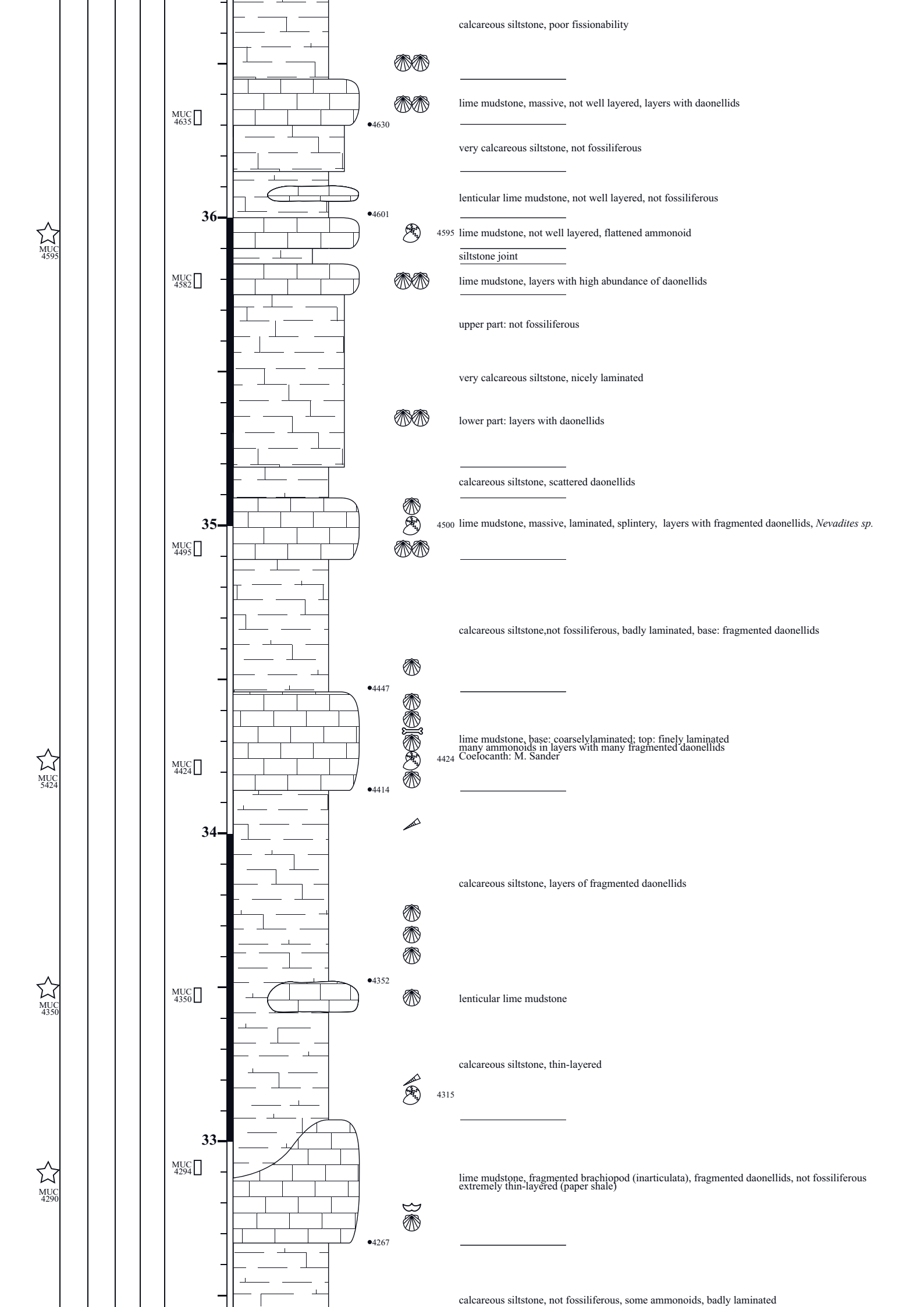
calcareous siltstone, poor fissionability
lime mudstone, massive, not well layered, layers with daonellids
MUC 4635
4630
very calcareous siltstone, not fossiliferous
lenticular lime mudstone, not well layered, not fossiliferous
36
4601
MUC 4595
4595
lime mudstone, not well layered, flattened ammonoid
siltstone joint
MUC 4582
lime mudstone, layers with high abundance of daonellids
upper part: not fossiliferous
very calcareous siltstone, nicely laminated
lower part: layers with daonellids
calcareous siltstone, scattered daonellids
35
4500
lime mudstone, massive, laminated, splintery, layers with fragmented daonellids, Nevadites sp.
MUC 4495
calcareous siltstone,not fossiliferous, badly laminated, base: fragmented daonellids
4447
lime mudstone, base: coarselylaminated; top: finely laminated
many ammonoids in layers with many fragmented daonellids
MUC 4424
4424
Coelocanth: M. Sander
MUC 5424
4414
34
calcareous siltstone, layers of fragmented daonellids
4352
MUC 4350
lenticular lime mudstone
MUC 4350
calcareous siltstone, thin-layered
4315
33
MUC 4294
lime mudstone, fragmented brachiopod (inarticulata), fragmented daonellids, not fossiliferous
extremely thin-layered (paper shale)
MUC 4290
4267
calcareous siltstone, not fossiliferous, some ammonoids, badly laminated

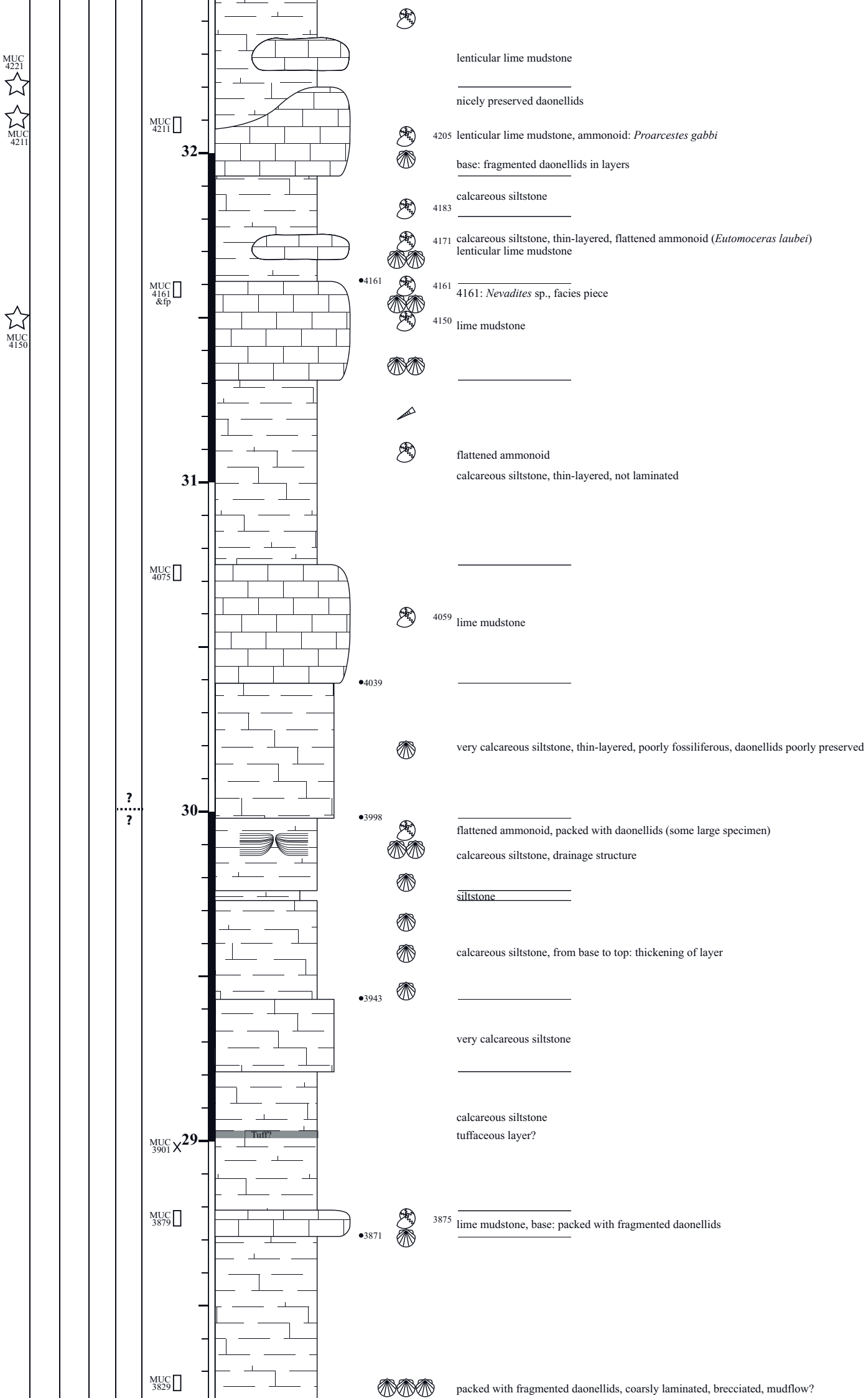
MUC 4221
MUC 4211
MUC 4211
32
MUC 4161 &fp
MUC 4150
31
MUC 4075
?
?
30
MUC 3901
29
MUC 3879
MUC 3829
Tuff?
lenticular lime mudstone
nicely preserved daonellids
4205 lenticular lime mudstone, ammonoid: Proarcestes gabbi
base: fragmented daonellids in layers
calcareous siltstone
4183
4171 calcareous siltstone, thin-layered, flattened ammonoid (Eutomoceras laubei)
lenticular lime mudstone
•4161
4161
4161: Nevadites sp., facies piece
4150 lime mudstone
flattened ammonoid
calcareous siltstone, thin-layered, not laminated
4059 lime mudstone
•4039
very calcareous siltstone, thin-layered, poorly fossiliferous, daonellids poorly preserved
•3998
flattened ammonoid, packed with daonellids (some large specimen)
calcareous siltstone, drainage structure
siltstone
calcareous siltstone, from base to top: thickening of layer
•3943
very calcareous siltstone
calcareous siltstone
tuffaceous layer?
3875 lime mudstone, base: packed with fragmented daonellids
•3871
packed with fragmented daonellids, coarsly laminated, brecciated, mudflow?

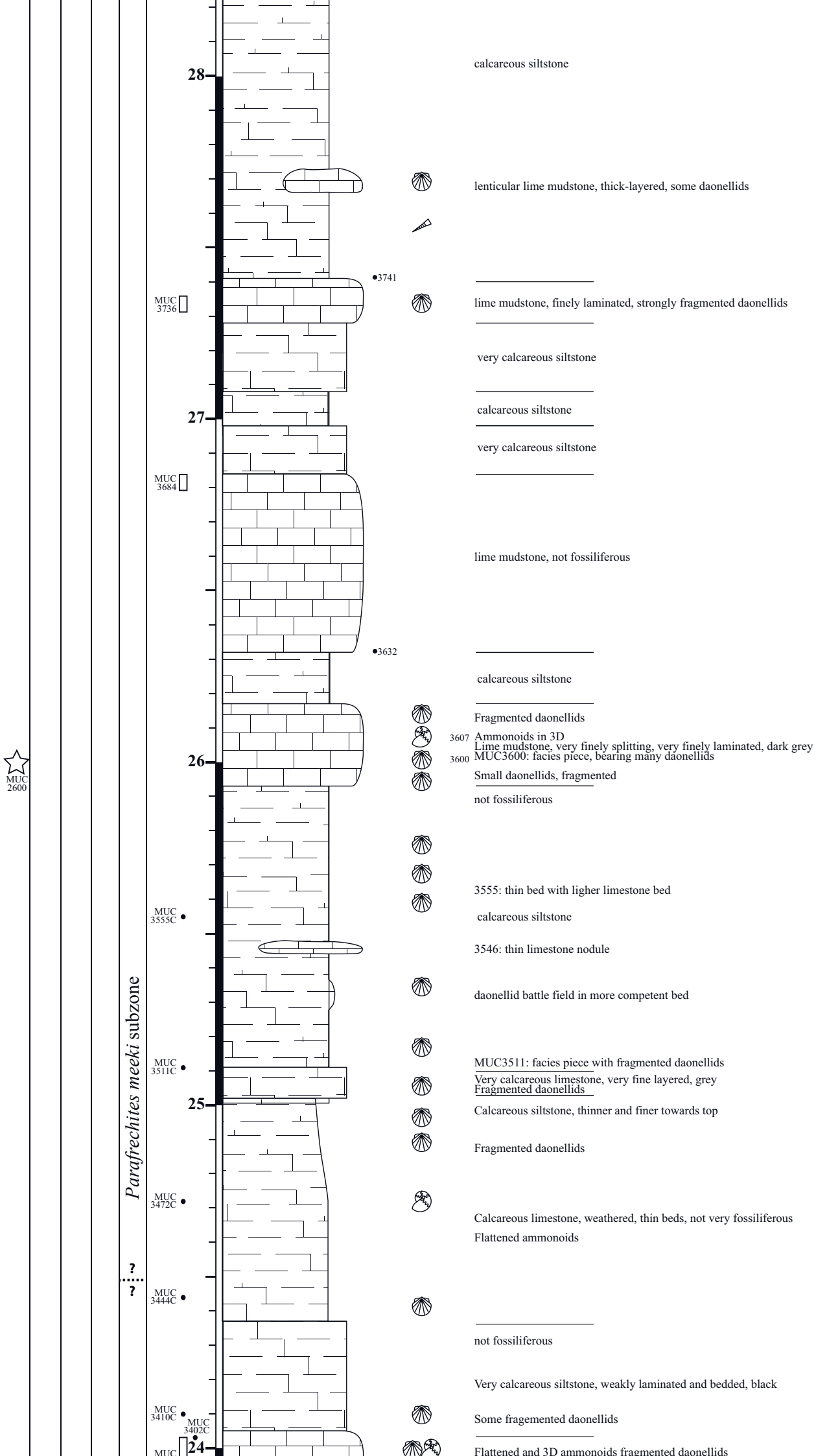
28
27
26
25
24
MUC 2600
MUC 3736
MUC 3684
MUC 3555C
MUC 3511C
MUC 3472C
MUC 3444C
MUC 3410C
MUC 3402C
MUC
●3741
●3632
Parafrechites meeki subzone
?
?
calcareous siltstone
lenticular lime mudstone, thick-layered, some daonellids
lime mudstone, finely laminated, strongly fragmented daonellids
very calcareous siltstone
calcareous siltstone
very calcareous siltstone
lime mudstone, not fossiliferous
calcareous siltstone
Fragmented daonellids
3607 Ammonoids in 3D
Lime mudstone, very finely splitting, very finely laminated, dark grey
3600 MUC3600: facies piece, bearing many daonellids
Small daonellids, fragmented
not fossiliferous
3555: thin bed with ligher limestone bed
calcareous siltstone
3546: thin limestone nodule
daonellid battle field in more competent bed
MUC3511: facies piece with fragmented daonellids
Very calcareous limestone, very fine layered, grey
Fragmented daonellids
Calcareous siltstone, thinner and finer towards top
Fragmented daonellids
Calcareous limestone, weathered, thin beds, not very fossiliferous
Flattened ammonoids
not fossiliferous
Very calcareous siltstone, weakly laminated and bedded, black
Some fragemented daonellids
Flattened and 3D ammonoids fragmented daonellids

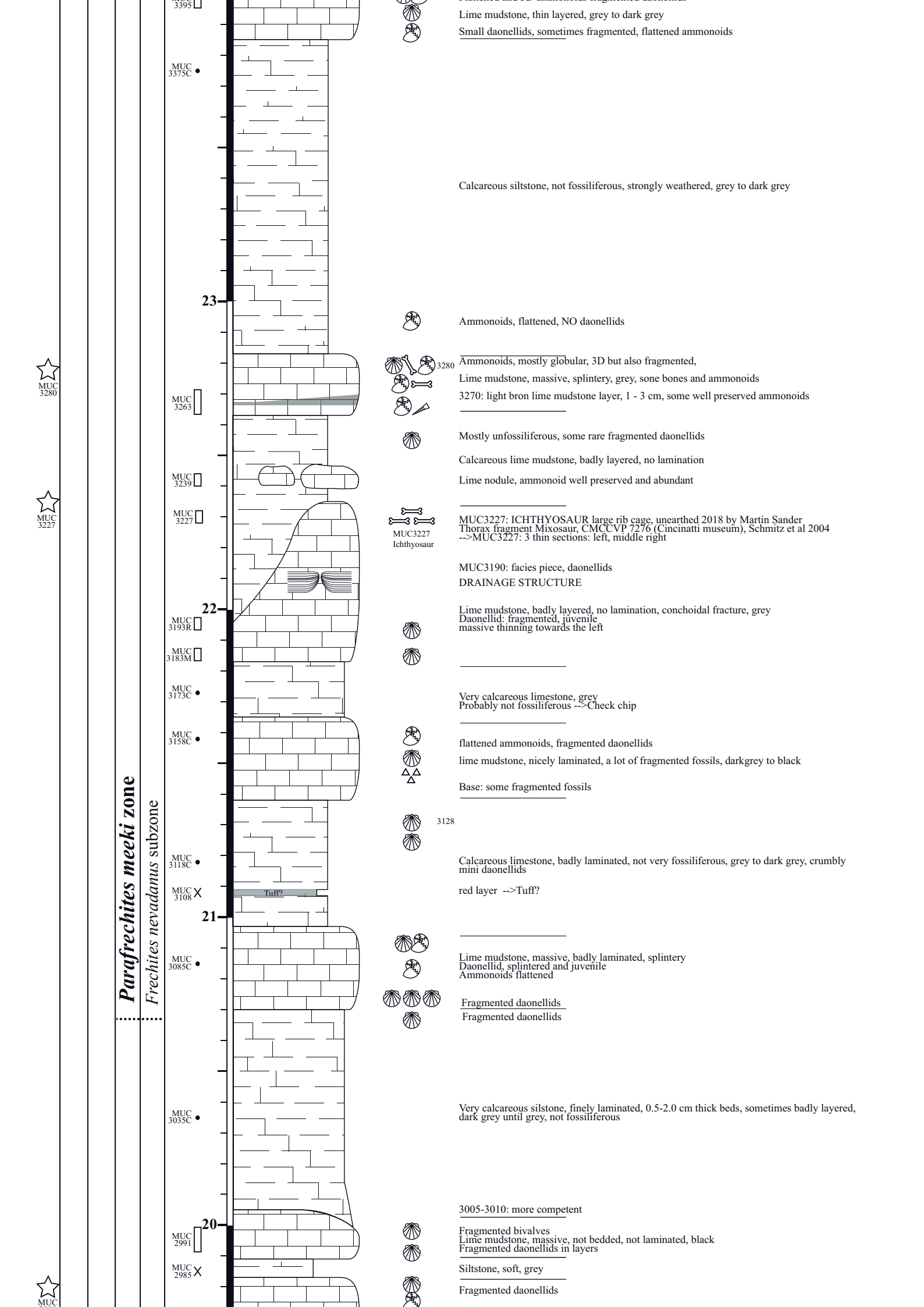
Parafrechites meeki zone
Frechites nevadanus subzone
MUC 3395
MUC 3375C
Lime mudstone, thin layered, grey to dark grey
Small daonellids, sometimes fragmented, flattened ammonoids
Calcareous siltstone, not fossiliferous, strongly weathered, grey to dark grey
23
Ammonoids, flattened, NO daonellids
MUC 3280
MUC 3263
3280
Ammonoids, mostly globular, 3D but also fragmented,
Lime mudstone, massive, splintery, grey, sone bones and ammonoids
3270: light bron lime mudstone layer, 1 - 3 cm, some well preserved ammonoids
Mostly unfossiliferous, some rare fragmented daonellids
Calcareous lime mudstone, badly layered, no lamination
MUC 3239
Lime nodule, ammonoid well preserved and abundant
MUC 3227
MUC3227
Ichthyosaur
MUC3227: ICHTHYOSAUR large rib cage, unearthed 2018 by Martin Sander
Thorax fragment Mixosaur, CMCCVP 7276 (Cincinatti museum), Schmitz et al 2004
-->MUC3227: 3 thin sections: left, middle right
MUC3190: facies piece, daonellids
DRAINAGE STRUCTURE
22
Lime mudstone, badly layered, no lamination, conchoidal fracture, grey
Daonellid: fragmented, juvenile
massive thinning towards the left
MUC 3193R
MUC 3183M
MUC 3173C
Very calcareous limestone, grey
Probably not fossiliferous -->Check chip
MUC 3158C
flattened ammonoids, fragmented daonellids
lime mudstone, nicely laminated, a lot of fragmented fossils, darkgrey to black
Base: some fragmented fossils
3128
MUC 3118C
Calcareous limestone, badly laminated, not very fossiliferous, grey to dark grey, crumbly
mini daonellids
MUC 3108
Tuff?
red layer -->Tuff?
21
MUC 3085C
Lime mudstone, massive, badly laminated, splintery
Daonellid, splintered and juvenile
Ammonoids flattened
Fragmented daonellids
Fragmented daonellids
MUC 3035C
Very calcareous silstone, finely laminated, 0.5-2.0 cm thick beds, sometimes badly layered,
dark grey until grey, not fossiliferous
3005-3010: more competent
20
MUC 2991
Fragmented bivalves
Lime mudstone, massive, not bedded, not laminated, black
Fragmented daonellids in layers
MUC 2985
Siltstone, soft, grey
Fragmented daonellids
MUC

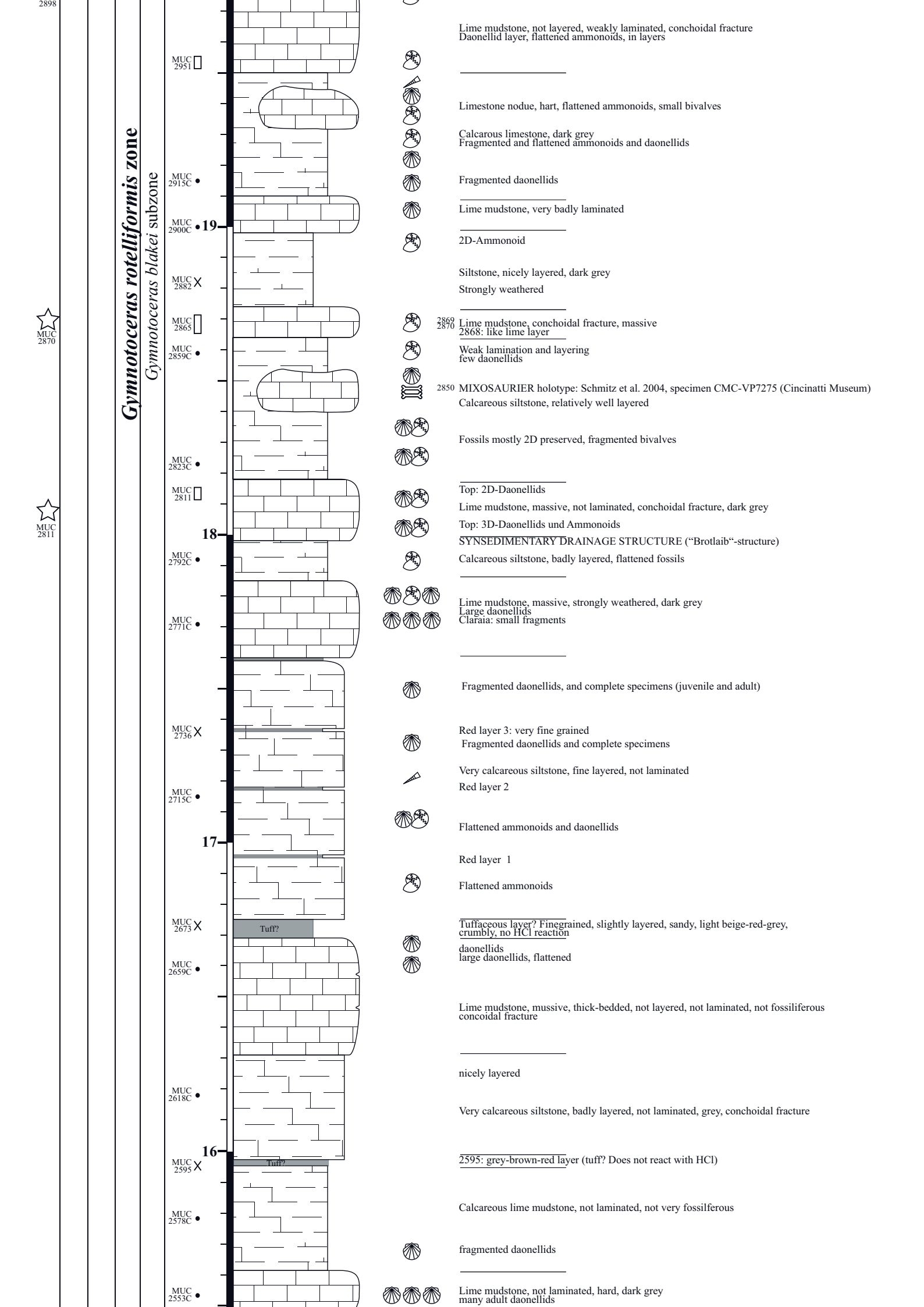
2898
Gymnotoceras rotelliformis zone
Gymnotoceras blakei subzone
MUC 2951
MUC 2915C
MUC 2900C
19
MUC 2882
MUC 2865
MUC 2870
MUC 2859C
MUC 2823C
MUC 2811
MUC 2811
18
MUC 2792C
MUC 2771C
MUC 2736
MUC 2715C
17
MUC 2673
Tuff?
MUC 2659C
MUC 2618C
16
MUC 2595
Tuff?
MUC 2578C
MUC 2553C
Lime mudstone, not layered, weakly laminated, conchoidal fracture
Daonellid layer, flattened ammonoids, in layers
Limestone nodue, hart, flattened ammonoids, small bivalves
Calcarous limestone, dark grey
Fragmented and flattened ammonoids and daonellids
Fragmented daonellids
Lime mudstone, very badly laminated
2D-Ammonoid
Siltstone, nicely layered, dark grey
Strongly weathered
2869
2870
Lime mudstone, conchoidal fracture, massive
2868: like lime layer
Weak lamination and layering
few daonellids
2850
MIXOSAURIER holotype: Schmitz et al. 2004, specimen CMC-VP7275 (Cincinatti Museum)
Calcareous siltstone, relatively well layered
Fossils mostly 2D preserved, fragmented bivalves
Top: 2D-Daonellids
Lime mudstone, massive, not laminated, conchoidal fracture, dark grey
Top: 3D-Daonellids und Ammonoids
SYNSEDIMENTARY DRAINAGE STRUCTURE (“Brotlaib“-structure)
Calcareous siltstone, badly layered, flattened fossils
Lime mudstone, massive, strongly weathered, dark grey
Large daonellids
Claraia: small fragments
Fragmented daonellids, and complete specimens (juvenile and adult)
Red layer 3: very fine grained
Fragmented daonellids and complete specimens
Very calcareous siltstone, fine layered, not laminated
Red layer 2
Flattened ammonoids and daonellids
Red layer 1
Flattened ammonoids
Tuffaceous layer? Finegrained, slightly layered, sandy, light beige-red-grey,
crumbly, no HCl reaction
daonellids
large daonellids, flattened
Lime mudstone, mussive, thick-bedded, not layered, not laminated, not fossiliferous
concoidal fracture
nicely layered
Very calcareous siltstone, badly layered, not laminated, grey, conchoidal fracture
2595: grey-brown-red layer (tuff? Does not react with HCl)
Calcareous lime mudstone, not laminated, not very fossilferous
fragmented daonellids
Lime mudstone, not laminated, hard, dark grey
many adult daonellids

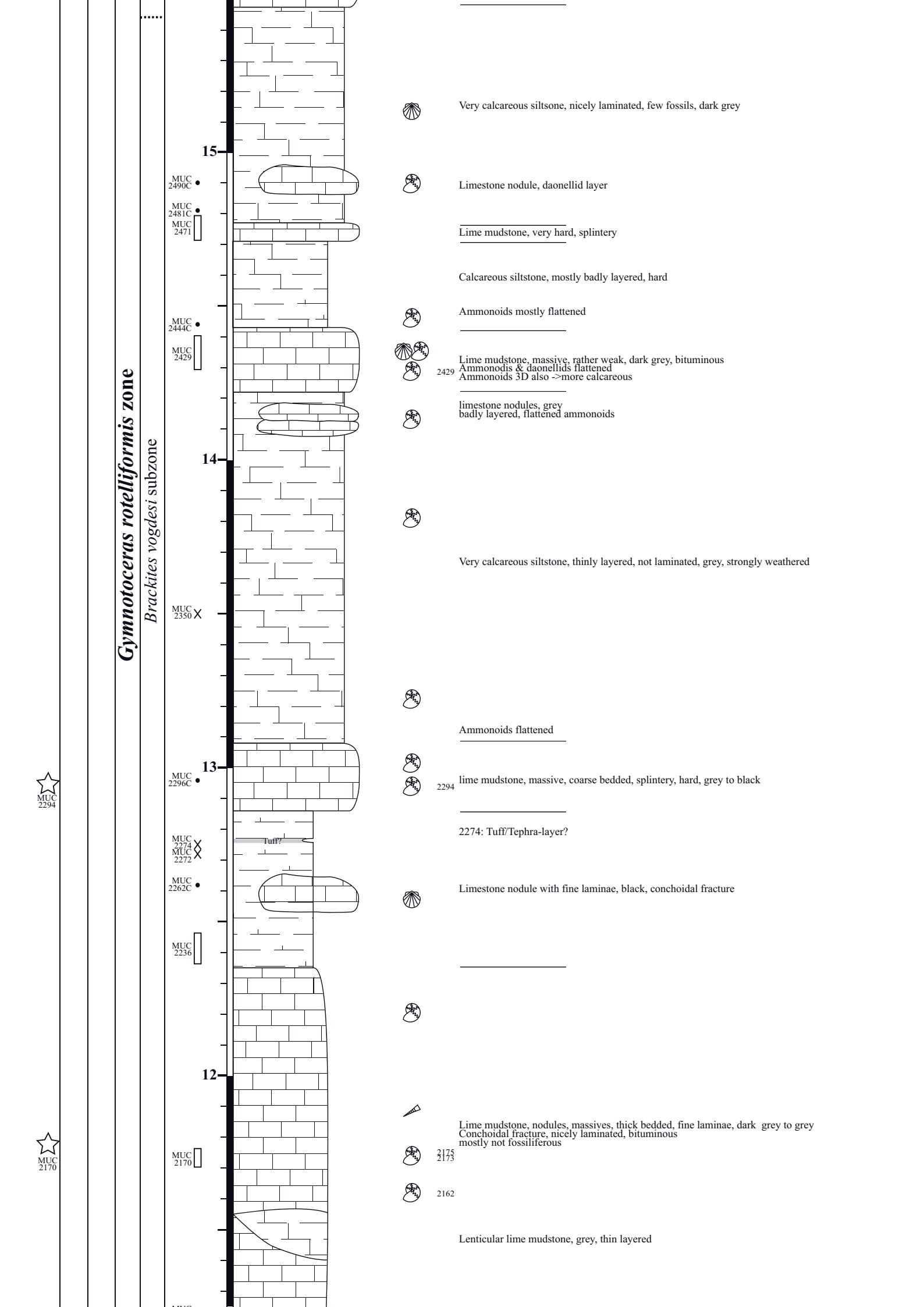
Gymnotoceras rotelliformis zone
Brackites vogdesi subzone
15
14
13
12
MUC 2490C
MUC 2481C
MUC 2471
MUC 2444C
MUC 2429
MUC 2350
MUC 2296C
MUC 2294
MUC 2274
MUC 2272
Tuff?
MUC 2262C
MUC 2236
MUC 2170
2429
2294
2175
2173
2162
Very calcareous siltsone, nicely laminated, few fossils, dark grey
Limestone nodule, daonellid layer
Lime mudstone, very hard, splintery
Calcareous siltstone, mostly badly layered, hard
Ammonoids mostly flattened
Lime mudstone, massive, rather weak, dark grey, bituminous
Ammonodis & daonellids flattened
Ammonoids 3D also ->more calcareous
limestone nodules, grey
badly layered, flattened ammonoids
Very calcareous siltstone, thinly layered, not laminated, grey, strongly weathered
Ammonoids flattened
lime mudstone, massive, coarse bedded, splintery, hard, grey to black
2274: Tuff/Tephra-layer?
Limestone nodule with fine laminae, black, conchoidal fracture
Lime mudstone, nodules, massives, thick bedded, fine laminae, dark grey to grey
Conchoidal fracture, nicely laminated, bituminous
mostly not fossiliferous
Lenticular lime mudstone, grey, thin layered

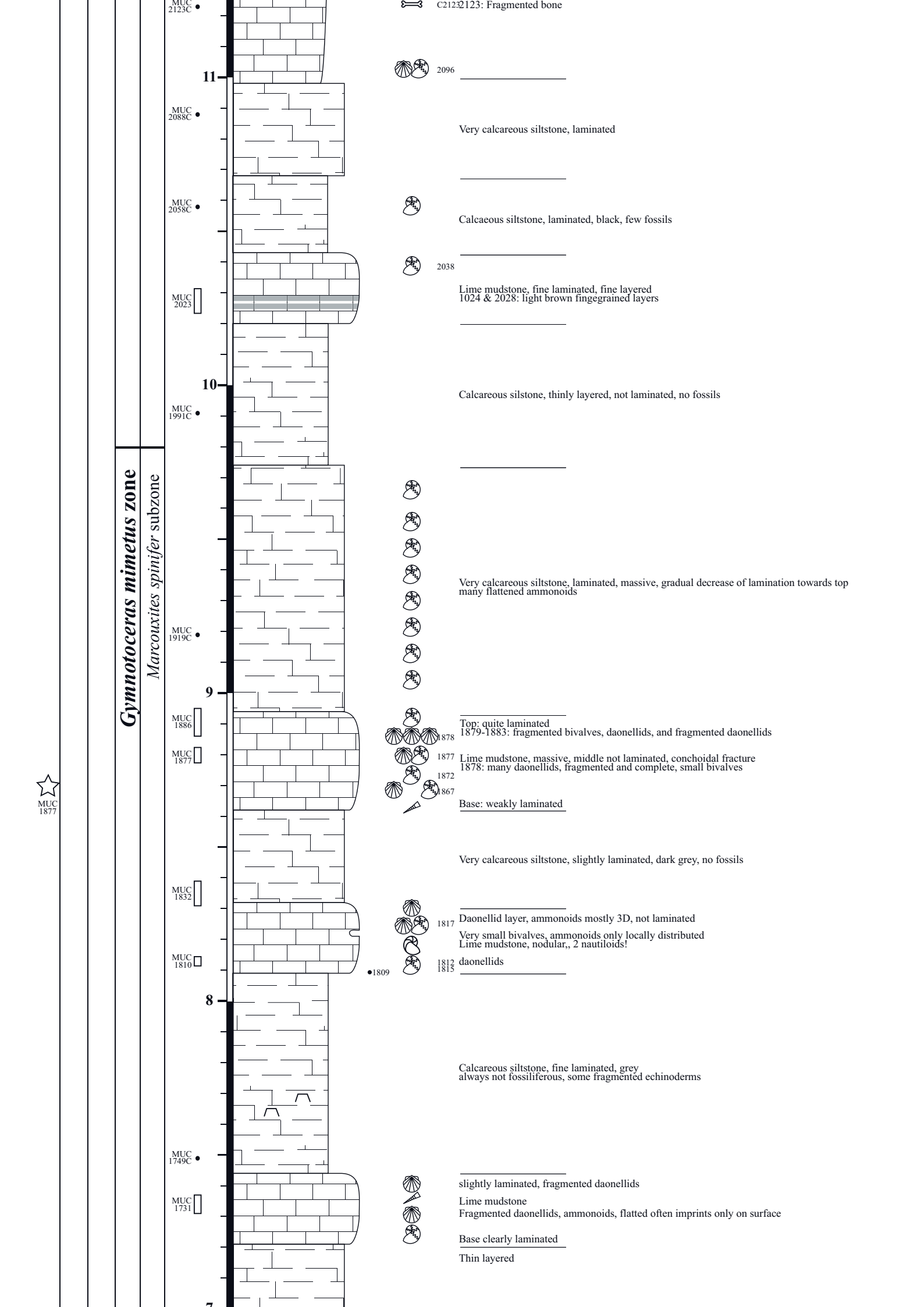
Gymnotoceras mimetus zone
Marcouxites spinifer subzone
MUC 2123C
MUC 2088C
MUC 2058C
MUC 2023
MUC 1991C
MUC 1919C
MUC 1886
MUC 1877
MUC 1832
MUC 1810
MUC 1749C
MUC 1731
MUC 1877
11
10
9
8
7
C2123
2123: Fragmented bone
2096
Very calcareous siltstone, laminated
Calcaeous siltstone, laminated, black, few fossils
2038
Lime mudstone, fine laminated, fine layered
1024 & 2028: light brown fingegrained layers
Calcareous silstone, thinly layered, not laminated, no fossils
Very calcareous siltstone, laminated, massive, gradual decrease of lamination towards top
many flattened ammonoids
Top: quite laminated
1879-1883: fragmented bivalves, daonellids, and fragmented daonellids
1878
1877
Lime mudstone, massive, middle not laminated, conchoidal fracture
1878: many daonellids, fragmented and complete, small bivalves
1872
1867
Base: weakly laminated
Very calcareous siltstone, slightly laminated, dark grey, no fossils
1817
Daonellid layer, ammonoids mostly 3D, not laminated
Very small bivalves, ammonoids only locally distributed
Lime mudstone, nodular,, 2 nautiloids!
1812
1815
daonellids
1809
Calcareous siltstone, fine laminated, grey
always not fossiliferous, some fragmented echinoderms
slightly laminated, fragmented daonellids
Lime mudstone
Fragmented daonellids, ammonoids, flatted often imprints only on surface
Base clearly laminated
Thin layered

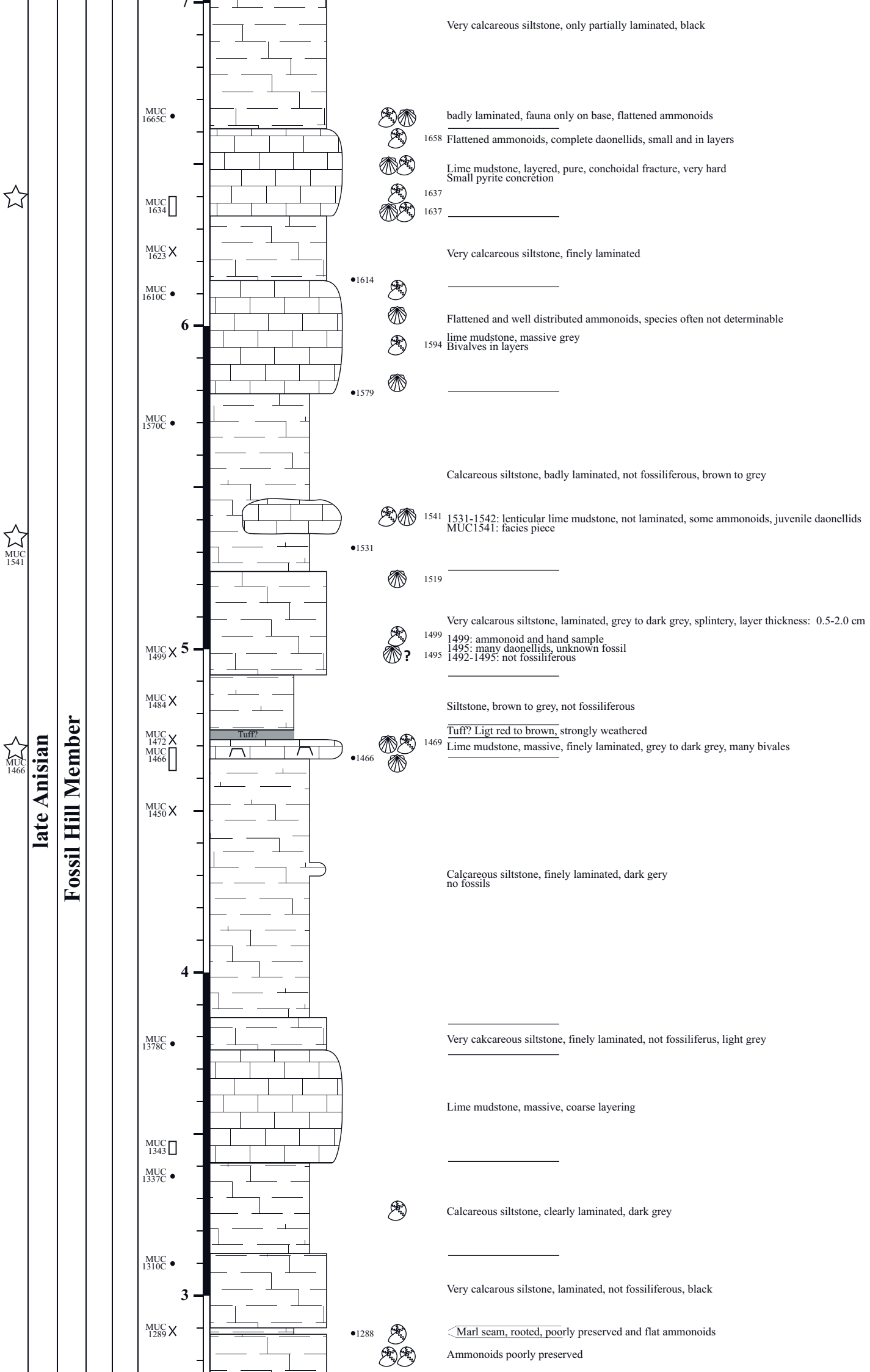
late Anisian
Fossil Hill Member
MUC 1466
MUC 1541
7
6
5
4
3
MUC 1665C
MUC 1634
MUC 1623
MUC 1610C
MUC 1570C
MUC 1499
MUC 1484
MUC 1472
MUC 1466
MUC 1450
MUC 1378C
MUC 1343
MUC 1337C
MUC 1310C
MUC 1289
Tuff?
1658
1637
1637
1614
1594
1579
1541
1531
1519
1499
1495
1469
1466
1288
?
Very calcareous siltstone, only partially laminated, black
badly laminated, fauna only on base, flattened ammonoids
Flattened ammonoids, complete daonellids, small and in layers
Lime mudstone, layered, pure, conchoidal fracture, very hard
Small pyrite concretion
Very calcareous siltstone, finely laminated
Flattened and well distributed ammonoids, species often not determinable
lime mudstone, massive grey
Bivalves in layers
Calcareous siltstone, badly laminated, not fossiliferous, brown to grey
1531-1542: lenticular lime mudstone, not laminated, some ammonoids, juvenile daonellids
MUC1541: facies piece
Very calcarous siltstone, laminated, grey to dark grey, splintery, layer thickness: 0.5-2.0 cm
1499: ammonoid and hand sample
1495: many daonellids, unknown fossil
1492-1495: not fossiliferous
Siltstone, brown to grey, not fossiliferous
Tuff? Ligt red to brown, strongly weathered
Lime mudstone, massive, finely laminated, grey to dark grey, many bivales
Calcareous siltstone, finely laminated, dark gery
no fossils
Very cakcareous siltstone, finely laminated, not fossiliferus, light grey
Lime mudstone, massive, coarse layering
Calcareous siltstone, clearly laminated, dark grey
Very calcarous silstone, laminated, not fossiliferous, black
Marl seam, rooted, poorly preserved and flat ammonoids
Ammonoids poorly preserved

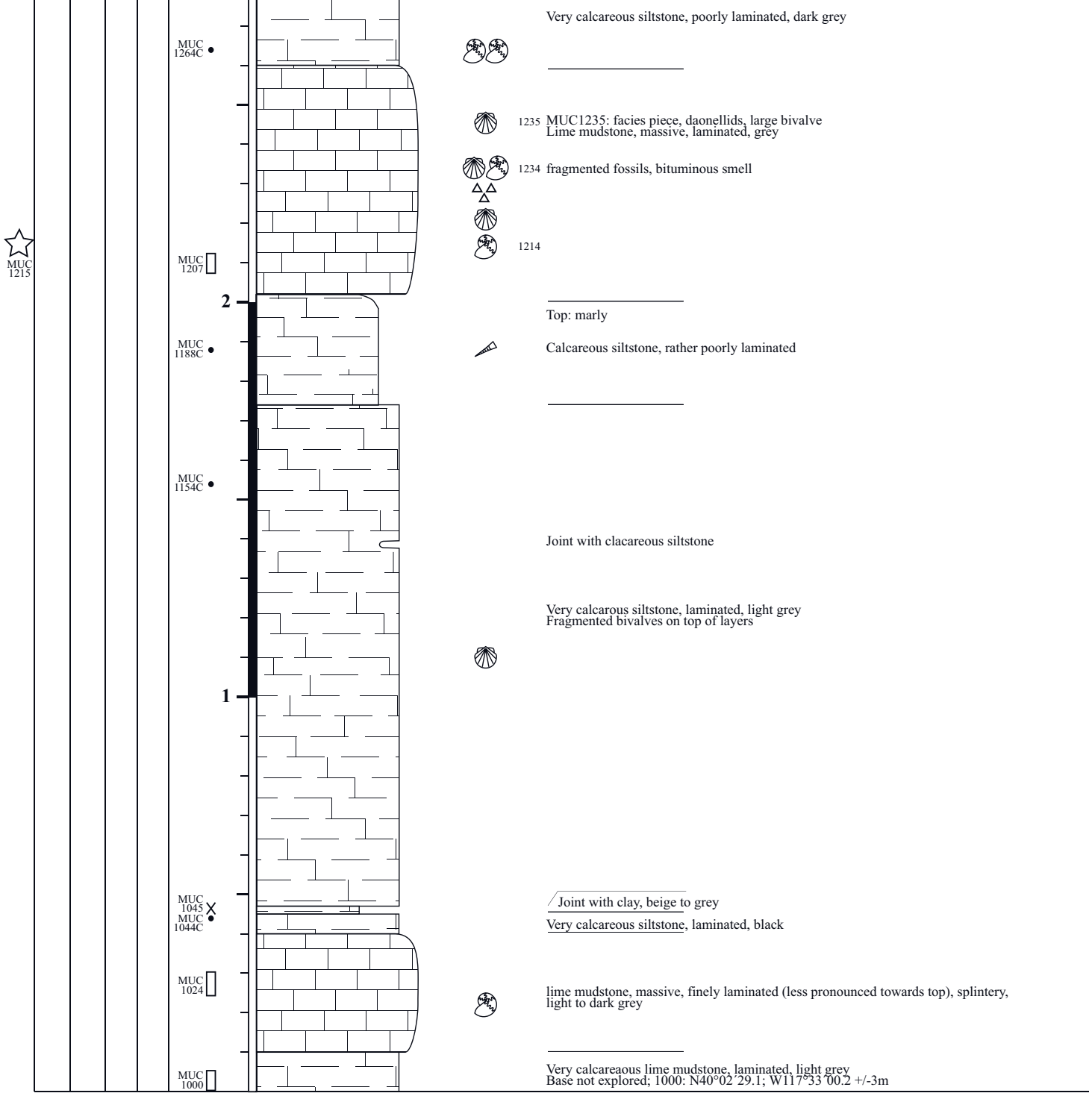
Very calcareous siltstone, poorly laminated, dark grey
MUC 1264C
1235
MUC1235: facies piece, daonellids, large bivalve
Lime mudstone, massive, laminated, grey
1234
fragmented fossils, bituminous smell
1214
MUC 1215
MUC 1207
2
Top: marly
MUC 1188C
Calcareous siltstone, rather poorly laminated
MUC 1154C
Joint with clacareous siltstone
Very calcarous siltstone, laminated, light grey
Fragmented bivalves on top of layers
1
MUC 1045
MUC 1044C
Joint with clay, beige to grey
Very calcareous siltstone, laminated, black
MUC 1024
lime mudstone, massive, finely laminated (less pronounced towards top), splintery,
light to dark grey
MUC 1000
Very calcareaous lime mudstone, laminated, light grey
Base not explored; 1000: N40°02´29.1; W117°33´00.2 +/-3m
stage
member
zone
subzone
samples
scale [m]
spikes
fossils

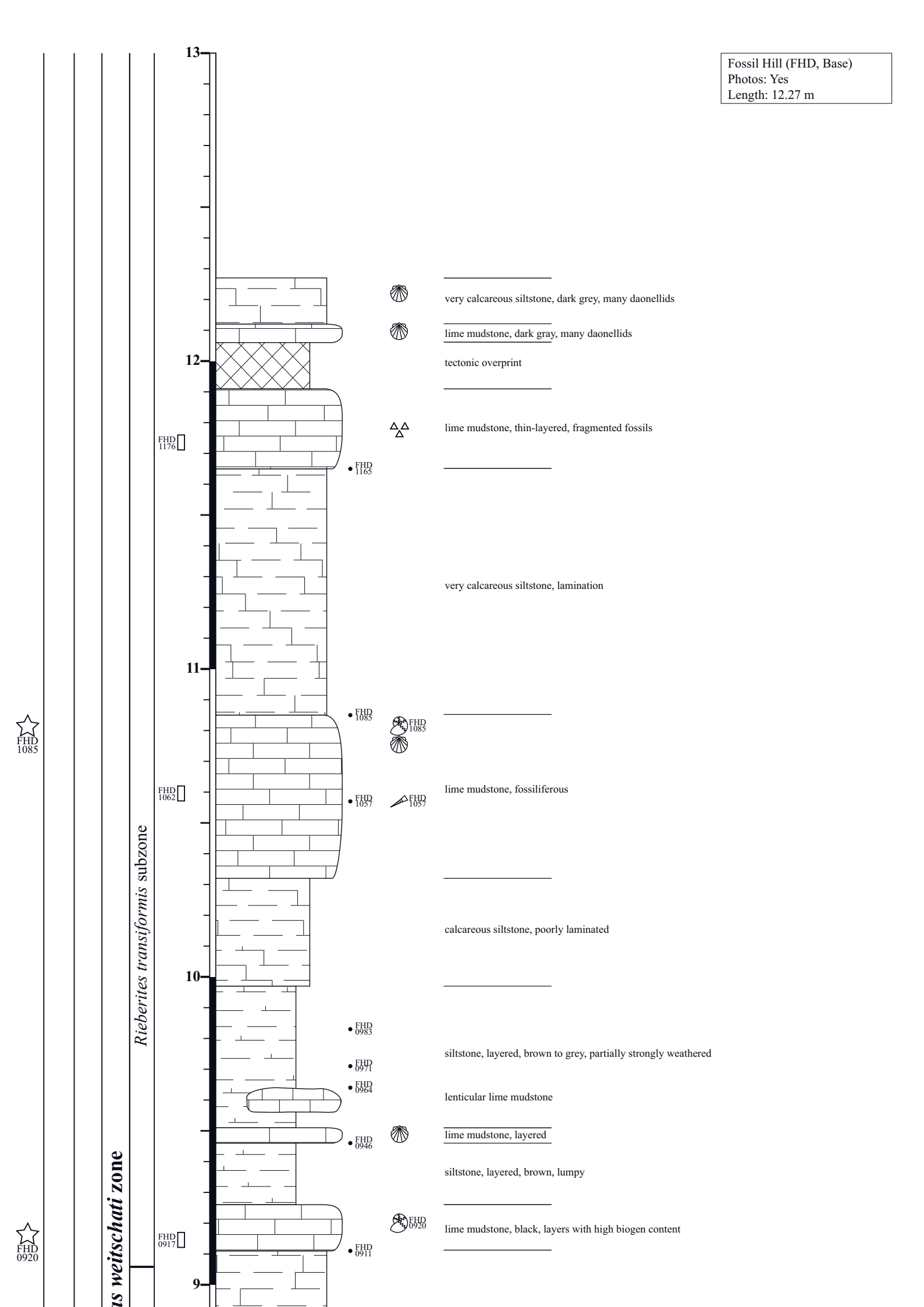
Fossil Hill (FHD, Base)
Photos: Yes
Length: 12.27 m
13
12
11
10
9
FHD 1176
FHD 1165
FHD 1085
FHD 1062
FHD 1057
FHD 0983
FHD 0971
FHD 0964
FHD 0946
FHD 0917
FHD 0911
FHD 1085
FHD 1085
FHD 1057
FHD 0920
very calcareous siltstone, dark grey, many daonellids
lime mudstone, dark gray, many daonellids
tectonic overprint
lime mudstone, thin-layered, fragmented fossils
very calcareous siltstone, lamination
lime mudstone, fossiliferous
calcareous siltstone, poorly laminated
siltstone, layered, brown to grey, partially strongly weathered
lenticular lime mudstone
lime mudstone, layered
siltstone, layered, brown, lumpy
lime mudstone, black, layers with high biogen content
Rieberites transiformis subzone
Daonella weitschati zone
FHD 1085
FHD 0920

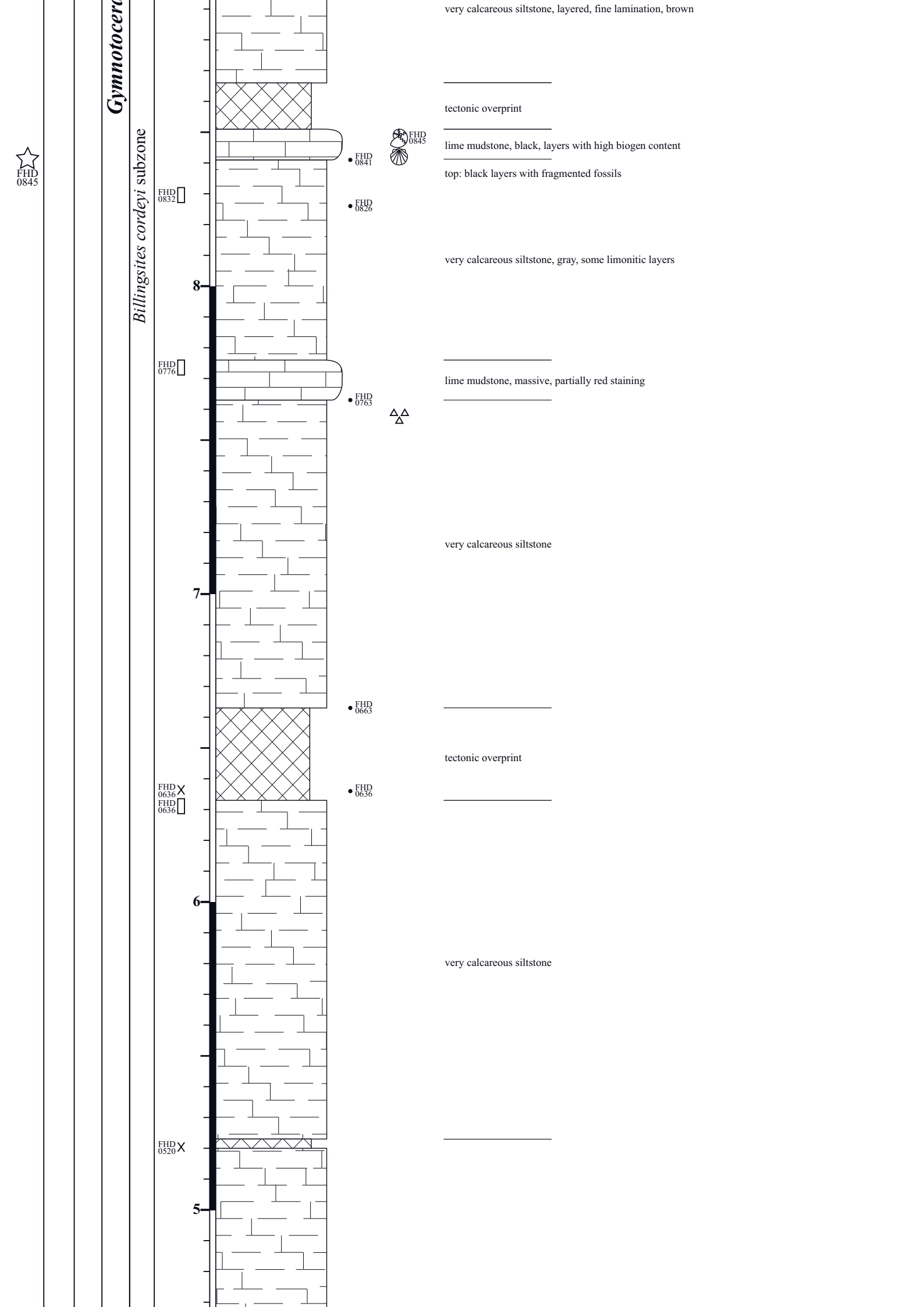
Gymnotoceras
Billingsites cordeyi subzone
FHD 0845
very calcareous siltstone, layered, fine lamination, brown
tectonic overprint
FHD 0845
lime mudstone, black, layers with high biogen content
FHD 0841
top: black layers with fragmented fossils
FHD 0832
FHD 0826
very calcareous siltstone, gray, some limonitic layers
8
FHD 0776
lime mudstone, massive, partially red staining
FHD 0763
very calcareous siltstone
7
FHD 0663
tectonic overprint
FHD 0636
FHD 0636
FHD 0636
6
very calcareous siltstone
FHD 0520
5

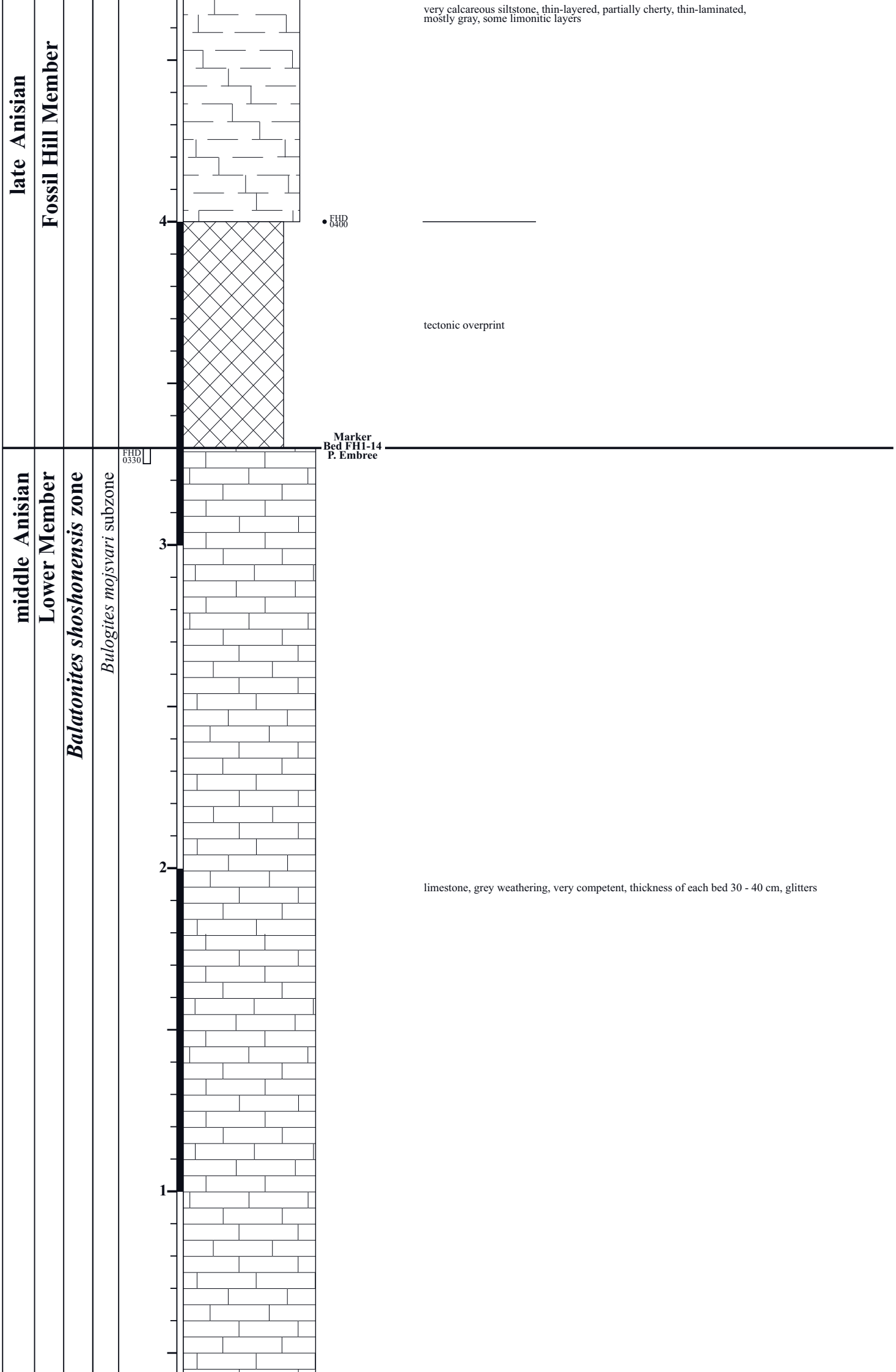
late Anisian
Fossil Hill Member
middle Anisian
Lower Member
Balatonites shoshonensis zone
Bulogites mojsvari subzone
very calcareous siltstone, thin-layered, partially cherty, thin-laminated, mostly gray, some limonitic layers
FHD 0400
tectonic overprint
Marker Bed FH1-14 P. Embree
FHD 0330
limestone, grey weathering, very competent, thickness of each bed 30 - 40 cm, glitters
4
3
2
1

FHD
0040
stage
member
zone
subzone
samples
scale [m]
spikes
fossils

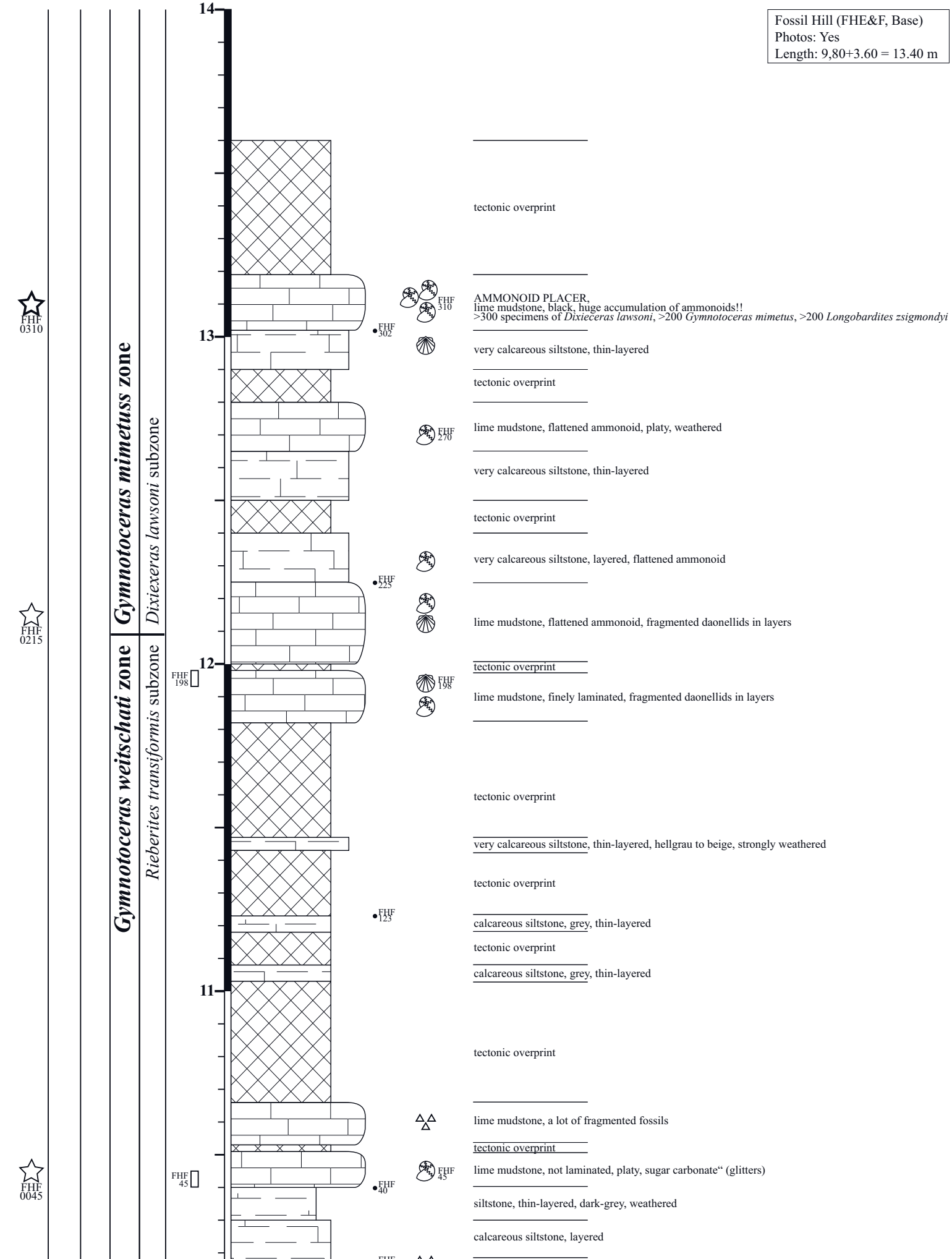
Fossil Hill (FHE&F, Base)
Photos: Yes
Length: 9,80+3.60 = 13.40 m
Gymnotoceras mimetuss zone
Dixiexeras lawsoni subzone
Gymnotoceras weitschati zone
Rieberites transiformis subzone
14
13
12
11
FHF 0310
FHF 0215
FHF 0045
FHF 302
FHF 310
FHF 270
FHF 225
FHF 198
FHF 123
FHF 45
FHF 40
AMMONOID PLACER,
lime mudstone, black, huge accumulation of ammonoids!!
>300 specimens of Dixieceras lawsoni, >200 Gymnotoceras mimetus, >200 Longobardites zsigmondyi
very calcareous siltstone, thin-layered
tectonic overprint
lime mudstone, flattened ammonoid, platy, weathered
very calcareous siltstone, thin-layered
tectonic overprint
very calcareous siltstone, layered, flattened ammonoid
lime mudstone, flattened ammonoid, fragmented daonellids in layers
tectonic overprint
lime mudstone, finely laminated, fragmented daonellids in layers
tectonic overprint
very calcareous siltstone, thin-layered, hellgrau to beige, strongly weathered
tectonic overprint
calcareous siltstone, grey, thin-layered
tectonic overprint
calcareous siltstone, grey, thin-layered
tectonic overprint
lime mudstone, a lot of fragmented fossils
tectonic overprint
lime mudstone, not laminated, platy, sugar carbonate“ (glitters)
siltstone, thin-layered, dark-grey, weathered
calcareous siltstone, layered

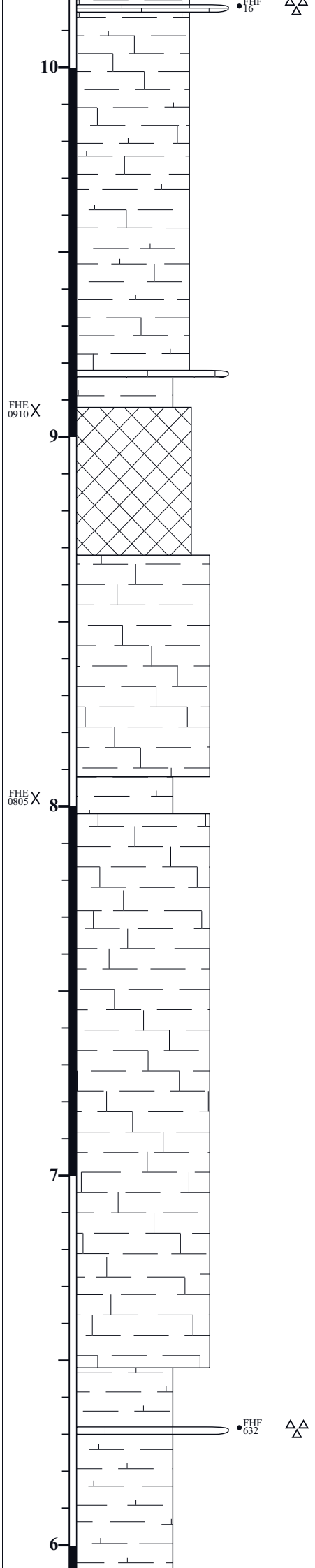
FHF 16
10
calcareous siltstone, layered
lime mudstone, SAND?
siltstone, dark-grey to black, SAND?
FHE 0910
9
tectonic overprint
very calcareous siltstone, layered
siltstone, dark-grey to black, SAND?
FHE 0805
8
very calcareous siltstone, layered, partially weathered
7
siltstone, thin-layered, not fossiliferous
FHF 632
lime mudstone, fragmented fossils
6

FHE 475

late Anisian

Fossil Hill Member

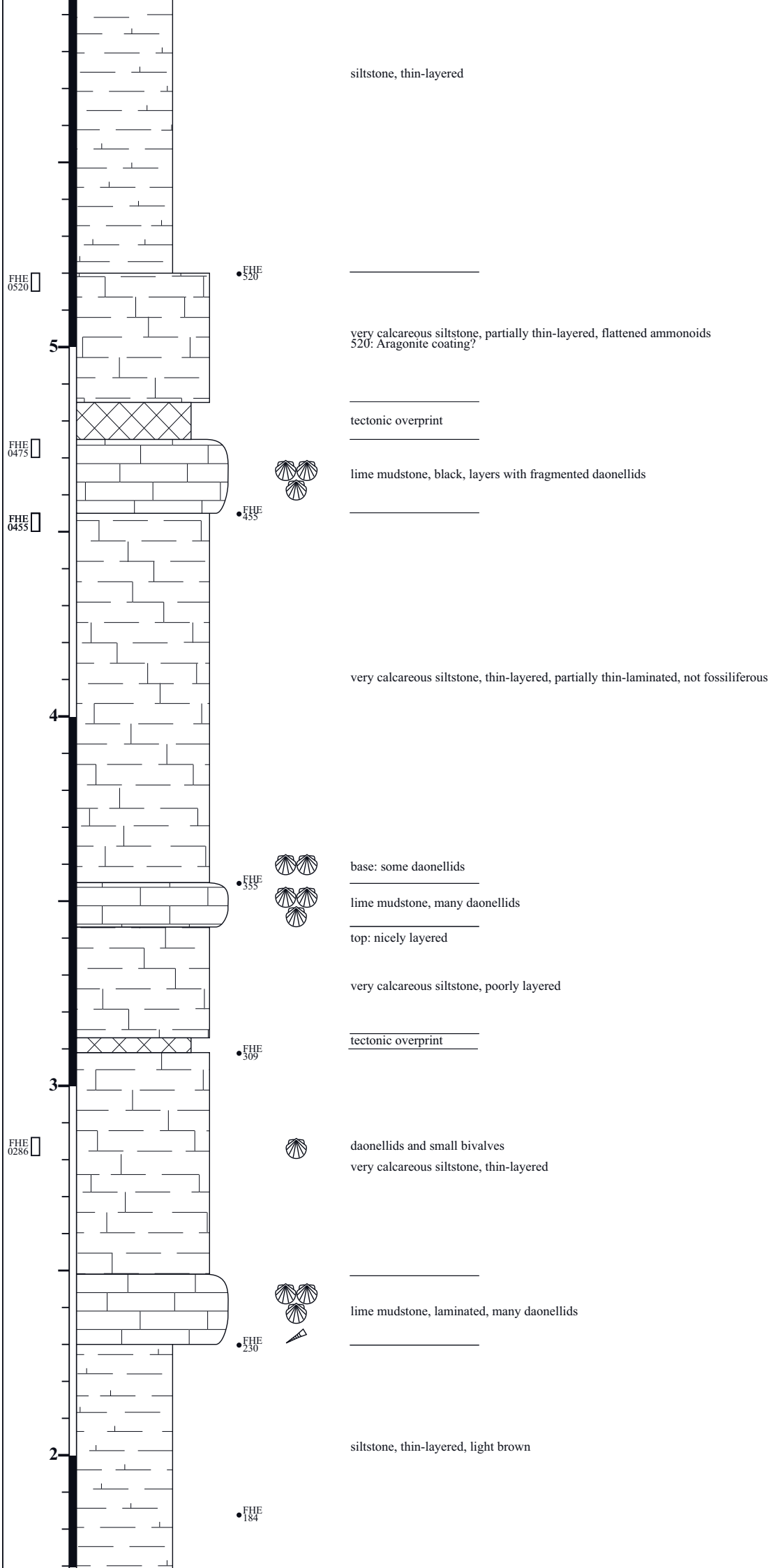

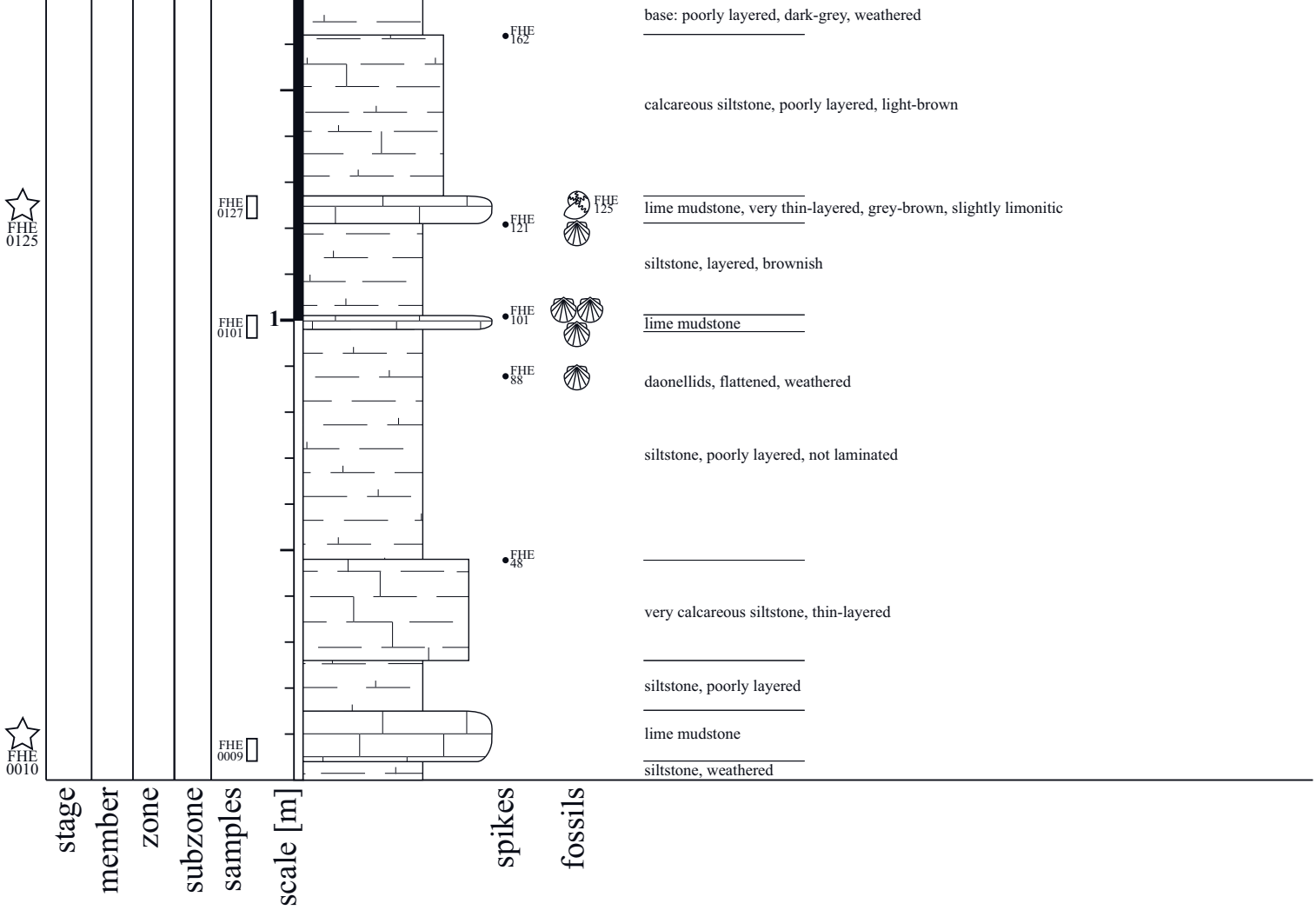
FHE 0125
FHE 0010
FHE 0127
FHE 0101
FHE 0009
1
FHE 162
FHE 121
FHE 101
FHE 88
FHE 48
FHE 125
base: poorly layered, dark-grey, weathered
calcareous siltstone, poorly layered, light-brown
lime mudstone, very thin-layered, grey-brown, slightly limonitic
siltstone, layered, brownish
lime mudstone
daonellids, flattened, weathered
siltstone, poorly layered, not laminated
very calcareous siltstone, thin-layered
siltstone, poorly layered
lime mudstone
siltstone, weathered
stage
member
zone
subzone
samples
scale [m]
spikes
fossils

Fossil Hill (FHR)
Photos: No
Length: 15.31 m

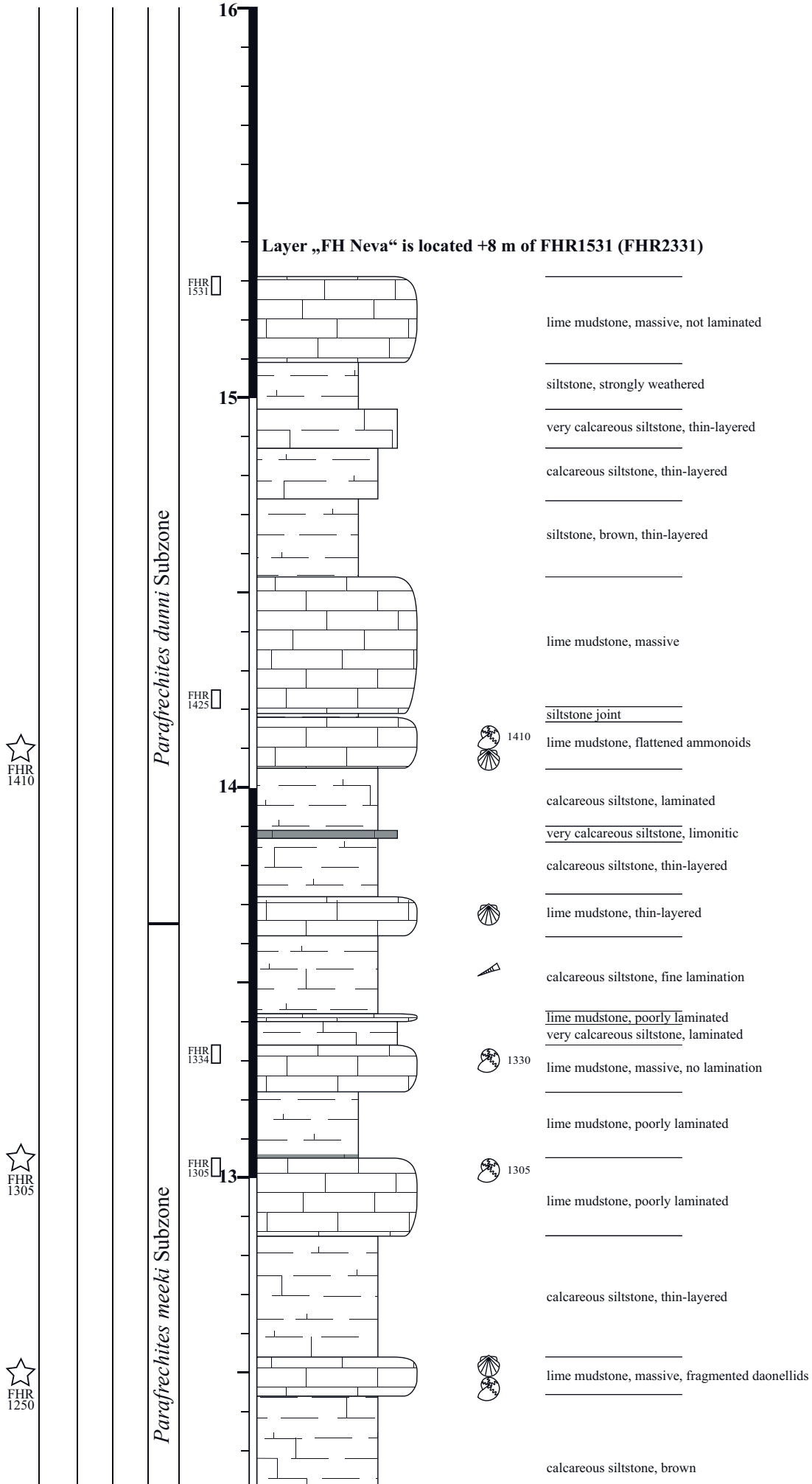

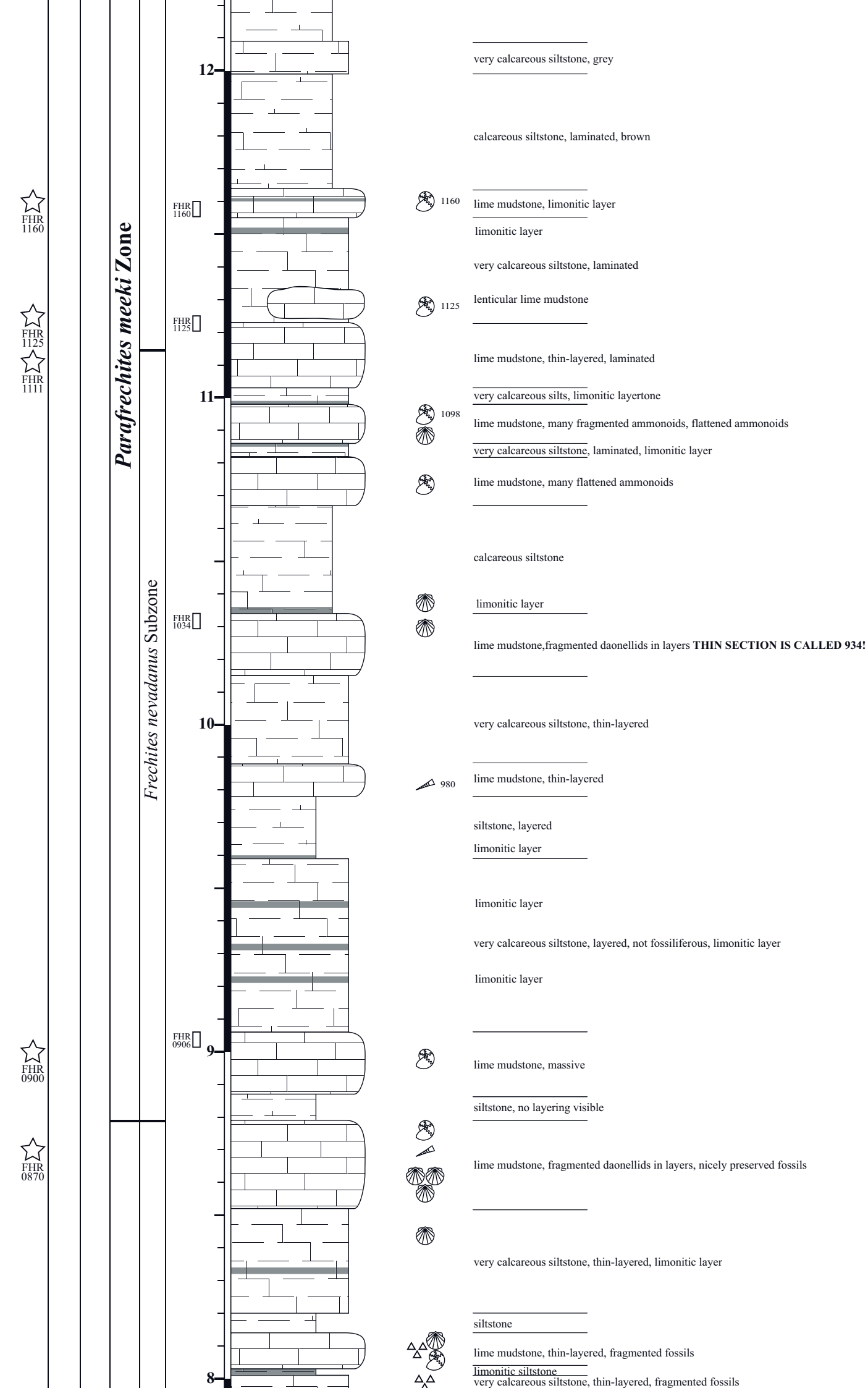
Parafrechites meeki Zone
Frechites nevadanus Subzone
FHR 1160
FHR 1125
FHR 1111
FHR 0900
FHR 0870
FHR 1160
FHR 1125
FHR 1034
FHR 0906
12
11
10
9
8
very calcareous siltstone, grey
calcareous siltstone, laminated, brown
1160
lime mudstone, limonitic layer
limonitic layer
very calcareous siltstone, laminated
1125
lenticular lime mudstone
lime mudstone, thin-layered, laminated
very calcareous silts, limonitic layertone
1098
lime mudstone, many fragmented ammonoids, flattened ammonoids
very calcareous siltstone, laminated, limonitic layer
lime mudstone, many flattened ammonoids
calcareous siltstone
limonitic layer
lime mudstone,fragmented daonellids in layers THIN SECTION IS CALLED 934!
very calcareous siltstone, thin-layered
980
lime mudstone, thin-layered
siltstone, layered
limonitic layer
limonitic layer
very calcareous siltstone, layered, not fossiliferous, limonitic layer
limonitic layer
lime mudstone, massive
siltstone, no layering visible
lime mudstone, fragmented daonellids in layers, nicely preserved fossils
very calcareous siltstone, thin-layered, limonitic layer
siltstone
lime mudstone, thin-layered, fragmented fossils
limonitic siltstone
very calcareous siltstone, thin-layered, fragmented fossils

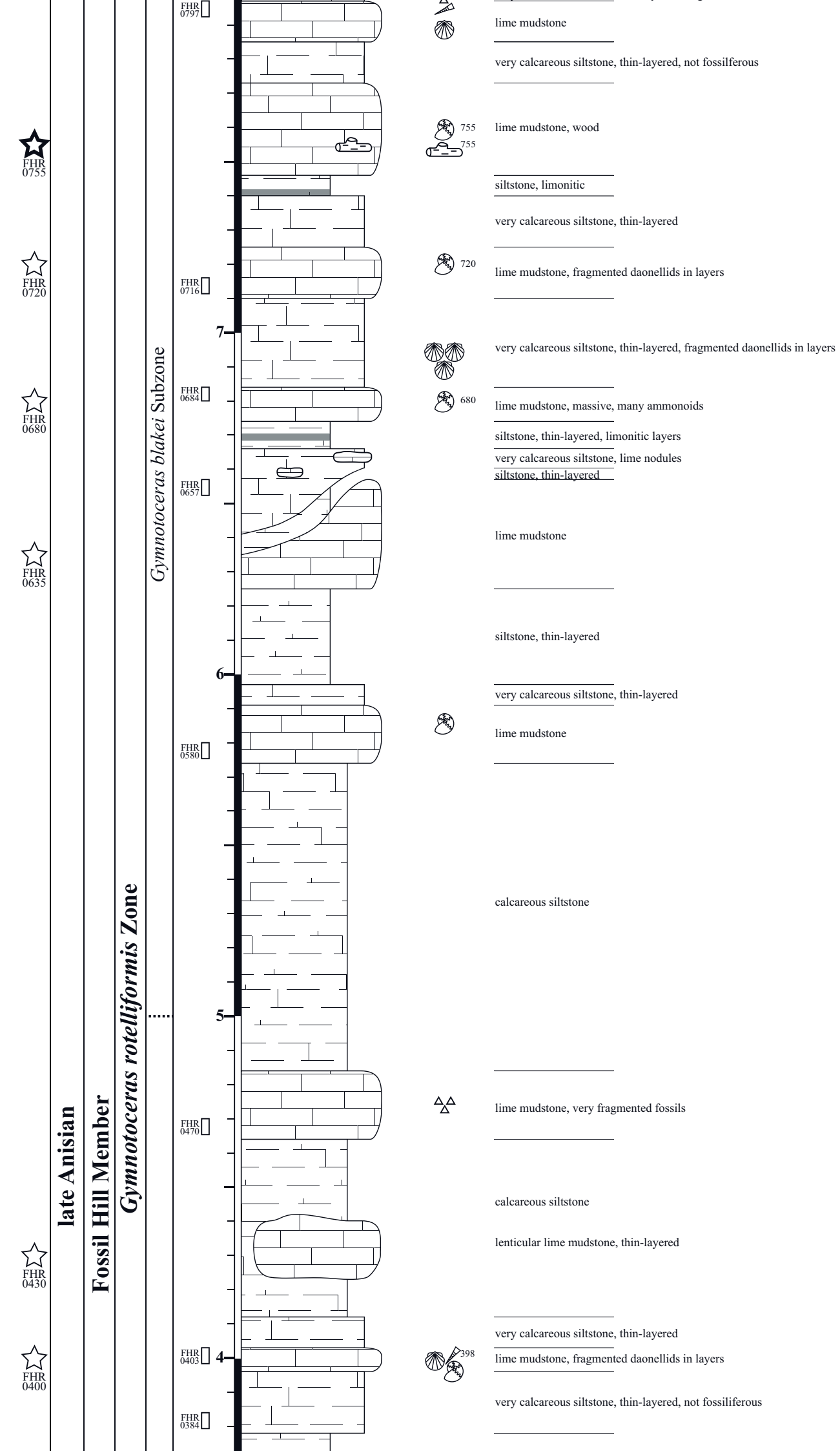
late Anisian
Fossil Hill Member
Gymnotoceras rotelliformis Zone
Gymnotoceras blakei Subzone
FHR 0797
FHR 0755
FHR 0720
FHR 0716
FHR 0684
FHR 0680
FHR 0657
FHR 0635
FHR 0580
FHR 0470
FHR 0430
FHR 0403
FHR 0400
FHR 0384
7
6
5
4
755
755
720
680
398
lime mudstone
very calcareous siltstone, thin-layered, not fossilferous
lime mudstone, wood
siltstone, limonitic
very calcareous siltstone, thin-layered
lime mudstone, fragmented daonellids in layers
very calcareous siltstone, thin-layered, fragmented daonellids in layers
lime mudstone, massive, many ammonoids
siltstone, thin-layered, limonitic layers
very calcareous siltstone, lime nodules
siltstone, thin-layered
lime mudstone
siltstone, thin-layered
very calcareous siltstone, thin-layered
lime mudstone
calcareous siltstone
lime mudstone, very fragmented fossils
calcareous siltstone
lenticular lime mudstone, thin-layered
very calcareous siltstone, thin-layered
lime mudstone, fragmented daonellids in layers
very calcareous siltstone, thin-layered, not fossiliferous

stage
member
zone
subzone
samples
scale [m]
spikes
fossils
Brackites vogdesi Subzone
FHR 0310
FHR 0240
FHR 0140
FHR 0090
FHR 0321
FHR 0270
FHR 0250
FHR 0205
FHR 0136
FHR 0016
FHR 0009
3
2
1
90
54
siltstone, thin-layered, laminated, layers of fragmented fossils
lime mudstone, thin-layered, flattened and fragmented ammonoid
siltstone, thin-layered
lime mudstone
siltstone, poorly laminated
lime mudstone
siltstone, poorly laminated
lime mudstone, backhoe
siltstone, poorly laminated
lime mudstone
siltstone, thin-layered, brown
lime mudstone
siltstone, laminated
very calcareous siltstone, laminated, flattened ammonoid
lime mudstone, fragmented aulacoceratid, fragmented daonellids
very calcareous siltstone, brown lamination
lime mudstone, flattened ammonoid, fragmented daonellids in layers
lenticular lime mudstone
siltstone
lenticular lime mudstone
lenticular lime mudstone
lime mudstone
siltstone, base not explored

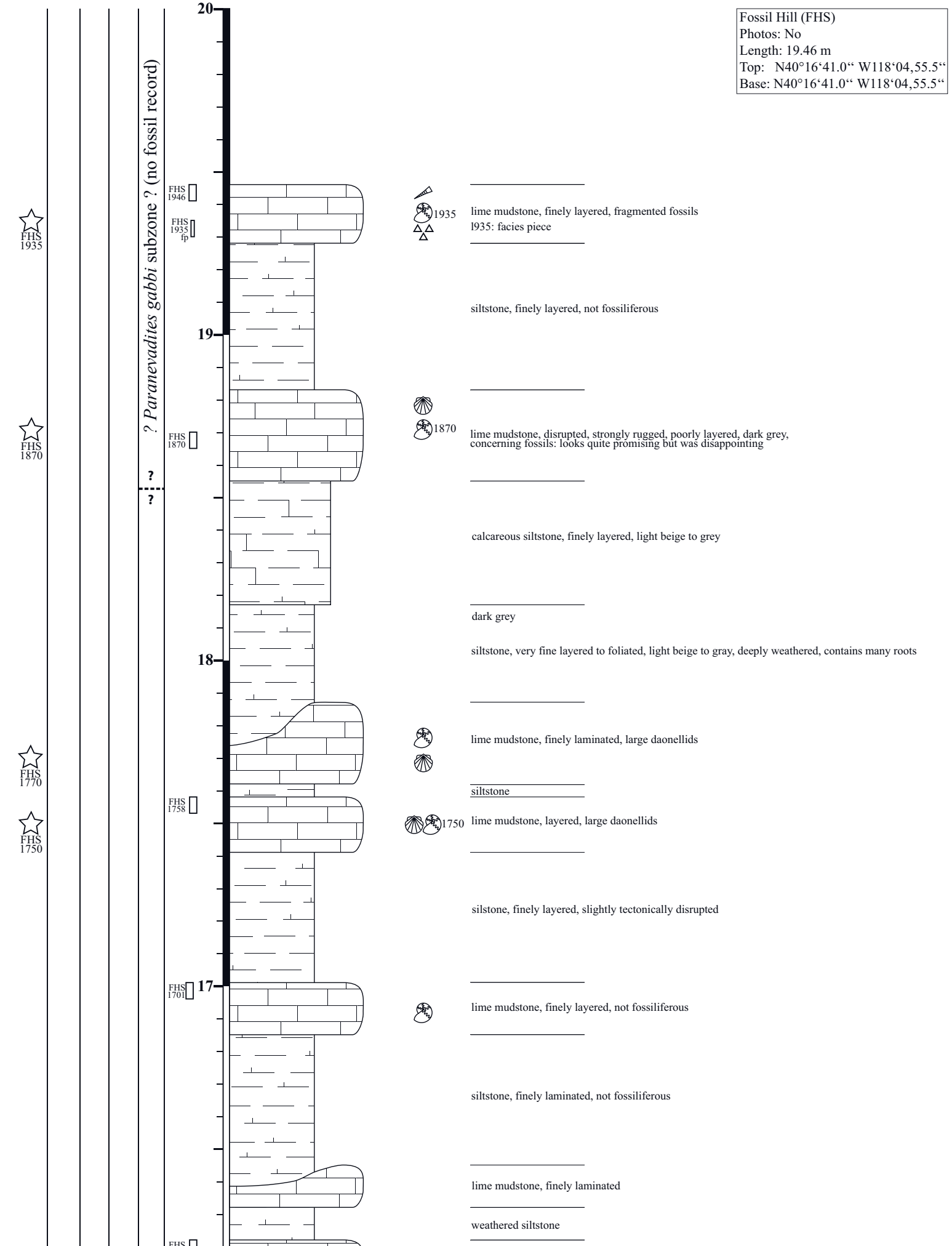
Fossil Hill (FHS)
Photos: No
Length: 19.46 m
Top: N40°16‘41.0“ W118‘04,55.5“
Base: N40°16‘41.0“ W118‘04,55.5“
? Paranevadites gabbi subzone ? (no fossil record)
20
19
18
17
FHS 1946
FHS 1935 fp
FHS 1935
1935
l935: facies piece
lime mudstone, finely layered, fragmented fossils
siltstone, finely layered, not fossiliferous
FHS 1870
1870
lime mudstone, disrupted, strongly rugged, poorly layered, dark grey,
concerning fossils: looks quite promising but was disappointing
?
?
calcareous siltstone, finely layered, light beige to grey
dark grey
siltstone, very fine layered to foliated, light beige to gray, deeply weathered, contains many roots
FHS 1770
lime mudstone, finely laminated, large daonellids
siltstone
FHS 1758
FHS 1750
1750
lime mudstone, layered, large daonellids
silstone, finely layered, slightly tectonically disrupted
FHS 1701
lime mudstone, finely layered, not fossiliferous
siltstone, finely laminated, not fossiliferous
lime mudstone, finely laminated
weathered siltstone
FHS

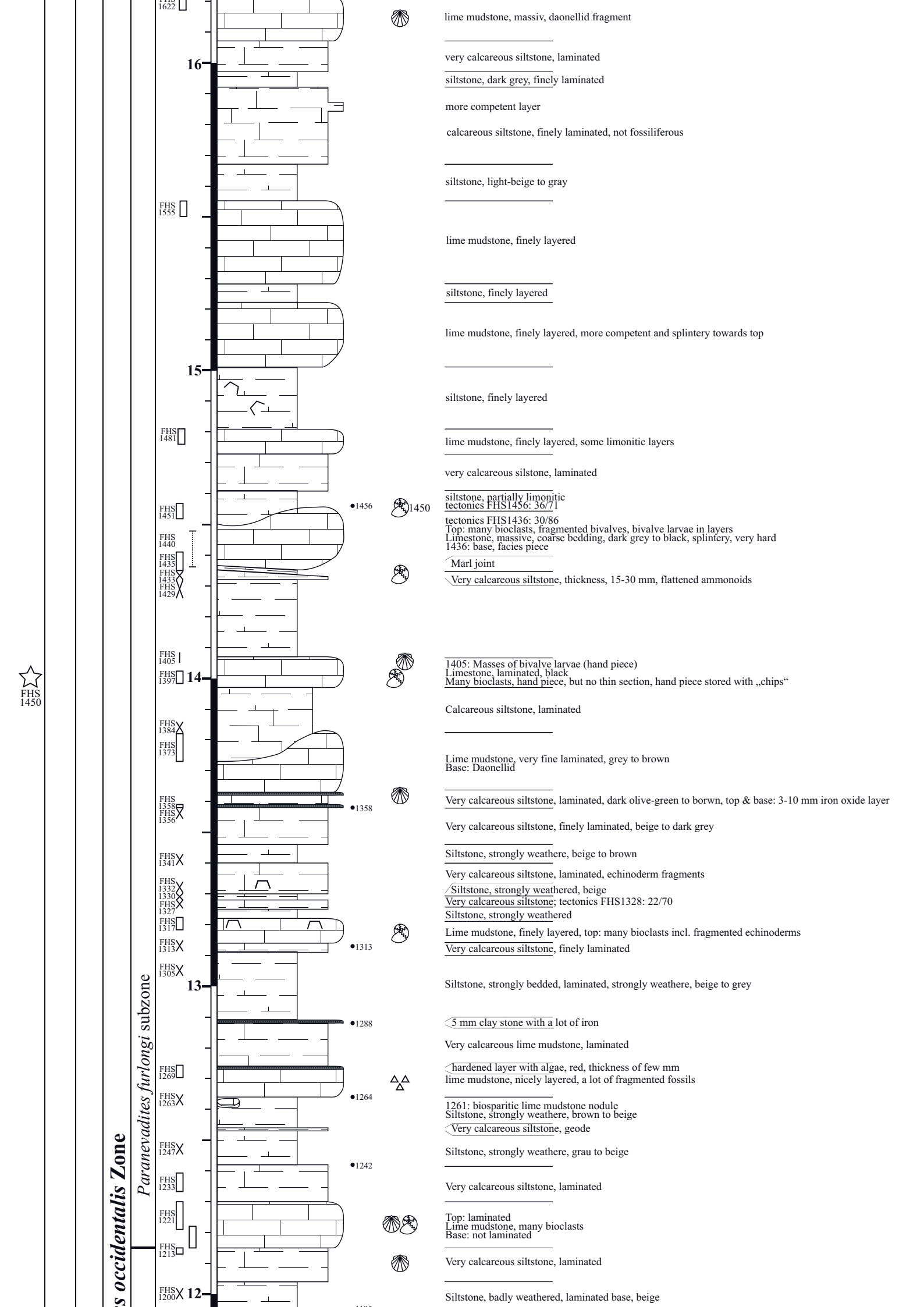
lime mudstone, massiv, daonellid fragment
very calcareous siltstone, laminated
siltstone, dark grey, finely laminated
more competent layer
calcareous siltstone, finely laminated, not fossiliferous
siltstone, light-beige to gray
lime mudstone, finely layered
siltstone, finely layered
lime mudstone, finely layered, more competent and splintery towards top
siltstone, finely layered
lime mudstone, finely layered, some limonitic layers
very calcareous silstone, laminated
siltstone, partially limonitic
tectonics FHS1456: 36/71
tectonics FHS1436: 30/86
Top: many bioclasts, fragmented bivalves, bivalve larvae in layers
Limestone, massive, coarse bedding, dark grey to black, splintery, very hard
1436: base, facies piece
Marl joint
Very calcareous siltstone, thickness, 15-30 mm, flattened ammonoids
1405: Masses of bivalve larvae (hand piece)
Limestone, laminated, black
Many bioclasts, hand piece, but no thin section, hand piece stored with „chips“
Calcareous siltstone, laminated
Lime mudstone, very fine laminated, grey to brown
Base: Daonellid
Very calcareous siltstone, laminated, dark olive-green to borwn, top & base: 3-10 mm iron oxide layer
Very calcareous siltstone, finely laminated, beige to dark grey
Siltstone, strongly weathere, beige to brown
Very calcareous siltstone, laminated, echinoderm fragments
Siltstone, strongly weathered, beige
Very calcareous siltstone; tectonics FHS1328: 22/70
Siltstone, strongly weathered
Lime mudstone, finely layered, top: many bioclasts incl. fragmented echinoderms
Very calcareous siltstone, finely laminated
Siltstone, strongly bedded, laminated, strongly weathere, beige to grey
5 mm clay stone with a lot of iron
Very calcareous lime mudstone, laminated
hardened layer with algae, red, thickness of few mm
lime mudstone, nicely layered, a lot of fragmented fossils
1261: biosparitic lime mudstone nodule
Siltstone, strongly weathere, brown to beige
Very calcareous siltstone, geode
Siltstone, strongly weathere, grau to beige
Very calcareous siltstone, laminated
Top: laminated
Lime mudstone, many bioclasts
Base: not laminated
Very calcareous siltstone, laminated
Siltstone, badly weathered, laminated base, beige
1456
1450
1358
1313
1288
1264
1242
FHS 1450
16
15
14
13
12
Paranevadites furlongi subzone
Gonioclymenia occidentalis Zone

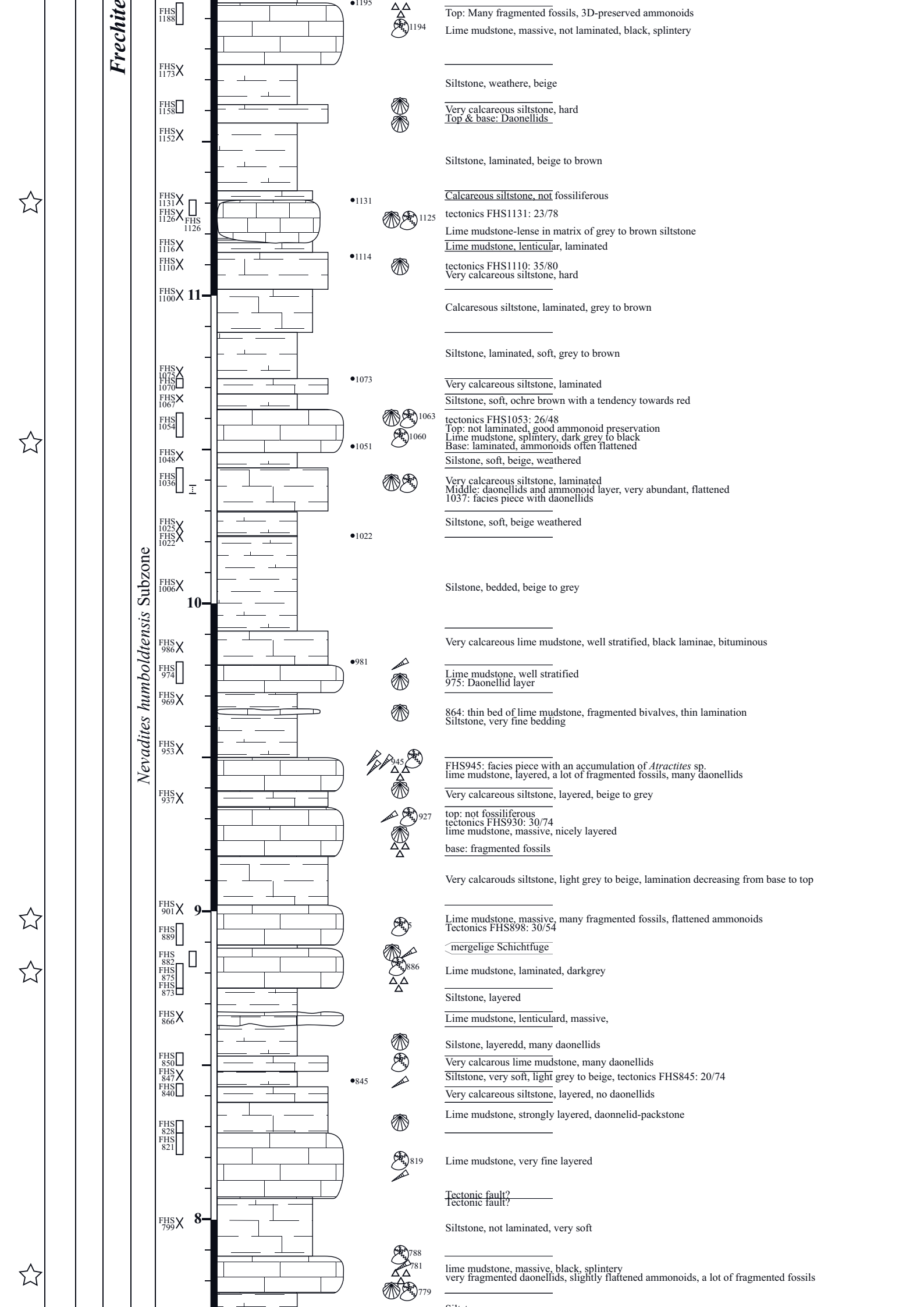
Frechites
Nevadites humboldtensis Subzone
FHS 1188
FHS 1173
FHS 1158
FHS 1152
FHS 1131
FHS 1126
FHS 1126
FHS 1116
FHS 1110
FHS 1100
11
FHS 1075
FHS 1070
FHS 1067
FHS 1054
FHS 1048
FHS 1036
FHS 1025
FHS 1022
FHS 1006
10
FHS 986
FHS 974
FHS 969
FHS 953
FHS 937
FHS 901
9
FHS 889
FHS 882
FHS 875
FHS 873
FHS 866
FHS 850
FHS 847
FHS 840
FHS 828
FHS 821
FHS 799
8
1195
1194
1131
1125
1114
1073
1063
1060
1051
1022
981
945
927
886
845
819
788
781
779
Top: Many fragmented fossils, 3D-preserved ammonoids
Lime mudstone, massive, not laminated, black, splintery
Siltstone, weathere, beige
Very calcareous siltstone, hard
Top & base: Daonellids
Siltstone, laminated, beige to brown
Calcareous siltstone, not fossiliferous
tectonics FHS1131: 23/78
Lime mudstone-lense in matrix of grey to brown siltstone
Lime mudstone, lenticular, laminated
tectonics FHS1110: 35/80
Very calcareous siltstone, hard
Calcaresous siltstone, laminated, grey to brown
Siltstone, laminated, soft, grey to brown
Very calcareous siltstone, laminated
Siltstone, soft, ochre brown with a tendency towards red
tectonics FHS1053: 26/48
Top: not laminated, good ammonoid preservation
Lime mudstone, splintery, dark grey to black
Base: laminated, ammonoids often flattened
Silstone, soft, beige, weathered
Very calcareous siltstone, laminated
Middle: daonellids and ammonoid layer, very abundant, flattened
1037: facies piece with daonellids
Siltstone, soft, beige weathered
Silstone, bedded, beige to grey
Very calcareous lime mudstone, well stratified, black laminae, bituminous
Lime mudstone, well stratified
975: Daonellid layer
864: thin bed of lime mudstone, fragmented bivalves, thin lamination
Siltstone, very fine bedding
FHS945: facies piece with an accumulation of Atractites sp.
lime mudstone, layered, a lot of fragmented fossils, many daonellids
Very calcareous siltstone, layered, beige to grey
top: not fossiliferous
tectonics FHS930: 30/74
lime mudstone, massive, nicely layered
base: fragmented fossils
Very calcarouds siltstone, light grey to beige, lamination decreasing from base to top
Lime mudstone, massive, many fragmented fossils, flattened ammonoids
Tectonics FHS898: 30/54
mergelige Schichtfuge
Lime mudstone, laminated, darkgrey
Siltstone, layered
Lime mudstone, lenticulard, massive,
Silstone, layeredd, many daonellids
Very calcarous lime mudstone, many daonellids
Siltstone, very soft, light grey to beige, tectonics FHS845: 20/74
Very calcareous siltstone, layered, no daonellids
Lime mudstone, strongly layered, daonnelid-packstone
Lime mudstone, very fine layered
Tectonic fault?
Tectonic fault?
Siltstone, not laminated, very soft
lime mudstone, massive, black, splintery
very fragmented daonellids, slightly flattened ammonoids, a lot of fragmented fossils

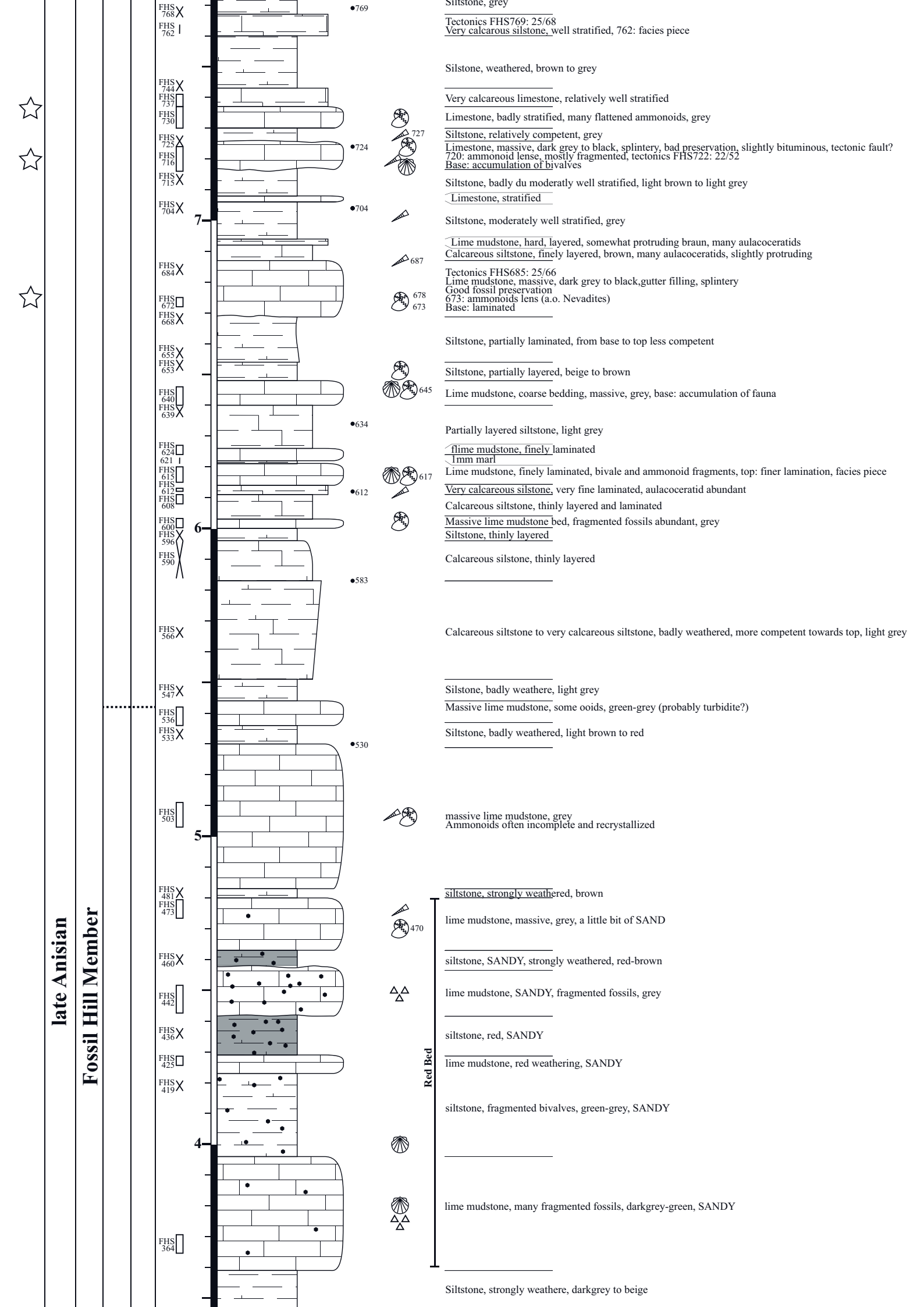
late Anisian
Fossil Hill Member
FHS 768
FHS 762
FHS 744
FHS 737
FHS 730
FHS 725
FHS 716
FHS 715
FHS 704
FHS 684
FHS 672
FHS 668
FHS 655
FHS 653
FHS 640
FHS 639
FHS 624
621
FHS 615
FHS 612
FHS 608
FHS 600
FHS 596
FHS 590
FHS 566
FHS 547
FHS 536
FHS 533
FHS 503
FHS 481
FHS 473
FHS 460
FHS 442
FHS 436
FHS 425
FHS 419
FHS 364
7
6
5
4
•769
•724
•704
•634
•612
•583
•530
727
687
678
673
645
617
470
Red Bed
Siltstone, grey
Tectonics FHS769: 25/68
Very calcarous silstone, well stratified, 762: facies piece
Siltstone, weathered, brown to grey
Very calcareous limestone, relatively well stratified
Limestone, badly stratified, many flattened ammonoids, grey
Siltstone, relatively competent, grey
Limestone, massive, dark grey to black, splintery, bad preservation, slightly bituminous, tectonic fault?
720: ammonoid lense, mostly fragmented, tectonics FHS722: 22/52
Base: accumulation of bivalves
Siltstone, badly du moderatly well stratified, light brown to light grey
Limestone, stratified
Siltstone, moderately well stratified, grey
Lime mudstone, hard, layered, somewhat protruding braun, many aulacoceratids
Calcareous siltstone, finely layered, brown, many aulacoceratids, slightly protruding
Tectonics FHS685: 25/66
Lime mudstone, massive, dark grey to black,gutter filling, splintery
Good fossil preservation
673: ammonoids lens (a.o. Nevadites)
Base: laminated
Siltstone, partially laminated, from base to top less competent
Siltstone, partially layered, beige to brown
Lime mudstone, coarse bedding, massive, grey, base: accumulation of fauna
Partially layered siltstone, light grey
flime mudstone, finely laminated
1mm marl
Lime mudstone, finely laminated, bivale and ammonoid fragments, top: finer lamination, facies piece
Very calcareous silstone, very fine laminated, aulacoceratid abundant
Calcareous siltstone, thinly layered and laminated
Massive lime mudstone bed, fragmented fossils abundant, grey
Siltstone, thinly layered
Calcareous silstone, thinly layered
Calcareous siltstone to very calcareous siltstone, badly weathered, more competent towards top, light grey
Silstone, badly weathere, light grey
Massive lime mudstone, some ooids, green-grey (probably turbidite?)
Siltstone, badly weathered, light brown to red
massive lime mudstone, grey
Ammonoids often incomplete and recrystallized
siltstone, strongly weathered, brown
lime mudstone, massive, grey, a little bit of SAND
siltstone, SANDY, strongly weathered, red-brown
lime mudstone, SANDY, fragmented fossils, grey
siltstone, red, SANDY
lime mudstone, red weathering, SANDY
siltstone, fragmented bivalves, green-grey, SANDY
lime mudstone, many fragmented fossils, darkgrey-green, SANDY
Siltstone, strongly weathere, darkgrey to beige

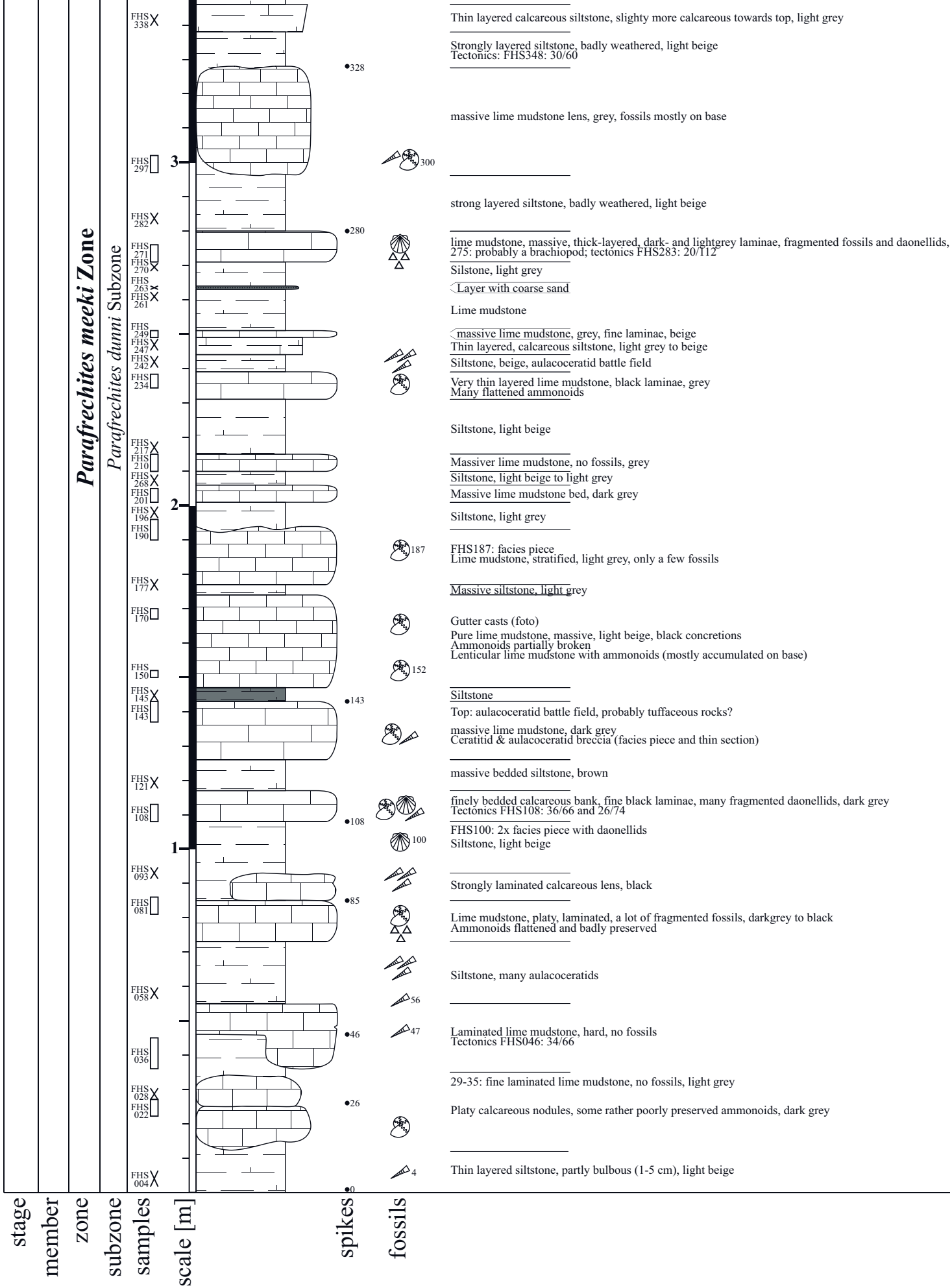
stage
member
zone
subzone
samples
scale [m]
spikes
fossils
Parafrechites meeki Zone
Parafrechites dunni Subzone
FHS 338
FHS 297
FHS 282
FHS 271
FHS 270
FHS 263
FHS 261
FHS 249
FHS 247
FHS 242
FHS 234
FHS 217
FHS 210
FHS 268
FHS 201
FHS 196
FHS 190
FHS 177
FHS 170
FHS 150
FHS 145
FHS 143
FHS 121
FHS 108
FHS 093
FHS 081
FHS 058
FHS 036
FHS 028
FHS 022
FHS 004
3
2
1
328
300
280
187
152
143
108
100
85
56
47
46
26
4
0
Thin layered calcareous siltstone, slighty more calcareous towards top, light grey
Strongly layered siltstone, badly weathered, light beige
Tectonics: FHS348: 30/60
massive lime mudstone lens, grey, fossils mostly on base
strong layered siltstone, badly weathered, light beige
lime mudstone, massive, thick-layered, dark- and lightgrey laminae, fragmented fossils and daonellids,
275: probably a brachiopod; tectonics FHS283: 20/112
Silstone, light grey
Layer with coarse sand
Lime mudstone
massive lime mudstone, grey, fine laminae, beige
Thin layered, calcareous siltstone, light grey to beige
Siltstone, beige, aulacoceratid battle field
Very thin layered lime mudstone, black laminae, grey
Many flattened ammonoids
Siltstone, light beige
Massiver lime mudstone, no fossils, grey
Siltstone, light beige to light grey
Massive lime mudstone bed, dark grey
Siltstone, light grey
FHS187: facies piece
Lime mudstone, stratified, light grey, only a few fossils
Massive siltstone, light grey
Gutter casts (foto)
Pure lime mudstone, massive, light beige, black concretions
Ammonoids partially broken
Lenticular lime mudstone with ammonoids (mostly accumulated on base)
Siltstone
Top: aulacoceratid battle field, probably tuffaceous rocks?
massive lime mudstone, dark grey
Ceratitid & aulacoceratid breccia (facies piece and thin section)
massive bedded siltstone, brown
finely bedded calcareous bank, fine black laminae, many fragmented daonellids, dark grey
Tectonics FHS108: 36/66 and 26/74
FHS100: 2x facies piece with daonellids
Siltstone, light beige
Strongly laminated calcareous lens, black
Lime mudstone, platy, laminated, a lot of fragmented fossils, darkgrey to black
Ammonoids flattened and badly preserved
Siltstone, many aulacoceratids
Laminated lime mudstone, hard, no fossils
Tectonics FHS046: 34/66
29-35: fine laminated lime mudstone, no fossils, light grey
Platy calcareous nodules, some rather poorly preserved ammonoids, dark grey
Thin layered siltstone, partly bulbous (1-5 cm), light beige

Fossil Hill Red Bed (FHSRB)
Photos: Yes
Length: 2.29 m
N40°16′42.1″ ; W118°04′51.7″
± 3 m
stage
member
zone
subzone
samples
scale [m]
spikes
fossils
late Anisian
Fossil Hill Member
? Frechites occidentalis zone?
Parafrechites meeki zone
? Nevadites humboldtensis subzone? (no fossil record)
Parafrechites dunni subzone
?
?
?
?
3
2
1
FHE 0455
FHS RB164
FHS RB 155
FHS RB150
FHS RB139
FHS RB133
FHS RB111
FHS RB85
FHS RB75
FHS RB20
very calcareous siltstone, layered
lime mudstone, massive, very competent, splintery
calcareous siltstone, thin-layered, contains some thin mudstone layers
very calcareous siltstone, layered, very competent, light-grey
lime mudstone, massive, light-grey, „sugar carbonate“ (glitters), a lot of fossil fragments
very calcareous siltstone, layered, competent, red weathering, thin-laminated, brown to dark grey

Appendix 2 Fossil Material

Zone	N. taylori	N. taylori	N. taylori	N. taylori	N. taylori	N. taylori	B. shoshonensis	B. shoshonensis	n.a.	G. mimetus	G. mimetus	G. mimetus	G. mimetus	G. mimetus	G. mimetus	G. rotelliformis
Subzone	P. praebalatonensis	P. praebalatonensis	P. praebalatonensis	P. praebalatonensis	P. praebalatonensis	P. praebalatonensis	F. rieberi	F. ransomei	n.a.	M. spinifer	M. spinifer	M. spinifer	M. spinifer	M. spinifer	M. spinifer	B. vogdesi
Species	**FCE 115**	**FCE 380**	**FCE 500**	**FCE 570**	**FCE 700**	**FCE 920**	**FCE 1445**	**FCE 1600**	**FCE loose**	**MUC 1214**	**MUC 1535**	**MUC 1594**	**MUC 1630-1858**	**MUC 1815-1818**	**MUC 1872-1877**	**MUC 2038**
Anagymnites sp.											3					
Ussurites cf. arthaberi	3						1	29								
Aplococeras cf. smithi																
Aplococeras cf. vogdesi																
Aplococeras parvus																
Aplococeras smithi																
Aplococeras sp.																
Aplococeras vogdesi																
Favreticeras ransomei								37								
Eogymnotoceras tuberculatum							20	73								
?Eogymnotoceras tuberculatum juv.							274									
Brackites vogdesi																
Billingsites cf. escuargeli																
Billingsites cordeyi																
Dixieceras lawsoni																
Gymnotoceras praecursor							20									
Gymnotoceras weitschati																
Gymnotoceras rotelliformis																
Gymnotoceras rotelliformis-blakei													96	1	37	5
Gymnotoceras cf. blakei																
Gymnotoceras blakei																
Gymnotoceras mimetus																
Parafrechites dunni																
Parafrechites meeki																
Frechites nevadanus																
Frechites occidentalis																
Humboldtites septentrionalis																
Intornites nevadanus		1		1	2		4	31								
Longobardites cf. parvus														3		
Longobardites parvus																
Longobardites sp.																1
Longobardites zsigmondyi															7	
Nevadisculites depressus							11									
Nevadisculites smithi								28	5							
Acrochordiceras carolinae	8	4	1		1	1	45	78								
Jenksites flexicostatus																
Rieppelites boletzkyi																
Rieberites transiformis																
Silberlingia clarkei														125		
Silberlingia praecursor																
Ceccaceras stecki										1						
Eutomoceras dunni																
Eutomoceras laubei																
Eutomoceras sp.										2		1		9	5	
Marcouxites spinifer ad.										23	6					
Marcouxites spinifer juv.										39	4				11	
Metadinarites desertorus											6			41	30	
Nevadites humboldtensis																
Nevadites hyatti																
Nevadites sp.																
Paranevadites furlongi																
Platycuccoceras cainense								25								
Proarcestes bramantei																
Proarcestes cf. P. balfouri																
Proarcestes cf. P. bramantei										1	3			1	1	
Proarcestes gabbi																
Proarcestes sp.																
Proarcestes-Humboldtites																
Ptychites gradinarui								1								
Ptychites guloensis								1								
Ptychites embreei														2		
Sageceras walteri																
Thanamites cf. contractus																
Tozerites gemmelaroi																
Tozerites humboldtensis																
Tozerites polygyratus																
Tropigastrites cf. louderbacki																
Tropigastrites lohantanus																
Tropigastrites louderbacki																
Tropigastrites sp.										19				3		
sp. indet.	1	3									1			5		
Atractites sp.				1			7	4								
Nautilid							2							3	1	
Paranautilus smithi																
Bivalve		2							1	1						
Brachiopod									1							
Gastropod							3									
Wood																
Sum:	**12**	**10**	**1**	**2**	**3**	**1**	**387**	**307**	**7**	**86**	**23**	**1**	**96**	**193**	**92**	**6**

Sum	730 specimens	1816 specimens
Sum juveniles	46 specimens	42 specimens
Total:	**776 specimens**	**1858 specimens**

Zone	G. rotellifor mis	G. rotellifor mis	G. rotellifor mis	G. rotellifor mis	G. rotellifor mis	G. rotellifor mis	P. meeki	P. meeki	P. meeki	P. meeki	F. occidenta lis	F. occidenta lis	F. occidenta lis	F. occidenta lis	F. occidenta lis	F. occidenta lis
Subzone	B. vogdesi	B. vogdesi	B. vogdesi	G. blakei	G. blakei	G. blakei	F. nevadanu s	F. nevadanu s	F. nevadanu s	P. dunni	N. hyatti	N. hyatti	N. hyatti	N. hyatti	N. hyatti	N. hyatti
Species	**MUC 2175**	**MUC 2294**	**MUC 2429**	**MUC 2800**	**MUC 2870**	**MUC 2980**	**MUC 3239**	**MUC 3280**	**MUC 3607**	**MUC 3875-4059**	**MUC 4150-4315**	**MUC 4424-4440**	**MUC 4500**	**MUC 4595**	**MUC 4740**	**MUC 4770**
Anagymnites sp.	0	0	0	0	0	0	0	0	0	0	0	0	0	0	0	0
Ussurites cf. arthaberi	0	0	0	0	0	0	0	0	0	0	0	0	0	0	0	0
Aplococeras cf. smithi	0	0	0	0	3	67	0	0	0	0	0	0	0	0	0	0
Aplococeras cf. vogdesi	0	0	0	0	6	0	0	0	0	0	0	0	0	0	0	0
Aplococeras parvus	0	0	0	0	0	0	0	0	0	0	0	0	0	0	0	0
Aplococeras smithi	0	0	0	0	0	0	1	0	0	0	0	0	0	0	0	0
Aplococeras sp.	0	0	0	0	0	0	0	0	0	1	0	0	0	0	0	0
Aplococeras vogdesi	0	0	0	0	0	0	0	0	5	0	0	0	0	0	0	0
Favreticeras ransomei	0	0	0	0	0	0	0	0	0	0	0	0	0	0	0	0
Eogymnotoceras tuberculatum	0	0	0	0	0	0	0	0	0	0	0	0	0	0	0	0
?Eogymnotoceras tuberculatum juv.	0	0	0	0	0	0	0	0	0	0	0	0	0	0	0	0
Brackites vogdesi	1	0	0	0	0	0	0	0	0	0	0	0	0	0	0	0
Billingsites cf. escuargeli	0	0	0	0	0	0	0	0	0	0	0	0	0	0	0	0
Billingsites cordeyi	0	0	0	0	0	0	0	0	0	0	0	0	0	0	0	0
Dixieceras lawsoni	0	0	0	0	0	0	0	0	0	0	0	0	0	0	0	0
Gymnotoceras praecursor	0	0	0	0	0	0	0	0	0	0	0	0	0	0	0	0
Gymnotoceras weitschati	0	0	0	0	0	0	0	0	0	0	0	0	0	0	0	0
Gymnotoceras rotelliformis	0	0	0	0	0	0	0	0	0	0	0	0	0	0	0	0
Gymnotoceras rotelliformis-blakei	18	16	0	45	119	23	6	10	4	0	0	0	0	0	0	0
Gymnotoceras cf. blakei	0	0	0	33	0	0	0	0	0	0	0	0	0	0	0	0
Gymnotoceras blakei	0	0	0	2	0	0	16	0	0	0	0	0	0	0	0	0
Gymnotoceras mimetus	0	0	0	0	0	0	0	0	0	0	0	0	0	0	0	0
Parafrechites dunni	0	0	0	0	0	0	0	0	0	0	0	0	0	0	0	0
Parafrechites meeki	0	0	0	0	0	0	12	0	0	1	0	0	0	0	0	0
Frechites nevadanus	0	0	0	0	0	0	0	0	0	0	0	0	0	0	0	0
Frechites occidentalis	0	0	0	0	0	0	0	0	0	0	3	1	4	0	0	0
Humboldtites septentrionalis	0	0	0	0	0	0	0	0	0	0	2	0	0	0	0	0
Intornites nevadanus	0	0	0	0	0	0	0	0	0	0	0	0	0	0	0	0
Longobardites cf. parvus	0	0	0	0	0	21	0	0	0	0	0	0	0	0	0	0
Longobardites parvus	0	0	0	0	0	0	0	0	0	0	0	0	0	0	0	0
Longobardites sp.	0	0	0	0	0	0	0	0	1	0	0	0	0	0	0	0
Longobardites zsigmondyi	0	0	0	0	0	0	0	0	0	2	0	16	1	0	1	2
Nevadisculites depressus	0	0	0	0	0	0	0	0	0	0	0	0	0	0	0	0
Nevadisculites smithi	0	0	0	0	0	0	0	0	0	0	0	0	0	0	0	0
Acrochordiceras carolinae	0	0	0	0	0	0	0	0	0	0	0	0	0	0	0	0
Jenksites flexicostatus	0	0	0	0	0	0	0	0	0	0	0	0	0	0	0	0
Rieppelites boletzkyi	0	0	0	0	0	0	0	0	0	0	0	0	0	0	0	0
Rieberites transiformis	0	0	0	0	0	0	0	0	0	0	0	0	0	0	0	0
Silberlingia clarkei	0	0	1	0	0	0	0	0	0	0	0	0	0	0	0	0
Silberlingia praecursor	0	0	0	0	0	0	0	0	0	0	0	0	0	0	0	0
Ceccaceras stecki	0	0	0	0	0	0	0	0	0	0	0	0	0	0	0	0
Eutomoceras dunni	0	0	0	0	0	0	0	0	0	0	0	0	0	0	0	0
Eutomoceras laubei	0	0	0	0	0	0	0	0	0	0	2	0	0	0	0	0
Eutomoceras sp.	8	0	0	4	5	7	4	0	0	0	0	0	0	0	0	0
Marcouxites spinifer ad.	0	0	0	0	0	0	0	0	0	0	0	0	0	0	0	0
Marcouxites spinifer juv.	0	0	0	0	0	0	0	0	0	0	0	0	0	0	0	0
Metadinarites desertorus	79	0	0	0	0	0	0	0	0	0	0	0	0	0	0	0
Nevadites humboldtensis	0	0	0	0	0	0	0	0	0	0	0	0	0	0	0	0
Nevadites hyatti	0	0	0	0	0	0	0	0	0	0	15	10	1	0	2	1
Nevadites sp.	0	0	0	0	0	0	0	0	0	0	0	0	0	1	0	0
Paranevadites furlongi	0	0	0	0	0	0	0	0	0	0	0	0	0	0	0	0
Platycuccoceras cainense	0	0	0	0	0	0	0	0	0	0	0	0	0	0	0	0
Proarcestes bramantei	0	0	0	0	0	0	0	0	0	0	0	0	0	0	0	0
Proarcestes cf. P. balfouri	0	0	0	0	0	0	0	0	0	0	0	0	0	0	0	0
Proarcestes cf. P. bramantei	2	0	0	0	0	0	0	0	0	0	0	0	0	0	0	0
Proarcestes gabbi	0	0	0	0	0	0	0	0	0	0	5	2	2	0	4	4
Proarcestes sp.	0	0	0	1	0	0	4	7	0	0	0	0	0	0	0	0
Proarcestes-Humboldtites	0	0	0	0	0	0	0	0	3	0	0	0	0	0	0	0
Ptychites gradinarui	0	0	0	0	0	0	0	0	0	0	0	0	0	0	0	0
Ptychites guloensis	0	0	0	0	0	0	0	0	0	0	0	0	0	0	0	0
Ptychites embreei	10	0	0	0	1	19	6	0	0	0	0	0	0	0	0	0
Sageceras walteri	1	0	0	0	0	0	0	0	0	0	0	0	0	0	0	0
Thanamites cf. contractus	0	0	0	0	0	0	0	0	0	0	0	0	0	0	0	0
Tozerites gemmelaroi	0	0	0	0	0	0	0	0	0	0	0	0	0	0	0	0
Tozerites humboldtensis	0	0	0	0	0	0	0	0	0	0	2	0	0	0	0	0
Tozerites polygyratus	0	0	0	0	0	0	0	0	0	0	0	0	0	0	0	0
Tropigastrites cf. louderbacki	0	2	0	0	0	0	0	1	0	0	0	0	0	0	0	0
Tropigastrites lohantanus	0	0	0	8	28	6	0	0	0	0	0	0	0	0	0	0
Tropigastrites louderbacki	0	0	0	0	0	0	0	0	0	0	0	0	0	0	0	0
Tropigastrites sp.	0	0	0	0	0	0	2	0	0	0	0	0	0	0	0	0
sp. indet.	1	1	0	0	12	5	2	0	0	1	0	0	0	0	0	0
Atractites sp.	0	0	0	0	0	2	0	0	1	0	1	1	0	0	2	0
Nautilid	0	0	0	0	0	0	0	0	0	0	0	0	0	0	0	0
Paranautilus smithi	0	0	0	0	0	0	0	0	0	0	0	0	0	0	0	0
Bivalve	2	0	0	0	0	0	0	0	1	0	0	0	1	0	0	0
Brachiopod	0	0	0	0	0	0	0	0	0	0	0	0	0	0	0	0
Gastropod	0	0	0	0	0	0	0	0	0	0	0	0	0	0	0	0
Wood	0	0	0	0	0	0	0	0	0	0	0	0	0	0	0	0
Sum:	**122**	**19**	**1**	**93**	**174**	**150**	**53**	**18**	**15**	**5**	**30**	**30**	**9**	**1**	**9**	**7**
Sum																
Sum juveniles																
Total:																

	Zone	F. occidentalis	F. occidentalis	F. occidentalis	F. occidentalis	F. occidentalis	F. occidentalis	F. occidentalis	F. occidentalis	F. occidentalis	F. occidentalis	F. occidentalis	F. occidentalis	F. occidentalis	F. occidentalis	F. occidentalis	F. occidentalis
	Subzone	N. hyatti	N. hyatti	N. hyatti	N. humboldtensis	N. humboldtensis	N. humboldtensis	N. humboldtensis	P. furlongi	P. furlongi	P. furlongi	P. furlongi	P. furlongi	P. furlongi	P. furlongi	P. furlongi	P. furlongi
Species		**MUC 4796**	**MUC 5064**	**MUC 5090**	**MUC 5118**	**MUC 5140-5146**	**MUC 5185**	**MUC 5196-5200**	**MUC 5257-5260**	**MUC 5280**	**MUC 5290**	**MUC 5307-5315**	**MUC 5357**	**MUC 5490**	**MUC 5520**	**MUC 5720-5730**	**MUC 5740-5745**
Anagymnites sp.		0	0	0	0	0			0		0				0	0	0
Ussurites cf. arthaberi		0	0	0	0	0			0		0				0	0	0
Aplococeras cf. smithi		0	0	0	0	0			0		0				0	0	0
Aplococeras cf. vogdesi		0	0	0	0	0			0		0				0	0	0
Aplococeras parvus		0	0	0	1	0			35		2				0	0	0
Aplococeras smithi		0	0	0	0	0			0		0				0	0	0
Aplococeras sp.		0	0	0	0	0			0		0				0	0	0
Aplococeras vogdesi		0	0	0	0	0			0		0				0	0	0
Favreticeras ransomei		0	0	0	0	0			0		0				0	0	0
Eogymnotoceras tuberculatum		0	0	0	0	0			0		0				0	0	0
?Eogymnotoceras tuberculatum juv.		0	0	0	0	0			0		0				0	0	0
Brackites vogdesi		0	0	0	0	0			0		0				0	0	0
Billingsites cf. escuargeli		0	0	0	0	0			0		0				0	0	0
Billingsites cordeyi		0	0	0	0	0			0		0				0	0	0
Dixieceras lawsoni		0	0	0	0	0			0		0				0	0	0
Gymnotoceras praecursor		0	0	0	0	0			0		0				0	0	0
Gymnotoceras weitschati		0	0	0	0	0			0		0				0	0	0
Gymnotoceras rotelliformis		0	0	0	0	0			0		0				0	0	0
Gymnotoceras rotelliformis-blakei		0	0	0	0	0			0		0				0	0	0
Gymnotoceras cf. blakei		0	0	0	0	0			0		0				0	0	0
Gymnotoceras blakei		0	0	0	0	0			0		0				0	0	0
Gymnotoceras mimetus		0	0	0	0	0			0		0				0	0	0
Parafrechites dunni		0	0	0	0	0			0		0				0	0	0
Parafrechites meeki		0	0	0	0	0			0		0				0	0	0
Frechites nevadanus		0	0	0	0	0			0		0				0	0	0
Frechites occidentalis		0	0	0	0	9	2		145	2	4	1	1	2	0	6	3
Humboldtites septentrionalis		0	0	0	8	0			0		0				0	0	0
Intornites nevadanus		0	0	0	0	0			0		0				0	0	0
Longobardites cf. parvus		0	0	0	0	0			0		0				0	0	0
Longobardites parvus		0	0	0	0	0			0		0				12	5	5
Longobardites sp.		0	0	0	0	0			0		0				0	0	0
Longobardites zsigmondyi		0	0	0	3	2		1	14		4				0	0	0
Nevadisculites depressus		0	0	0	0	0			0		0				0	0	0
Nevadisculites smithi		0	0	0	0	0			0		0				0	0	0
Acrochordiceras carolinae		0	0	0	0	0			0		0				0	0	0
Jenksites flexicostatus		0	0	0	0	0			0		0				0	0	0
Rieppelites boletzkyi		0	0	0	0	0			0		0				0	0	0
Rieberites transiformis		0	0	0	0	0			0		0				0	0	0
Silberlingia clarkei		0	0	0	0	0			0		0				0	0	0
Silberlingia praecursor		0	0	0	0	0			0		0				0	0	0
Ceccaceras stecki		0	0	0	0	0			0		0				0	0	0
Eutomoceras dunni		0	0	0	0	0			0		0				0	0	0
Eutomoceras laubei		0	0	0	0	0			0		0				0	0	0
Eutomoceras sp.		0	0	0	0	0			0		0				0	0	0
Marcouxites spinifer ad.		0	0	0	0	0			0		0				0	0	0
Marcouxites spinifer juv.		0	0	0	0	0			0		0				0	0	0
Metadinarites desertorus		0	0	0	0	0			0		0				0	0	0
Nevadites humboldtensis		0	0	0	10	16			60	2	1	2			22	11	0
Nevadites hyatti		1	0	3	0	0	1		0		0				0	0	0
Nevadites sp.		0	0	0	0	0			0		0				0	0	0
Paranevadites furlongi		0	0	0	0	0			13		0				3	0	1
Platycuccoceras cainense		0	0	0	0	0			0		0				0	0	0
Proarcestes bramantei		0	0	0	0	0			0		0				0	0	0
Proarcestes cf. P. balfouri		0	0	0	0	0			0		0				0	0	0
Proarcestes cf. P. bramantei		0	0	0	0	0			0		0				0	0	0
Proarcestes gabbi		0	0	8	34	18	1	1	29	1	3				0	0	0
Proarcestes sp.		0	0	0	0	0			0		0				0	0	0
Proarcestes-Humboldtites		0	0	0	0	0			0		0				0	0	0
Ptychites gradinarui		0	0	0	0	0			0		0				0	0	0
Ptychites guloensis		0	0	0	0	0			0		0				0	0	0
Ptychites embreei		0	0	0	0	0			0		0				0	0	0
Sageceras walteri		0	0	0	0	0			0		0				0	0	0
Thanamites cf. contractus		0	0	0	12	1			2		0				0	0	0
Tozerites gemmelaroi		0	0	0	0	0			0		0				0	0	0
Tozerites humboldtensis		0	0	0	0	0			0		0				0	0	0
Tozerites polygyratus		0	1	0	0	0			0		0				17	2	4
Tropigastrites cf. louderbacki		0	0	0	0	0			0		0				0	0	0
Tropigastrites lohantanus		0	0	0	0	0			0		0				0	0	0
Tropigastrites louderbacki		0	0	0	0	0			0		0				0	0	0
Tropigastrites sp.		0	0	0	0	0			0		0				0	0	0
sp. indet.		0	0	0	0	0			0		0				0	0	0
Atractites sp.		0	0	0	2	4			0		0				3	0	1
Nautilid		0	0	0	0	0			1		0				0	0	0
Paranautilus smithi		0	0	0	0	0			0		0				0	0	0
Bivalve		0	1	0	1	3			0		0				0	0	1
Brachiopod		0	0	0	0	0			0		0				0	0	0
Gastropod		0	0	0	0	0			0		0				0	0	0
Wood		0	0	0	1	0			1		0				0	0	0
Sum:		**1**	**2**	**11**	**72**	**53**	**4**	**2**	**300**	**5**	**14**	**3**	**1**	**2**	**57**	**24**	**15**
Sum																	
Sum juveniles																	
Total:																	

	Zone	F. occidentalis	F. occidentalis	F. occidentalis	F. occidentalis	F. occidentalis	F. occidentalis	F. occidentalis	G. weitschati	G. weitschati	G. weitschati	G. weitschati	G. weitschati	G. weitschati	G. weitschati	G. weitschati	G. weitschati
	Subzone	P. furlongi	P. furlongi	P. furlongi	P. furlongi	P. furlongi	P. furlongi	P. furlongi	B. cordeyi	B. cordeyi	R. transformis	R. transformis	R. transformis	R. transformis	R. transformis	R. transformis	R. transformis
Species		**MUC 5865**	**MUC 5570**	**MUC 5880**	**MUC 6036**	**MUC 5080**	**MUC 6245**	**MUC 6070-6080**	**FHD 845**	**FHD 911**	**FHD 1060**	**FHD 1065**	**FHD 1085**	**FHE 10**	**FHE 45**	**FHE 125**	**FHE 198**
Anagymnites sp.									0	0	0	0	0	0	0	0	
Ussurites cf. arthaberi									0	0	0	0	0	0	0	0	
Aplococeras cf. smithi									0	0	0	0	0	0	0	0	
Aplococeras cf. vogdesi									0	0	0	0	0	0	0	0	
Aplococeras parvus									0	0	0	0	0	0	0	0	
Aplococeras smithi									0	0	0	0	0	0	0	0	
Aplococeras sp.									0	0	0	0	0	0	0	0	
Aplococeras vogdesi									0	0	0	0	0	0	0	0	
Favreticeras ransomei									0	0	0	0	0	0	0	0	
Eogymnotoceras tuberculatum									0	0	0	0	0	0	0	0	
?Eogymnotoceras tuberculatum juv.									0	0	0	0	0	0	0	0	
Brackites vogdesi									0	0	0	0	0	0	0	0	
Billingsites cf. escuargeli									0	0	0	0	3	5	0	0	
Billingsites cordeyi									0	0	0	0	195	21	0	4	
Dixieceras lawsoni									0	0	0	0	0	0	0	0	
Gymnotoceras praecursor									0	0	0	0	0	0	0	0	
Gymnotoceras weitschati									0	3	0	0	7	34	24	3	
Gymnotoceras rotelliformis									0	0	0	0	0	0	0	0	
Gymnotoceras rotelliformis-blakei									0	0	0	0	0	0	0	0	
Gymnotoceras cf. blakei									0	0	0	0	0	0	0	0	
Gymnotoceras blakei									0	0	0	0	0	0	0	0	
Gymnotoceras mimetus									0	0	0	0	0	0	0	0	
Parafrechites dunni									0	0	0	0	0	0	0	0	
Parafrechites meeki									0	0	0	0	0	0	0	0	
Frechites nevadanus									0	0	0	0	0	0	0	0	
Frechites occidentalis								1	0	0	0	0	0	0	0	0	
Humboldtites septentrionalis									0	0	0	0	0	0	0	0	
Intornites nevadanus									0	0	0	0	0	0	0	0	
Longobardites cf. parvus									0	0	0	0	0	0	0	0	
Longobardites parvus								1	0	0	0	0	61	2	0	0	
Longobardites sp.									0	0	0	0	0	0	0	0	
Longobardites zsigmondyi									0	0	0	0	0	0	2	0	
Nevadisculites depressus									0	0	0	0	0	0	0	0	
Nevadisculites smithi									0	0	0	0	0	0	0	0	
Acrochordiceras carolinae									0	0	0	0	0	0	0	0	
Jenksites flexicostatus									2	3	0	0	6	0	0	0	
Rieppelites boletzkyi									3	5	0	0	9	0	0	0	
Rieberites transiformis									0	8	0	0	48	0	0	0	
Silberlingia clarkei									0	0	0	0	0	0	0	0	
Silberlingia praecursor									0	0	0	0	38	1	0	0	
Ceccaceras stecki									0	0	0	0	0	0	0	0	
Eutomoceras dunni									0	0	0	0	0	0	0	0	
Eutomoceras laubei									0	0	0	0	0	0	0	0	
Eutomoceras sp.									0	0	0	0	0	0	0	0	
Marcouxites spinifer ad.									0	0	0	0	0	0	0	0	
Marcouxites spinifer juv.									0	0	0	0	0	0	0	0	
Metadinarites desertorus									0	0	0	0	0	0	0	0	
Nevadites humboldtensis				2					0	0	0	0	0	0	0	0	
Nevadites hyatti									0	0	0	0	0	0	0	0	
Nevadites sp.									0	0	0	0	0	0	0	0	
Paranevadites furlongi		1						1	0	0	0	0	0	0	0	0	
Platycuccoceras cainense									0	0	0	0	0	0	0	0	
Proarcestes bramantei									0	0	0	0	0	1	16	0	
Proarcestes cf. P. balfouri									0	0	0	0	0	0	0	0	
Proarcestes cf. P. bramantei									0	0	0	0	0	0	0	0	
Proarcestes gabbi								1	0	0	0	0	0	0	0	0	
Proarcestes sp.									0	0	0	0	0	0	0	0	
Proarcestes-Humboldtites									0	0	0	0	0	0	0	0	
Ptychites gradinarui									0	0	0	0	0	0	0	0	
Ptychites guloensis									0	0	0	0	0	0	0	0	
Ptychites embreei									0	0	0	0	0	0	0	0	
Sageceras walteri									0	1	0	0	0	0	0	0	
Thanamites cf. contractus									0	0	0	0	0	0	0	0	
Tozerites gemmelaroi									0	0	0	0	0	0	0	0	
Tozerites humboldtensis									0	0	0	0	0	0	0	0	
Tozerites polygyratus							1	2	0	0	0	0	0	0	0	0	
Tropigastrites cf. louderbacki									0	0	0	0	0	0	0	0	
Tropigastrites lohantanus									0	0	0	0	0	0	0	0	
Tropigastrites louderbacki									0	0	0	0	0	0	0	0	
Tropigastrites sp.									0	0	0	0	0	0	0	0	
sp. indet.									0	7	0	0	0	1	0	0	
Atractites sp.									0	1	1	0	0	0	2	0	
Nautilid									0	0	0	0	0	1	0	0	
Paranautilus smithi									0	0	0	0	0	0	0	0	
Bivalve			1	3	1	2			0	0	0	1	0	0	0	0	2
Brachiopod									0	0	0	0	0	0	0	0	
Gastropod									0	0	0	0	0	0	0	0	
Wood									0	0	0	0	0	0	0	0	
Sum:		**1**	**1**	**5**	**1**	**2**	**1**	**6**	**5**	**28**	**1**	**1**	**367**	**66**	**44**	**7**	**2**
Sum									402 specimens					959 specimens			
Sum juveniles									172 specimens					123 specimens			
Total:									**574 specimens**					**1082 specimens**			

Zone	G. weitschati	G. mimetus	G. mimetus	G. mimetus	G. rotelliformis	G. rotelliformis	G. rotelliformis	G. rotelliformis	G. rotelliformis	G. rotelliformis	G. rotelliformis	G. rotelliformis	G. rotelliformis	G. rotelliformis	G. rotelliformis	G. rotelliformis
Subzone	R. transiformis	D. lawsoni	D. lawsoni	D. lawsoni	B. vogdesi	B. vogdesi	B. vogdesi	B. vogdesi	B. vogdesi	B. vogdesi	B. vogdesi	B. vogdesi	B. vogdesi	G. blakei	G. blakei	G. blakei
Species	**FHE 270**	**FHF 215**	**FHF 310**	**FHI**	**FHR 54**	**FHR 90**	**FHR 140**	**FHR 240**	**FHR 270**	**FHR 310**	**FHR 340**	**FHR 398**	**FHR 430**	**FHR 635**	**FHR 755**	**FHR 870**
Anagymnites sp.		2	12	0	0	0	0	0	0	0	0	0	0	0	0	0
Ussurites cf. arthaberi			0	0	0	0	0	0	0	0	0	0	0	0	0	0
Aplococeras cf. smithi			0	0	0	0	0	0	0	0	0	0	0	0	0	0
Aplococeras cf. vogdesi			0	0	0	0	0	0	0	0	0	0	0	0	0	0
Aplococeras parvus			0	0	0	0	0	0	0	0	0	0	0	0	0	0
Aplococeras smithi			0	0	0	0	0	0	0	0	0	0	0	0	5	0
Aplococeras sp.			0	0	0	0	0	0	0	0	0	0	0	0	0	0
Aplococeras vogdesi			0	0	0	0	0	0	0	0	0	0	0	0	0	0
Favreticeras ransomei			0	0	0	0	0	0	0	0	0	0	0	0	0	0
Eogymnotoceras tuberculatum			0	0	0	0	0	0	0	0	0	0	0	0	0	0
?Eogymnotoceras tuberculatum juv.			0	0	0	0	0	0	0	0	0	0	0	0	0	0
Brackites vogdesi			0	0	0	4	1	1	42	13	1	0	5	0	0	0
Billingsites cf. escuargeli			0	0	0	0	0	0	0	0	0	0	0	0	0	0
Billingsites cordeyi			0	0	0	0	0	0	0	0	0	0	0	0	0	0
Dixieceras lawsoni		1	333	19	0	0	0	0	0	0	0	0	0	0	0	0
Gymnotoceras praecursor			0	0	0	0	0	0	0	0	0	0	0	0	0	0
Gymnotoceras weitschati			0	0	0	0	0	0	0	0	0	0	0	0	0	0
Gymnotoceras rotelliformis			0	0	1	49	19	10	308	66	6	0	104	0	0	0
Gymnotoceras rotelliformis-blakei			0	0	0	0	0	0	0	0	0	0	0	0	0	0
Gymnotoceras cf. blakei			0	0	0	0	0	0	0	0	0	0	0	0	0	0
Gymnotoceras blakei			0	0	0	0	0	0	0	0	0	0	0	12	54	1
Gymnotoceras mimetus			218	17	0	0	0	0	0	0	0	0	0	0	0	0
Parafrechites dunni			0	0	0	0	0	0	0	0	0	0	0	0	0	0
Parafrechites meeki			0	0	0	0	0	0	0	0	0	0	0	0	0	0
Frechites nevadanus			0	0	0	0	0	0	0	0	0	0	0	0	8	0
Frechites occidentalis			0	0	0	0	0	0	0	0	0	0	0	0	0	0
Humboldtites septentrionalis			0	0	0	0	0	0	0	0	0	0	0	0	0	0
Intornites nevadanus			0	0	0	0	0	0	0	0	0	0	0	0	0	0
Longobardites cf. parvus			0	0	0	0	0	0	0	0	0	0	0	0	0	0
Longobardites parvus			0	0	0	0	0	0	0	0	0	0	3	0	39	7
Longobardites sp.			0	0	0	0	0	0	0	0	0	0	0	0	0	0
Longobardites zsigmondyi		1	236	10	0	5	0	0	0	0	0	0	0	0	0	0
Nevadisculites depressus			0	0	0	0	0	0	0	0	0	0	0	0	0	0
Nevadisculites smithi			0	0	0	0	0	0	0	0	0	0	0	0	0	0
Acrochordiceras carolinae			0	0	0	0	0	0	0	0	0	0	0	0	0	0
Jenksites flexicostatus			0	0	0	0	0	0	0	0	0	0	0	0	0	0
Rieppelites boletzkyi			0	0	0	0	0	0	0	0	0	0	0	0	0	0
Rieberites transiformis			0	0	0	0	0	0	0	0	0	0	0	0	0	0
Silberlingia clarkei			0	0	0	0	0	0	0	0	0	0	0	0	0	0
Silberlingia praecursor			0	0	0	0	0	0	0	0	0	0	0	0	0	0
Ceccaceras stecki			0	0	0	0	0	0	0	0	0	0	0	0	0	0
Eutomoceras dunni			0	0	0	0	0	0	0	0	0	0	0	0	4	1
Eutomoceras laubei			0	0	0	0	0	0	0	0	0	0	0	0	0	0
Eutomoceras sp.			0	0	0	0	0	0	0	1	0	0	6	0	0	0
Marcouxites spinifer ad.			0	0	0	0	0	0	0	0	0	0	0	0	0	0
Marcouxites spinifer juv.			0	0	0	0	0	0	0	0	0	0	0	0	0	0
Metadinarites desertorus			0	0	0	0	0	0	1	0	0	0	0	0	0	0
Nevadites humboldtensis			0	0	0	0	0	0	0	0	0	0	0	0	0	0
Nevadites hyatti			0	0	0	0	0	0	0	0	0	0	0	0	0	0
Nevadites sp.			0	0	0	0	0	0	0	0	0	0	0	0	0	0
Paranevadites furlongi			0	0	0	0	0	0	0	0	0	0	0	0	0	0
Platycuccoceras cainense			0	0	0	0	0	0	0	0	0	0	0	0	0	0
Proarcestes bramantei		1	28	0	0	0	0	0	0	0	0	0	0	0	0	0
Proarcestes cf. P. balfouri			0	0	0	0	0	0	0	0	0	0	2	1	3	0
Proarcestes cf. P. bramantei			0	0	0	0	0	0	0	0	0	0	0	0	0	0
Proarcestes gabbi			0	0	0	0	0	0	0	0	0	0	0	0	0	0
Proarcestes sp.			0	0	0	0	0	0	1	0	0	0	0	0	0	0
Proarcestes-Humboldtites			0	0	0	0	0	0	0	0	0	0	0	0	0	0
Ptychites gradinarui			0	0	0	0	0	0	0	0	0	0	0	0	0	0
Ptychites guloensis			0	0	0	0	0	0	0	0	0	0	0	0	0	0
Ptychites embreei			0	0	0	0	0	0	0	0	0	0	0	0	0	0
Sageceras walteri			0	0	0	0	0	0	0	0	0	0	0	0	0	0
Thanamites cf. contractus			0	0	0	0	0	0	0	0	0	0	0	0	0	0
Tozerites gemmelaroi			0	0	0	0	0	0	0	0	0	0	0	0	0	0
Tozerites humboldtensis			0	0	0	0	0	0	0	0	0	0	0	0	0	0
Tozerites polygyratus			0	0	0	0	0	0	0	0	0	0	0	0	0	0
Tropigastrites cf. louderbacki			0	0	0	0	0	0	0	0	0	0	0	0	0	0
Tropigastrites lohantanus			0	0	0	0	0	0	0	0	0	0	0	0	9	1
Tropigastrites louderbacki			0	0	0	0	0	0	0	0	0	0	0	0	0	0
Tropigastrites sp.			0	0	0	0	0	0	0	0	0	0	0	0	0	0
sp. indet.	1		0	0	0	0	0	1	3	0	1	0	0	0	0	0
Atractites sp.		1	3	0	0	1	0	0	4	1	2	1	3	0	5	1
Nautilid			0	0	0	0	0	0	0	0	0	0	0	0	0	0
Paranautilus smithi			0	0	0	0	0	0	0	0	0	0	0	0	0	0
Bivalve		3	0	0	0	0	0	0	0	0	0	0	0	0	0	0
Brachiopod			0	0	0	0	0	0	0	0	0	0	0	0	0	0
Gastropod			0	0	0	0	0	0	0	0	0	0	0	0	0	0
Wood			0	0	0	0	0	0	0	0	0	0	0	0	1	0
Sum:	**1**	**9**	**830**	**46**	**1**	**59**	**20**	**12**	**359**	**81**	**10**	**1**	**123**	**13**	**128**	**11**

Sum	46 specimens	1282 specimens
Sum juveniles	17 specimens	57 specimens
Total:	**63 specimens**	**1339 specimens**

Zone	P. meeki	P. meeki	P. meeki	P. meeki	P. meeki	P. meeki	P. meeki	P. meeki	P. meeki	P. meeki	P. meeki	P. meeki	P. meeki	P. meeki	F. occidentalis	F. occidentalis
Subzone	F. nevadanus	F. nevadanus	F. nevadanus	F. nevadanus	P. meeki	P. meeki	P. meeki	P. meeki	P. dunni	P. dunni	P. dunni	P. dunni	P. dunni	P. dunni	N. hyatti	N. hyatti
Species	**FHR 900**	**FHR 980**	**FHR 1086**	**FHR 1111**	**FHR 1125**	**FHR 1160**	**FHR 1250**	**FHR 1350**	**FHR 1410**	**FHS 16**	**FHS 26**	**FHS 83**	**FHS 120**	**FHS 151-170**	**FHS 672-673**	**FHS 678**
Anagymnites sp.																
Ussurites cf. arthaberi																
Aplococeras cf. smithi																
Aplococeras cf. vogdesi																
Aplococeras parvus															13	33
Aplococeras smithi									1							
Aplococeras sp.																
Aplococeras vogdesi					1									7		
Favreticeras ransomei																
Eogymnotoceras tuberculatum																
?Eogymnotoceras tuberculatum juv.																
Brackites vogdesi																
Billingsites cf. escuargeli																
Billingsites cordeyi																
Dixieceras lawsoni																
Gymnotoceras praecursor																
Gymnotoceras weitschati																
Gymnotoceras rotelliformis																
Gymnotoceras rotelliformis-blakei																
Gymnotoceras cf. blakei																
Gymnotoceras blakei																
Gymnotoceras mimetus																
Parafrechites dunni									22	4		1	2	35		
Parafrechites meeki				10	240	9	2	4	12		18			31		
Frechites nevadanus				112												
Frechites occidentalis															37	51
Humboldtites septentrionalis																2
Intornites nevadanus																
Longobardites cf. parvus																
Longobardites parvus				1				1	8							
Longobardites sp.														5		
Longobardites zsigmondyi														15	38	54
Nevadisculites depressus																
Nevadisculites smithi																
Acrochordiceras carolinae																
Jenksites flexicostatus																
Rieppelites boletzkyi																
Rieberites transiformis																
Silberlingia clarkei																
Silberlingia praecursor																
Ceccaceras stecki																
Eutomoceras dunni				1	1				1							
Eutomoceras laubei											2			1	11	9
Eutomoceras sp.																
Marcouxites spinifer ad.																
Marcouxites spinifer juv.																
Metadinarites desertorus																
Nevadites humboldtensis																
Nevadites hyatti															24	33
Nevadites sp.																
Paranevadites furlongi																
Platycuccoceras cainense																
Proarcestes bramantei																
Proarcestes cf. P. balfouri																
Proarcestes cf. P. bramantei																
Proarcestes gabbi															4	3
Proarcestes sp.																
Proarcestes-Humboldtites															4	5
Ptychites gradinarui																
Ptychites guloensis																
Ptychites embreei																
Sageceras walteri																
Thanamites cf. contractus																
Tozerites gemmelaroi											4			8		
Tozerites humboldtensis															11	17
Tozerites polygyratus																
Tropigastrites cf. louderbacki																
Tropigastrites lohantanus																
Tropigastrites louderbacki				5	1			5								
Tropigastrites sp.																
sp. indet.															2	2
Atractites sp.	1	1		11	7		1		5	1				1	3	4
Nautilid																
Paranautilus smithi																
Bivalve			1												2	
Brachiopod																
Gastropod																
Wood																
Sum:	**1**	**1**	**1**	**140**	**250**	**9**	**3**	**10**	**49**	**5**	**24**	**1**	**2**	**103**	**149**	**213**

Sum	1538 specimens
Sum juveniles	217 specimens
Total:	**1755 specimens**

	Zone	F. occidentalis	F. occidentalis	F. occidentalis	F. occidentalis	F. occidentalis	F. occidentalis	F. occidentalis	F. occidentalis	F. occidentalis	F. occidentalis	F. occidentalis	F. occidentalis	F. occidentalis	F. occidentalis	F. occidentalis	F. occidentalis
	Subzone	N. humbol.	N. humbol.	N. humbol.	N. humbol.	N. humbol.	N. humbol.	N. humbol.	N. humbol.	N. humbol.	N. humbol.	N. humbol./ P. furlongi	P. furlongi	P. furlongi	P. furlongi	P. furlongi	P. furlongi
Species		**FHS 720**	**FHS 737**	**FHS 780-788**	**FHS 819**	**FHS 886-895**	**FHS 927**	**FHS 945**	**FHS 1050-1063**	**FHS 1125**	**FHS 1194**	**FHS 1215**	**FHS 1400-1410**	**FHS 1450**	**FHS 1750**	**FHS 1870**	**FHS 1935**
Anagymnites sp.		0	0	0	0	0	0		0	0	0	0	0	0	0	0	0
Ussurites cf. arthaberi		0	0	0	0	0	0		0	0	0	0	0	0	0	0	0
Aplococeras cf. smithi		0	0	0	0	0	0		0	0	0	0	0	0	0	0	0
Aplococeras cf. vogdesi		0	0	0	0	0	0		0	0	0	0	0	0	0	0	0
Aplococeras parvus		0	0	7	0	0	0		0	0	0	0	0	0	0	0	0
Aplococeras smithi		0	0	0	0	0	0		0	0	0	0	0	0	0	0	0
Aplococeras sp.		0	0	0	0	0	0		0	0	0	0	0	0	0	0	0
Aplococeras vogdesi		0	0	0	0	0	0		0	0	0	0	0	0	0	0	0
Favreticeras ransomei		0	0	0	0	0	0		0	0	0	0	0	0	0	0	0
Eogymnotoceras tuberculatum		0	0	0	0	0	0		0	0	0	0	0	0	0	0	0
?Eogymnotoceras tuberculatum juv.		0	0	0	0	0	0		0	0	0	0	0	0	0	0	0
Brackites vogdesi		0	0	0	0	0	0		0	0	0	0	0	0	0	0	0
Billingsites cf. escuargeli		0	0	0	0	0	0		0	0	0	0	0	0	0	0	0
Billingsites cordeyi		0	0	0	0	0	0		0	0	0	0	0	0	0	0	0
Dixieceras lawsoni		0	0	0	0	0	0		0	0	0	0	0	0	0	0	0
Gymnotoceras praecursor		0	0	0	0	0	0		0	0	0	0	0	0	0	0	0
Gymnotoceras weitschati		0	0	0	0	0	0		0	0	0	0	0	0	0	0	0
Gymnotoceras rotelliformis		0	0	0	0	0	0		0	0	0	0	0	0	0	0	0
Gymnotoceras rotelliformis-blakei		0	0	0	0	0	0		0	0	0	0	0	0	0	0	0
Gymnotoceras cf. blakei		0	0	0	0	0	0		0	0	0	0	0	0	0	0	0
Gymnotoceras blakei		0	0	0	0	0	0		0	0	0	0	0	0	0	0	0
Gymnotoceras mimetus		0	0	0	0	0	0		0	0	0	0	0	0	0	0	0
Parafrechites dunni		2	0	0	0	0	0		0	0	0	0	0	0	0	0	0
Parafrechites meeki		0	0	0	0	0	0		0	0	0	0	0	0	0	0	0
Frechites nevadanus		0	0	0	0	0	0		0	0	0	0	0	0	0	0	0
Frechites occidentalis		17	11	4	0	3	2		708	3	1	1	21	6	1	0	0
Humboldtites septentrionalis		2	6	4	0	0	0		0	0	0	0	0	0	0	0	0
Intornites nevadanus		0	0	0	0	0	0		0	0	0	0	0	0	0	0	0
Longobardites cf. parvus		0	0	0	0	0	0		0	0	0	0	0	0	0	0	0
Longobardites parvus		0	0	0	0	0	0		0	0	0	0	0	0	0	0	0
Longobardites sp.		0	0	0	0	0	0		0	0	0	0	0	0	0	0	0
Longobardites zsigmondyi		10	12	8	1	1	5		0	0	0	0	0	0	0	0	0
Nevadisculites depressus		0	0	0	0	0	0		0	0	0	0	0	0	0	0	0
Nevadisculites smithi		0	0	0	0	0	0		0	0	0	0	0	0	0	0	0
Acrochordiceras carolinae		0	0	0	0	0	0		0	0	0	0	0	0	0	0	0
Jenksites flexicostatus		0	0	0	0	0	0		0	0	0	0	0	0	0	0	0
Rieppelites boletzkyi		0	0	0	0	0	0		0	0	0	0	0	0	0	0	0
Rieberites transiformis		0	0	0	0	0	0		0	0	0	0	0	0	0	0	0
Silberlingia clarkei		0	0	0	0	0	0		0	0	0	0	0	0	0	0	0
Silberlingia praecursor		0	0	0	0	0	0		0	0	0	0	0	0	0	0	0
Ceccaceras stecki		0	0	0	0	0	0		0	0	0	0	0	0	0	0	0
Eutomoceras dunni		0	0	0	0	0	0		0	0	0	0	0	0	0	0	0
Eutomoceras laubei		0	1	0	0	0	0		0	0	0	0	0	0	0	0	0
Eutomoceras sp.		1	0	2	0	0	0		0	0	0	0	0	0	0	0	0
Marcouxites spinifer ad.		0	0	0	0	0	0		0	0	0	0	0	0	0	0	0
Marcouxites spinifer juv.		0	0	0	0	0	0		0	0	0	0	0	0	0	0	0
Metadinarites desertorus		0	0	0	0	0	0		0	0	0	0	0	0	0	0	0
Nevadites humboldtensis		24	6	18	4	2	0		2	0	1	1	0	0	0	0	0
Nevadites hyatti		0	0	0	0	0	0		0	0	0	0	0	0	0	0	0
Nevadites sp.		0	0	0	0	0	0		0	0	0	0	0	0	0	0	0
Paranevadites furlongi		0	0	0	0	0	0		0	0	0	1	10	1	0	1	1
Platycuccoceras cainense		0	0	0	0	0	0		0	0	0	0	0	0	0	0	0
Proarcestes bramantei		0	0	0	0	0	0		0	0	0	0	0	0	0	0	0
Proarcestes cf. P. balfouri		0	0	0	0	0	0		0	0	0	0	0	0	0	0	0
Proarcestes cf. P. bramantei		0	0	0	0	0	0		0	0	0	0	0	0	0	0	0
Proarcestes gabbi		5	1	9	0	0	0		0	0	0	0	22	4	0	0	0
Proarcestes sp.		0	0	0	0	0	0		0	0	0	0	0	0	0	0	0
Proarcestes-Humboldtites		1	0	4	0	0	0		0	0	0	0	0	0	0	0	0
Ptychites gradinarui		0	0	0	0	0	0		0	0	0	0	0	0	0	0	0
Ptychites guloensis		0	0	0	0	0	0		0	0	0	0	0	0	0	0	0
Ptychites embreei		0	0	0	0	0	0		0	0	0	0	0	0	0	0	0
Sageceras walteri		0	0	0	0	0	0		0	0	0	0	0	0	0	0	0
Thanamites cf. contractus		0	0	0	0	0	0		0	0	0	0	0	0	0	0	0
Tozerites gemmelaroi		0	0	0	0	0	0		0	0	0	0	0	0	0	0	0
Tozerites humboldtensis		8	7	0	0	1	0		0	0	0	0	1	0	0	0	0
Tozerites polygyratus		0	0	0	0	0	0		0	0	0	0	0	0	0	0	0
Tropigastrites cf. louderbacki		0	0	0	0	0	0		0	0	0	0	0	0	0	0	0
Tropigastrites lohantanus		0	0	0	0	0	0		0	0	0	0	0	0	0	0	0
Tropigastrites louderbacki		0	0	0	0	0	0		0	0	0	0	0	0	0	0	0
Tropigastrites sp.		0	0	0	0	0	0		0	0	0	0	0	0	0	0	0
sp. indet.		1	1	3	0	0	0		0	0	0	0	2	0	0	0	1
Atractites sp.		1	5	8	0	1	0	15	1	0	0	0	4	1	0	1	0
Nautilid		0	0	0	0	0	0		0	0	0	0	0	0	0	0	0
Paranautilus smithi		0	0	0	0	0	0		0	0	1	0	0	0	0	0	0
Bivalve		0	1	1	0	0	0		2	0	0	2	2	0	1	0	0
Brachiopod		0	0	0	0	0	0		0	0	0	0	0	0	0	0	0
Gastropod		0	0	0	0	0	0		7	0	0	0	4	0	0	0	0
Wood		0	0	0	0	0	0		0	0	0	0	0	0	0	0	0
Sum:		**72**	**51**	**68**	**5**	**8**	**7**	**15**	**720**	**3**	**3**	**5**	**66**	**12**	**2**	**2**	**2**
Sum																	
Sum juveniles																	
Total:																	

Zone	Parafrechites meeki	Parafrechites meeki	Parafrechites meeki	Frechites occidentalis				
Subzone	Parafrechites dunni	Parafrechites dunni	Parafrechites dunni	Nevadites humboldtensis				
Species	**FHS-RB 133**	**FHS-RB 144**	**FHS-RB 155**	**FH-Neva**	**Absolute abundance**	**Relative abundance**	**Relative abundance of family**	**average relative abundance of species in family**
Anagymnites sp.	0	0	0	0	17	0.24	0.24	0.24
Ussurites cf. arthaberi	0	0	0	0	33	0.46	0.46	0.46
Aplococeras cf. smithi	0	0	0	0	70	0.98		
Aplococeras cf. vogdesi	0	0	0	0	6	0.08		
Aplococeras parvus	0	0	0	3	94	1.32		
Aplococeras smithi	0	0	0	0	7	0.10		
Aplococeras sp.	0	0	0	0	1	0.01		
Aplococeras vogdesi	0	1	5	0	19	0.27	2.77	0.46
Favreticeras ransomei	0	0	0		37	0.52		
Eogymnotoceras tuberculatum	0	0	0	0	93	1.31		
?Eogymnotoceras tuberculatum juv.	0	0	0	0	274	3.85		
Brackites vogdesi	0	0	0	0	68	0.95		
Billingsites cf. escuargeli	0	0	0	0	8	0.11		
Billingsites cordeyi	0	0	0	0	220	3.09		
Dixieceras lawsoni	0	0	0	0	353	4.96		
Gymnotoceras praecursor	0	0	0	0	20	0.28		
Gymnotoceras weitschati	0	0	0	0	71	1.00		
Gymnotoceras rotelliformis	0	0	0	0	563	7.90		
Gymnotoceras rotelliformis-blakei	0	0	0	0	380	5.33		
Gymnotoceras cf. blakei	0	0	0		33	0.46		
Gymnotoceras blakei	0	0	0	0	85	1.19		
Gymnotoceras mimetus	0	0	0	0	235	3.30		
Parafrechites dunni	0	4	10	0	80	1.12		
Parafrechites meeki	0	3	27	5	374	5.25		
Frechites nevadanus	0	0	0	0	120	1.68		
Frechites occidentalis	0	0	0	442	1492	20.94	63.25	3.51
Humboldtites septentrionalis	0	0	0	0	24	0.34	0.34	0.34
Intornites nevadanus	0	0	0	0	39	0.55		
Longobardites cf. parvus	0	0	0	0	24	0.34		
Longobardites parvus	0	0	1	0	146	2.05		
Longobardites sp.	0	0	0	0	7	0.10		
Longobardites zsigmondyi	0	0	0	10	461	6.47	9.50	1.90
Nevadisculites depressus	0	0	0		11	0.15		
Nevadisculites smithi	0	0	0	0	33	0.46	0.62	0.31
Acrochordiceras carolinae	0	0	0	0	138	1.94	1.94	1.94
Jenksites flexicostatus	0	0	0	0	11	0.15		
Rieppelites boletzkyi	0	0	0	0	17	0.24		
Rieberites transiformis	0	0	0	0	56	0.79		
Silberlingia clarkei	0	0	0	0	126	1.77		
Silberlingia praecursor	0	0	0	0	39	0.55		
Ceccaceras stecki	0	0	0	0	1	0.01		
Eutomoceras dunni	0	0	0	0	8	0.11		
Eutomoceras laubei	0	1	6	2	35	0.49		
Eutomoceras sp.	0	0	0		55	0.77		
Marcouxites spinifer ad.	0	0	0	0	29	0.41		
Marcouxites spinifer juv.	0	0	0	0	54	0.76		
Metadinarites desertorus	0	0	0	0	157	2.20		
Nevadites humboldtensis	0	0	0	0	184	2.58		
Nevadites hyatti	0	0	0	0	91	1.28		
Nevadites sp.	0	0	0	0	1	0.01		
Paranevadites furlongi	0	0	0	0	33	0.46	12.59	0.79
Platycuccoceras cainense	0	0	0		25	0.35	0.35	
Proarcestes bramantei	0	0	0	0	46	0.65		
Proarcestes cf. P. balfouri	0	0	0	0	6	0.08		
Proarcestes cf. P. bramantei	0	0	0	0	8	0.11		
Proarcestes gabbi	0	0	0	13	174	2.44		
Proarcestes sp.	0	0	0	0	13	0.18		
Proarcestes-Humboldtites	0	0	0	0	17	0.24	3.71	0.62
Ptychites gradinarui	0	0	0	0	1	0.01		
Ptychites guloensis	0	0	0		1	0.01		
Ptychites embreei	0	0	0	0	38	0.53	0.56	0.19
Sageceras walteri	0	0	0	1	3	0.04	0.04	0.04
Thanamites cf. contractus	0	0	0	0	15	0.21	0.21	0.21
Tozerites gemmelaroi	1	0	1	0	14	0.20		
Tozerites humboldtensis	0	0	0	0	47	0.66		
Tozerites polygyratus	0	0	0	8	35	0.49		
Tropigastrites cf. louderbacki	0	0	0	0	3	0.04		
Tropigastrites lohantanus	0	0	0	0	52	0.73		
Tropigastrites louderbacki	0	0	0	0	11	0.15		
Tropigastrites sp.	0	0	0		24	0.34	2.61	0.37
sp. indet.	0	0	0	0	58	0.81	0.81	0.81
Atractites sp.	0	0	3	1				
Nautilid	0	0	1	0				
Paranautilus smithi	0	0	0	0				
Bivalve	0	0	0	0				
Brachiopod	0	0	3	0				
Gastropod	0	0	1	0				
Wood	0	0	0	0				
Sum:	**1**	**9**	**58**	**485**	**7124**	**100.00**	**100.00**	

		7124	**Total sum adult ammonoid specimens**
Sum	68 specimens	485	**7326 Total sum adult ammonoid specimens incl. other fossil**
Sum juveniles	1 specimens	16	**691 Total sum juvenile ammonoid specimens**
Total:	**69 specimens**	**501**	**8017 Total sum fossil specimens**

7326 Total sum adult ammonoid specimen incl. other fossil
691 Total sum juvenile ammonoid specimen
8017 Total sum fossil specimen